

University of Wollongong - Research Online

Thesis Collection

Title: Low-velocity pneumatic transportation of bulk solids

Author: Bo Mi

Year: 1994

Repository DOI:

Copyright Warning

You may print or download ONE copy of this document for the purpose of your own research or study. The University does not authorise you to copy, communicate or otherwise make available electronically to any other person any copyright material contained on this site.

You are reminded of the following: This work is copyright. Apart from any use permitted under the Copyright Act 1968, no part of this work may be reproduced by any process, nor may any other exclusive right be exercised, without the permission of the author. Copyright owners are entitled to take legal action against persons who infringe their copyright. A reproduction of material that is protected by copyright may be a copyright infringement. A court may impose penalties and award damages in relation to offences and infringements relating to copyright material.

Higher penalties may apply, and higher damages may be awarded, for offences and infringements involving the conversion of material into digital or electronic form.

Unless otherwise indicated, the views expressed in this thesis are those of the author and do not necessarily represent the views of the University of Wollongong.

Research Online is the open access repository for the University of Wollongong. For further information contact the UOW Library: research-pubs@uow.edu.au

University of Wollongong Thesis Collections

University of Wollongong Thesis Collection

University of Wollongong

Year 1994

Low-velocity pneumatic transportation of bulk solids

Bo Mi
University of Wollongong

Mi, Bo, Low-velocity pneumatic transportation of bulk solids, PhD thesis, Department of Mechanical Engineering, University of Wollongong, 1994. <http://ro.uow.edu.au/theses/830>

This paper is posted at Research Online.
<http://ro.uow.edu.au/theses/830>

NOTE

This online version of the thesis may have different page formatting and pagination from the paper copy held in the University of Wollongong Library.

UNIVERSITY OF WOLLONGONG

COPYRIGHT WARNING

You may print or download ONE copy of this document for the purpose of your own research or study. The University does not authorise you to copy, communicate or otherwise make available electronically to any other person any copyright material contained on this site. You are reminded of the following:

Copyright owners are entitled to take legal action against persons who infringe their copyright. A reproduction of material that is protected by copyright may be a copyright infringement. A court may impose penalties and award damages in relation to offences and infringements relating to copyright material. Higher penalties may apply, and higher damages may be awarded, for offences and infringements involving the conversion of material into digital or electronic form.

LOW-VELOCITY PNEUMATIC TRANSPORTATION OF BULK SOLIDS

A thesis submitted in fulfilment of the requirements
for the award of the degree of

DOCTOR OF PHILOSOPHY

from

UNIVERSITY OF WOLLONGONG

by

BO MI

B.Sc. (USTB), M.Sc. (USTB)

Department of Mechanical Engineering

1994

DECLARATION

This is to certify that the work presented in this thesis was carried out by the author in the Department of Mechanical Engineering at the University of Wollongong and has not been submitted for a degree to any other university or institution.

Bo Mi

ACKNOWLEDGMENTS

I would like to thank my supervisor, Dr P. W. Wypych, Senior Lecturer in the Department of Mechanical Engineering at the University of Wollongong, for his supervision, generous assistance and encouragement during the period of this study. I am indebted to Professor P. C. Arnold, Dr A. Mclean, Mr O. Kennedy, Dr Z. Gu and Dr R. Pan, the staff of the Bulk Materials Handling group, for their constructive suggestions in the development of the theory.

I gratefully acknowledge the financial support of the University of Wollongong under the Postgraduate Research Award scheme and the financial contribution by the Bulk Materials Handling and Physical Processing research program.

Acknowledgment also is made of the assistance given by other staff of the department, especially that of Mrs R. Hamlet and Mrs B. Butler, who completed many of the administrative tasks associated with this project. My thanks are extended to the technical staff in the Workshop and Bulk Solids Handling Laboratory with whose help and expertise the experimental apparatus was constructed. In particular, I would like to express my gratitude to Mr D. Cook, Mr I. Frew, Mrs W. Halford, Mr I. McColm and Mr S. Dunster.

Finally, special acknowledgment is made to my dear wife Yao Feng and my parents for their unfailing help and encouragement.

SUMMARY

Low-velocity pneumatic conveying is being used increasingly in industry to transport a wide range of bulk solids due to reasons of low power consumption and low product damage, etc. However, investigations into this type of conveying still are at an elementary stage. For example, the existing procedures to estimate pipeline pressure drop during low-velocity pneumatic conveying still are inaccurate and inefficient. For this reason, this thesis aims at developing a pressure prediction model that is a function of the physical properties of the material, pipeline configuration and conveying condition.

During low-velocity pneumatic conveying, particles are conveyed usually in the form of slugs. This thesis studies initially the pressure drop across a single particle slug and the stress state and distribution in the slug through theoretical analysis.

To obtain detailed information on low-velocity pneumatic conveying, a test rig is set up and four types of coarse granular material are conveyed in the rig. Major parameters such as mass flow-rate of air and solids, pipeline pressure, slug velocity and wall pressure, etc. are measured over a wide range of low-velocity conveying conditions.

Based on the experimental results and a dimensional analysis, the relationship between the slug velocity and superficial air velocity is established in terms of the physical properties of the material and pipe size. Also by using particulate mechanics, a semi-empirical correlation is developed to determine the stress transmission coefficient for the slugs flowing in the pipe with rigid and parallel walls. A model then is developed to predict the overall horizontal pipeline pressure drop of low-velocity pneumatic conveying.

This model is used to predict the pneumatic conveying characteristics and static air pressure distribution for different test rig pipelines and materials. Good agreement is obtained between the predicted and experimental results. Based on the developed model, a method for determining the economical operating point in low-velocity pneumatic conveying is presented.

Additional experimental results from the conveying of semolina show that the performance of fine powders is quite different in low velocity. Based on these experimental results, an appropriate modification to the model is made so that it can be applied to the prediction of pressure drop in low-velocity pneumatic conveying of fine powders.

TABLE OF CONTENTS

ACKNOWLEDGMENTS	i
SUMMARY	ii
TABLE OF CONTENTS	iv
LIST OF FIGURES	ix
LIST OF TABLES	xvii
NOMENCLATURE	xix
CHAPTER	
1 INTRODUCTION	1
2 LITERATURE SURVEY	7
2.1 Introduction	8
2.2 Suitability of Bulk Material	8
2.3 Performance of Low-Velocity Pneumatic Conveying	15
2.3.1 Flow Pattern	15
2.3.2 Pipeline Pressure Drop	17
2.3.2.1 Pressure Drop in Horizontal Flow	17
2.3.2.2 Pressure Drop in Vertical Flow	24
2.3.2.3 Pressure Drop Around Bends	26
2.4 Design of Low-Velocity Conveying System	27
3 THEORY ON LOW-VELOCITY PNEUMATIC CONVEYING	32
3.1 Introduction	33
3.2 Flow Pattern and Formation of Particle Slugs	33
3.3 State of Particle Slug	35
3.4 Pressure Gradient of Horizontal Slug	39
3.4.1 Stresses Acting on Moving Slug	40
3.4.2 Force Balance and Pressure Gradient of Horizontal Slug	44

3.5	Axial Stress and Transmission Radial Stress	46
3.5.1	Distribution of Axial Stress	46
3.5.2	Average Axial Stress	48
3.6	Stress on Front and Back Surface of Slug	49
4	TEST FACILITY AND PROCEDURES	51
4.1	Introduction	52
4.2	General Arrangement of Main Test Rig	52
4.2.1	Material Feeders	52
4.2.1.1	High Pressure Rotary Valve	55
4.2.1.2	Blow Tank	58
4.2.2	Feed Hopper and Receiving Silo	59
4.2.3	Conveying Pipeline	59
4.3	Air Supply and Control	62
4.3.1	Air Supply	62
4.3.2	Air Flow Control	62
4.4	Experimental Instrumentation and Technique	64
4.4.1	Mass Flow-Rate of Solids	65
4.4.2	Mass Flow-Rate of Air	65
4.4.3	Static Air Pressure	66
4.4.4	Wall Pressure	66
4.4.5	Stationary Bed Thickness	68
4.4.6	Slug Velocity	68
4.5	Data Acquisition and Processing Systems	69
4.5.1	Hewlett Packard 3044A System	69
4.5.2	PC Based Quick Data Acquisition System	70
4.5.3	Data Processing	71
4.6	Test Procedures	74
4.6.1	System Check	74

4.6.2	Calibration	75
4.6.2.1	Load Cell Calibration	76
4.6.2.2	Pressure Transducer Calibration	77
4.6.3	Test Programs	79
5	TEST MATERIAL AND PROPERTIES	82
5.1	Introduction	83
5.2	Particle Size and Distribution	84
5.3	Density Analysis and Measurement	87
5.3.1	Particle Density	87
5.3.2	Bulk Density	89
5.3.3	Bulk Voidage	90
5.4	Flow Properties of Bulk Material	91
5.4.1	Internal and Effective Friction Angle	91
5.4.2	Wall Friction Angle	95
5.5	Test Material	99
6	VELOCITY OF PARTICLE SLUG	101
6.1	Introduction	102
6.2	Definitions of Velocity	104
6.2.1	Velocities for Fluid Medium	104
6.2.2	Velocities for Particulate Medium	105
6.3	Experimental Determination of Slug Velocity	107
6.3.1	Principle and Method of Slug Velocity Measurement	107
6.3.2	Calculation of Cross Correlation Function	111
6.3.3	Resolution of Velocity	114
6.4	Experimental Results of Slug Velocity	117
6.4.1	Presentation of Results vs Mass Flow-Rate of Air	118
6.4.2	Presentation of Results vs Mass Flow-Rate of Solids	122
6.4.3	Presentation of Results vs Superficial Air Velocity	124

6.5	Empirical Correlation for Slug Velocity	127
6.5.1	Linear Model of Slug Velocity	127
6.5.2	Regression Slope for Linear Model	128
6.5.3	Dimensional Analysis	130
6.5.4	Minimum Air Velocity	131
7	WALL PRESSURE AND STRESS TRANSMISSION COEFFICIENT	136
7.1	Introduction	137
7.2	Wall Pressure Measurement	139
7.2.1	Method of Wall Pressure Measurement	139
7.2.2	Installation of Transducers	140
7.2.3	Test Procedures and Special Requirements	142
7.2.3.1	Re-calibration of Transducers	142
7.2.3.2	Check Test	142
7.2.3.3	Improvement of Phase Difference of Signals	145
7.2.4	Data Processing	147
7.3	Experimental Results	147
7.4	Strength of Particulate Medium	155
7.5	Stress Transmission Coefficient	159
7.5.1	Stress Transmission Coefficient in Pipe	159
7.5.2	Discussion on Stress Transmission Coefficient	162
7.6	Correlation of Static Internal Friction Angle	166
8	TOTAL HORIZONTAL PIPELINE PRESSURE DROP	171
8.1	Introduction	172
8.2	Geometrical Parameters of Low-Velocity Pneumatic Conveying	173
8.2.1	Air Gap Length	174
8.2.2	Slug Length	186
8.2.3	Stationary Bed Thickness	189
8.2.3.1	Measurement of Stationary Bed Thickness	190

8.2.3.2	Results of Stationary Bed Thickness	192
8.3	Pneumatic Conveying Characteristics	195
8.4	Effect of Bends on Pressure Drop	201
8.5	Correlation of Horizontal Pipeline Pressure Drop	206
8.6	Comparison of Experimental and Predicted Results	208
9	PRACTICAL APPLICATIONS	213
9.1	Introduction	214
9.2	Prediction of Pneumatic Conveying Characteristics	214
9.2.1	Test Materials	215
9.2.2	Test Rigs	216
9.2.3	Test Results	219
9.2.4	Predicted Pneumatic Conveying Characteristics	220
9.3	Prediction of Pipeline Pressure Distribution	227
9.4	Determination of Economical Operating Point	231
9.5	Application of Model to Fine Powders	235
9.5.1	Test Material and Properties	236
9.5.2	Test Results	237
9.5.3	Modification of Model and Predicted Results	239
10	CONCLUSIONS AND SUGGESTIONS FOR FURTHER WORK	241
10.1	Conclusions	242
10.2	Suggestions for Further Work	245
11	REFERENCES	247
	APPENDICES	262
A	EXPERIMENTAL DATA OF MAIN TESTS	263
B	LOCATIONS OF PRESSURE TRANSDUCERS	276
C	COMPUTER PROGRAMME FOR PRESSURE DROP PREDICTION	277
D	WALL PRESSURE DISTRIBUTION IN VERTICAL SLUG-FLOW	279
E	PUBLICATIONS WHILE PHD CANDIDATE	280

LIST OF FIGURES

Figure	Title	Page
1.1	Phase diagram of pneumatic conveying	2
1.2	Flow patterns of pneumatic conveying in horizontal pipe	3
2.1	Dixon's slugging diagram for a 100 mm diameter pipe [28]	10
2.2	Pressure gradient vs permeability factor [78]	13
2.3	Pressure gradient vs term accounting for de-aeration factor and particle density [78]	14
2.4	Schematic graph of measuring pipe from Legel and Schwedes [71]	23
2.5	Dissipated energy versus air flow-rate from Daoud et al. [23]	30
3.1	Flow pattern of horizontal low-velocity pneumatic conveying	33
3.2	Particle in air stream	34
3.3	Formation process of slug	35
3.4	Fluidisation rig and schematic illustration of aggregative fluidisation	36
3.5	Pressure gradient of bed versus superficial air velocity	37
3.6	Forces and stresses acting on a horizontal particle slug	41
3.7	Total wall pressure and its components	42
3.8	Cross section of a slug	43
3.9	Pressure to maintain movement of a particle slug in a pipe [17]	45
3.10	Distribution curve of axial stress of a moving slug	47
3.11	Stresses acting on the frontal surface of a slug	50
4.1	Schematic layout of low-velocity pneumatic conveying test rig	53
4.2	Feed devices and receiving silo	54
4.3	ZGR-250 high pressure rotary valve	55
4.4	Air leakage curves of ZGR-250 rotary valve	57

4.5	Configuration of 0.9 m ³ low-velocity blow tank feeder	58
4.6	Details of 96 m x 105 mm ID test rig pipeline	61
4.7	General arrangement of compressed air supply	63
4.8	Sonic nozzles	64
4.9	Orifice plate device	66
4.10	Exploded view of typical air pressure tapping location	67
4.11	Wall pressure measuring assembly	68
4.12	Data acquisition systems	70
4.13	Typical graphic outputs from "HPPLT"	73
4.14	Linear relationship between physical phenomena and electrical signal	76
4.15	Calibration of load cells	77
4.16	Calibration line of a pressure transducer	78
4.17	Range of low-velocity pneumatic conveying for a given m_s	79
5.1	Regular and irregular shaped particles	84
5.2	Particle size distribution	86
5.3	Schematic of stereo pycnometer	88
5.4	Different arrangement of particles [120]	90
5.5	Jenike shearing test [121]	91
5.6	Mohr circle and yield locus of cohesive material	92
5.7	Jenike direct shear tester	93
5.8	Typical measured yield locus	95
5.9	Arrangement for wall yield locus test	96
5.10	Wall yield locus	96
5.11	Wall yield locus for polystyrene chips	98
6.1	Slug flowing in a horizontal pipe	106
6.2	Time history records	108
6.3	Typical cross-correlation plot	108

6.4	Correlated signals taken by two neighbouring sensors	110
6.5	Discrete sequences sampled from continuous time signals	111
6.6	Discrete cross correlation function	114
6.7	Discrete cross correlation function with the peak value not at sampling point	115
6.8	Graph of an actual cross correlation function, obtained from the experiment where $m_f = 0.0498 \text{ kgs}^{-1}$ and $m_s = 0.840 \text{ kgs}^{-1}$	118
6.9	Slug velocity vs mass flow-rate of air for white plastic pellets	119
6.10	Slug velocity vs mass flow-rate of air for black plastic pellets	119
6.11	Slug velocity vs mass flow-rate of air for wheat	120
6.12	Slug velocity vs mass flow-rate of air for barley	120
6.13	Slug velocity vs mass flow-rate of solids for white plastic pellets, carried out in the 105 mm ID mild steel pipeline	122
6.14	Slug velocity vs mass flow-rate of solids for black plastic pellets, carried out in the 105 mm ID mild steel pipeline	123
6.15	Slug velocity vs mass flow-rate of solids for wheat, carried out in the 105 mm ID mild steel pipeline	123
6.16	Slug velocity vs mass flow-rate of solids for barley, carried out in the 105 mm ID mild steel pipeline	124
6.17	Slug velocity vs superficial air velocity for white plastic pellets, carried out in the 105 mm ID mild steel pipeline	125
6.18	Slug velocity vs superficial air velocity for black plastic pellets, carried out in the 105 mm ID mild steel pipeline	125
6.19	Slug velocity vs superficial air velocity for wheat, carried out in the 105 mm ID mild steel pipeline	126
6.20	Slug velocity vs superficial air velocity for barley, carried out in the 105 mm ID mild steel pipeline	126
6.21	Goodness of fit of K correlation	129

6.22	Idealised slug with acting forces at initial motion	132
7.1	Pressures acting on the sensitive surfaces of transducers	139
7.2	Location requirement of pressure transducers	141
7.3	Type-B transducer installed flush with pipe wall	141
7.4	Typical graphs of the pressures and processed results from check tests	144
7.5	Phase difference of signals	145
7.6	Plots of wall pressure and air pressure for black plastic pellets, $m_f = 0.0643 \text{ kgs}^{-1}$, $m_s = 0.849 \text{ kgs}^{-1}$	148
7.7	Plots of wall pressure and air pressure for black plastic pellets, $m_f = 0.0498 \text{ kgs}^{-1}$, $m_s = 0.840 \text{ kgs}^{-1}$	149
7.8	Wall pressure versus mass flow-rate of air for white plastic pellets	150
7.9	Wall pressure versus mass flow-rate of air for black plastic pellets	151
7.10	Wall pressure versus mass flow-rate of air for wheat	151
7.11	Wall pressure versus mass flow-rate of air for barley	152
7.12	Stresses acting on a particle slug	152
7.13	Stresses on element P in particulate medium and Mohr circle representation	156
7.14	Possible state of stress at element P represented by a series of Mohr circles	157
7.15	Possible states of stress at element P in passive stress state	158
7.16	Particles flowing in a vertical pipe	159
7.17	Diagram of strength	160
7.18	Particles moving in a silo	164
7.19	Variation trend of stress transmission coefficient in active case	165
7.20	Possible Mohr circles representing the stress state of a particle slug	167
7.21	Goodness of fit	170

8.1	Geometrical parameters of slug-flow	174
8.2	Various positions of slugs during low-velocity pneumatic conveying	176
8.3	Time history records of static air and wall pressures	177
8.4	Plot of air gap length versus mass flow-rate of air for white plastic pellets	182
8.5	Plot of air gap length versus mass flow-rate of solids for white plastic pellets	182
8.6	Plot of air gap length versus mass flow-rate of air for black plastic pellets	183
8.7	Plot of air gap length versus mass flow-rate of solids for black plastic pellets	183
8.8	Plot of air gap length versus mass flow-rate of air for wheat	184
8.9	Plot of air gap length versus mass flow-rate of solids for wheat	184
8.10	Plot of air gap length versus mass flow-rate of air for barley	185
8.11	Plot of air gap length versus mass flow-rate of solids for barley	185
8.12	Cross section of stationary bed	190
8.13	Measurement of stationary bed thickness with a camera	191
8.14	A typical photograph of the stationary bed of barley for the experiment of $m_s = 1.32 \text{ kgs}^{-1}$, $m_f = 0.088 \text{ kgs}^{-1}$, conducted in the 96 m long pipeline	192
8.15	Cross-sectional area ratio of stationary bed to pipe versus slug velocity for white plastic pellets	193
8.16	Cross-sectional area ratio of stationary bed to pipe versus slug velocity for black plastic pellets	193
8.17	Cross-sectional area ratio of stationary bed to pipe versus slug velocity for wheat	194

8.18	Cross-sectional area ratio of stationary bed to pipe versus slug velocity for barley	194
8.19	General form of steady state pneumatic conveying characteristics for a given material and pipeline	196
8.20	Experimental conveying characteristics of black plastic pellets conveyed in the 52 m long pipeline	197
8.21	Experimental conveying characteristics of wheat conveyed in the 52 m long pipeline	198
8.22	Pressure distribution along a horizontal pipe for white plastic pellets	199
8.23	Pressure distribution along a horizontal pipe for black plastic pellets	199
8.24	Pressure distribution along a horizontal pipe for wheat	200
8.25	Pressure distribution along a horizontal pipe for barley	200
8.26	Arrangement of transducers for the investigation into bend effect	201
8.27	Comparison of pressure gradient for black plastic pellets	203
8.28	Comparison of pressure gradient for white plastic pellets	203
8.29	Slug flowing through pipeline with a bend and the corresponding idealised pressure wave form	204
8.30	Predicted conveying characteristics of white plastic pellets in the horizontal pipe $L_{th} = 36$ m and $D = 0.105$ m, showing the curves of constant m_s	209
8.31	Predicted conveying characteristics of white plastic pellets in the horizontal pipe $L_{th} = 78$ m and $D = 0.105$ m, showing the curves of constant m_s	209
8.32	Predicted conveying characteristics of black plastic pellets in the horizontal pipe $L_{th} = 36$ m and $D = 0.105$ m, showing the curves of constant m_s	210

8.33	Predicted conveying characteristics of black plastic pellets in the horizontal pipe $L_{th} = 78$ m and $D = 0.105$ m, showing the curves of constant m_s	210
8.34	Predicted conveying characteristics of wheat in the horizontal pipe $L_{th} = 36$ m and $D = 0.105$ m, showing the curves of constant m_s	211
8.35	Predicted conveying characteristics of wheat in the horizontal pipe $L_{th} = 78$ m and $D = 0.105$ m, showing the curves of constant m_s	211
8.36	Predicted conveying characteristics of barley in the horizontal pipe $L_{th} = 36$ m and $D = 0.105$ m, showing the curves of constant m_s	212
8.37	Predicted conveying characteristics of barley in the horizontal pipe $L_{th} = 78$ m and $D = 0.105$ m, showing the curves of constant m_s	212
9.1	Pneumatic conveying test rig with 80.5 mm ID pipeline	218
9.2	Procedure for determining pneumatic conveying characteristics	221
9.3	Relationship between slug velocity and superficial air velocity	222
9.4	Predicted PCC of the horizontal pipeline of Rig 1 for conveying polystyrene chips, $L_{th} = 78$ m, $D = 105$ mm	223
9.5	Predicted PCC of the horizontal pipeline of Rigs 2 and 3 for conveying polystyrene chips, $L_{th} = 40$ m, $D = 156$ mm	224
9.6	Predicted PCC of the horizontal pipeline of Rig 4 for conveying black plastic pellets, $L_{th} = 116$ m, $D = 80.5$ mm	224
9.7	Predicted pressure drop compared with experimental pressure drop obtained on Rig 1 for polystyrene chips	225
9.8	Predicted pressure drop compared with experimental pressure drop obtained on Rigs 2 and 3 for polystyrene chips	226

9.9	Predicted pressure drop compared with experimental pressure drop obtained on Rig 4 for black plastic pellets	226
9.10	Pipeline pressure distribution for white plastic pellets and $D = 105$ mm	228
9.11	Pipeline pressure distribution for black plastic pellets and $D = 105$ mm	228
9.12	Pipeline pressure distribution for wheat and $D = 105$ mm	229
9.13	Pipeline pressure distribution for barley and $D = 105$ mm	229
9.14	Variation of pressure gradient	230
9.15	Economical operating curve of white plastic pellets shown on PCC graph for 36 m horizontal pipeline	233
9.16	Economical operating curve of black plastic pellets shown on PCC graph for 36 m horizontal pipeline	233
9.17	Economical operating curve of wheat shown on PCC graph for 78 m horizontal pipeline	234
9.18	Economical operating curve of barley shown on PCC graph for 36 m horizontal pipeline	234
9.19	Particle size distribution of semolina	236
9.20	Semolina shown in Dixon's slugging diagram	237
9.21	Low-velocity pneumatic conveying characteristics of 105 mm ID, 52 m mild steel pipeline for semolina	238
9.22	Plot of slug velocity versus superficial air velocity for semolina	239
9.23	Predicted pneumatic conveying characteristics of semolina and 36 m horizontal pipeline by using modified model	240
B.1	Schematic layout of 96 m long pipeline and transducer locations	276
D.1	A particle slug in a vertical pipe	279

LIST OF TABLES

Table	Title	Page
5.1	Physical properties of test material	100
6.1	K , U_{amin} and γ^2 for lines of various test materials	127
6.2	Optimal coefficient	129
7.1	Experimental wall pressure and stress transmission coefficient for wheat	154
7.2	Stress transmission coefficient λ for different test materials	155
7.3	Static internal friction angles for test materials	168
7.4	Coefficient of best fit	169
9.1	Conveying pipelines	217
9.2	Steady-state dense-phase results for black plastic pellets	219
9.3	Steady-state dense-phase results for polystyrene chips	220
9.4	Economical superficial air velocity	232
A.1	Experimental values of major parameters for conveying white plastic pellets in 52 m long pipeline	264
A.2	Experimental values of major parameters for conveying white plastic pellets in 96 m long pipeline	265
A.3	Experimental values of major parameters for conveying black plastic pellets in 96 m long pipeline	266
A.4	Experimental values of major parameters for conveying black plastic pellets in 52 m long pipeline	267
A.5	Experimental values of major parameters for conveying wheat in 52 m long pipeline	268
A.6	Experimental values of major parameters for conveying wheat in 96 m long pipeline	269

A.7	Experimental values of major parameters for conveying barley in 96 m long pipeline	270
A.8	Experimental values of major parameters for conveying barley in 52 m long pipeline	271
A.9	Experimental values of pressure along 96 m long pipeline for white plastic pellets	272
A.10	Experimental values of pressure along 96 m long pipeline for black plastic pellets	273
A.11	Experimental values of pressure along 96 m long pipeline for wheat	274
A.12	Experimental values of pressure along 96 m long pipeline for barley	275
B.1	Pressure transducer locations (distance from end of pipeline)	276

NOMENCLATURE

A	Cross sectional area of pipe (m^2)
A_c	Cross sectional area of the shear ring of a Jenike shearing tester
A_f	De-aeration factor ($mbar \cdot sm^{-1}$)
A_{st}	Cross sectional area of stationary bed, m^2
a, b	Ergun constant
C	Integration constant in Equation (3.10)
c	Interparticle cohesion
c_d	Coefficient in Equation (6.29)
c_w	Particle-wall cohesion
D	Diameter of pipe (m)
d	Particle diameter (mm)
F_d	Drag force of fluid (N)
F_b	Buoyant force (N)
F_r, F_s	Friction forces for particles (N)
Fr	Froude number of material, $Fr = U_s^2/gD$
Fr_{cF}	Variable in Equation (2.10)
F_w	Gravity force (N)
f	Sampling frequency (Hz)
f_K	Constant in Equation (6.23)
g	Acceleration due to gravity (ms^{-2})
H_b	Height of fixed bed (m)
h_c	Critical depth of the shearing flow at transition (m)
h_s	Stationary bed thickness (mm)
ID	Internal diameter of pipe (m)

K	Slope in Equation (6.25)
k	Constant in Equation (6.35) and (6.36)
k_1	Constant in Equation (6.1)
L	Distance of two neighbouring pressure transducers (m)
L_h	Length of horizontal pipe (m)
L_t	Total pipeline length (m)
L_{th}	Total horizontal pipeline length (m)
L_v	Vertical pipeline length (m)
l_A	Distance between a test point and pipe end (m)
l_d	Distance between two neighbouring slugs (m)
l_g	Air gap length (m)
l_s	Single slug length (m)
M	Total mass of the moving solids in a pipe (kg)
m	Mass of particles (kg)
m_f	Mass flow-rate of air (kgs^{-1})
m_{fl}	Rotary valve air leakage (kgs^{-1})
m_{ft}	Total supplied mass flow-rate of air (kgs^{-1})
m_s	Mass flow-rate of solids (kgs^{-1})
m_{st}	Mass of particles collected by a slug per unit time (kgs^{-1})
m^*	Mass flow ratio
NB	Number of bends
N_s	Number of the pressure peaks in a certain period of time
n	Number of test materials
n_b	Number of the particles contained in the back area of a slug
n_f	Number of the particles contained in the front area of a slug
n_i	Number of the particles having velocity u_{pi} , $i = 1, \dots, n$
n_m	Number of the particles contained in the middle area of a slug
n_p	Numbers of the particles of a given mass

P_i	Air pressure at different points along a pipe (Pag), $i = 1, \dots, n$
P_B	Air pressure during a slug flowing through a bend (Pag)
P_S	Air pressure during a slug flowing in a straight pipe (Pag)
P_{f1}, P_{f2}	Pressure force (N)
P_n	Nominal power
P_u	Dissipated energy (J/kgm)
p	Interstitial air pressure (Pag)
p_2, p_3	Pressure in Equation (5.2) (Psig)
p_f	Permeability factor (m^3skg^{-1})
Q_g	Air flow rate (m^3s^{-1})
Q_w	Shearing force acting on a slug (N)
R	Radius of pipe (m)
R_b	Radius of Bend (m)
Re	Reynold's number
R_f	Friction force between the sliding slug and pipe wall (N)
R_{s1}, R_{s2}	Resistant forces (N)
R_{xy}	Cross correlation function
\hat{R}_{xy}	Estimation of R_{xy}
r	Radius of Mohr circle
S, S', S'', S'''	Shearing forces in Jenike shearing test
S_v	Specific surface (i.e. particle surface per unit particle volume) (m^{-1})
S_{xy}	Cross spectral density
\hat{S}_{xy}	Estimation of S_{xy}
T	Time range of a signal record (s)
T_s	Sampling time interval (s)
t_i	Different times (s), $i = 0, 1, \dots, n$
t_f, t_l	Time of the first and last slug occurring in a pressure record (s)
t_p	Closing time of a solenoid valve (s)

t_s	Time taken by the slug to travel across a pipeline (s)
t_T	Opening and closing time of a solenoid valve (s)
U_a	Superficial air velocity (ms^{-1})
U_{amin}	Minimum superficial air velocity (ms^{-1})
U_{mf}	Incipient fluidisation air velocity (ms^{-1})
U_{ra}	Mean air velocity (ms^{-1})
U_p	Superficial particle velocity (ms^{-1})
U_{pb}	Particle velocity in the back area of a slug (ms^{-1})
U_{pf}	Particle velocity in the front area of a slug (ms^{-1})
U_{pm}	Particle velocity in the middle area of a slug (ms^{-1})
U_{pst}	Particle velocity in stationary bed (ms^{-1})
U_s	Slug velocity (ms^{-1})
U_{sb}	Velocity of the back surface of a slug (ms^{-1})
U_{sf}	Velocity of the front surface of a slug (ms^{-1})
U_{sp}	Slip velocity (ms^{-1})
U_t	Single particle terminal velocity (ms^{-1})
u_{pi}	Velocity of each particle contained in a slug (ms^{-1}), $i = 0, 1, \dots, n$
V, V', V'', V'''	Normal forces in Jenike shearing test
V_1, V_2	Principle forces
V_a	Added cell volume of a stereo pycnometer (cm^3)
V_c	Sealed sample cell volume of a stereo pycnometer (cm^3)
V_p	Powder sample volume (cm^3)
V_s	Total volume of the moving solids in a pipe
X	Variable in Figure 2.3
x, y, z	Co-ordinates
x_1, \dots, x_5	Coefficients in Equations (6.26) and (7.19)
$x(t), y(t), z(t)$	Time history records
α	Cross sectional area ratio of stationary bed to pipe

α_b	Incline angle of bend with respect to the horizontal ($^\circ$)
β	Coefficient in Equation (6.36)
β_b	Incline angle of the back surface of a slug ($^\circ$)
β_f	Incline angle of the front surface of a slug ($^\circ$)
δ	Effective internal friction angle ($^\circ$)
$\Delta\theta=\theta_1-\theta_2$	Radian of bend in Equation (2.15) ($^\circ$)
Δp	Pressure drop across a single slug (Pa)
Δp_i	Pipeline pressure drops at different locations (Pa), $i = 1, \dots, n$
Δp_t	Total pipeline pressure drop (Pa)
Δp_{th}	Total horizontal pipeline pressure drop (Pa)
Δt	Interval time (s)
ε	Bulk voidage
ϕ	Internal friction angle ($^\circ$)
ϕ_s	Static internal friction angle ($^\circ$)
ϕ_w	Wall friction angle ($^\circ$)
γ	Coefficient of correlation
γ_b	Bulk specific weight with respect to water at 4 $^\circ\text{C}$
γ_s	Particle specific weight with respect to water at 4 $^\circ\text{C}$
η	Dynamic viscosity of fluid, Nsm^{-2}
λ	Stress transmission coefficient
λ_A	Stress transmission coefficient at active failure
$\lambda_{\min}, \lambda_{\max}$	Minimum and maximum stress transmission coefficient
λ_o	Static stress transmission coefficient
$\lambda_{o\min}, \lambda_{o\max}$	Minimum and maximum static stress transmission coefficient
λ_P	Stress transmission coefficient at passive failure
μ	Coefficient of internal friction
μ_w	Coefficient of wall friction
θ	Angle in Figure (3.8) ($^\circ$)

θ_s	Angle in Figure (8.12) ($^\circ$)
ρ_a	Air density (kgm^{-3})
ρ_b	Bulk density (kgm^{-3})
ρ_{bst}	Bulk density of stationary bed (kgm^{-3})
ρ_s	Particle density (kgm^{-3})
σ	Normal stress (Pa)
σ_1, σ_2	Principle stresses (Pa)
σ_b	Stress on the back face of a slug (Pa)
σ_f	Stress on the front face of a slug (Pa)
σ_r	Radial stress (Pa)
σ_g	Gravity pressure (Pa)
σ_n	Normal stress coordinate
σ_{tw}	Total wall pressure (Pa)
σ_w	Wall pressure (Pa)
σ_{wm}	Average wall pressure (Pa)
$\sigma_x, \sigma_y, \sigma_z$	Normal stresses in x, y, z direction (Pa)
σ_{xm}	Average stress in x direction
τ	Shearing stress (Pa)
τ_d	Time delay between two signals (s)
τ_p	Specific time delay for the peak value of cross-correlation function (s)
τ_n	Shearing stress coordinate
τ_{tw}	Total shear stress at a wall (Pa)
$\tau_{xy}, \tau_{xz}, \tau_{yz}$	Shear stresses at the planes perpendicular to x, y, z coordinates
ω	Angle defined in Figure 7.17 ($^\circ$)

CHAPTER 1

INTRODUCTION

Pneumatic conveying is being used increasingly in industry to transport a wide range of bulk solids. Numerous efforts have been made to advance the research and application of this method of transport. Experience has demonstrated that pneumatic conveying exhibits different performances and flow patterns for different air mass flow rates (m_f). There are many ways of describing the different flow patterns. Among them, the concept of the phase diagram originally proposed by Zenz [118] is most well known by pneumatic conveying researchers. It is usually a graph of pressure gradient versus superficial air velocity, on which lines of constant mass flow-rate of solids m_s are shown. A log-log scale generally is used so that a wide range of values can be included, as shown in Figure 1.1.

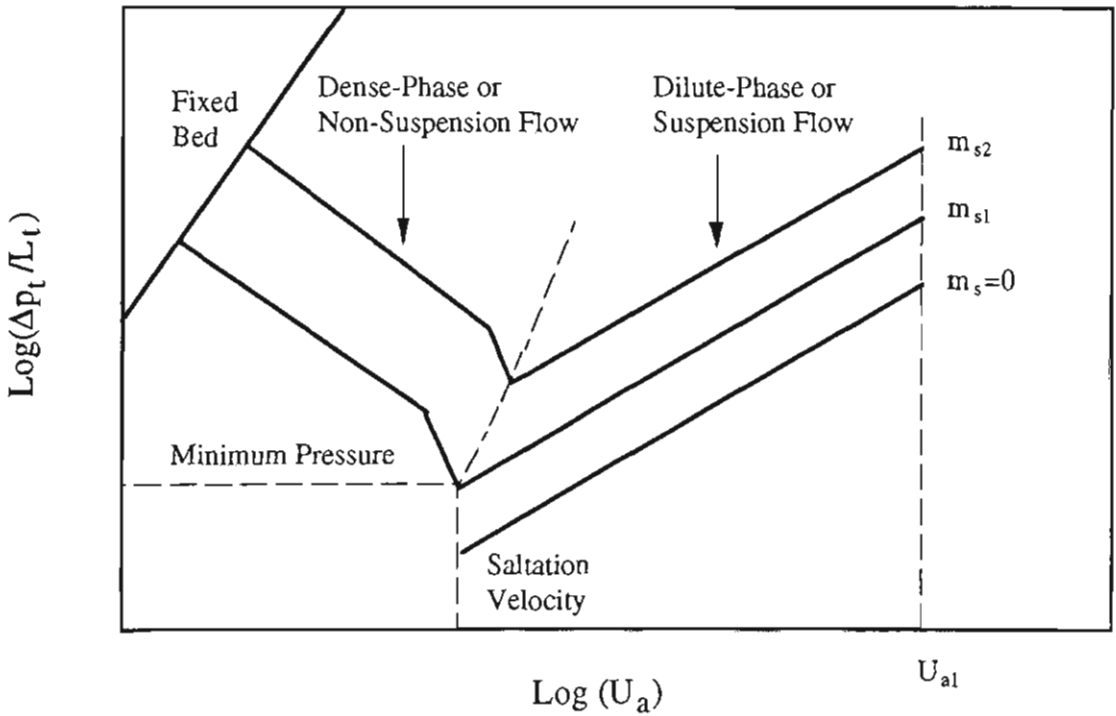
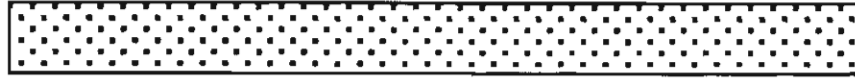


Figure 1.1 Phase diagram of pneumatic conveying.

By using the phase diagram, the flow patterns can be determined within a pipeline for a given set of conveying conditions. According to the different flow patterns, pneumatic conveying is classified primarily as dilute phase or dense phase.

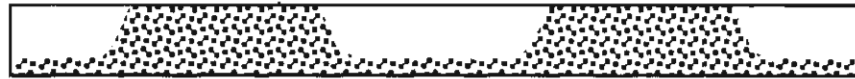
Dilute phase conveying in general employs large volumes of air at high velocity so that the individual particles are conveyed as a fully suspended flow, as shown in Figure 1.2(a). If the mass flow ratio (m^*), which is a ratio of the solids mass flow rate (m_s) to the conveying air mass flow rate (m_f), is in the range $0 < m^* < 15$, then the mode of flow usually is regarded as dilute phase conveying [17].



(a)



(b)



(c)



(d)



(e)

Figure 1.2 Flow patterns of pneumatic conveying in horizontal pipe.

Dense phase conveying is defined by Konrad et al.[68, 69] as the conveying of particles by air along a pipe that is filled with particles at one or more cross-sections, as shown in Figure 1.2(c), (d) and (e). The flow pattern and behaviour of dense phase conveying are much more complex than those of dilute phase conveying so that there is, as yet, no universally accepted definition for dense phase conveying. Some researchers [70, 74] define dense phase conveying when $m^* > 15$. This definition seems inappropriate for

some materials. For example, conveying white plastic pellets can display the dense phase flow pattern while $m^* = 6$. The different types of dense-phase shown in Figure 1.2(c), (d) and (e) are dependent on the material and method of conveying.

The conveying that has flow patterns shown in Figure 1.2(c) and (d) is defined in this thesis as dense phase low-velocity pneumatic conveying. Figure 1.2(c) shows the slug flow of fine and coarse granular products (e.g. wheat, semolina) displaying natural slugging ability and Figure 1.2(d) shows the plug flow of more cohesive-type products (e.g. milk powder).

The conveying shown in Figure 1.2 (e) is called fluidised dense phase conveying, which is achieved usually with powders, such as cement, pulverised coal and fly ash.

Besides dilute and dense phase conveying, for some products, there is an unstable dune flow between dilute and dense phase flow, as shown in Figure 1.2(b), where the occasional "dune" may grow to fill the pipe and cause temporary blockage and severe pipe vibrations. To achieve reliable pneumatic conveying, this unstable zone should be avoided.

Dilute phase conveying is most widely used in industry. Only in the last thirty years, there has been increasing interest in low-velocity dense phase pneumatic conveying due to the following reasons.

- Less amount of air is needed to transport a given mass of solids. This can be important if an expensive gas needs to be used for some reason, e.g. nitrogen to convey explosive powders.
- Particle velocity is able to be controlled in the range 0.25 to 5 ms^{-1} (depending on degradation and/or throughput requirements), and as a result, damage to the product (e.g. particle attrition or scratching) is minimised or even eliminated. Also pipe/bend wear is reduced dramatically.

- Only small filtration systems are required, due to the relatively low amounts of air used for transport.
- Material is transported at extremely high levels of volumetric concentration, which are not possible in conventional-type systems. Hence, reasonable conveying rates are obtained despite the relatively low velocities that are used for transport.
- A lower specific power consumption is needed.
- Electrostatic charging of the particles is reduced by using dense phase.

Certainly dense phase pneumatic conveying systems also have some disadvantages, such as:

- The precise mechanism by which the particles are conveyed has not yet been well understood, leading to anomalies in system performance, difficulties in design and to the danger of unforeseen pipe blockages.
- They can not provide "pure" continuous conveying due to the slugging or plugging mode of flow.

Although some commercial systems have been developed successfully to overcome the above disadvantages, e.g. using a bypass pipe [77] to convey conventionally difficult materials such as alumina, up till now the research for dense phase pneumatic conveying is still at an elementary stage. In particular, the pressure drop of dense phase conveying systems still can not be predicted accurately. Hence, the ultimate objective of this research is to investigate and develop a model for the prediction of pipeline pressure drop so as to provide a reliable design strategy for dense phase pneumatic conveying systems. It should be pointed out that this research is confined to horizontal low-velocity slug flow pneumatic conveying, as it appears currently to be the most attractive and widely applicable mode of transport in industry (e.g. food industry, chemical plants).

To achieve the ultimate goal of this research, the work is concentrated on the following aspects:

- (i) Reviewing published literature to assess the current state of the knowledge of low-velocity pneumatic conveying (Chapter 2),
- (ii) Introducing and further studying the behaviour of a single particle slug (Chapter 3),
- (iii) Organising low-velocity pneumatic conveying experiments and finalising the main test program (Chapters 4 and 5),
- (iv) Establishing an empirical correlation of slug velocity in terms of superficial air velocity, pipe size and the physical properties of the material (Chapter 6),
- (v) Measuring the pipe wall pressures exerted by moving slugs and establishing a semi-empirical relationship between the radial and axial stress in particle slug flow (Chapter 7),
- (vi) Exploring a broad range of conveying conditions so that the performance of low-velocity pneumatic conveying can be evaluated and finally developing a model for the prediction of total horizontal pipeline pressure drop which is a function of the physical properties of the material, conveying conditions and pipeline configuration (Chapter 8),
- (vii) Illustrating applications of the developed model into different conveying systems and providing guidelines for the optimal design of low-velocity pneumatic conveying systems (Chapter 9).

Finally, concluding remarks based on the investigations and suggestions for further work are given in Chapter 10.

CHAPTER 2

LITERATURE SURVEY

2.1 Introduction

This chapter reviews published literature to present the current state of knowledge on dense phase pneumatic conveying. The reviewing is very necessary for there still exists a lot of confusion even though dense phase pneumatic conveying has been in use for over thirty years. These problems focus on the following aspects:

- The definition of dense-phase conveying is still a matter of some debate.
- The precise mechanism by which the particles are conveyed has never been well understood, resulting in difficulties to predict conveying performance.
- Different flow patterns exist for different conveying methods and materials.
- Conflicting experimental work causes numerous controversies and there is a lack of a coherent theory to explain the discrepancies.

As a large amount of literature has been published in the field of dense phase conveying, this reviewing is confined only to dense phase low-velocity pneumatic conveying and encompasses the following three aspects:

- Suitability of bulk material for low-velocity pneumatic conveying.
- Performance of low-velocity pneumatic conveying.
- Design considerations of conveying systems.

2.2 Suitability of Bulk Material

Experience has demonstrated that the range of materials that can be conveyed successfully in a dense phase mode of flow is more limited than that of dilute phase. An appropriate procedure for assessing the suitability of material for conveying in dense phase pneumatic conveying is necessary for design and industrial applications.

Geldart [39] firstly classified bulk materials into four groups according to the mean particle size and density difference for the purpose of predicting fluidisation behaviour. Group A materials retain aeration and if fluidised, generally expand before bubbling. Group B materials do not retain aeration and bubble immediately after fluidisation. Group C materials are cohesive and generally difficult to be fluidised. The materials in Group D have similar behaviour to the materials in Group B but require much larger air flows to maintain fluidisation. Geldart's classification was proposed by some researchers (e.g. Marcus [124]) as a method to indicate the potential of conveying material in dense phase (i.e. as this mode of flow was analogous to the mechanism to fluidisation). Unfortunately, Geldart's classification does not appear [78] to give a reliable prediction for pneumatic conveying.

Dixon [28] conveyed ten different materials ranging from fine powder to coarse pellets in dense phase systems of different pipe diameter and also recognised that the fluidisation properties of a product have significant influences on its suitability to dense phase conveying. He suggested that some materials have a natural tendency to slug in dense phase conveying systems whereas others tend towards dune-flow. Fine powders form neither slugs nor dunes but flow naturally as a well-mixed 'fluidised' column. Based on Geldart's classification of fluidisation, Dixon [28] generated the slugging diagram for assessing the suitability of material for conveying in dense phase pneumatic conveying. He further produced theoretical criteria for classifying materials into groups based on the argument that an air slug will be destroyed by particle entrainment if the relative slug velocity exceeds the single particle terminal velocity. As example of a Dixon [28] slugging diagram for a 100 mm diameter pipe is presented in Figure 2.1. The Group AB boundary is defined by Equation (2.1):

$$U_t = 0.35 (2gD)^{0.5} \quad (2.1)$$

where U_t is the single particle terminal velocity, and

$$U_t = \frac{(\rho_s - \rho_a)gd^2}{18\eta} \quad \text{Re} < 2.0$$

$$U_t = \frac{0.152g^{0.714}d^{1.14}(\rho_s - \rho_a)^{0.714}}{\eta^{0.428}\rho_a^{0.285}} \quad 2.0 < \text{Re} < 500$$

Please see print copy for image

Figure 2.1 Dixon's slugging diagram for a 100 mm diameter pipe [28].

The Group BD boundary is defined by Equation (2.2):

$$U_{mf} = 0.35(gD)^{0.5} \quad (2.2)$$

where U_{mf} is the minimum fluidisation velocity, and determined by the following equation with $\epsilon = 0.45$,

$$150 \frac{(1-\epsilon)\eta U_{mf}}{d^2 \epsilon^3} + 1.75 \frac{\rho_a U_{mf}^2}{d \epsilon^3} = \rho_s g$$

The boundary between Group A and C is an empirical relationship, and is not as well defined (e.g. Dixon [28] simply reproduced this boundary from the Geldart [39] diagram).

Dixon [28] then concluded that the materials in Groups A and D can be conveyed in dense phase. The materials in Group D have strong natural slugging tendency and are the best candidates for low-velocity pneumatic conveying, with slugs moving slower than the air in dense phase. The materials in Group A have no slugging tendency but can be conveyed at very high m^* values. They can be made to slug by commercial techniques. The materials in Group B have weak natural slugging tendency and can be troublesome in dense phase conveying.

Dixon [29] undertook further work to modify slightly his slugging diagram, as he found that it was more appropriate to replace the equations for calculating U_t and U_{mf} by

$$U_t = \frac{(\rho_s - \rho_a)gd^2}{18\eta} \quad \text{Re} < 0.4$$

$$U_t = \left[\frac{4(\rho_s - \rho_a)^2 g^2}{225 \rho_a \eta} \right]^{\frac{1}{3}} d \quad 0.4 < \text{Re} < 500$$

and

$$U_{mf} = \frac{(\rho_s - \rho_a)gd^2}{1650\eta} \quad \text{Re} < 20$$

$$U_{mf} = \left[\frac{(\rho_s - \rho_a)gd}{24.5\rho_a} \right]^{\frac{1}{2}} \quad \text{Re} > 1000$$

To date Dixon's slugging diagram [28, 29] has been used most commonly for assessing the suitability of material for conveying in dense phase pneumatic conveying. However, Dixon's work is still imprecise as the behaviour of solids are extremely complex.

Jodlowski [57] successfully conveyed some materials, which are classified as "difficult" products for dense phase conveying in Dixon's classification, by using the dense phase

systems with careful selection of the mass flow ratio, conveying velocity, pipe diameter and the distribution of air flow along the conveying length. Hence, Jodlowski [57] believed that the Geldart and Dixon classifications based on mean particle size and density difference is insufficient. Other parameters of material properties must be taken into account, such as particle size range, particle shape, hardness, compressibility, cohesion, product behaviour after subjection to fluidisation and friction coefficient, etc. Jodlowski [57] further stressed that the design of conveying systems also has equal importance for successful dense phase conveying.

Ginestet et al. [41] attempted to use the results of the air-solids, solids-solids and solids-wall interaction factors to predict the suitability of material for dense phase conveying. Unfortunately, Ginestet's work had not been completed entirely by the time he published his paper. Therefore no valuable conclusions were given.

Jones et al. [58] carried out conveying experiments to determine the conveying characteristics for five products. Based on the detailed information provided by these conveying characteristics, Jones et al. [58] studied the potential of the product to be conveyed in dense phase and pointed out that the two properties which are identified as most useful for the determining conveyability are the permeability of a product to air and the ability of a product to retain air. Jones et al. [58] found that products that exhibit good air retention properties are the most likely candidates for dense phase conveying and products that exhibit relatively poor air permeability characteristics are also good candidates for dense phase conveying. Jones et al. [58] did not establish criteria for identifying the good air retention properties and poor air permeability characteristics. However, they believed the air retention and air permeability properties of a product can be determined by analysing a small sample of the product so that the conveyability of the product can be predicted.

Mainwaring and Reed [78] recognised the unreliability of the Geldart and Dixon classifications. They agreed that the air retention properties and air permeability characteristics influence the conveyability of the material. Hence they proposed an approach based on the measured permeability and de-aeration characteristics of the materials in their research. The approach is reviewed below.

Please see print copy for image



Figure 2.2 Pressure gradient vs permeability factor [78].

Mainwaring and Reed [78] firstly generated a diagram for the potential of dense phase conveying according to the permeability of material, as shown in Figure 2.2. They found that the materials exhibiting high values of permeability factor (p_f) generally can be

conveyed in a plug type mode of dense phase conveying, while the other materials are conveyed either in dense phase moving bed type flow or not at all in dense phase. The line of constant superficial air velocity drawn on the diagram represents the boundary between these two modes of flow and is defined by the equation $U_{mf} = p_f(\Delta p/H_b) = 50 \text{ mms}^{-1}$.

Please see print copy for image




Figure 2.3 Pressure gradient vs term accounting for de-aeration factor and particle density [78].

Mainwaring and Reed [78] also found that materials that have high values of de-aeration factor divided by particle density can be conveyed in a moving bed type of flow while

others are conveyed either in the slug type flow or cannot be conveyed in dense phase at all. Hence they produced another graph for dense phase potential according to the de-aeration characteristics of materials, as shown in Figure 2.3. The boundary line is represented by the equation $(\Delta p/H_b)X = A_f/\rho_s$ with the constant $X = 0.001\text{m}^3\text{skg}^{-1}$.

Mainwaring and Reed [78] claimed that this approach enables the potential for dense phase conveying to be established with more certainty than the Dixon's method.

2.3 Performance of Low-Velocity Pneumatic Conveying

2.3.1 Flow Pattern

The earliest research into dense phase pneumatic conveying probably was carried out by Albright et al. [1], where pulverized coal was conveyed through horizontal pipes at mass flow ratios up to ≈ 200 . As the pipes used for conveying were made of copper, the flow pattern could not be observed.

Wen and Simons [109] were the first to outline the flow pattern of dense phase pneumatic conveying based on visual observation. Since the conveyed materials appear to belong to the Dixon [28] Group B, more descriptions were given to the dune-flow pattern in their paper.

Konrad et al. [69] photographed low-velocity pneumatic conveying and to date provided one of the most comprehensive descriptions for this flow pattern. A brief summary is given below.

For horizontal conveying, the solids flow in discrete slugs. Between the slugs, the upper part of the pipe contains moving air with some dispersed particles while the lower part of the pipe is filled with stationary particles. Each slug sweeps up the stationary particles in front and leaves behind a stationary layer of approximately the same thickness.

For vertical flow, the flow pattern resembles that of square-nosed slugging in a fluidized bed. The solids move up as plug of particles that occupy the entire cross-section of the pipe. Particles are seen to rain down from the back of one plug and then to be collected by the front of the next plug.

Similar descriptions also were given by several other researchers [16, 48, 71, 105]. Hitt [48] defined this type of slug flow as full bore flow and further pointed out that at low pipeline pressure gradients, horizontal conveying takes the form of shearing flow, i.e. a series of plugs shearing across a stationary layer of particles. Hitt [48] also developed a model for predicting the critical depth of the shearing flow at the transition to full bore flow. For cohesionless material, Hitt's model is given by Equation (2.3):

$$\frac{h_c}{R} = \frac{\mu_w}{\mu} \quad (2.3)$$

Tsuji et al. [105] introduced a new concept to assist in the research of low-velocity pneumatic conveying. They used simulation technology to study low-velocity flow from a microscopic point of view, since they believed that although the flow structure is complicated, the most basic mechanism of particle-to-particle interaction is fundamental and simple to model. That is, for single particles in a conveying system, the state and position of the particles are determined only by the contacting force and fluid drag force. The contacting force can be calculated by simplifying the particle by a spring model with dashpot and slider. The fluid force acting on the particles can be evaluated by applying Ergun's equation [32]. Therefore the simulation of low-velocity pneumatic conveying can be conducted by using a computer. The results were presented in the form of graphical output showing the flow pattern involved.

According to the simulated graphs, Tsuji et al. [105] gave a very similar description for the flow pattern to that given by Konrad et al. [69] and other researchers [16, 48, 71] through actual observations. They also deduced that there exists a critical value of the quantity of particles per unit length of pipe to form slug flow.

With the simulation, the motion of individual particles, especially the particles marked with different colours near the middle and rear end of a slug, can be observed easily and clearly. Theoretically, the flow pattern can be defined numerically by using this technology. That is, the geometrical sizes reflecting the nature of the flow pattern, such as the particle slug length, air gap length and the shape of the air-particle interface between two slugs, can be predicted, although Tsuji et al. [105] did not mention this in their paper. It is extremely difficult to determine such parameters through visual observations and photograph records. With the simulation technology, slug velocity and the normal pressure exerted on the wall by the particles also were obtained by Tsuji et al. [105]. Simulation is a very promising method for the study of pneumatic conveying.

2.3.2 Pipeline Pressure Drop

One of the most important aspects of pneumatic conveying research is to investigate pipeline pressure drop and the influence of conveying conditions and other factors. Numerous studies of course have been undertaken for low-velocity pneumatic conveying, as described in the following sections.

2.3.2.1 Pressure Drop in Horizontal Flow

Albright et al. [1] are believed to have undertaken the first research into dense phase pneumatic conveying. They conveyed pulverized coal through horizontal pipes with different pipe diameters in dense phase and measured the pipeline pressure drop. Two empirical equations were presented for predicting the pressure drop of the dense phase flow based on the measured results. As the flow pattern could not be observed from the experiments (the flow pattern used by Albright et al. was most likely fluidized dense-phase as Dixon [28] Group A materials were conveyed), it is difficult to evaluate whether the equations of Albright et al. [1] are suitable for low-velocity pneumatic conveying (viz. slug flow). That is, the flow pattern defines the mechanisms that have to be investigated in order to predict the pressure drop.

Wen and Simons [109] studied the flow characteristics of dense phase horizontal conveying of glass beads and coal powders of various sizes (0.071 to 0.754 mm). Based on their experimental finding that the average interstitial air velocity is about twice as large as the average particle velocity, they presented an empirical correlation for the pipeline pressure gradient in terms of the pipe and particle properties and conveying conditions. The correlation by Konrad [68] converted to SI units is

$$\frac{\Delta p_t}{L_t} = 41.82 m_s A^{-0.45} \left(\frac{d}{D} \right)^{0.25} \left(\frac{m_f}{2\rho_a} + \frac{m_s}{\rho_s} \right)^{-0.55} \quad (2.4)$$

Wen and Simons [109] observed four types of flow pattern that occurred in their dense phase conveying experiments, but they did not indicate clearly the one that their model represented. According to the type of materials they conveyed, i.e. materials in Dixon [28] Group B, the conveying is believed most likely to be dune-flow. Hence their model is most likely suitable to dune-flow. In addition, the experimental work of Wen and Simons [109] was only for a test section of approximately 3 m length. Hence any effects due to changing air density might not be large enough to be correlated reliably. Therefore, the correlation is probably only valid at air pressures close to ambient.

Dickson et al. [27] carried out a set of experiments to investigate the pressure drop required to sustain the movement of a single particle plug in a horizontal pipe. In these experiments, the plugs were confined loosely at their ends by porous fibre slugs. The discs were connected to each other by a length of string passing through the plug. The test materials, glass beads and bentonite, were conveyed through perspex and galvanised iron pipes. To investigate the difference between pneumatic propulsion of the plug and mechanical propulsion, the propelling force required to move the slug by mechanical means also was determined. They found that the pressure required to move a plug of granular material by pneumatic propulsion is proportional to the length of the plug, i.e. the pressure gradient in the plug is constant. However, in mechanical propulsion the force to sustain the continuous movement of the plug is proportional to exponent of the

length of the plug. Their work was preliminary since no correlations for pressure drop in terms of particle properties and conveying conditions were presented. Despite this, the method and conclusions of their work are still very meaningful to the present research on low-velocity conveying.

Butters [16] presented a calculation method for the total pipeline pressure drop of low-velocity pneumatic conveying by equating the air pressure force to the friction force caused by the slug weight. The research of this thesis has found that the friction force caused by the slug weight only takes up a minor part of the pressure drop, hence this method may not be reliable for predicting the pipeline pressure.

According to the conclusion of Dickson et al. [27] that the pressure required to move a plug of granular material by pneumatic propulsion is proportional to the length of the plug, Konrad et al. [69] firstly derived a theoretical equation to predict the pressure drop required to move a single particle slug in a horizontal pipe by using the method of Janssen (1895). That is, for cohesionless material:

$$\frac{\Delta p}{l_s} = \frac{4\mu_w \lambda}{D} \sigma_f + 2\rho_b g \mu_w \quad (2.5)$$

The significance of Equation (2.5) is that it has laid a foundation for the research of low-velocity pneumatic conveying. It also indicates that the pressure loss across a single slug is composed of two parts, i.e. the pressure loss caused by the slug collecting stationary particles and the pressure loss caused by the friction force due to particle weight.

A low-velocity pneumatic conveying system usually includes several particle slugs flowing in the pipeline. In order to predict the total pipeline pressure drop, the relationship between the single slug pressure drop and the total pipeline pressure drop must be established. For this purpose, Konrad et al. [69] treated all the slugs moving at an average slug velocity (U_s) (i.e. the average particle velocity designated by Konrad et al. [69]) in the horizontal section of the pipeline as one slug.

As Konrad et al. [69] believed that the particle slugs can be considered as a packed bed model, they applied Ergun's equation [32] to the bed resulting in:

$$\frac{\Delta p}{l_s} = \frac{150\eta(1-\epsilon)^2(U_a + U_p - U_s)}{d^2\epsilon^3} + \frac{1.75\rho_a(1-\epsilon)(U_a + U_p - U_s)^2}{d\epsilon^3} \quad (2.6)$$

Obviously combination of Equation (2.6) with Equation (2.5) can determine the slug velocity (U_s).

A correlation for L_s in terms of the mass flow rate of solids (m_s), the bulk density of the slugs (ρ_b), the total length of the horizontal pipeline (L_t) and slug velocity (U_s) was given by Konrad et al. [69] as

$$L_s = \frac{m_s L_t}{A\rho_b U_s} \quad (2.7)$$

By replacing the single slug pressure drop (Δp) and length (l_s) with the total pipeline pressure drop (Δp_t) and total slug length (L_s), Konrad et al. [69] at last gave a model for predicting the total horizontal pipeline pressure drop of low-velocity pneumatic conveying:

$$\frac{\Delta p_t}{L_s} = \frac{2.168\mu_w \lambda \sqrt{g} U_s}{\sqrt{D}} \left(1 - \frac{m_s}{A\rho_b U_s - m_s} \right) + 2\rho_b g \mu_w \quad (2.8)$$

Compared with their experimental results, Konrad et al. [69] claimed that the model gave good predictions with the passive failure selection of the value of the stress transmission coefficient λ in Equation (2.8). These results were for the conveying of 4 mm diameter polyethylene granules through a 47.3 mm diameter horizontal pipelines, 6.36 m in length.

The models of Konrad et al. [69], particularly the model for the pressure gradient of a single slug, i.e. Equation (2.5), are introduced and cited most extensively by the researchers of low-velocity pneumatic conveying. However, comparisons between the predictions of Konrad's model and practical experimental pressure drops of full-scale

conveying systems are rarely found. In the research of this thesis, the comparisons between the predicted results and the author's experimental data show that Equation (2.8) always overpredicts the total horizontal pipeline pressure drop, in some cases by a factor of 2.5. The experimental results obtained in this research were for the conveying of 3.76 mm diameter black plastic pellets through 105 mm diameter mild steel horizontal pipelines, 36 m and 78 m in length. There are two possible reasons to cause this over prediction.

One reason is that the determination of the stress transmission coefficient λ in passive failure case may be inappropriate. Konrad et al. [69] derived formulae for evaluating two extremes of λ , known as the passive and active failure solutions according to particle mechanics. That is,

$$\text{for active failure:} \quad \lambda_A = \frac{1 - \sin\phi \cos(\omega - \phi_w)}{1 + \sin\phi \cos(\omega - \phi_w)}$$

$$\text{for passive failure:} \quad \lambda_P = \frac{1 + \sin\phi \cos(\omega + \phi_w)}{1 - \sin\phi \cos(\omega + \phi_w)}$$

$$\text{where } \sin\omega = \frac{\sin\phi_w}{\sin\phi}.$$

Konrad et al. [69] pointed out that in theory, λ should occur between these two extreme solutions. Borzone and Klinzing [10] also indicated this fact. However, as it is difficult to determine exactly the real value of λ between these two extremes, Konrad et al. [69] further recommended using λ_P for slug-flow pneumatic conveying according to their experimental results. In fact, the range of the two extremes of λ for some materials is quite large. For example, $\lambda_A = 0.178$ and $\lambda_P = 3.566$ for white plastic pellets. Hence, using λ_P instead of the real value of λ may cause large deviations in predicted values. For example, if the real value of λ for white plastic pellets is taken as the average of the two extremes, i.e. $\lambda = 1.8$, then $\lambda_P/\lambda = 2.0$, then the predicted pressure gradient in a single slug when using λ_P may be twice as large as the real pressure gradient.

Another reason probably is that applying Ergun's equation [32] to the particle slugs in slug flow is not applicable as the particle slugs are found to be fluidized in this research, refer to Chapter 3.

Hence Equation (2.8) for the prediction of the total pipeline pressure drop does not appear to be reliable.

Legel and Schwedes [71] derived an equation similar to Equation (2.5) from a force balance for determining the pressure drop required to move a single slug.

$$\frac{\Delta p}{l_s} = \frac{4\mu_w \lambda}{D} \sigma_f + \rho_b g \mu_w \quad (2.9)$$

The difference is that the second term in the right hand Equation (2.9), which represents the friction force due to the weight of the slug, is half the corresponding term in Equation (2.5). Legel and Schwedes [71] believed that the weight of slug only exerts pressure on the lower half of the pipe wall. However, this consideration appears incorrect. For example, if the upper half of the pipe was removed, obviously the particles in the slug in the upper half part of the pipe will flow outwards without the restriction of the pipe wall. This indicates that the weight of the slug generates the stress exerted on the upper half of the pipe wall, resulting in the friction force. For the stress transmission coefficient, Legel and Schwedes [71] considered that its value can be set equal to the coefficient of earth pressure at static state, i.e. $\lambda \approx 1 - \sin \phi$. For most cases, $\lambda \approx 0.5$. This consideration [71] conflicts with that of Konrad et al. [69].

Legel and Schwedes [71] generated slugs in their experiments by means of pulses of pressured air that were introduced periodically into the particle column by a solenoid valve. Hence the length of each slug was able to be controlled and adjusted by the operating frequency of the solenoid valve, and from the operating frequency of the solenoid valve, the total length of slugs was calculated. Based on this work, Legel and

Schwedes [71] gave a semi-empirical model for predicting the total horizontal pipeline pressure drop:

$$\Delta p_t = (1 + 2.9 Fr_{cF}^{0.25}) \rho_b g \mu_w L_t \frac{t_p}{t_T} \quad (2.10)$$

$$\text{where } Fr_{cF}^{0.25} = \left(\frac{m_s}{A \rho_b} \right)^2 \left(\frac{t_p}{t_T} \right)^2 \frac{1}{Dg}$$

The model given by Equation (2.10) may not be suitable for natural slugging pneumatic conveying systems since the model was developed based on the experiments that slugs were not generated naturally.

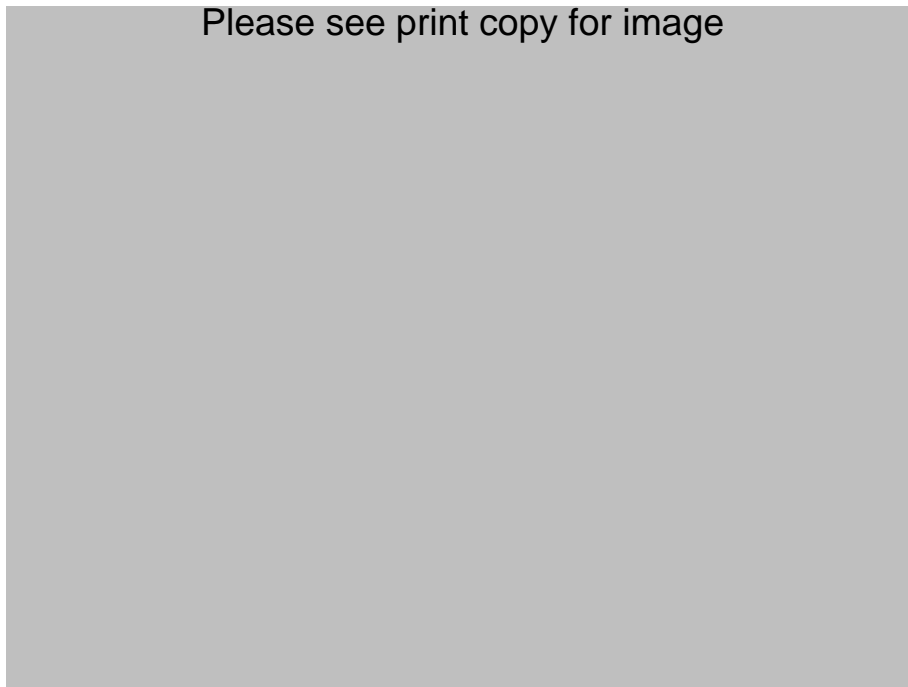


Figure 2.4 Schematic graph of measuring pipe from Legel and Schwedes [71].

Legel and Schwedes [71] also measured friction forces of slugs by using load cells, as shown in Figure 2.4. This is very valuable work. If analysing the measurement only from the test schematic graph they presented, the signals measured by the load cells should include the vibration effects in the axial direction of flow. Legel and Schwedes [71] did not mention any steps to eliminate the vibration effects and did not publish directly the experimental data for the friction force in their paper. Therefore, the results of

this work cannot be evaluated and used for further research. Also test results for the wedge number [71] obtained from the measurement of the friction force are considered with some scepticism.

2.3.2.2 Pressure Drop in Vertical Flow

Studies into dense phase vertical conveying commenced in the 1960's. However, the earlier work seldom dealt with "typical" or "conventional" low-velocity pneumatic conveying. For example, Lippert's study [77] was related to the bypass system, Sandy [95] researched the moving bed system and the flow pattern in the study of Tomita et al. [101] for dense phase vertical flow was unclear. This unfortunately hinders the use of their findings in the current world on low-velocity pneumatic conveying. Also, as the earlier studies of vertical flow have been reviewed extensively by Leung [72] and Konrad [68], the review of this section will concentrate on the more recent developments of vertical slug flow.

Konrad et al. [69] developed an equation for estimating the pressure drop required to lift a single slug in a vertical pipe when they did similar work for horizontal flow. The following equation was given for cohesionless materials:

$$\frac{\Delta p}{l_s} = \frac{4\mu_w \lambda}{D} \sigma_f + \rho_b g \quad (2.11)$$

The pressure loss across a vertical slug is also composed of two parts, one represented slug weight, the other represented by the frontal stress (σ_f) of the slug. The particles raining down from the back of one slug cause this frontal stress.

In Equation (2.11), the stress transmission coefficient (λ) and frontal stress (σ_f) are parameters to be determined further. Konrad [66] presented an equation for calculating the frontal stress in 1987 from a momentum balance and continuity of flow, that is

$$\sigma_f = \frac{\epsilon_g \rho_s (1 - \epsilon)(u_p - u_g)^2}{(1 - \epsilon - \epsilon_g)} \quad (2.12)$$

Konrad and Totah [64] undertook further experimental work to measure the pressure drops across single slugs moving through the vertical section of a 50.8 mm diameter circulating unit. The length of slug, velocity of the particles within the slug and velocity of the front of the slug also were measured by using a high speed camera. The material conveyed by Konrad and Totah [64] was a mixture of black and white polyethylene with a particle diameter of 3 mm. The black polyethylene took up 5 % of the volume of the mixture. From the experimental results of the pressure gradient, Konrad and Totah [64] concluded that for a given frontal stress, the pressure drop across a moving slug of cohesionless solid is directly proportional to its length, and Equation (2.11) gave a good prediction if the stress transmission coefficient λ was selected between the active and passive failure solutions.

An immediate problem of the work of Konrad et al. [64, 66, 69] is that the model is not applicable for multi-slug vertical flow systems. Another problem is that the value of λ was still uncertain.

Borzone and Klinzing [10] derived models from the force balance for predicting the pressure drop to lift a single slug of cohesive solids in a vertical pipe.

$$\text{For passive case: } \frac{\Delta p}{l_s} = \rho_b g + \frac{4c\mu_w(\lambda_p + 1)\cos\phi\cos(\omega + \phi_w)}{D} + \frac{4c_w}{D} \quad (2.13)$$

$$\text{For active case: } \frac{\Delta p}{l_s} = \rho_b g - \frac{4c\mu_w(\lambda_A + 1)\cos\phi\cos(\omega - \phi_w)}{D} + \frac{4c_w}{D} \quad (2.14)$$

Borzone and Klinzing [10] then conducted experiments by conveying coal powders of various sizes (9.8 to 38.0 μm) through a 25.4 mm diameter vertical pipe, 3.05 m in length in low-velocity pneumatic conveying. Gu and Klinzing [42] continued the experiments with different diameters of vertical pipe (50 mm and 100 mm). The pressure drop across a single slug, slug length and slug velocity were measured. From the experimental results, Borzone, Gu and Klinzing [10, 42] achieved the same conclusion as that of Konrad and Totah [64] for the relationship between the pressure drop and slug

length, i.e. constant pressure gradient in the slug. Compared with the experimental results, the models of Borzone, Gu and Klinzing [10, 42] provided estimates of the pressure drop across a single slug of cohesive material. They also found that the slug velocity is independent of the slug length and depends mainly on the air velocity. In their experiments, the slug velocity appears to be 90 % of the superficial air velocity.

According to the work of Borzone, Gu and Klinzing [10, 42], using the passive case or active case models to predict pressure drop of a single slug of cohesive material seems not important as the predictions made by the two models were very close. However the relationship between the total pipeline pressure drop and single slug pressure drop was not established in their work making it difficult to apply their model directly to multi-slug vertical flow systems.

Hikita et al. [47] conveyed coke particles of 0.21 mm diameter in vertical acrylic resin pipes of 50 and 150 mm diameter, 4 m in length. The particles were observed to rise in the pipe with an alternate pattern of particle and air slug, accompanied by a collapse of the particle slug. Experimental data for pressure drop across the transport pipe were presented by plotting against the solid static head. No models for the pressure drop were given by Hikita et al. [47].

2.3.2.3 Pressure Drop Around Bends

Investigations into the pressure drop caused by bends in low-velocity pneumatic conveying have not received much attention, except for the recent work by Aziz and Klinzing [5]. One possible reason is that the slug flow around bends has more complex mechanisms than the slug flow through straight pipes. Another reason is that experimental work of Hitt [48] displayed that the bends had no significant effect on the conveying characteristics since the particles moved at rather low velocity during flow. Hence in this section, only the work of Aziz and Klinzing [5] is reviewed.

Aziz and Klinzing [5] found that the pressure loss around bends is dependent on the material properties and the parameters of the bends. By analysing the behaviour of the slugs flowing around bends with a packed bed model and using a force balance on a differential length of the slug contained in a bend, they derived the following model for predicting the pressure drop across the slug.

$$\frac{\Delta p}{R_b} = 4\mu_w \rho_b g \Delta \theta [1 + \lambda Fr (\frac{U_s}{U_a} - 1)] + 2\rho_b g \sin \alpha_b [\cos(\frac{\theta_1}{2}) - \cos(\frac{\theta_2}{2})] \quad (2.15)$$

This model is a function of the physical properties of the material, bend parameters and slug and air velocity.

Aziz and Klinzing [5] also conveyed pulverised coal in slug-flow pattern in the 25.4 mm and 50.8 mm clear PVC pipes which included bends of different radii. The bends were inclined at 0, 45 and 90 degrees with respect to the horizontal. They claimed that both bend model predictions and the experimental pressure drop data showed a linear variation between bend pressure drop and slug length. Also the pressure drop increases with increasing air velocity but decreases with increasing pipe diameter and bend radius. They noted that a minimum bend radius is necessary to allow a given length of slug to flow easily through the bend.

2.4 Design of Low-Velocity Conveying System

Although the precise mechanism of low-velocity pneumatic conveying has not been well understood, leading to difficulties in system design, researchers continue to make efforts to establish a standardised and universally agreed technique for the proper design of low-velocity pneumatic conveying systems.

Wypych and Hauser [116] proposed basic principles for the design of low-velocity pneumatic conveying systems after summarising the progress in research and technology. They indicated that the design considerations must include the following three aspects:

- (i) Selecting a most suitable pattern of conveying for the given material by analysing the material characteristics and using the existing methods of material/conveying phase classification,
- (ii) Selecting the most suitable conveying system to confirm flow pattern and avoid pipeline blockages,
- (iii) Establishing reliable and economical operating conditions according to conveying characteristics.

Wypych and Hauser [116] further recommended using the classification work of Geldart [39], Dixon [28, 29], Jones et al. [58], Mainwaring and Reed [78] to assist the selection of flow pattern.

The unclear mechanism of the flow also led to the danger of unforeseen pipe blockages. Hence a great amount of work [34, 35, 36, 37, 77] was carried out to assist in the development of various conveying systems to ensure proper flow pattern and the reliability of conveying. Wypych and Hauser [116] mentioned some of these conveying systems (e.g. blow tanks and its method of air injection, by-pass systems and pipe-boosters systems) and set up some principles for the selection of these systems.

Since the classifications of material have been reviewed in Section 2.2 of this chapter and the different conveying systems have been reviewed extensively by Klintworth and Marcus [61] yielding qualitative diagrams for selecting the appropriate conveying system, this section mainly reviews the work on establishing reliable and economical operating conditions.

Daoud et al. [23] conveyed polyethylene pellets of 3.09 mm diameter in pipelines of 50 mm diameter. The pipelines were 25 to 70 m in length and made of stainless steel except for the first 10 m. The pipe of the first 10 m was made of Plexiglas to allow a visual study of the flow pattern. During the experiments, slug flow patterns were observed. The

solids flow rate, air flow rate and pipeline pressures were also measured. Using the experimental results, Daoud et al. [23] studied the behaviour of low-velocity pneumatic conveying and presented a flow diagram which gave the pressure drop as a function of the air flow rate for a constant solids flow rate. The trend of the flow diagram agrees with that shown on the phase diagram of Zenz [118], i.e. the pressure drop decreases when the air flow-rate increases during low-velocity pneumatic conveying.

In dilute phase conveying, it is usually accepted that the minimum pressure drop point in the phase diagram of Zenz [118] is considered as the optimum transport condition. However, for low-velocity pneumatic conveying, Daoud et al. [23] re-defined the optimum operating point as the minimum point in the dissipated energy which is defined as the power consumed for conveying a unit weight of material through a unit length of pipe, that is

$$P_u = \frac{\Delta p_t}{L_t} \frac{Q_g}{m_s} \quad (2.16)$$

Using measured results, Daoud et al. [23] calculated the dissipated energy in each experiment and plotted the calculated values against the volumetric air flow-rate. Figure 2.5 shows the graph presented by Daoud et al. [23].

From the graph representing the dissipated energy (Figure 2.5), Daoud et al. [23] found that the minimum pressure drop point is different from the minimum dissipated energy point. The results of Daoud et al. [23] showed that the optimum transport point is located on the left side of the minimum pressure drop point. On the right side of the optimum transport point, the dissipated energy increases when the air flow-rate increases.

Although the optimum transport point was defined by Daoud et al. [23], it still is difficult to design a low-velocity pneumatic conveying system according to Equation (2.16) if the correlations of pressure drop in terms of the air velocity and mass flow rate of solids have not been developed reliably.

Please see print copy for image

Figure 2.5 Dissipated energy versus air flow-rate from Daoud et al. [23].

Rao and Ramakrishnan [89] undertook an experimental study to investigate the influence of conveying air and system pressure drop to arrive at the optimum pressure drop and corresponding minimum energy consumed. For this purpose, data for air flow rate, solids flow rate, solid-air mass flow ratio and specific power consumption were collected from the experiments. These experiments were for conveying four types of material (i.e. cement, flyash, pulverized coal and rawmeal) in dense phase. A turbuflow system was employed in the experiments to ensure dense phase conveying since some of the test materials were classified as conventionally difficult dense phase products.

Rao and Ramakrishnan [89] established an experimental program to identify the optimum point of conveying performance. They firstly presented the collected data by plotting the specific power consumption against the air mass flow rate with constant solid-air mass flow ratios for a test material. Then according to the plot the minimum specific power consumption was evaluated and the corresponding operation point was considered as the optimum for conveying. Rao and Ramakrishnan [89] also presented another plot

showing a group of curves for the conveying pressure versus air mass flow rate with constant solid-air mass flow ratios. From this plot, Rao and Ramakrishnan [89] finally identified the optimum conveying pressure corresponding to the maximum solid-air mass flow ratio according to the determined optimum air mass flow rate.

Rao and Ramakrishnan [89] also found from the plots of conveying pressure that the conveying of pulverised coal used low power consumption compared with other materials. Hence they concluded that from the point of view of saving power, the pulverised coal appeared to be the best for dense phase conveying.

Although this work did not contribute to the ultimate aim of accurate pressure drop prediction, it still is helpful for the optimal design of low-velocity pneumatic conveying systems. It should be noted that as the conveying system employed by Rao and Ramakrishnan [89] was the turbuflow system, the data they collected may not be applicable to dense phase conveying in general.

CHAPTER 3

THEORY ON LOW-VELOCITY PNEUMATIC CONVEYING

3.1 Introduction

The ultimate objective of this research is to develop a model which can predict the pipeline pressure drop in low-velocity pneumatic conveying. To attain this goal, a theoretical analysis is carried out in this chapter concentrating on single particle slugs.

Firstly, the work considers a study and description of the flow pattern of low-velocity pneumatic conveying and the state of particles for the purpose of establishing suitable theories for low-velocity pneumatic conveying.

Secondly, the work of previous researchers [69, 71] in applying the two phase theory and the principles of particle mechanics to single slugs is introduced. Further study is undertaken based on their work.

3.2 Flow Pattern and Formation of Particle Slugs

A steady state flow pattern of horizontal low-velocity pneumatic conveying can be described as follows:

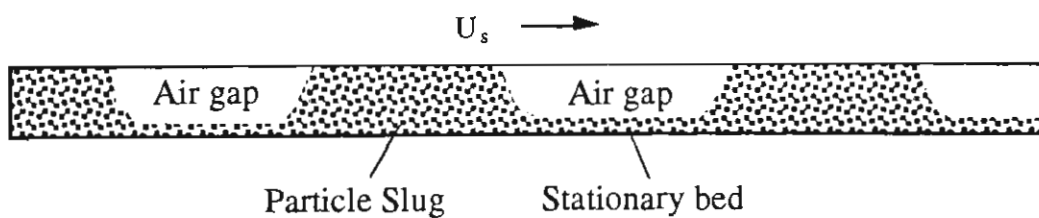


Figure 3.1 Flow pattern of horizontal low-velocity pneumatic conveying

Particles are conveyed in the form of discrete slugs, as shown in Figure 3.1. Between the slugs the pipe is filled with air (i.e. air gap) and a stationary bed of particles. Each slug sweeps up some quantity of the particles from the stationary bed in front of it and delivers about the same quantity of particles to the pipe behind it while it travels forward along the pipe. Observations of numerous low-velocity pneumatic conveying experiments undertaken by the author in this thesis agree to this description. The slug obviously is a

distinct feature of low-velocity pneumatic conveying. The following introduces the concept of slug formation.

Figure 3.2 shows a particle being transported by air flowing through horizontal pipe. The particle is acted upon by a drag force F_d , friction forces for the particle F_s and F_r , weight force F_w , buoyant force F_b . It is known that if the air velocity is less than the saltation velocity, then $F_b + F_r < F_w$, the particle will fall down to the bottom of the pipe.

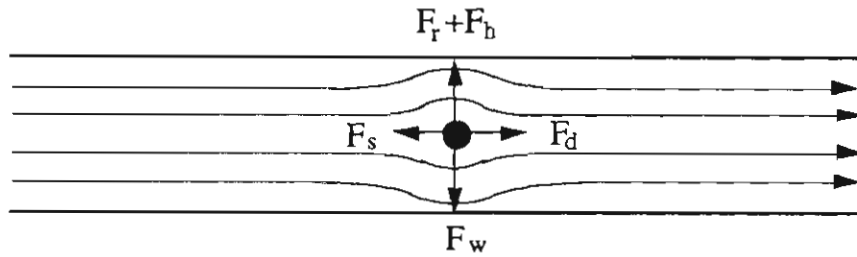


Figure 3.2 Particle in air stream.

For a low-velocity pneumatic conveying system, the particles entering the conveying pipe of the system through a material feeder fall down to the bottom of the pipe and remain stationary after moving some distance downstream (i.e. instead of flowing away directly like in dilute-phase conveying), see Figure 3.3(a). The air velocity generally is much lower than the saltation velocity of the conveyed material. As more particles are added to the pipe, like the previous particles, they also drop down and lay above the previous particles, see Figure 3.3(b). This process continues until the whole cross-section of the pipe is occupied, resulting in slug formation, see Figure 3.3(c). As soon as the slug is formed, the pressure in the pipe increases sharply to a value enough to drive the slug forward, see Figure 3.3(d). After the slug moves away, the next slug starts to form.

It is observed that while a slug moves forward, it delivers particles to the pipe and generates a stationary bed of particles behind it, refer to Figure 3.3(d). If the slug is the first slug in the system, the slug eventually "disappears" after it travels a certain distance along the pipe (i.e. the slug spreads out along the pipeline and runs out of particles). The following slug also deposits particles, but it is also observed to collect approximately the

same quantity of particles from the stationary bed which is left by the first slug. This slug disappears at a farther distance than the first one (i.e. the length of the stationary bed is extended). Slug-flow cannot reach "equilibrium" until the bottom of the entire pipe contains a stationary bed.

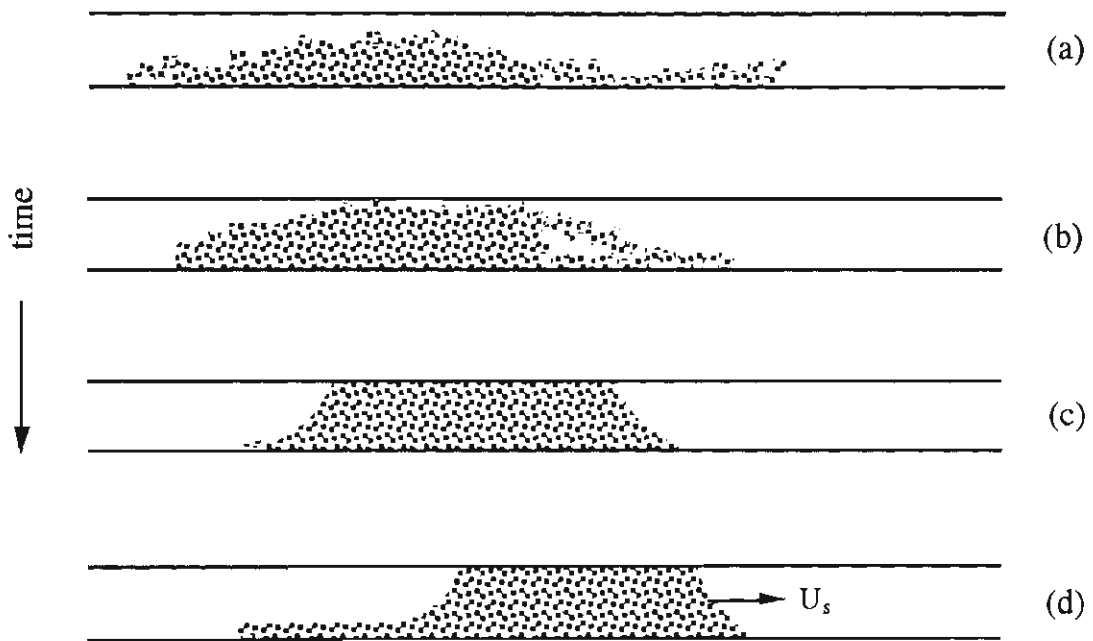


Figure 3.3 Formation process of slug.

3.3 State of Particle Slug

In order to apply appropriate theories to low-velocity pneumatic conveying, the state of the slug must be known. For this purpose, a group of fluidisation experiments were undertaken for packed beds of plastic pellets, wheat and barley. A schematic illustration of the fluidisation rig is shown in Figure 3.4(a).

The rig is composed of a glass tube with a plastic porous base and a cover with filter. Fluidising air is introduced into the tube from a tap located at the bottom of the rig. The mass flow-rate of air is monitored by an orifice plate. A differential pressure meter is connected to the bottom and top end of the tube to measure the pressure drop across the bed.

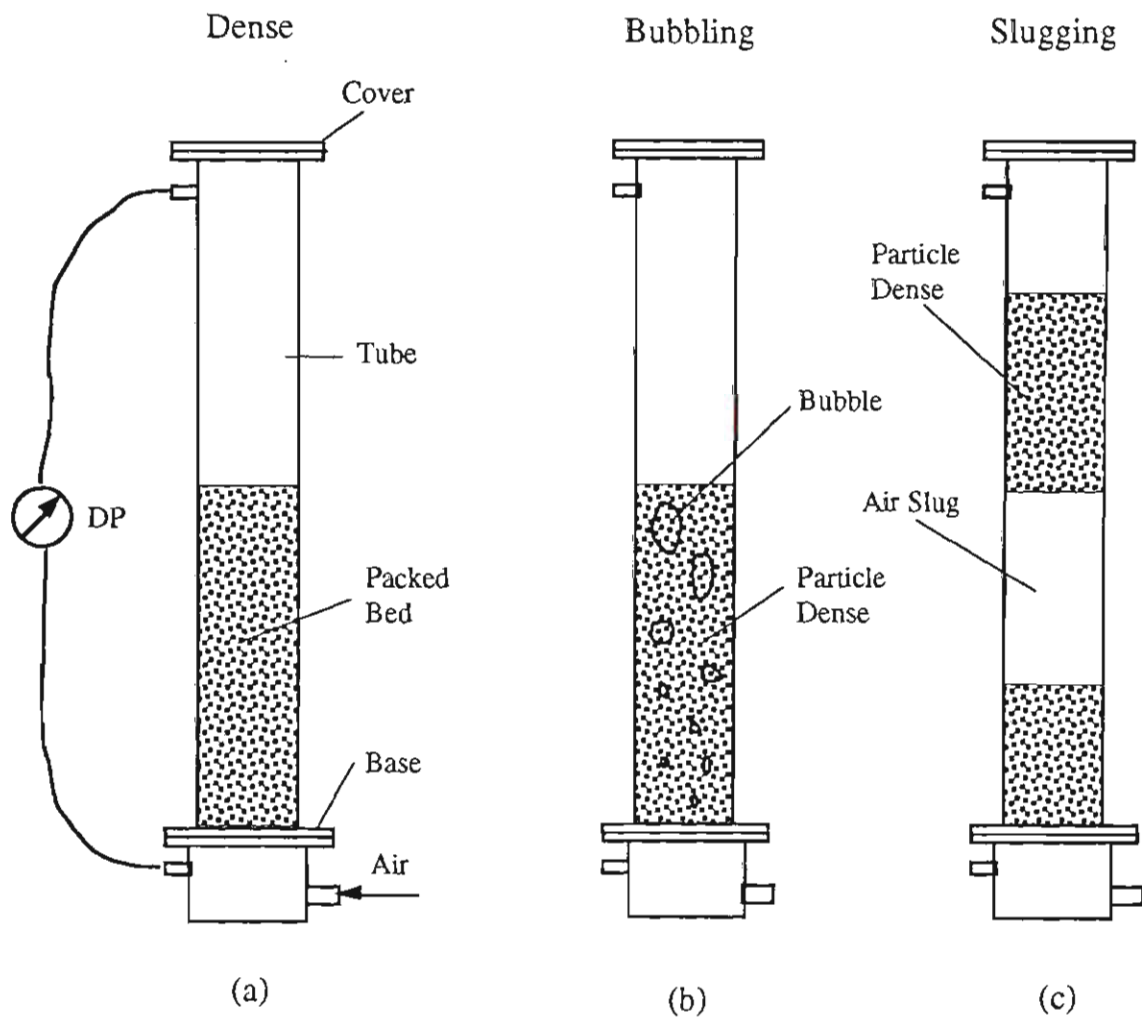


Figure 3.4 Fluidisation rig and schematic illustration of aggregative fluidisation.

The experiments were carried out using the following procedure:

- (i) Remove the cover of the rig and pour a known mass of material into the tube, then screw on the cover tightly.
- (ii) Measure the height of the particle bed.
- (iii) Introduce air into the fluidisation rig and observe the state of the bed.
- (iv) When the system is stable, measure the mass flow-rate of air and the pressure drop across the bed.
- (v) Increase the mass flow-rate of air, then repeat step (iv) until the bed is fully fluidised.

Figure 3.5 presents the test results with the plot of average bed pressure gradient against superficial air velocity for black plastic pellets, wheat and barley.

From an observation of the experiments and the curves shown in Figure 3.5, it is found that each experiment presents three stages. At the initial stage of the experiment, air passes upward at low velocity through a bed of particles, encounters frictional resistance and exhibits a pressure drop as it flows through the interstices. As the pressure drop is insufficient to support the weight of particles, the particles remain in their original position in contact with each other. This fixed bed condition is depicted in Figure 3.4(a). The pressure drop of the bed increases quickly as the mass flow-rate of air increases and has been correlated for all combinations of fluids, solids, and packed bed densities by a number of investigators (e.g. Ergun [32], Carman [18], etc.).

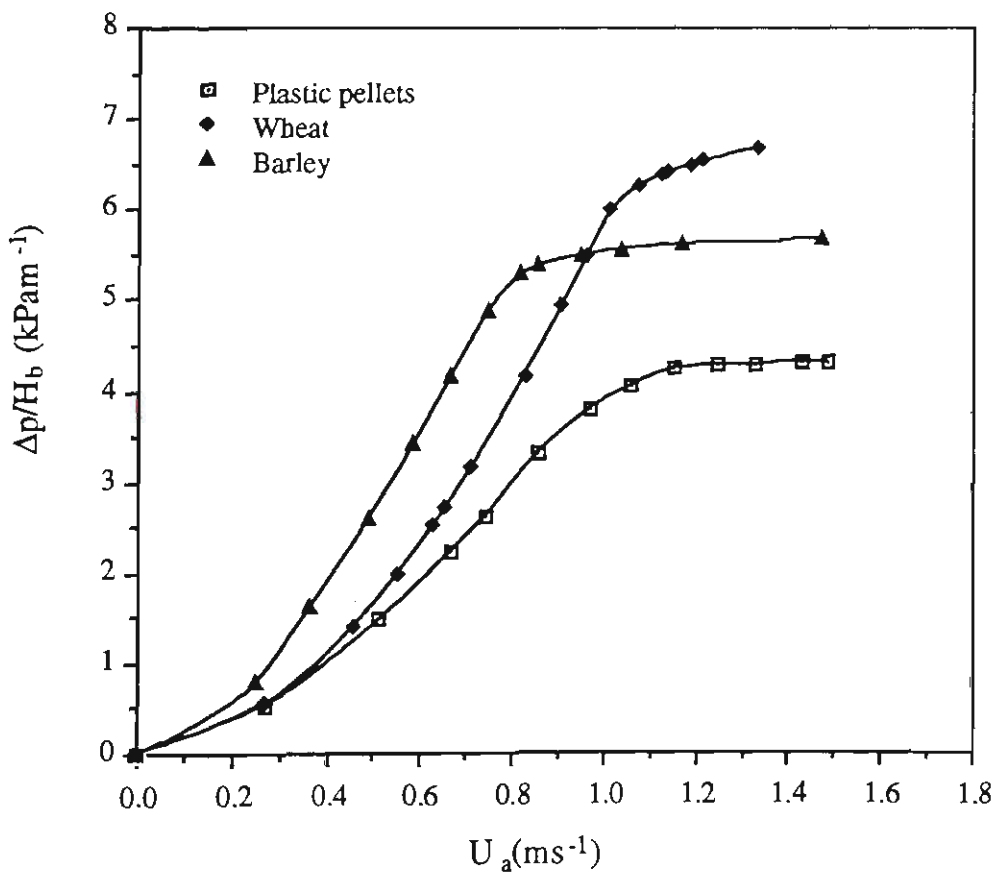


Figure 3.5 Pressure gradient of bed versus superficial air velocity.

As the air velocity is increased to the point at which the pressure drop caused by the air passing up through the bed of particles is just equal to the weight of the particle bed, the weight of each particle theoretically is balanced by the pressure drop across the particle. Hence, the inter particle stress disappears, although the particles still are in contact with each other. There is no motion of particles (i.e. particles keep fixed relative to each other). The pressure drop of the bed arrives at its maximum theoretical value. The particle state at this stage is called incipient fluidisation. The flow rate of the air corresponding to this point is termed as the incipient fluidisation rate.

If velocities above the incipient fluidisation rate, for some materials, the bed expands in volume, the particles in the bed move further apart and open up the interstices to allow easy passage of the air, thus the bulk density decreases (i.e. the bulk voidage increases), and all the particles are no longer touching each other. The bed is in the so-called "fluid" state. This system is said to exhibit particulate fluidisation. On the other hand, for some other materials such as the materials used in this investigation, any excessive air passes up through the bed in the form of bubbles, as shown in Figure 3.4(b). This system is said to exhibit aggregative fluidisation. If the flow rate of air is increased further, more bubbles occur in the bed, and coalesce to form larger bubbles. During aggregative fluidisation, the bed is divided into two phases: particle dense phase, in which the particles are believed to exhibit fixed bed configuration and the volume of the air passes through the phase just at the incipient fluidisation rate; and particle dilute phase, i.e. bubbles, which are formed by the excessive air and small numbers of particles "free-fall" in the bubbles. In theory, the pressure drop across the bed no longer increases after the bed is fluidised. In practice, the pressure drop still increases slightly with the fluid flow rate increasing, see Figure 3.5. From these figures, a transition area between the fixed bed and fluidised bed regions can be observed.

If the flow rate of air provided for fluidisation is sufficiently high to achieve an aggregative fluidisation bed, the volume of some bubbles increases until the diameter is

equal to the diameter of the bed, see Figure 3.4(c). At this time the particle dense phase is lifted and slug-flow appears. According to the flow pattern of low-velocity pneumatic conveying and the fluidisation experiments, the following conclusions can be obtained for low-velocity pneumatic conveying:

- 1 Low-velocity pneumatic conveying can be represented by an aggregative fluidised bed model.
- 2 Two particle phases exist in low-velocity pneumatic conveying. One is the particle dense phase (i.e. the particle slugs), the other is the particle dilute-phase (i.e. the air gaps). These constitute the discontinuous flow pattern of low-velocity pneumatic conveying.
- 3 The particle slugs are a special case of dense phase (i.e. incipient fluidisation), in which the air flow-rate is equal to that required just to fluidise the material. The air gaps are formed by using air in excess of that needed to fluidise the material. Therefore, for a low-velocity pneumatic conveying system and a given mass flow-rate of solids, increasing the mass flow-rate of air in theory does not change the pressure gradient of the slugs and only increases the length of the air gaps or forms new air gaps. The air gaps are axisymmetric for vertical slug flow and asymmetric for horizontal slug flow which results in the existence of a stationary bed.
- 4 From the definition of incipient fluidisation it is known that the particle slugs have a conventional fixed-bed configuration (i.e. the particles in the slugs are just in contact and are fixed relative to each other), with a bulk density similar to the loose-poured bulk density.

3.4 Pressure Gradient of Horizontal Slug

The following section introduces the theoretical analysis for the pressure gradient of a single slug, as conducted by K. Konrad [69] based on the Janssen's method for

analysing hopper flow problems. Further studies then are given by the author for the stress state of a single slug. For this purpose, the following assumptions are made:

- All the air flows through a slug in the axial direction of the slug (i.e. there is no motion of the air in a direction perpendicular to the axis of the slug).
- When low-velocity pneumatic conveying reaches steady state, the acceleration of the slug is not significant, so that the motion of slug can be regarded as uniform.
- The axial stress and transmission radial stress in a slug are functions of the length of slug only, i.e. their values are constant at a particular cross section of slug.
- The ratio of the axial stress to the transmission radial stress is constant, although the stresses themselves are functions of the length of slug.
- The length of slug is much greater than its diameter, i.e. $l_s \gg D$.
- The particle slug is cohesionless and obeys the Coulomb failure criterion.

3.4.1 Stresses Acting on Moving Slug

Figure 3.6 shows a moving particle slug in a horizontal pipe. The average length of the slug is l_s and the inner pipe diameter (i.e. the diameter of the slug) is D . During conveying, the slug is subjected to the pressure forces P_1 and P_2 , collecting and delivering resistant forces R_{s1} and R_{s2} , as well as the friction force R_f between the sliding slug and pipe wall, as shown in Figure 3.6(a).

The external forces acting on the slug generate various stresses. The stresses acting on an element of the slug are shown in Fig 3.6(b). The notations in the figure are explained below.

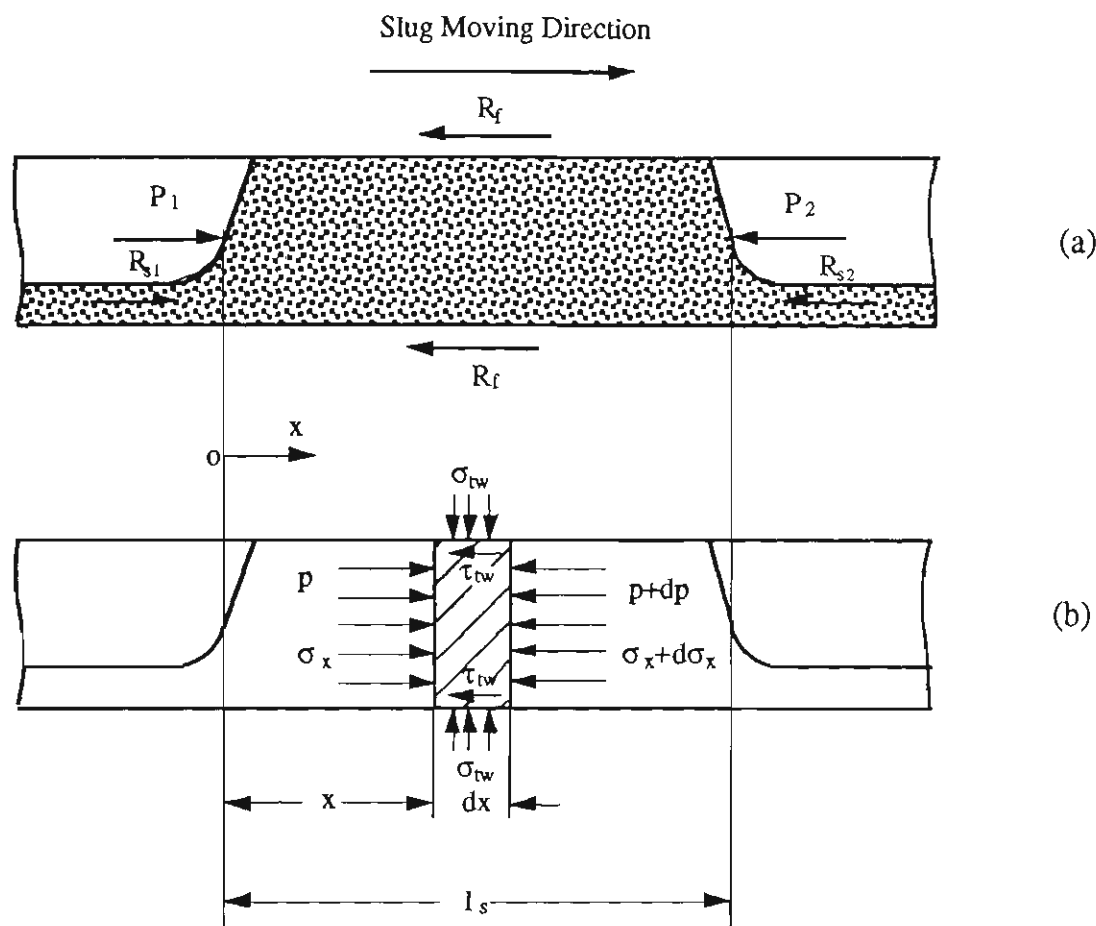


Figure 3.6 Forces and stresses acting on a horizontal particle slug.

p is the interstitial air pressure and it exerts a pressure force on each particle in the slug due to the porosity of the bulk solid. dp is the pressure drop across the element. The difference in the pressure force acting on the element is $dp \cdot A$, where cross-sectional area $A = \pi D^2/4$.

While the slug is compressed by the external forces, the particles in the slug react against each other to causes various stresses. These stresses are divided into axial and radial stress, as shown in Figure 3.6(b). The values of the stresses vary at the different locations of the slug. The radial stress at the wall is composed of the transmission radial stress and radial stress due to the weight of the slug for horizontal flow. For convenience and distinction, these stresses are called total wall pressure (σ_{tw}), wall pressure (σ_w) and gravity pressure (σ_g) due to weight, respectively. Figure 3.7 displays the total wall pressure (σ_{tw}) and its components (σ_w) and (σ_g).

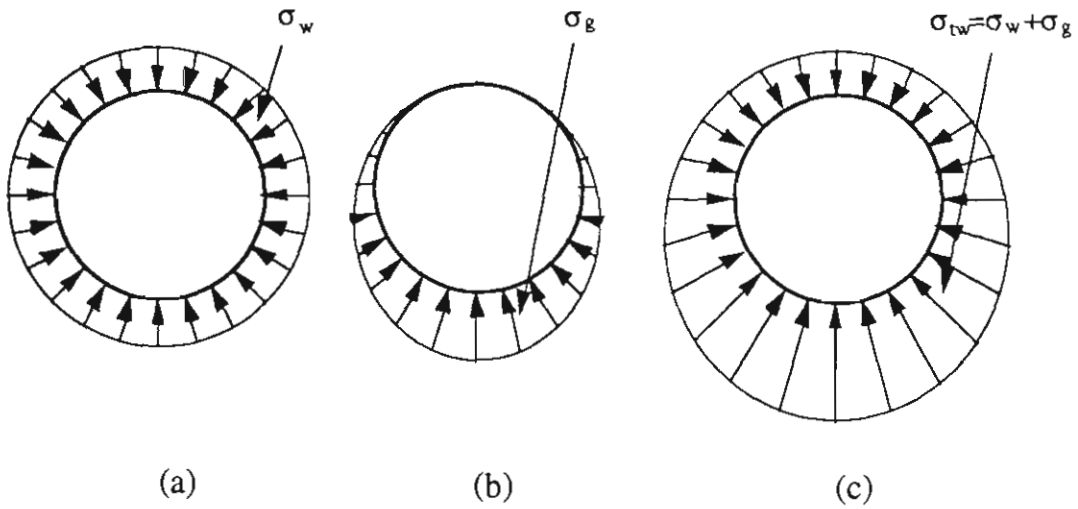


Figure 3.7: Total wall pressure and its components.

- (a) radial stress due to transmission at wall, called wall pressure,
- (b) radial stress at wall due to weight, called gravity pressure,
- (c) total wall pressure.

For vertical flow, the radial stress at wall due to weight (σ_g) is zero, thus $\sigma_{tw} = \sigma_w$. The wall pressure σ_w is caused by the pipe wall preventing the radial deformation of particles due to the axial force. The relationship between these two can be described by the ratio:

$$\lambda = \frac{\sigma_w}{\sigma_x} \quad (3.1)$$

which is defined and called the stress (force) transmission coefficient. It is analogous to the stress ratio of horizontal to vertical stress for the calculation of stresses in silos and hoppers. For slugs moving in pipes with rigid and parallel walls, the particles contained in the moving slugs can be observed fixed each other, i.e. no failures occur in the actual slugs. The determination of λ appears more difficult for this case and is investigated in more detail by theory and experiment in Chapter 7.

σ_g is a direct result of material weight. Wilson [111] and Konrad et al [69] considered in their research that the weight of bulk material in a horizontal pipe causes pressure on the whole pipe instead of only on the lower half of the pipe, as shown in Figure 3.7(b).

Their consideration appears to be reasonable since bulk material has some characteristics analogous to liquid. For example, if the upper half wall of a horizontal pipe is taken away, the bulk material on the upper half part of the pipe will flow down and can not maintain its original shape (i.e. cylinder shape) without the restriction of the pipe wall. This indicates that the upper half wall of the pipe should react with a force against the bulk material flowing down. Hence, Wilson's consideration [111] for σ_g is applied to this research.

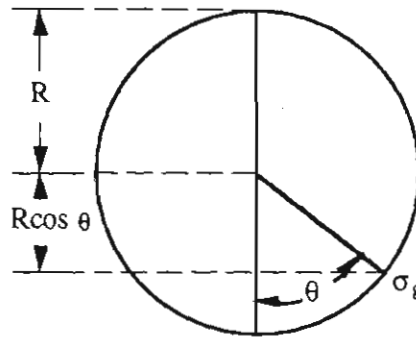


Figure 3.8 Cross section of a slug.

As shown in Figure 3.8, the stress distribution can be [111]:

$$\sigma_g = (1 + \cos\theta) \rho_b g R \quad (3.2)$$

τ_{tw} is the total shear stress at the wall. If the material obeys the Coulomb failure criterion, then $\tau_{tw} = \mu_w \sigma_{tw} + c_w$, where $\mu_w = \tan\phi_w$ and c_w is the particle wall cohesion. Note for cohesionless material, $c_w = 0$. As this study is confined to free-flowing granular materials, thus

$$\tau_{tw} = \mu_w (\sigma_w + \sigma_g) \quad (3.3)$$

Substituting $\sigma_w = \lambda \sigma_x$ from Equation (3.1) and $\sigma_g = (1 + \cos\theta) \rho_b g R$ from Equation (3.2) gives

$$\tau_{tw} = \mu_w [\lambda \sigma_x + (1 + \cos\theta) \rho_b g R] \quad (3.4)$$

3.4.2 Force Balance and Pressure Gradient of Horizontal Slug

Because the motion of a slug is regarded as uniform, there exists an equilibrium of the forces acting on the element of length dx , so that:

$$\frac{dp}{dx} + \frac{d\sigma_x}{dx} + \frac{Q_w}{A} = 0 \quad (3.5)$$

where Q_w in Equation (3.5) is the total shear stress acting on the wall around the pipe, therefore:

$$Q_w = \int_0^{2\pi} \tau_{tw} R d\theta \quad (3.6)$$

From Equation (3.4),

$$Q_w = \int_0^{2\pi} \mu_w [\lambda \sigma_x + (1 + \cos\theta) \rho_b g R] R d\theta \quad (3.7)$$

Integrating the right hand side of Equation (3.7) gives

$$Q_w = 2\pi R \mu_w [\lambda \sigma_x + \rho_b g R] \quad (3.8)$$

If a deaerated particle slug is forced to move by a mechanical piston, the motive pressure usually is expected to be proportional to the exponential of the slug length, as shown in Figure 3.9. However, some researchers [17, 27] pointed out that the pressure to maintain the movement of a slug by using air is much smaller, as the slug may allow air to permeate through the particles and aerate the solids resulting in a reduced material to wall friction force. The pressure is expected to be proportional to the slug length raised to a power (n) as shown in Figure 3.9. The value of the exponent (n) depends on the properties of the material such as permeability, etc. and is in the range $1 \leq n \leq 2$ [17].



Figure 3.9 Pressure to maintain movement of a particle slug in a pipe [17].

This research is concentrated on the low-velocity pneumatic conveying of coarse granular material. This type of material has natural slugging behaviour and good permeability. It can form rather short slugs naturally while still being conveyed at low velocity. Hence, the conveying air can aerate the particles completely. It is assumed that the value of the exponent (n) approaches 1 and the pressure is proportional to the slug length (i.e. the pressure gradient in the coarse granular material slug is constant). Therefore, $\frac{dp}{dx} = -\frac{\Delta p}{l_s}$,

where l_s is the length of a single slug.

Substituting Equation (3.8) into Equation (3.5), and replacing A with πR^2 , results in:

$$\frac{d\sigma_x}{dx} + \frac{4\mu_w\lambda}{D}\sigma_x - \frac{\Delta p}{l_s} + 2\mu_w\rho_b g = 0 \quad (3.9)$$

where R has been replaced by $D/2$. The solution to Equation (3.9) is,

$$\sigma_x = C e^{-\frac{4\mu_w\lambda}{D}x} + (-2\rho_b g\mu_w + \frac{\Delta p}{l_s})\frac{D}{4\mu_w\lambda} \quad (3.10)$$

where C is the integration constant and can be determined by the following boundary conditions where the stresses on the front and back surface of a slug are σ_f and σ_b , respectively.

$$\sigma_x = \sigma_f, \text{ at } x = l_s,$$

$$\sigma_x = \sigma_b, \text{ at } x = 0.$$

Applying the above conditions to Equation (3.10) yields

$$\sigma_f = C e^{-\frac{4\mu_w \lambda}{D} l_s} + (-2\rho_b g \mu_w + \frac{\Delta p}{l_s}) \frac{D}{4\mu_w \lambda} \quad (3.11)$$

$$\sigma_b = C + (-2\rho_b g \mu_w + \frac{\Delta p}{l_s}) \frac{D}{4\mu_w \lambda} \quad (3.12)$$

Eliminating constant C yields

$$\sigma_f - \sigma_b e^{-\frac{4\mu_w \lambda}{D} l_s} = (1 - e^{-\frac{4\mu_w \lambda}{D} l_s}) (-2\rho_b g \mu_w + \frac{\Delta p}{l_s}) \frac{D}{4\mu_w \lambda} \quad (3.13)$$

Actual observations of low-velocity pneumatic conveying found that the stationary bed thickness on the two sides of a slug is very similar. It is mentioned by Konrad et al. [69] that the value of σ_b is approximately equal to the value of σ_f if the cross sectional area ratio of stationary bed to pipe is similar on average both in front of and behind a slug. Hence assume that $\sigma_f \approx \sigma_b$, as well as $l_s \gg D$, which is reasonable for a natural slug-flow system, an equation for the pressure gradient of a single horizontal slug is determined:

$$\frac{\Delta p}{l_s} = \frac{4\mu_w \lambda}{D} \sigma_f + 2\rho_b g \mu_w \quad (3.14)$$

3.5 Axial Stress and Transmission Radial Stress

3.5.1 Distribution of Axial Stress

Rearranging Equation (3.14):

$$\sigma_f = (-2\rho_b g \mu_w + \frac{\Delta p}{l_s}) \frac{D}{4\mu_w \lambda} \quad (3.15)$$

Replacing $(-2\rho_b g \mu_w + \frac{\Delta p}{l_s}) \frac{D}{4\mu_w \lambda}$ in Equations (3.10) and (3.12) with σ_f gives

$$\sigma_x = C e^{-\frac{4\mu_w \lambda}{D} x} + \sigma_f \quad (3.16)$$

$$\sigma_b = C + \sigma_f \quad (3.17)$$

Eliminating C in Equations (3.16) and (3.17), the distribution of axial stress is given by

$$\sigma_x = (\sigma_b - \sigma_f) e^{-\frac{4\mu_w \lambda}{D} x} + \sigma_f \quad (3.18)$$

Equation (3.18) shows that the axial stress of a slug is proportional to the exponential of the slug length (i.e. x -coordinate) and is a function of the stresses on the front and back surface of the slug. According to this equation, a curve can be drawn to display the stress distribution clearly, as shown in Figure 3.10.

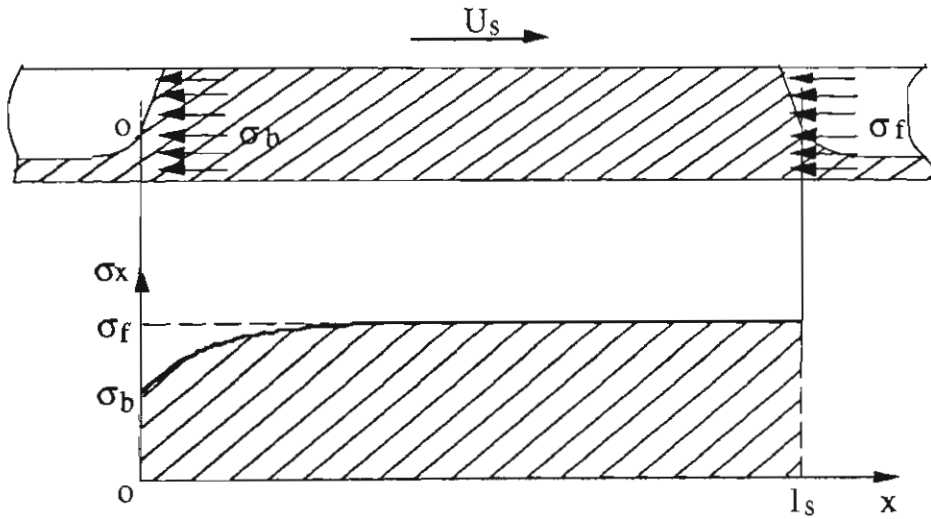


Figure 3.10 Distribution curve of axial stress of a moving slug.

From Equation (3.1):

$$\sigma_w = \lambda \sigma_x = \lambda \left[(\sigma_b - \sigma_f) e^{-\frac{4\mu_w \lambda}{D} x} + \sigma_f \right] \quad (3.19)$$

The distribution curve of this stress is similar to that of the axial stress shown in Figure 3.10 as λ is assumed as a constant.

3.5.2 Average Axial Stress

From Equation (3.18), the total axial stress of a slug can be obtained easily by integrating the axial stress along the slug length (i.e. calculating the shaded area in Figure 3.10). The average axial stress is the total stress divided by the slug length.

$$\sigma_{xm} = \frac{1}{l_s} \int_0^{l_s} \sigma_x dx = \frac{1}{l_s} \int_0^{l_s} [(\sigma_b - \sigma_f) e^{-\frac{2\mu_w \lambda}{R} x} + \sigma_f] dx \quad (3.20)$$

which results in:

$$\sigma_{xm} = \sigma_f \left[1 - \frac{D}{4\mu_w \lambda l_s} \left(1 - \frac{\sigma_b}{\sigma_f} \right) \left(1 - e^{-\frac{4\mu_w \lambda}{D} l_s} \right) \right] \quad (3.21)$$

As $\sigma_f \approx \sigma_b$ and $l_s \gg D$, therefore $\frac{D}{4\mu_w \lambda l_s} \left(1 - \frac{\sigma_b}{\sigma_f} \right) \left(1 - e^{-\frac{4\mu_w \lambda}{D} l_s} \right) \approx 0$, so that:

$$\sigma_{xm} \approx \sigma_f \quad (3.22)$$

This result can be observed clearly from Figure 3.10 where most of the axial stress is close to the value of the frontal stress of the slug.

If the average wall pressure of the slug is σ_{wm} , as λ is assumed as a constant in a slug, from Equation (3.1):

$$\lambda = \frac{\sigma_w}{\sigma_x} = \frac{\sigma_{wm}}{\sigma_{xm}} \quad (3.23)$$

Substituting $\sigma_{xm} \approx \sigma_f$ into Equation (3.23):

$$\lambda \approx \frac{\sigma_{wm}}{\sigma_f} \quad (3.24)$$

Equation (3.24) shows that the stress transmission coefficient of a slug can be approximated by the ratio of the average wall pressure to the frontal stress of the slug. This result is useful for determining λ by experiment, since it is difficult to measure the axial stress inside a slug and its corresponding transmission stress.

3.6 Stress on Front and Back Surface of Slug

While a slug moves in a horizontal pipe at a velocity U_s , the slug is in contact with the stationary bed in front of it, resulting in a reacting force R_{s2} , see Figure 3.6. A model to estimate the reacting force R_{s2} can be developed from a momentum balance.

Adding a velocity ($-U_s$) to the slug flow system, the particle slug can be regarded as a static object and the particles in the stationary bed flow toward the slug at velocity U_s . After the particles arrive at the slug, the velocity of the particles in the stationary bed changes to zero in direction of flow. Therefore,

$$R_{s2} = m_{st} U_s \quad (3.25)$$

where $m_{st} = \rho_{bst} A_{st} U_s$, which is the mass flow-rate of solids that flows into the slug from the stationary bed and U_s is the slug velocity which is defined as the mean velocity of the particles contained in a slug (see Chapter 6).

Substituting m_{st} into the above equation:

$$R_{s2} = \rho_{bst} A_{st} U_s^2 \quad (3.26)$$

where A_{st} is the cross sectional area of the stationary bed ahead of a slug, ρ_{bst} is the bulk density of solids in the stationary bed, which is approximately equal to the loose-poured bulk density of the material (ρ_b).

It is quite difficult to determine exactly the frontal stress (σ_f) due to its non-uniform distribution, as shown in Figure 3.11. However, the non-uniform distribution of σ_f caused by the external force R_{s2} only appears on the area very close to the surface of the slug. In order to calculate the stress easily, a uniform distribution is assumed. Such an assumption is not expected to cause a significant error as the stress gradually becomes uniform on the cross section further away from the front surface.

Hence,

$$\sigma_f = \alpha \rho_b U_s^2 \quad (3.27)$$

where α is the cross sectional area ratio of stationary bed to pipe.

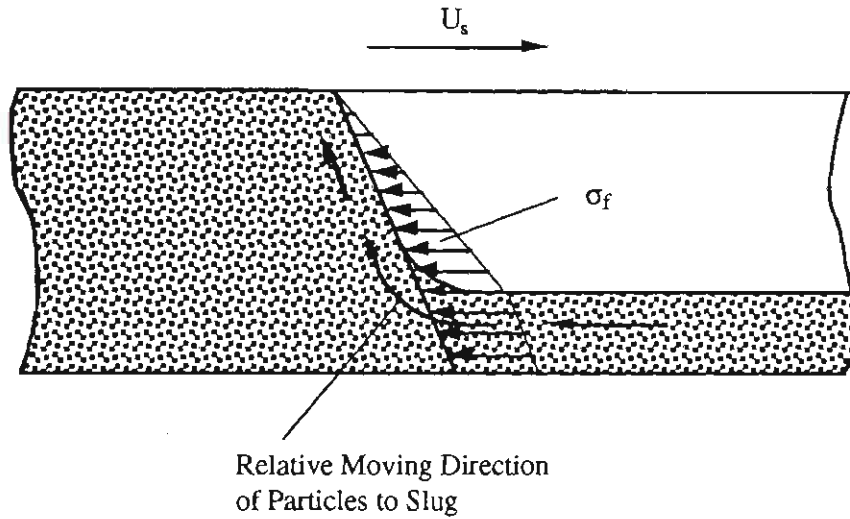


Figure 3.11 Stresses acting on the frontal surface of a slug.

While the moving slug deposits particles to the stationary bed behind the slug, the deposited particles impact the stationary bed, also resulting in a force R_{s1} . A similar method can be employed to estimate the stress on the back face of a slug, so that:

$$\sigma_b = \alpha \rho_b U_s^2 \quad (3.28)$$

CHAPTER 4
TEST FACILITY AND PROCEDURES

4.1 Introduction

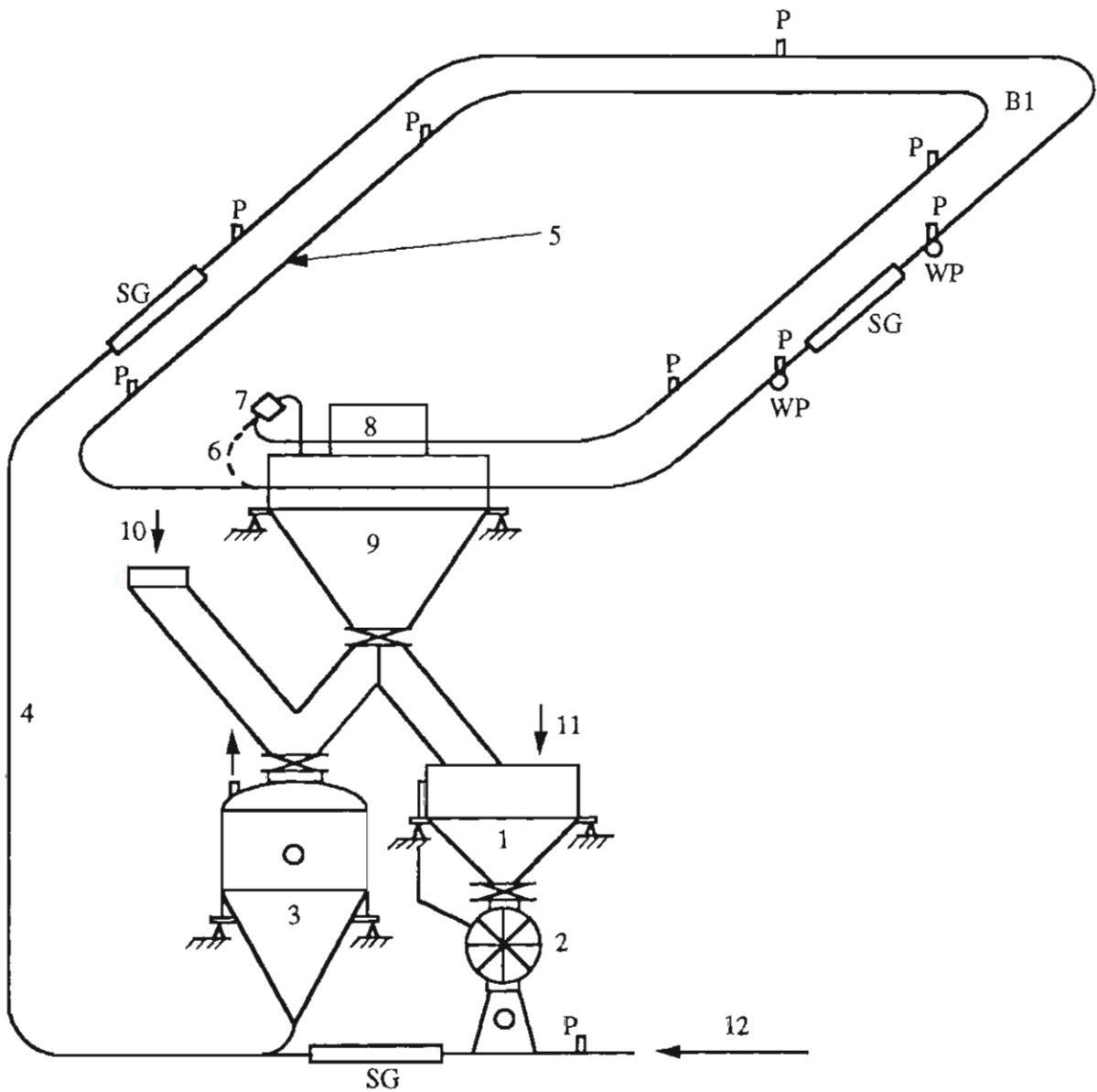
To understand the performance of low-velocity pneumatic conveying and determine some parameters which are difficult to predict theoretically, such as slug velocity and stress transmission coefficient λ , experimental investigations are necessary. Based on the experimental data, empirical correlations are established to demonstrate the influence and relationship of the major parameters of low-velocity pneumatic conveying. Substituting these empirical correlations into the theoretical models developed in Chapter 3 results in the final solution. More tests are carried out with different materials and pipelines and the data are used to verify the validity of the prediction model. The equipment described in this chapter is designed specifically for this purpose. The test rig allows product, air flow-rates and conveying distances to be of similar scale to industrial applications.

4.2 General Arrangement of Main Test Rig

The main low-velocity pneumatic conveying test rig consists primarily of material feeders (either a blow tank or high pressure rotary valve), a feed hopper, conveying pipelines, receiving silo mounted above the blow tank and rotary valve feed hopper and some instrumentation. A schematic layout of the low-velocity pneumatic conveying test rig is shown in Figure 4.1. If the conveying pressure of the system is no more than 350 kPag, the rotary valve is chosen as the feed device, otherwise, the blow tank is employed to allow tests to be carried out at higher pressures.

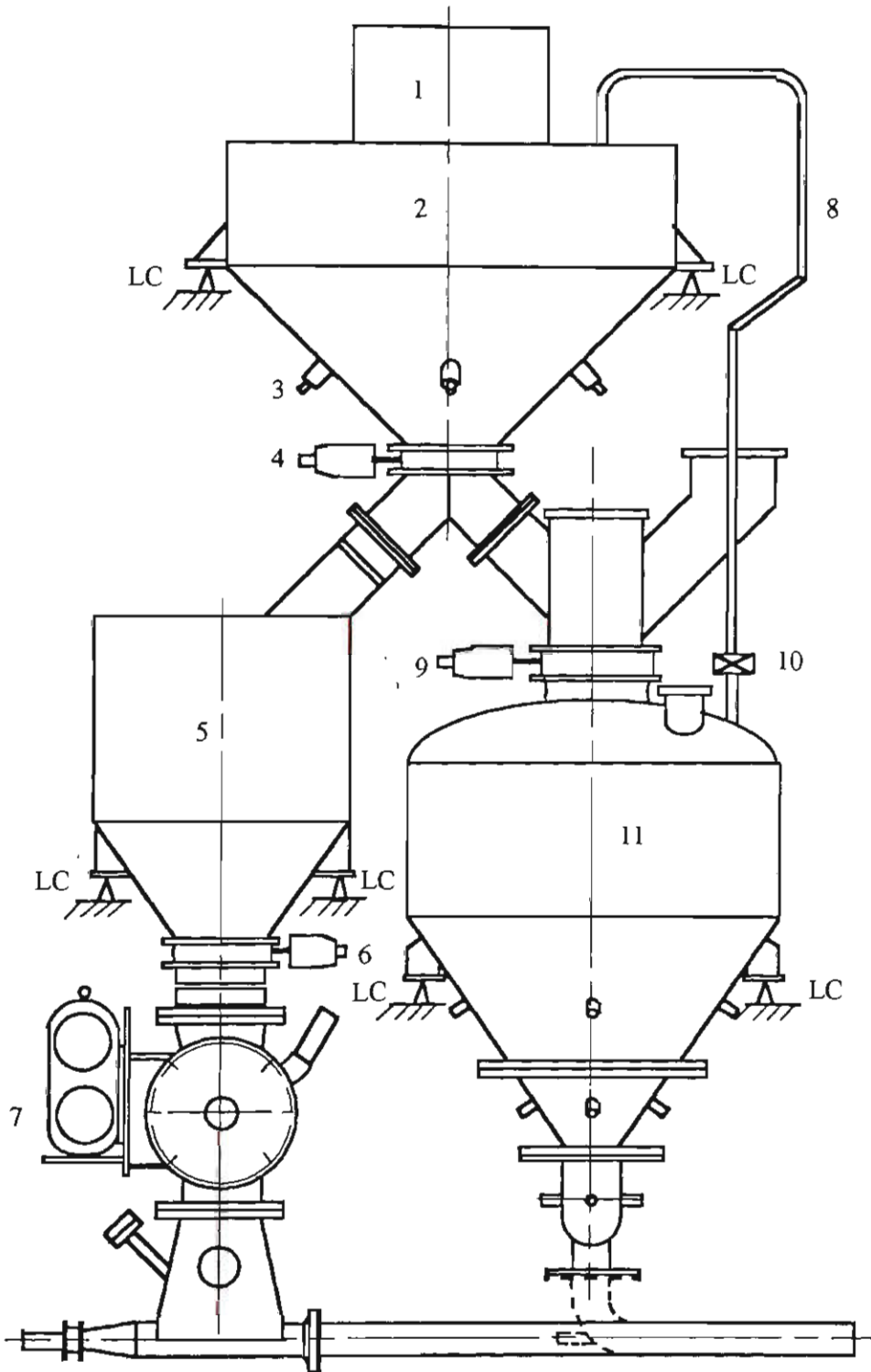
4.2.1 Material Feeders

There are many types of devices which have been used as material feeders successfully in pneumatic conveying. In this thesis, a high pressure rotary valve and blow tank feeder are available for dense-phase granular conveying in the low-velocity pneumatic conveying test rig, see Figure 4.2.



- | | | |
|---|-----------------------|-------------------------------|
| 1 Feed Hopper | 6 52 m Loop Connector | 11 Rotary Valve Filling |
| 2 ZGR-250 Rotary Valve | 7 Back Pressure Valve | 12 Conveying Air Inlet |
| 3 Blow Tank | 8 Reverse-jet Filter | P Static Air Pressure Tapping |
| 4 Vertical Lift, 6.5 m | 9 Receiving Silo | SG Sight Glass |
| 5 Transport Line 105 mm ID,
One Loop 52 m, Two Loops
96 m | 10 Blow Tank Filling | WP Wall Pressure Fittings |

Figure 4.1 Schematic layout of low-velocity pneumatic conveying test rig.



- | | | | |
|------------------|----------------|------------------------|----------------|
| 1 Filter | 4 Silo Valve | 7 ZGR-250 Rotary Valve | 10 Vent Valve |
| 2 Receiving Silo | 5 Feed Hopper | 8 Blow Tank Vent Pipe | 11 Blow Tank |
| 3 Pulse Valve | 6 Hopper Valve | 9 Blow Tank Fill Valve | LC - Load Cell |

Figure 4.2 Feed devices and receiving silo.

4.2.1.1 High Pressure Rotary Valve

The principle requirement of a feeder is that it should be capable of feeding the solids at a reliable rate from the supply hopper at one pressure to the conveying line at another pressure. For this reason rotary valves are an ideal selection for pneumatic conveying systems. Since rotary valves are used for feeding products from a low pressure area into a higher pressure area, air leakage automatically occurs between rotor and housing due to the existence of clearance between them. Conventional rotary valves (up to pressures of 100 kPag) are most commonly applied to dilute-phase systems. Feeding into high pressure systems almost always involves the use of a blow tank, which usually is capable of working at the pressures up to about 600 kPag. One disadvantage of the blow tank is that the feed rate cannot be controlled easily.

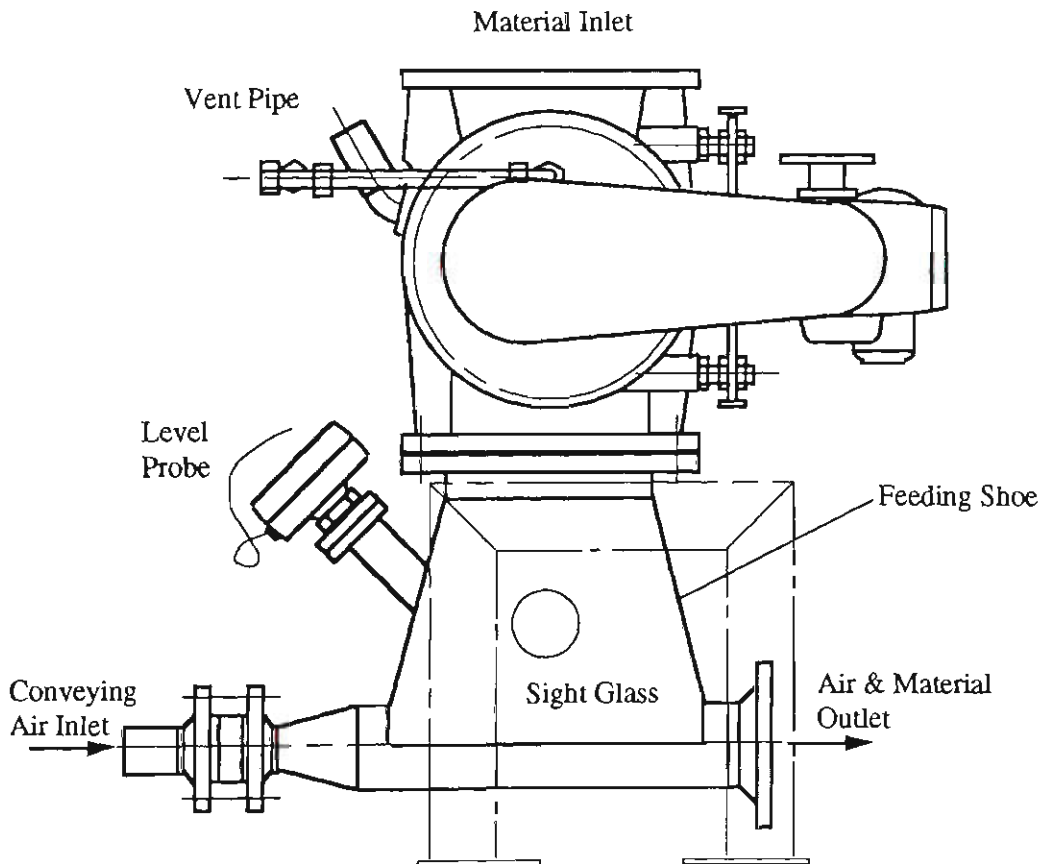


Figure 4.3 ZGR-250 high pressure rotary valve.

Thanks to the further systematic development of rotary valve technology, the application for rotary valves has been extended into dense-phase pneumatic conveying systems. The

ZGR-250 rotary valve shown in Figure 4.3 is a high performance rotary valve designed and manufactured specially for dense-phase pneumatic conveying by Waeschle Maschinenfabrick GmbH (Germany).

Designers of the company found new ways to seal off the rotor at the side by external, self-adjusting axial rotating mechanical seals to reduce air leakage under high pressure. A rotor shaft sealing ring also can be used to minimise air leakage further. The application of these new developments allows the ZGR-250 rotary valve to handle fine and coarse materials up to the conveying pressures of 350 kPag and reduce the air leakage by up to 60% compared to conventional rotary valves.

Although the air leakage of the ZGR-250 rotary valve is quite low (compared with conventional rotary valves), it still may be quite significant in low-velocity pneumatic conveying. That is, the effect of air leakage on systems cannot be ignored. In order to determine air leakage of the ZGR-250 rotary valve under different conveying pressures, experiments are undertaken as follows.

- (i) Block the air and material outlet of the ZGR-250 rotary with a steel plate, refer to Figure 4.3.
- (ii) Load a certain mass of material (e.g. plastic pellets) into the feed hopper and operate the rotary valve at a given rotor speed (e.g 20 rpm).
- (iii) Blow air from the conveying air inlet, see Figure 4.3, into the rotary valve. As the air and material outlet of the rotary valve is blocked, all the air escapes out of the rotary valve through the clearance between the rotor and housing.
- (iv) Measure the mass flow-rate of the blowing air by an orifice plate and the pressure in the feeding shoe of the rotary valve.

- (v) Repeat the test from step (iii) with blowing different mass flow-rate of air until enough data are obtained.

Figure 4.4 shows the curves of the air leakage of the ZGR-250 rotary valve versus conveying pressure obtained by experiment.

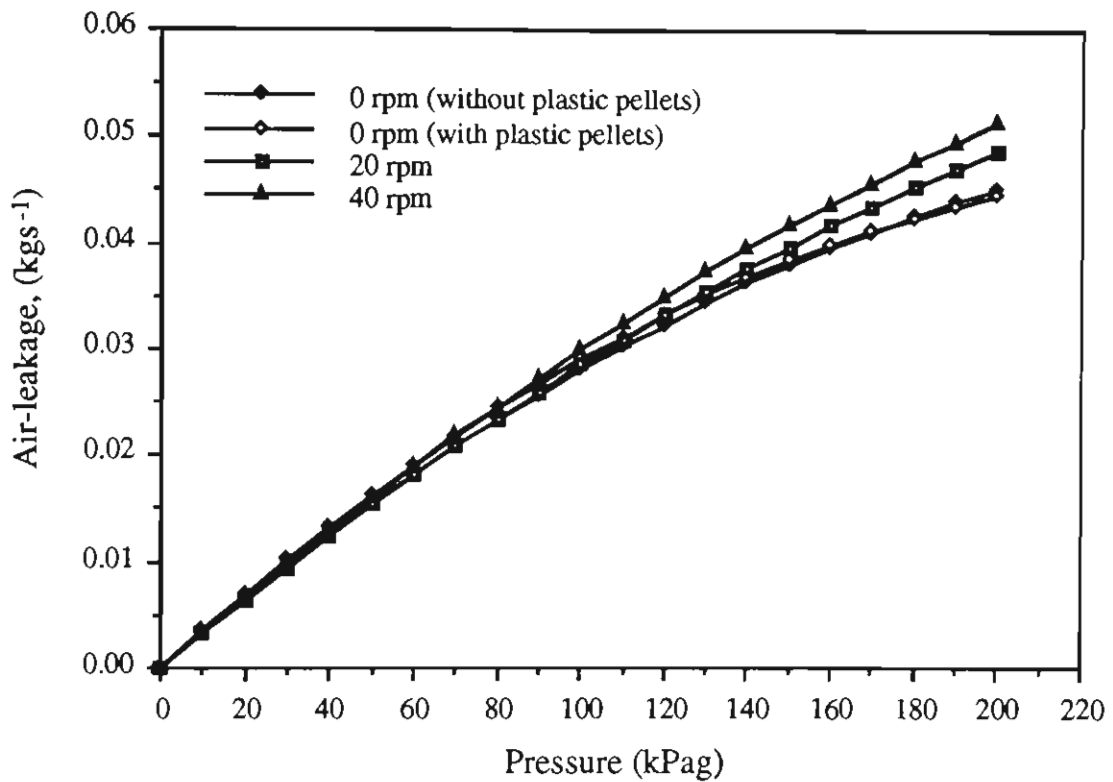


Figure 4.4 Air leakage curves of ZGR-250 rotary valve.

To determine the actual value of mass flow-rate of air for conveying, the conveying pressure is recorded during each experiments so that the relevant air leakage may be calculated. The actual mass flow-rate of air in the pipeline is the difference between the total supplied mass flow-rate of air and air leakage of the rotary valve.

The ZGR-250 rotary valve is installed underneath a feed hopper, and its outlet is linked to the conveying pipe of the system through a feed shoe in which a level probe is installed to limit the height of material that could build up underneath the rotary valve. When feeding a conveying line with a rotary valve, the air leakage through the valve can impede the material flowing into the rotor pockets and therefore reduce the feed rate. To

overcome this problem, venting has been developed and installed by manufacturers and/or users of rotary valves. This is achieved usually by the provision of vent holes on the valve casing (i.e. on the empty or return side of the valve), see Figure 4.3.

4.2.1.2 Blow Tank

The ZGR-250 high pressure rotary valve enables material to be fed against a pressure of 350 kPag without its air leakage exceeding the rate normally experienced with conventional dilute-phase conveying systems. However, the pressures in some conveying trials may exceed the maximum allowed value of 350 kPag. In this case, a 0.9 m³ blow tank is engaged to enable the conveying tests to be completed. A general arrangement of the blow tank is presented in Figure 4.5.

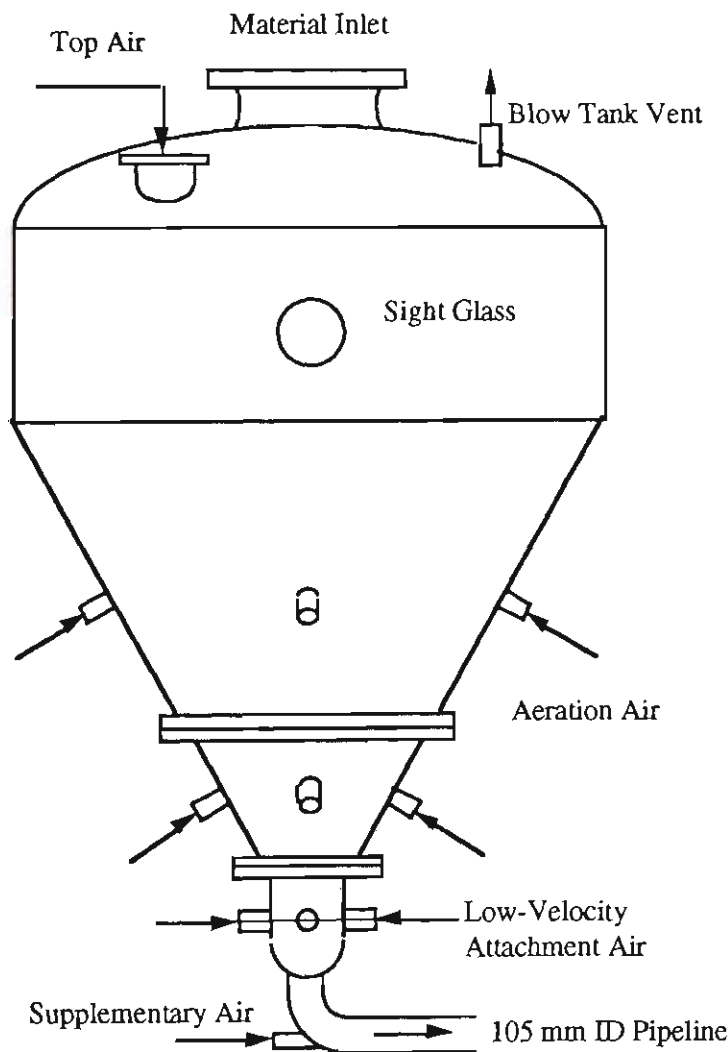


Figure 4.5 Configuration of 0.9 m³ low-velocity blow tank feeder.

This blow tank was developed jointly by the University of Wollongong and NEI John Thompson (Australia) to allow friable and/or granular products to be conveyed with extremely low levels of product degradation or damage (e.g. solids conveying velocities usually occur in the range 0.25 to 2 ms^{-1}). The blow tank is supported on load cells which are fixed on a supporting structure. The mass of product discharged from or loaded into the blow tank can be measured by the load cells.

4.2.2 Feed Hopper and Receiving Silo

A 0.9 m^3 feed hopper providing material for the rotary valve is supported within a framework by load cells, see Figure 4.2. The mass of material discharged from or loaded into the hopper can be measured by the load cells. The hopper is connected to the rotary valve via a flexible tube to avoid the influence of vibration of the working rotary valve on the output of the load cells.

The receiving silo is designed to be slightly larger in capacity than the blow tank or feed hopper to allow for the loss of volumetric capacity by uneven distribution of the received material within the silo. The mass of the received material can be measured by the load cells which support the receiving silo. A filter is installed on top of the silo to separate the air from the conveyed solids. Four pulse valves, see Figure 4.2, are mounted on the conical hopper of the silo to assist in the complete discharge of material from the silo.

4.2.3 Conveying Pipeline

The low-velocity pneumatic conveying test rig consists of a mild steel closed loop pipeline, see Figure 4.1, either 96 m or 52 m in length (105 mm ID), fitted with flanges connected properly to provide continuous uninterrupted flow. The main section of the pipeline is constructed horizontally above the roof of the Bulk Solids Handling Laboratory. A 6.5 m vertical lift required to send material up to this horizontal section is located at the beginning of the conveying line. The total pipeline comprises various

lengths of pipe and the length of each pipe is shown in Figure 4.6. Ten 90° 1.2 m radius bends are installed along the pipeline with a back pressure valve and a 45° 1.2 m radius bend at the end of the line.

Two sight glasses (each 1.0 m in length), see Figure 4.1, can be fitted to the test pipeline for the visual study of slug-flow. The effect of the sight glasses, in particular due to the different frictional characteristics between the steel and glass with the conveyed products, is unknown. However, the length of each sight glass is very small compared to the total length of the pipeline and the effect on flow performance is assumed negligible.

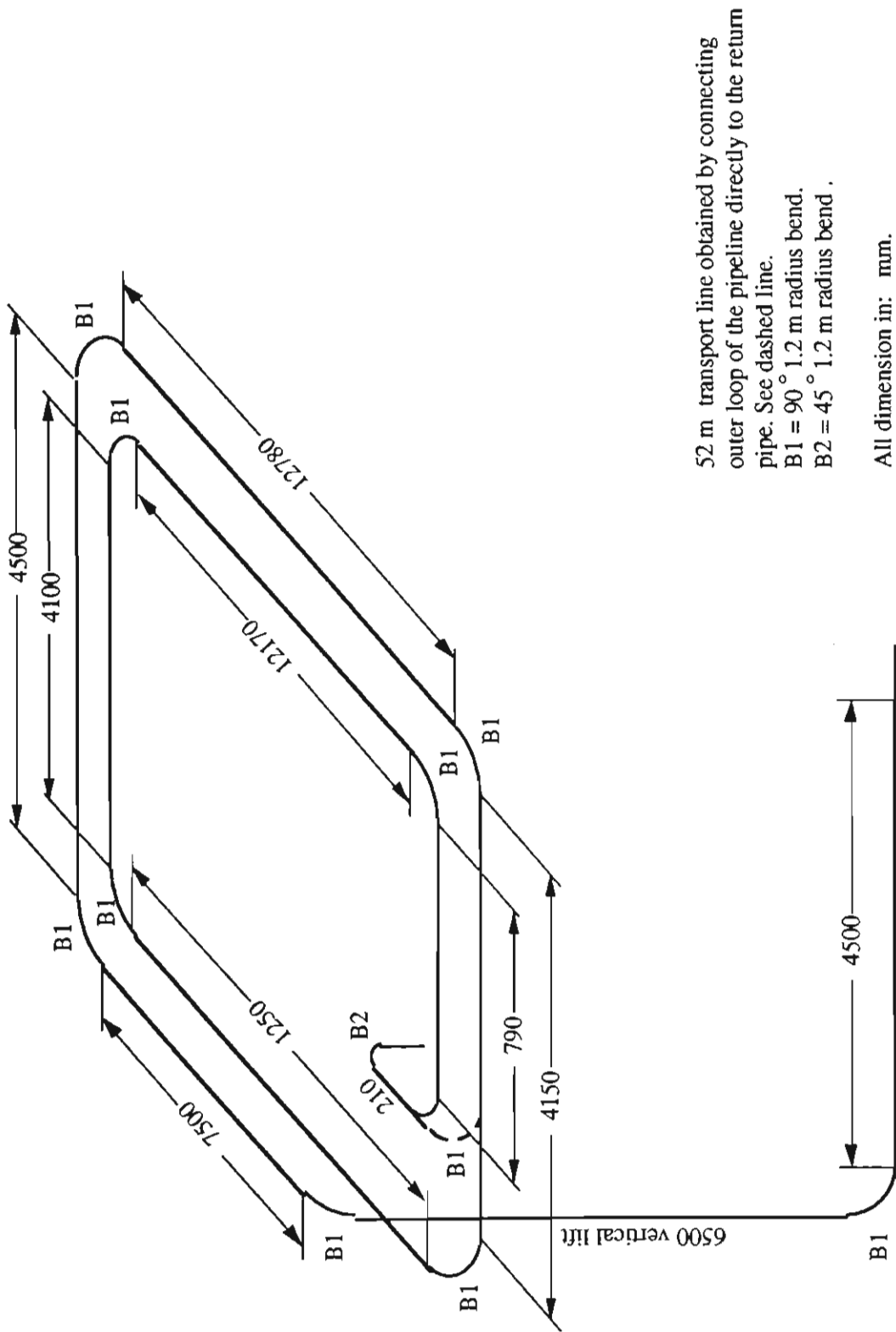


Figure 4.6 Details of 96 m x 105 mm ID test rig pipeline.

4.3 Air Supply and Control

4.3.1 Air Supply

The major consideration in the selection of an air supply plant for a test rig is that sufficient air is available for all experiments. In the Bulk Solids Handling Laboratory, air at a maximum pressure head of 800 kPag is supplied from the following rotary screw compressors:

- Atlas Copco electric-powered Model GA-308, $3.1 \text{ m}^3 \text{ min}^{-1}$ free air delivery.
- Ingersoll Rand diesel-powered Model P374-WP, $10.6 \text{ m}^3 \text{ min}^{-1}$ free air delivery.
- Ingersoll Rand diesel-powered Model P840-WGM, $24.1 \text{ m}^3 \text{ min}^{-1}$ free air delivery.

To handle a wide range of bulk solids through numerous sizes of pipeline (e.g. 50 to 150 mm), any combination of the above compressors can be employed for the test rig. The compressors are connected to an after-cooler, two refrigerated air dryers and two air receivers (1.74 and 6.0 m^3 volumetric capacity). Various filters and separators are installed in series with these compressors to ensure a dry and oil-free air supply. Figure 4.7 shows a general arrangement of the air supply system.

4.3.2 Air Flow Control

Cooled, dried and oil-free air is introduced into the conveying pipeline through an orifice plate or annubar where the air flow-rate is measured, as shown in Figure 4.7. It is a general requirement that the mass flow-rate of air is as constant as possible during a conveying trial. Due to the fluctuations in the air supply pressure, the mass flow-rate of air entering the pipeline normally will vary (i.e. without using mass flow-rate control device). For this reason, sonic nozzles are installed before the entrance of the pipeline of the low-velocity pneumatic conveying test rig, as shown in Figure 4.8.

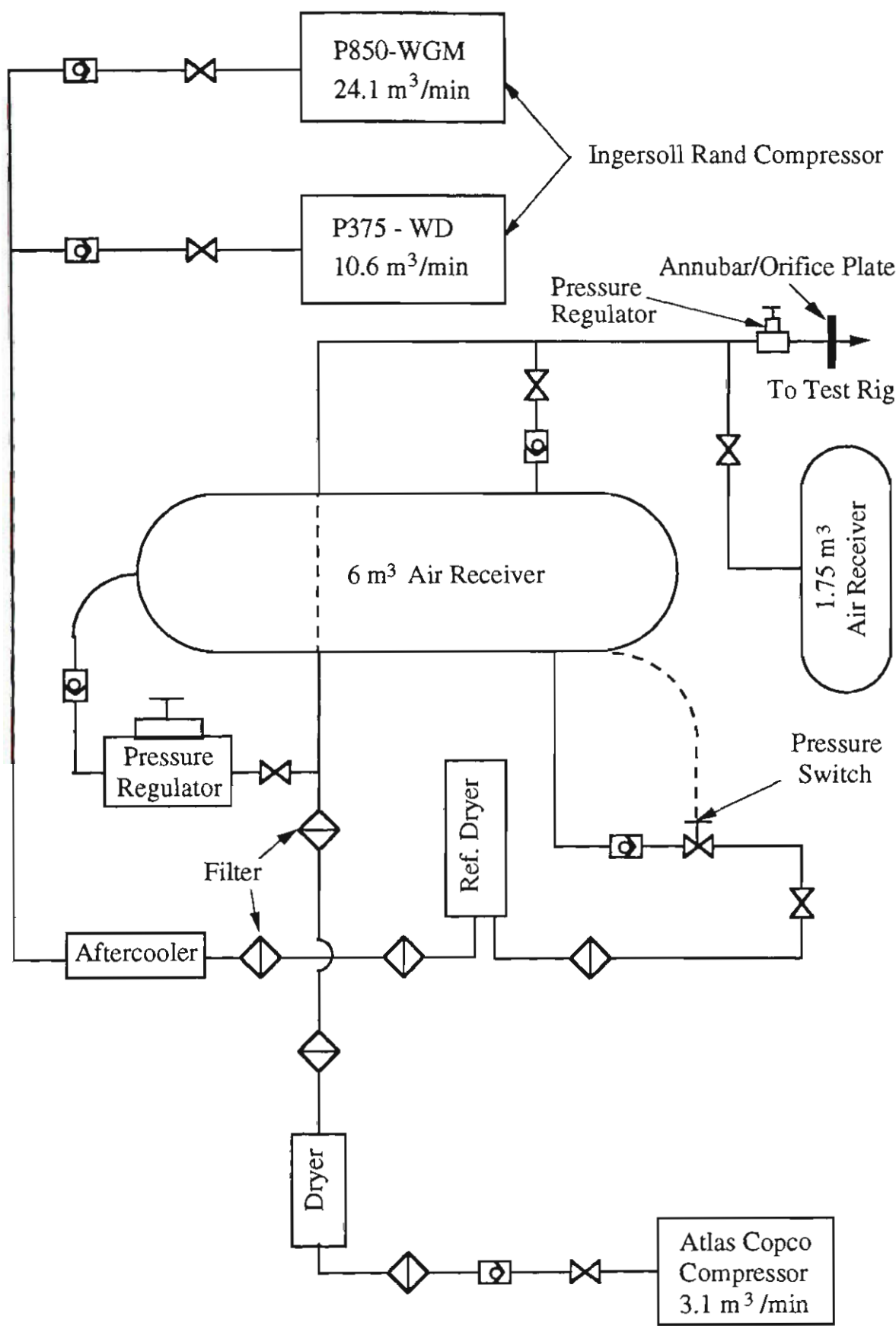


Figure 4.7 General arrangement of compressed air supply.

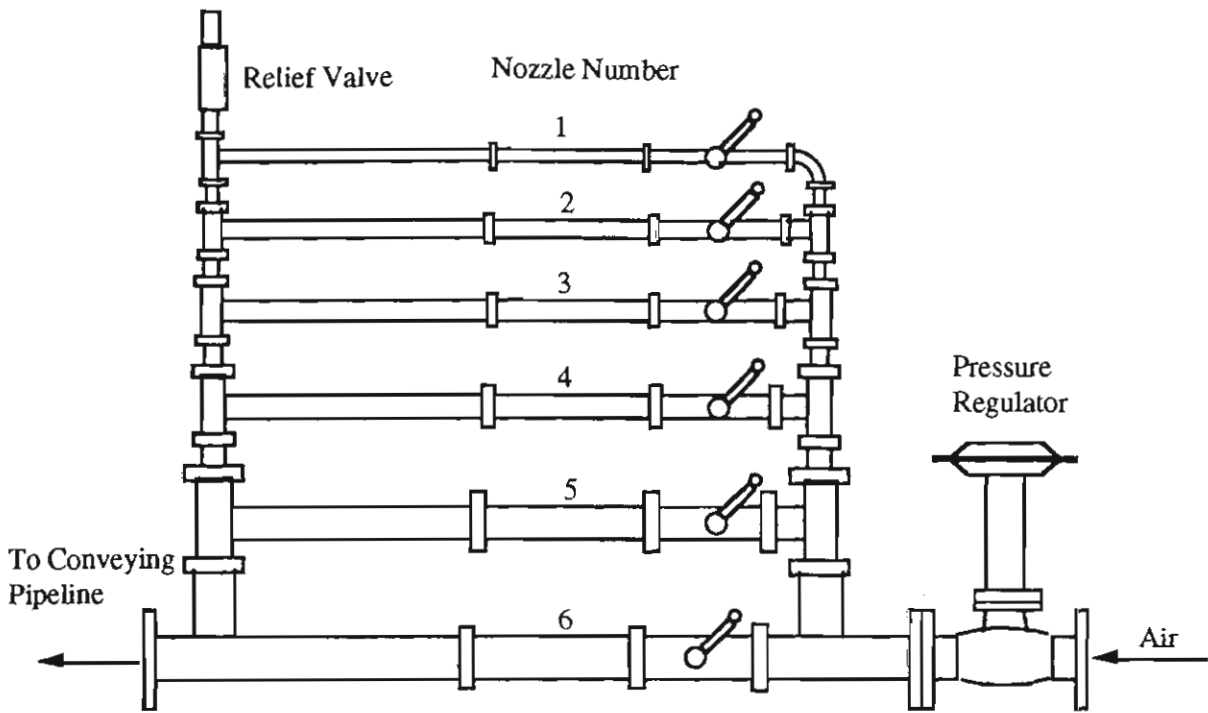


Figure 4.8 Sonic nozzles.

Air mass flow-rate control is achieved with any combination of nozzles and a pressure regulator that maintains a fairly constant upstream pressure. As each nozzle is manufactured to have an accurate internal diameter, the flow-rate of air through a nozzle will be constant irrespective of downstream air pressure fluctuations. The pressure regulator can be set at 500 kPag or 300 kPag.

4.4 Experimental Instrumentation and Technique

The instrumentation and techniques are designed to measure directly the following parameters during the experiments on low-velocity pneumatic conveying:

- mass flow rate of solids (m_s),
- mass flow rate of air (m_f),
- static air pressures at various points of the system (P),
- wall pressure (σ_w),
- stationary bed thickness (h_s).

In addition, some parameters are to be obtained indirectly from the above measured signals by using signal analysis technology. These parameters include:

- slug velocity (U_s),
- slug and air gap length (l_s, l_g).

The following sections describe the instrumentation and relevant technology used for measurement.

4.4.1 Mass Flow-Rate of Solids

Shear-beam-type load cells (model KA-500kg) support the blow tank, feed hopper and receiving silo (see Figure 4.2). The mass of material discharged from or loaded into these containers over a period of time (e.g. ranging from 50 to 150 seconds) can be measured by these load cells. An average mass flow-rate of solids is obtained by calculating the slope of the line of best fit.

4.4.2 Mass Flow-Rate of Air

The mass flow-rate of air is measured by an orifice plate, which is simply a thin, flat plate having a central hole. Figure 4.9 shows the orifice plate device used in this project. Inserting this device into an air supply pipeline, the flow-rate of air through the device can be calculated from a measurement of the upstream pressure and the difference between the pressures on the wall of the pipe at specified distances upstream and downstream of the orifice plate. The numerical relationship between the flow-rate of air and pressure difference depends on the shape of the orifice and the positions of the pressure tapping. The orifice plate and positions of the pressure tapping used in this project are designed according to B.S. 1042. The equation for calculation of the flow-rate is listed in B.S. 1042. The pressure difference is measured by a 150 inch H₂O full-scale DP (differential pressure) transmitter connected to the pressure tapping holes.

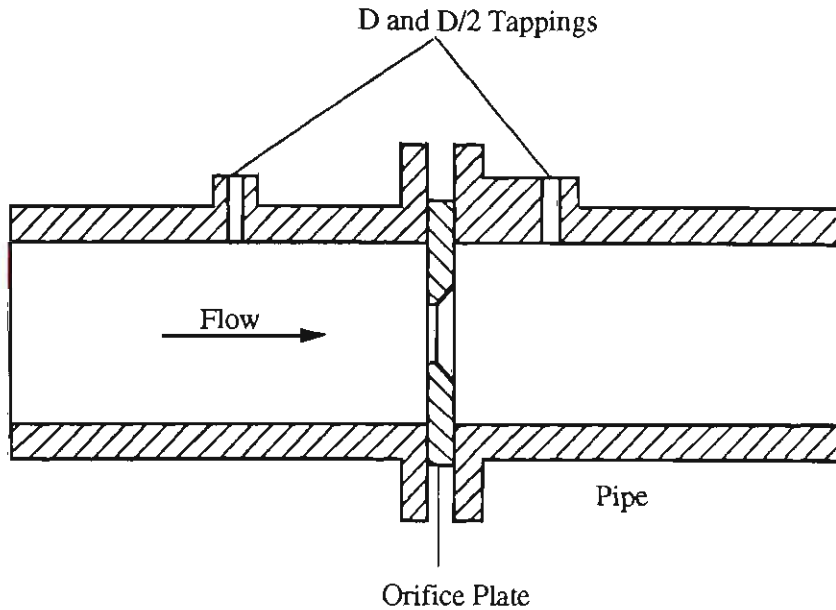


Figure 4.9 Orifice plate device.

4.4.3 Static Air Pressure

Static air pressures at different locations such as air supply, blow tank and pipeline are measured simply with strain-gauge pressure transducers type-A (model BHL-4400 range 0-6 bar and -3040 range 0-10 bar), see Figure 4.1. Refer to Figure 4.10 for an exploded view of a typical pipeline air pressure tapping location. The pressure transducer is connected to the pipe socket by a quick connector.

4.4.4 Wall Pressure

Figure 4.11 shows a wall pressure measuring assembly which mainly consists of two types of pressure transducer (i.e. type-A and -B). As above mentioned, the type-A pressure transducer measures the static air pressure on the pipe wall. The type-B (model AB/HP-40G) pressure transducer, which is installed at the bottom of the pipe, measures the total values of the static air pressure and total wall pressure. The wall pressure is obtained by subtracting the static air pressure from the total pressure.

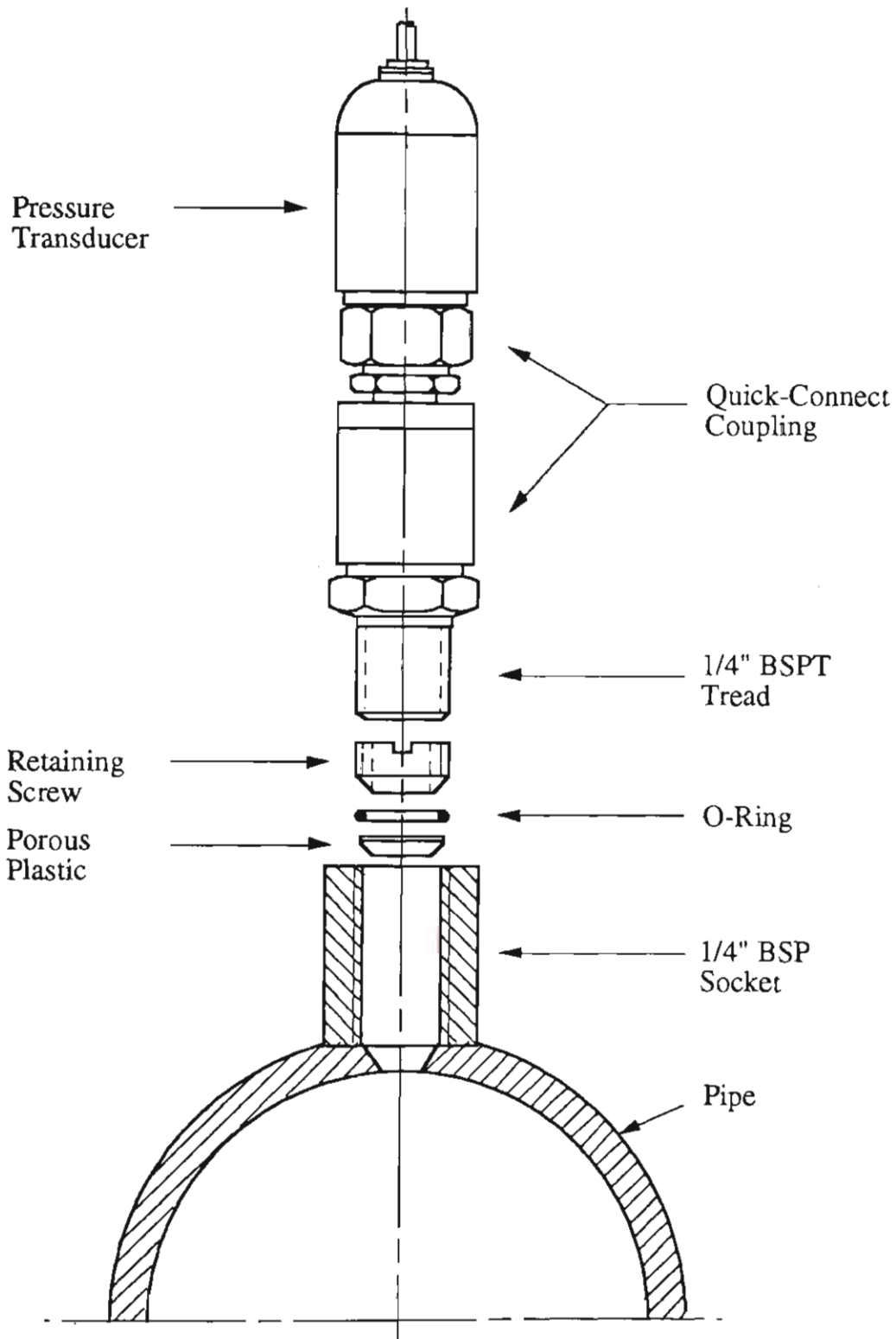


Figure 4.10 Exploded view of typical air pressure tapping location.

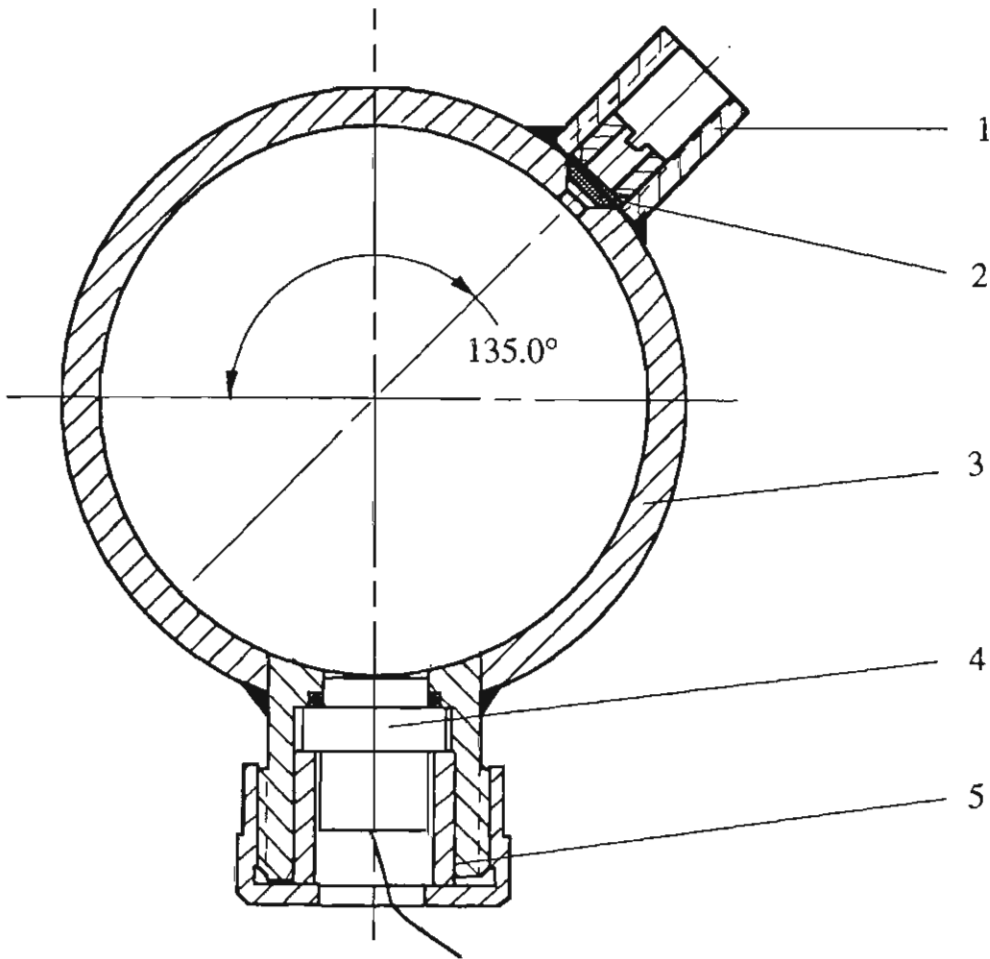


Figure 4.11 Wall pressure measuring assembly.

1 - Air Pressure Tapping, 2 - Porous Plastic, 3 - Pipe, 4 - AB/HP-40G Pressure Transducer, 5 - AB/HP-40G Transducer Fitting

4.4.5 Stationary Bed Thickness

Stationary bed thickness is measured directly by taking photographs of the stationary bed through a sight glass, and scaling the height with respect to the known pipe diameter.

4.4.6 Slug Velocity

A cross correlation function analysis technique is used for determining slug velocity in low-velocity pneumatic conveying. This method uses the characteristics of the cross correlation function to determine the time (τ_d) taken by a slug to travel through two neighbouring test points along a pipe. If the distance between two neighbouring test

points is known as L , then the slug velocity can be determined (i.e. $U_s = L/\tau_d$). The accuracy of this technique is dependent on the selection of the correlated signals, sampling rate of a data acquisition system and the distance between the two neighbouring test points. Here the wall pressure signals are selected to carry out the cross-correlation function analysis. Further details on this measurement are discussed in Chapter 6.

4.5 Data Acquisition and Processing Systems

Since a major part of this research is reliant on the collection and analysis of a large amount of experimental data, the development of a data acquisition system (DAS) of sufficient capacity and reliability to handle the required tasks is crucial. The DAS employed in this research is shown in Figure 4.12.

4.5.1 Hewlett Packard 3044A System

The basic DAS used for this experimental investigation was developed during previous research work and was based on a portable Hewlett-Packard 3044A system, consisting of a HP-85B desk-top computer and a HP-3497A DVM capable of reading down to μV , see Figure 4.12. The scanning capacity of this system was about 20 Hz, which was adequate for most requirements. Due to the limited memory capacity of the HP-85B computer, the time history responses coming from the pressure transducers and load cells were stored firstly in the HP-85B computer and then unpacked and transferred to a Tektronix 4923 digital tape recorder before commencing the next experiment. This procedure was slow and tedious and limited the number of tests that could be completed in one day.

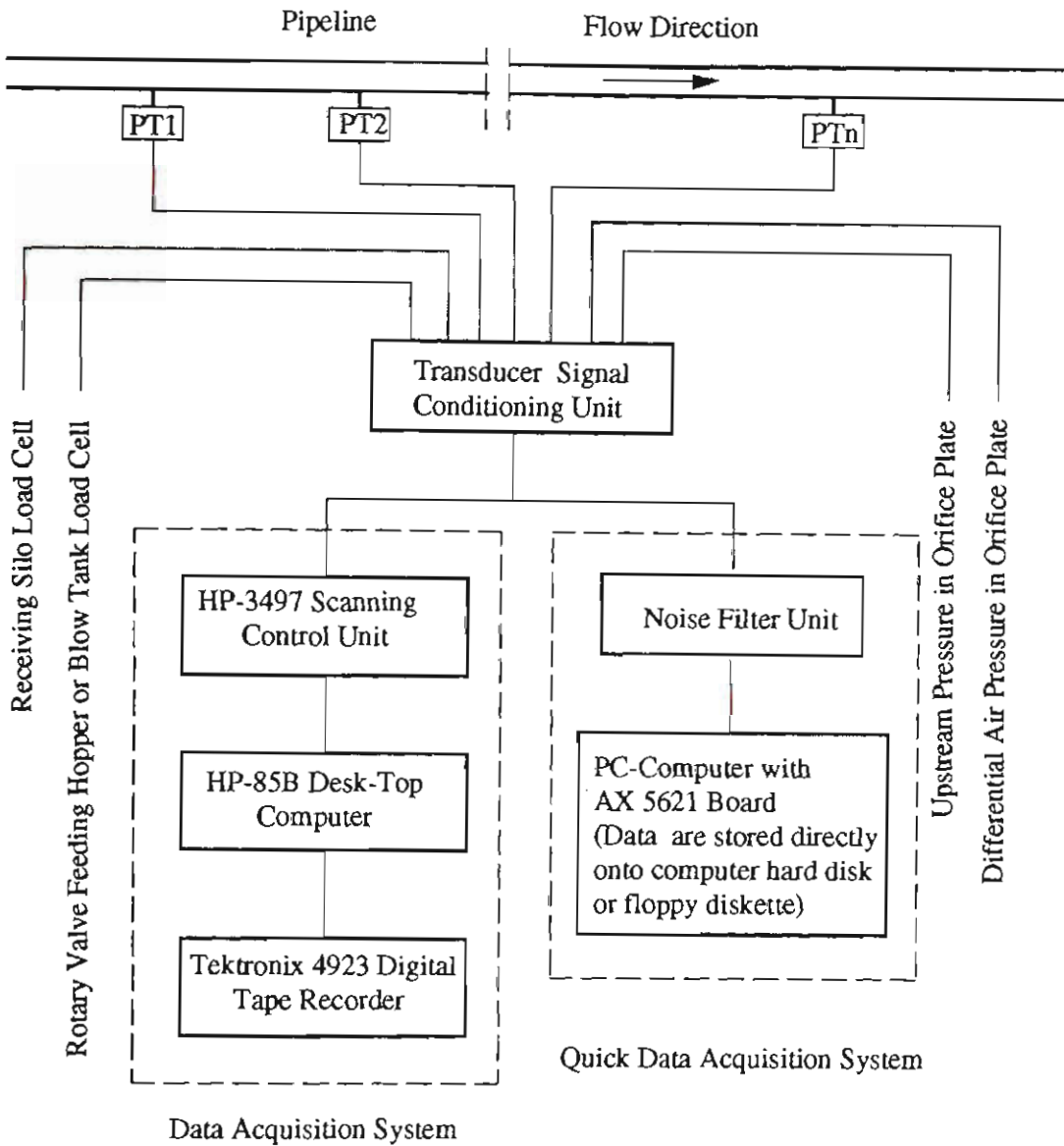


Figure 4.12 Data acquisition systems.

4.5.2 PC Based Quick Data Acquisition System

Due to the quite low sampling rate of the Hewlett-Packard 3044A system, it was not adequate for some requirements of measurement. For example, the determination of slug velocity by using cross correlation function technique required a high sampling rate to ensure good accuracy of results. Another reason for needing a high speed data acquisition system was that the pressure fluctuation in low-velocity pneumatic conveying is much more evident compared with dilute-phase conveying. A low speed data acquisition system may lose some frequency components and result in incorrect

information. Hence a new PC based "quick" data acquisition system was developed for this study on low-velocity pneumatic conveying, see Figure 4.12.

A compatible IBM-PC/XT or AT computer was selected. An AX5621 board, which is a high-speed, high-resolution analog-digital converter, was plugged into an expansion slot of the computer. Signal scanning was carried out by the board. A software package was written to control the operation of the board and arrange the collection and storage of the data in a useful format. A software package called "logger" was designed for this purpose. This new system was able to scan a maximum of 1000 scans for eight channels at a scanning rate of 160 Hz.

4.5.3 Data Processing

A data processing software package "HPPLT" was developed by previous researchers of the Bulk Solids Handling Research group and modified by the author with FORTRAN 77 language based on a compatible IBM-PC/XT or AT computer. The software supporting this processing was DOS and PLOTPACKAGE, which was developed by the University of Wollongong. All time history signals sampled by either the DAS or quick DAS were stored finally onto floppy diskettes as data files. A data processing computer can read the data files directly from the diskettes, then display the signals as required or carry out further calculations on the signals. The functions of "HPPLT" are listed below:

- 1 Print calibrated transducer responses with respect to cycle time
- 2 Plot pipeline air pressures at a particular cycle time
- 3 Plot multiple pipeline transducer responses
- 4 Calculate and plot mass flow-rate of air with respect to cycle time
- 5 Calculate flow characteristics

- 6 Plot conveying parameter relationships
- 7 Change the data (in Engineering Units)
- 8 Plot multiple pipeline transducer responses and mass flow-rate of air onto one screen
- 9 Finish

In these functions, Functions 3, 4, 5 and 8 are most commonly used. Functions 3 and 8 are similar, but Function 3 only displays one type of transducer response (e.g. air pressure), whereas Function 8 allows several types of transducer responses (e.g. air pressure, mass flow-rate of air etc.) to be shown simultaneously for ease of comparison. Typical graphic outputs generated by Function 8 are repeated in Figure 4.13, where the channels 0 and 1 are the wall pressure and static air pressure signals, respectively, the channels 8 and 9 represent the mass of material loaded into the silo and discharged from the feed hopper. Function 4 is used to calculate the mass flow-rate of air according to the orifice plate/annubar equation using the values of differential pressure and upstream pressure of the orifice plate/annubar. These calculated results can also be presented by Function 8, see Figure 4.13.

EXPERIMENT NO. 167 - 6
TOTAL MASS OF AIR USED (KGS) = 13.781
TEST DATE: 6/10/92

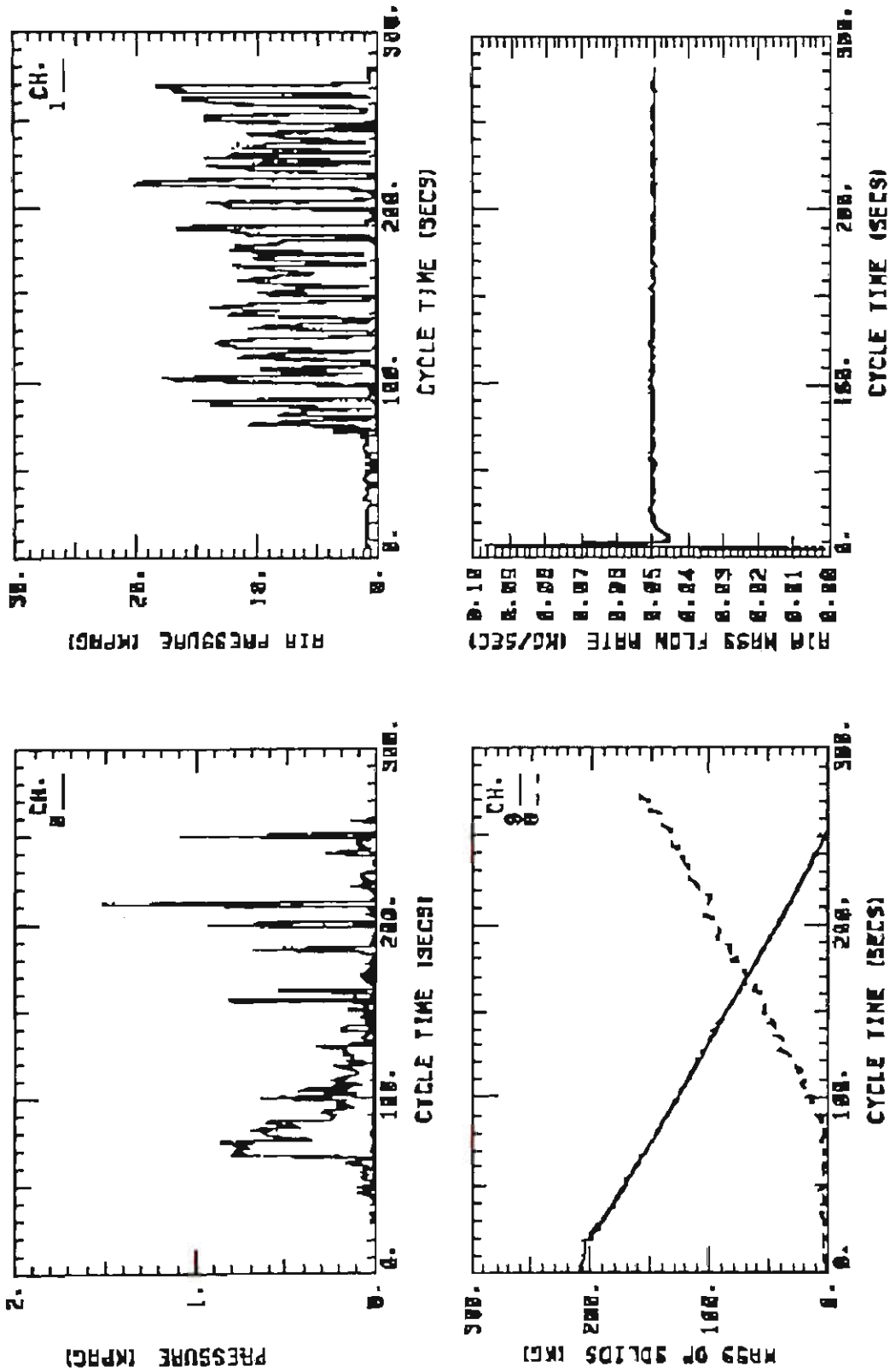


Figure 4.13 Typical graphic outputs from "HPPLT".

Function 5 is used for the statistical calculation of some major parameters, including the average value of the mass flow-rate of air in a specific time range, average air pressure and wall pressure, blow tank or rotary valve feed rate, etc.

If an experiment includes measurement of wall pressure, the wall pressure responses also can be subtracted from the total pressure by using the HPPLT software package.

Note that the slug velocity calculation based on cross correlation function analysis technique is not included in this software package.

4.6 Test Procedures

After all the instruments are installed as required, they are then connected to the relevant data acquisition system via a zero box. Experiments are carried out in the test rig using the following procedures.

4.6.1 System Check

To ensure the rig and experiments run smoothly and correctly, a system check is necessary. This work mainly includes double checking the installation of the pipeline system and various instruments, which can be verified easily via direct observation, and checking for air leakage at each pressure tapping point. For the low-velocity pneumatic conveying test rig, the air leakage check is carried out as the follows:

- (i) Block one end of the pipeline with a thin steel plate and close the back pressure valve, open the air supply valve to allow air into the pipeline.
- (ii) When the air pressure in the pipeline reaches a designated value (e.g. 100 kPag), close the air supply valve.
- (iii) Drop soapy water onto each tapping point and observe whether soapy bubbles appear.

- (iv) If so, open the back pressure valve to release the air in the pipeline, rectify the leak and then repeat the last step.

If wall pressures are to be measured, an extra check is needed for this measurement. This check is discussed in Chapter 7. After all these checks are completed, the test rig is ready for use.

4.6.2 Calibration

Transducers sense physical phenomena and provide electrical signals that a data acquisition system can accept. For example, load cells convert force into an analog electrical signal that the A/D converter (ADC) can measure and record. Other examples include pressure transducers, thermocouples and flow transducers which measure pressure, temperature and flow-rate, respectively. Although all the physical quantities are measured through different sensors, e.g. mass via load cells and air pressure via strain-gauge transducers, the actual engineering value cannot be read directly from the recorded values since they are all in the form of electrical output.

The electrical output of a good sensor should provide a linear relationship with the actual measuring quantity, as shown in Figure 4.14. The linearity represents the quality of the sensor. The slope of the line called the calibration factor of the transducer represents the sensitivity of the transducer. To obtain accurately the actual values of the measured quantities, the linear relationship must be determined by calibration. Generally, the calibration factor of a transducer is constant. However, variations in some environmental factors such as temperature, pressure, etc. will affect the characteristics of the sensor. Hence, it is required to calibrate various transducers periodically, especially before a new set of experiments. Standardised calibration procedures have been developed for load cells and pressure transducers by the Bulk Solids Handling Research group.

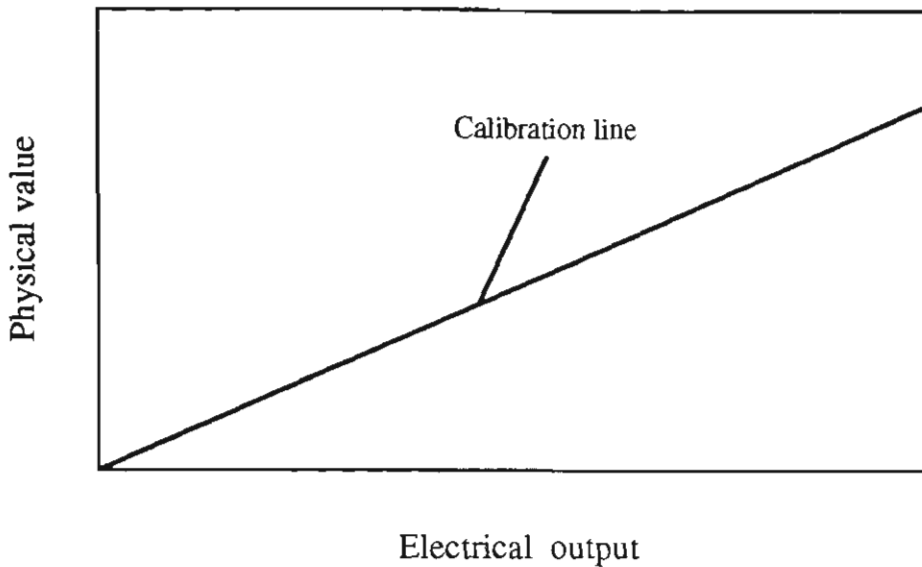


Figure 4.14 Linear relationship between physical phenomena and electrical signal.

4.6.2.1 Load Cell Calibration

Load cells which are used to support the rotary valve feed hopper, blow tank and product receiving silo, monitor the mass of material loaded in or discharged from these containers. Calibration of load cells is carried out by filling a given mass of product into the feed hopper. The detailed steps are:

- (i) Remove any previously conveyed material from the pneumatic conveying test rig and purge the rig with a high flow-rate of air until the pipeline and rig are believed clean. Record the voltage output of all load cells.
- (ii) Load a given mass of a product (say 40 kg) into the feed hopper or blow tank. Record the voltage output of the load cells.
- (iii) Transport this material to the receiving silo (using a high flow-rate of air to ensure no product is left in the pipeline) and record the voltage output from the load cells of the receiving silo.

- (iv) Discharge all the product from the receiving silo to the feed hopper (using the pulse valves to ensure no product is left in the receiving silo). Then add another given mass of product into the hopper and record the voltage.
- (v) Repeat steps (iii) and (iv) until all the designated product is loaded in the hopper.

The calibration of the load cells of the low-velocity pneumatic conveying test rig is presented in Figure 4.15. The linearity is quite good for each set of load cells. The calibration factors for the load cells of the feed hopper and receiving silo are 140.25 kg/mV and 376.67 kg/mV, respectively.

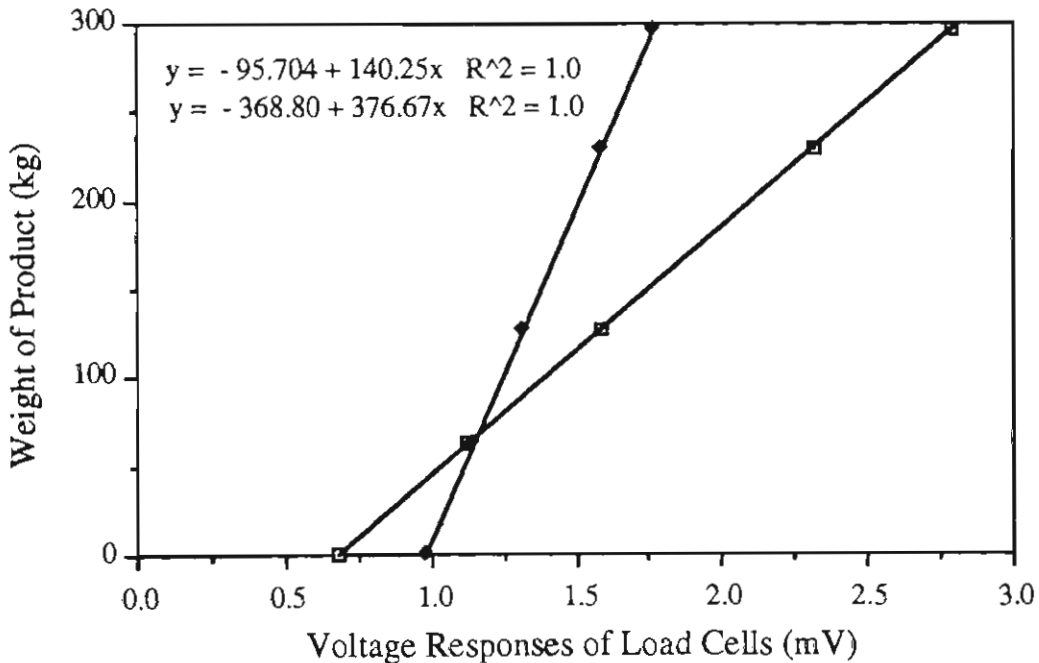


Figure 4.15 Calibration of load cells.

4.6.2.2 Pressure Transducer Calibration

All the pressure transducers used in the test program are calibrated by maintaining a constant pressure in the pipeline and recording simultaneously the voltage responses of the transducers. The calibration procedures can be summarised as follows.

- (i) Connect pressure transducers and a high accuracy pressure meter to the pipeline via pressure tappings.
- (ii) Purge the pipeline with a high flow-rate of air, block the pipeline at the product feed end with a steel plate and close the back pressure valve.
- (iii) Open the air supply valve, blow air into the pipeline until the pipeline pressure arrives at a designated value (e.g. 40 kPag), then close the air supply valve.
- (iv) Record the pressure value and the voltage responses of all the transducers after the pipeline pressure which is monitored by the pressure meter becomes stable.
- (v) Repeat steps (iii) and (iv) until the highest designated air pressure (i.e. the pressure slightly higher than the highest expected pressure occurring in the subsequent test program) is obtained. Open the back-pressure valve.

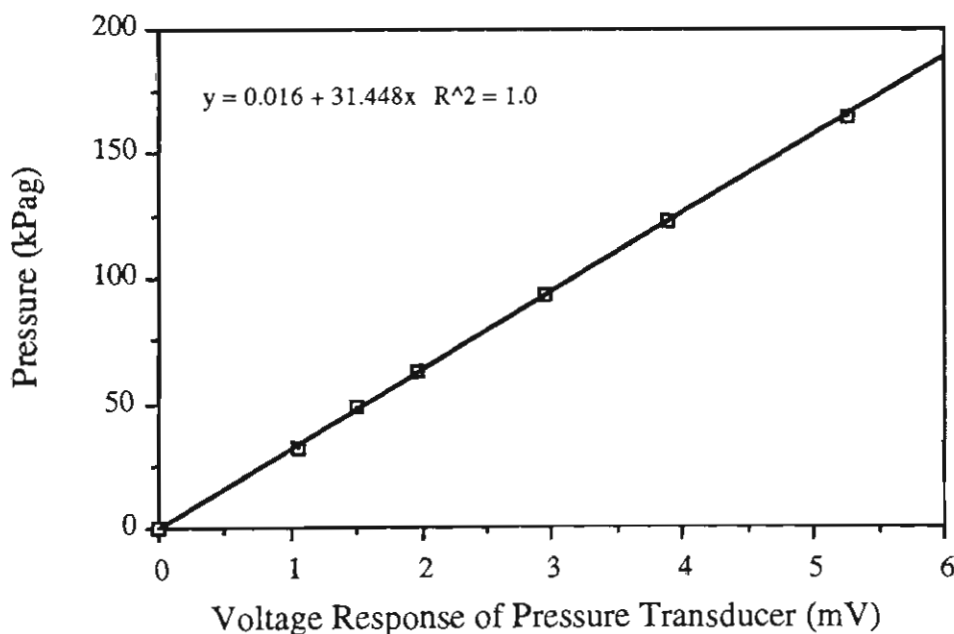


Figure 4.16 Calibration line of a pressure transducer.

A typical calibration line of a pressure transducer is presented in Figure 4.16. The calibration factor of the transducer is 31.448 kPa/mV.

4.6.3 Test Programs

The main test program is carried out on the low-velocity conveying test rig. Several materials are transported in the range of low-velocity pneumatic conveying. The selection and physical properties of these materials are discussed in the next chapter. The range of low-velocity pneumatic conveying is governed by the minimum and maximum possible mass flow-rate of air for a given mass flow-rate of solids, as shown in Figure 4.17.

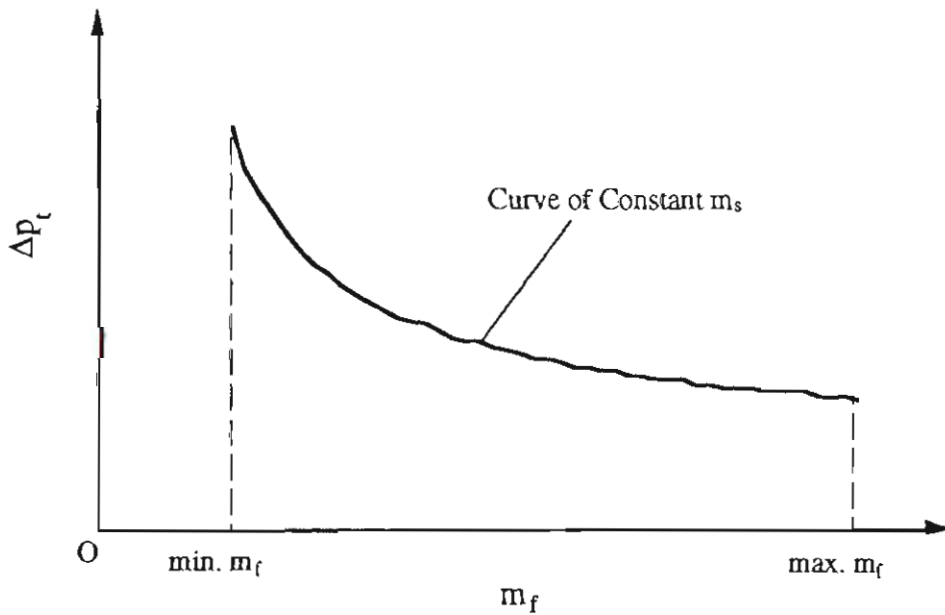


Figure 4.17 Range of low-velocity pneumatic conveying for a given m_s .

If a selected mass flow-rate of air is less than the minimum value, the rotary valve stops working due to material building up inside the feeding shoe. If the mass flow-rate of air is greater than the maximum value, the flow either goes unstable zone or changes to dilute-phase. The materials conveyed in this range (i.e. between the maximum and minimum mass flow-rate of air) form regular slugs without the aid of any slug forming device. Major parameters reflecting the features and affecting the pressure drops of low-velocity pneumatic conveying are measured during the main test program. In order to obtain relationships between the various parameters and low-velocity pneumatic conveying characteristics, the experiments on each type of material are divided into

several groups according to their mass flow-rate of solids to fulfil. The test program is designed as follows:

- (i) Adjust the rotary valve to a designated rotor speed (i.e. fix the mass flow-rate of solids), operate the first test with the minimum possible mass flow-rate of air.
- (ii) Still using the same rotor speed, conduct more experiments with increased values of m_f until the maximum mass flow-rate of air for low-velocity pneumatic conveying has been reached (i.e. for the given m_s).
- (iii) Alter the rotor speed, repeat steps (i) and (ii).

The operating procedures of each test are summarised below for the rig using the rotary valve feeder:

- (i) Open the silo valve and load sufficient material into the feed hopper, see Figure 4.2, then close the valve after loading.
- (ii) Adjust the rotor speed of the rotary valve to obtain a suitable mass flow-rate of solids.
- (iii) Predetermine a mass flow-rate of air by selection of the relevant critical flow nozzles, see Figure 4.8.
- (iv) Set the data acquisition system to scan the required channels at a suitable sampling rate.
- (v) Start the data acquisition system.
- (vi) After about 10 seconds, open the conveying air valve to introduce air into the pipeline.

- (vii) Operate the rotary valve and open the hopper valve to feed the material in the conveying pipeline.
- (viii) After all the material in the hopper has been conveyed into the silo, turn off the rotary valve.
- (ix) Keep the air blowing until all the material left in the rig and pipeline returns to the silo, then close the air supply valve.

In ensure good accuracy results, each test is repeated at least two times. In addition, each repeated experiment is scanned at different sampling rates to rationalise the memory limitation problem of the DAS. That is, at least one repeated experiment is scanned at a low sampling rate to make the total scanning time of the DAS cover the entire range of the test, and another repeated experiment is scanned at the maximum possible sampling rate of the DAS for measuring slug velocity.

In addition to the main experiments, other experiments were conducted on other test rigs with different configurations of pipeline (i.e. to confirm the validity of model predictions for different materials and pipe sizes). These experiments and relevant facilities are discussed in Chapter 9.

CHAPTER 5

TEST MATERIAL AND PROPERTIES

5.1 Introduction

Pneumatic conveying performance can vary considerably for different bulk materials. Some materials can be conveyed over a wide range of the flow conditions, from high-velocity, dilute-phase to low-velocity, dense-phase. Other materials, however, are restricted to dilute-phase only in conventional pneumatic conveying systems (i.e. using standard pipelines). Some cannot be conveyed pneumatically (e.g. 3 μm lead fume). In addition, materials which are capable of being conveyed pneumatically can exhibit for given conditions quite different levels of performance in terms of flow pattern, material throughput, etc., particularly at low velocity. It is believed that all these quite different performances are dependent on the properties of the materials to be conveyed. Hence for a pneumatic conveying system to be designed or upgraded to ensure satisfactory and efficient operation or the total pipeline pressure drop of an existing system to be predicted accurately, the influence of the properties of the materials must be considered properly. However, due to the complicated nature of two phase flow, it is quite difficult to determine how the properties of the materials exactly affect pneumatic conveying performance and behaviour.

A relatively reliable method for design and/or pressure prediction of a pneumatic conveying system accepted by most researchers and engineers is to undertake a series of experiments with a representative sample of the material in a pilot plant, then obtain the full scale plant data from the test rig results by using appropriate scale-up procedures. Obviously the pilot plant experimental results include the influence of the properties of the material, and this information is transferred to the full scale plant data by the scale-up procedures. A major disadvantage of this strategy is that it may be time consuming and costly. Therefore the ultimate aim of pneumatic conveying research is to design and/or predict pressure drop for a pneumatic conveying system without the need to carry out small or full scale conveying tests (i.e. to establish relationships between pneumatic conveying performance and the physical properties of the material).

In the case of bulk solids there are many terms that are used to describe the properties of a product. Many of these properties are used in qualitative, descriptive and empirical ways. They are often difficult to define precisely and even more difficult to measure. In this work, attention is given particularly to low-velocity pneumatic conveying. The properties possibly affecting the performance of this type of flow consist of particle size and distribution, density and flow properties. This chapter introduces these properties and their measurement method. In addition, four types of representative material are chosen according to the Dixon's classification [28] to carry out this research. Their properties are measured and presented.

5.2 Particle Size and Distribution

Particle size and distribution are the most often used characteristics of a bulk material. However, it is often difficult to define particle size. For regular shaped particles such as spherical or cubic particles, see Figure 5.1(a) and (b), the size can be defined easily as the largest linear dimension. For the spherical particle the size would be the diameter and for the cubic particle the corner-to-corner diagonal.

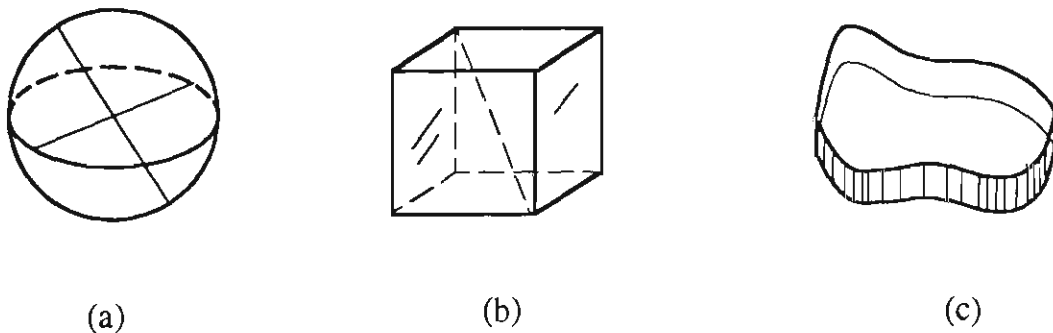


Figure 5.1 Regular and irregular shaped particles.

However, for irregular shaped particles, see Figure 5.1(c), terms such as length, thickness and diameter have little meaning as many different values for each can be determined from each single particle. In an attempt to represent the size of an irregularly shaped particle by a single quantity, the term most often used is equivalent diameter. This refers to the diameter of a sphere that exhibits the same behaviour as the particle when

subjected to the same sizing technique, e.g. the sphere that has the same projected area or mass or that just passes through a mesh aperture. Thus the measurement of the size (equivalent diameter) of particles is dependent on the method used to determine that parameter.

The particle size mentioned above actually indicates single particle size. The size and shape of particles that randomly make up a real bulk solid usually vary quite widely. In this case, a mean particle size is needed to represent the size nature of the bulk solid. Only after knowing the single particle size and distribution of a bulk solid, the mean particle size (equivalent diameter) of the bulk solid may be calculated by an appropriate method, such as the methods of arithmetic mean, geometric mean and log geometric mean, etc. Hence the size range (distribution) of the bulk solids also is an important parameter that defines the size nature of the bulk solid. There are many methods that can be used for determining the size distribution of particulate materials. These include:

- Mechanical sieving,
- Sedimentation,
- Microscopy,
- Electron microscopy,
- Scanning electron microscopy,
- Advanced optical methods (e.g. laser diffraction).

Mechanical sieving is the most widely used method for determining the size distribution of a bulk solid and is a process well known to most researchers and engineers, as it covers the range of particle sizes that are of considerable industrial importance. With this method, a bulk solid sample is placed on a nest of screens with precisely defined apertures. These sieves are either manually or mechanically shaken for a designated

period of time, resulting in a proportion of granules being retained on each screen. The particle size and distribution, as measured by sieving, can be defined by quoting the aperture of the two screens, one through which the particles pass and the other on which they are retained.

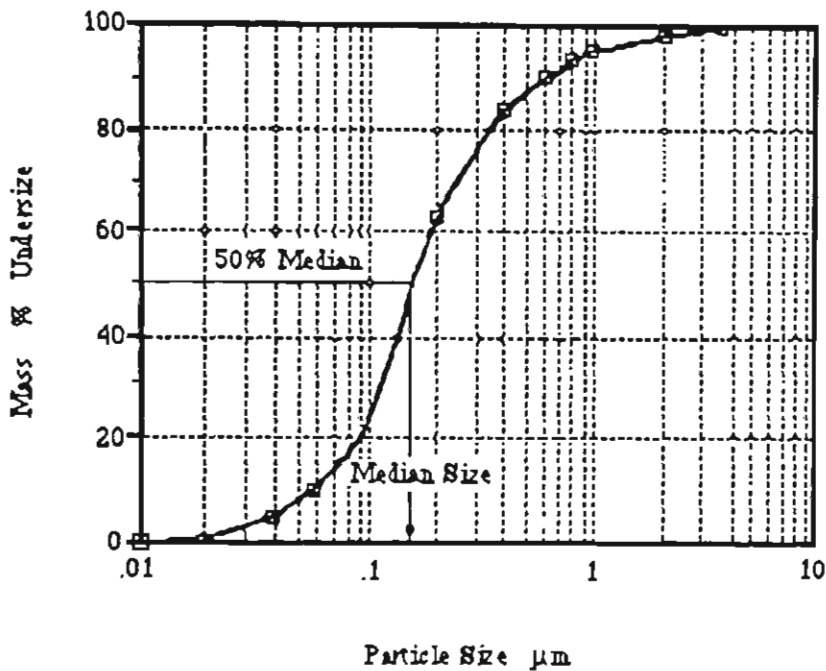


Figure 5.2 Particle size distribution.

For pneumatic conveying applications, the most useful approach is to plot the data graphically, as shown in Figure 5.2. This shows the particle size or equivalent diameter plotted against the mass percentage of the sample under a certain size. Such information gives an appreciation of the range of particle size constituting the bulk solid. A commonly used method for assigning a characteristic figure to this information is by quoting the median size. This is defined as the particle size which represents 50 % of the sample by mass.

In the case of monosized or nearly monosized particles, mean equivalent spherical size by mass is often employed. For large size particles like polyethylene pellets, the mean equivalent spherical size can be determined by the following equation as the numbers of known mass particles can be counted,

$$d = \sqrt[3]{\frac{6m}{\pi \rho_s n_p}} \quad (5.1)$$

where d is the mean equivalent particle diameter, m is the mass of particles, n_p is the number of the particles of the known mass, ρ_s is the particle density.

5.3 Density Analysis and Measurement

A bulk solid consists of many randomly grouped particles. This bulk material has an apparent bulk density, i.e. the mass of the bulk divided by the volume of the particles and voids contained in the bulk. Besides the bulk density, each particle that makes up the bulk solid has particle density. Generally speaking, the particle density is constant, the bulk density is not unique for a bulk material. It is dependent on the particle density, particle shape and how the particles are packed or positioned with respect to one another. The bulk density and particle density are both parameters of primary importance in the investigation of pneumatic conveying.

It is well known that specific weight is often used in fluid research instead of density. Since bulk materials have some similar features to fluid, specific bulk and particle weight of the bulk materials are defined as the bulk and particle density relative to the density of water at 4 °C.

5.3.1 Particle Density

Particle density can often be measured using an air comparison pycnometer or stereo pycnometer. In this study, a stereo pycnometer is used for most measurements of particle density. It employs Archimedes principle of fluid displacement to determine the volume of the solid objects. The displaced fluid is a gas which can penetrate the finest pores to assure maximum accuracy. A diagram displaying the principle of the stereo pycnometer is presented in Figure 5.3.

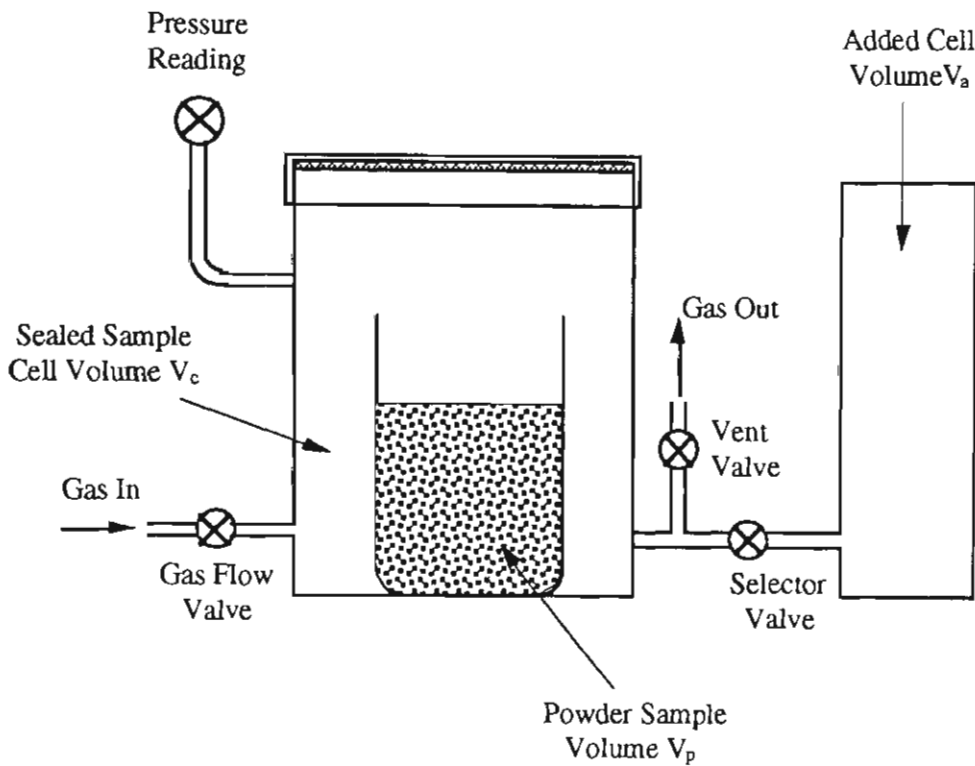


Figure 5.3 Schematic of stereo pycnometer.

The device consists of two cells (i.e. the sealed sample cell and added cell) with volumes V_c and V_a connected through a selector valve. A pressure transducer is installed in the sample cell to allow accurate monitoring the system pressure. The basic operating procedures are stated below:

- (i) Open the vent valve and selector valve to bring the system to ambient pressure, then close the selector valve carefully.
- (ii) Place a given volume of bulk solid sample in the sample cell, then close the vent valve and seal the sample cell.
- (iii) Open the air flow valve and pressurise the sample cell to a designated pressure p_2 (e.g. 17 psig) above ambient.
- (iv) Open the selector valve to connect the added cell with the sample cell, then the air in the sample cell flows into the added cell, the pressure will fall to a lower value p_3 .

- (v) Calculate the particle volume according to the following equation:

$$V_p = V_c + \frac{V_a}{1 - p_2/p_3} \quad (5.2)$$

It should be noted that either the comparison- or stereo- pycnometer only measures the average particle density of a bulk solid. The densities of different constituent particles in a blended product can be determined by measuring them before mixing. Also, the pycnometer yields the apparent particle density which is the mass of product divided by the occupied volume including closed pores but excluding open pores.

5.3.2 Bulk Density

Bulk density does not have an unique value for a particular bulk solid and it varies with the condition of the bulk solid. For example, a bulk solid that has been conveyed pneumatically may be aerated and have a lower bulk density than if it had been allowed to de-aerate. It is not always easy to determine the bulk density of a product under changing consolidation conditions. Since it has been concluded in Chapter 3 that particle slugs have approximately a loose-poured bulk density in low-velocity pneumatic conveying, only the loose-poured bulk density is discussed here.

Loose-poured bulk density usually can be obtained by the following steps:

- (i) Pour carefully and gently a certain volume of bulk solid into a measuring cylinder. Note that the measuring cylinder must be held at an angle of 45° to the horizontal when pouring to avoid compaction.
- (ii) Bring the cylinder upright and note the volume occupied by the bulk solid.
- (iii) Weigh the cylinder and bulk solid and deduce the mass of the bulk solid.
- (iv) Determine the loose-poured bulk density by knowing the mass and the poured volume of the bulk solid.

5.3.3 Bulk Voidage

The space of bulk material is not occupied completely by the particles that make up the bulk material. Part of the space is filled by voids. The volume ratio of the total voids to the bulk material is defined as the bulk voidage of the material. The bulk voidage can be calculated theoretically by using geometry for the bulk material which only consists of mono-sized spherical particles. However, due to the different arrangements of the particles, the bulk voidage can vary from 0.26 to 0.47 [120] even though the particle size does not change, as shown in Figure 5.4. Also for multi-sized particles, many other factors such as size, shape and distribution of particles and degree of consolidation affect the value of bulk voidage. Hence, it is very difficult to calculate bulk voidage directly from geometry.

Please see print copy for image



Figure 5.4 Different arrangements of particles [120].

However, bulk voidage has the following relationship with particle density and bulk density,

$$\varepsilon = 1 - \frac{\rho_b}{\rho_s} \quad (5.3)$$

Hence the bulk voidage of a bulk solid is often calculated from the above equation after measuring the bulk density and particle density of the bulk solid.

5.4 Flow Properties of Bulk Material

The flow properties of bulk material mainly include internal and effective friction angle and wall friction angle, which are of special interest to pneumatic conveying.

5.4.1 Internal and Effective Friction Angle

Figure 5.5 shows a Jenike shearing test [121]. The shear cell, see Figure 5.5, is composed of a base which is located on a frame, a shearing ring which rests on the top of the base, and a cover which has a loading bracket attached to it. The test apparatus permits failure to develop only along the shear plane.



Figure 5.5 Jenike shearing test [121].

A bulk solid is placed in the shear cell and loaded by a normal force V . After applying a shearing force S through the shearing ring, the normal stress $\sigma (= V/A_c)$ and shearing stress $\tau (= S/A_c)$ occur along the shear plane, where A_c is the cross-sectional area of the shear cell. If S is less than the maximum possible shearing force corresponding to a given normal force V , then no continuous deformation occurs. However slip takes place along the shear plane as soon as S reaches its maximum value. If a σ_n - τ_n coordinate system is introduced to generate a shear-compressive stress diagram, the stresses on the shear plane at shearing can be expressed by a circle C , as shown in Figure 5.6.

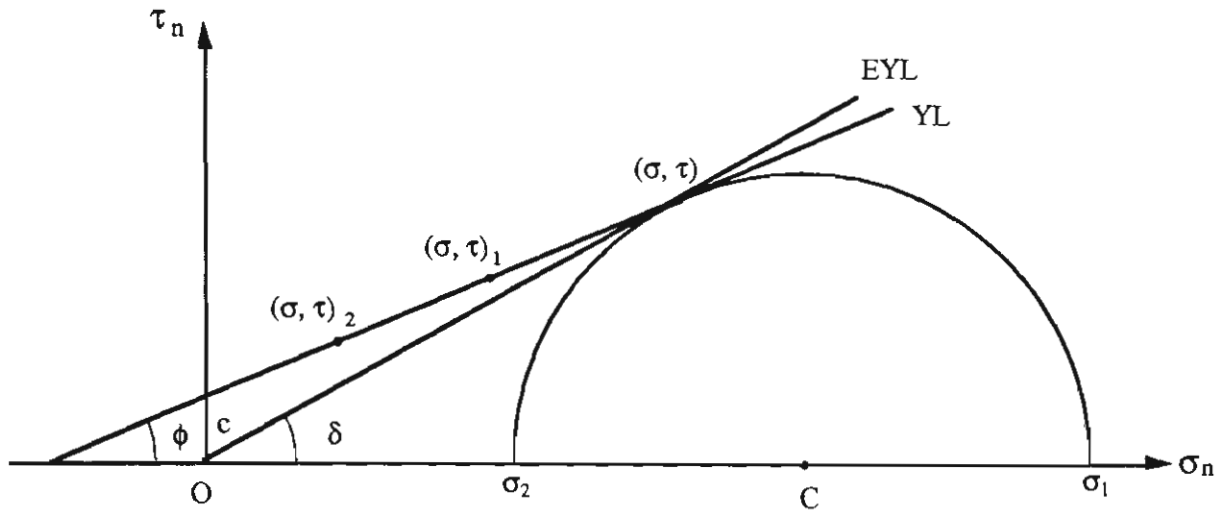


Figure 5.6 Mohr circle and yield locus of cohesive material.

This circle is called the Mohr circle. Note σ_1 and σ_2 are major and minor normal stress. If repeating the direct shear test for the sample with the same initial void ratio (i.e. same consolidating pressures) but with a range of constant V values, a yield locus (YL for short), which is called the Mohr failure envelope, can be obtained, see Figure 5.6. For the values of the normal stress and shearing stress (σ, τ) lying below that line, the solid can be considered to behave rigidly (or elastically), for the values lying on the line, failure or yield occurs. The locus (envelope) usually can be represented approximately by a straight line. If the slope and intercept of the line are designated as ϕ and c , respectively, then the locus in Figure 5.6 may be written as

$$\tau = \sigma \tan \phi + c \quad (5.4)$$

The form of Equation (5.4) was firstly given by Coulomb in 1776 and hence, is called the Coulomb failure criterion. ϕ and c in Equation (5.4) are called internal friction angle and cohesion of the bulk solid.

As shown in Figure 5.6, the tangent to the Mohr circle C and passing through the origin of the σ_n - τ_n coordinate system is called the effective yield locus (EYL for short). The angle δ between the effective yield locus and σ_n -coordinate in Figure 5.6 is called the

effective friction angle. Using angle δ , the following relationship between major stress and minor stress can be given [121],

$$\frac{\sigma_1}{\sigma_2} = \frac{1 + \sin \delta}{1 - \sin \delta} \quad (5.5)$$

For cohesionless solids, such as dry sand and plastic pellets, the yield locus passes through the origin of the normal stress and shearing stress axes. This yield locus coincides with the effective yield locus (EYL). The internal friction angle ϕ is equal to the effective internal friction angle δ . The discussion hereafter for flow properties of bulk materials is limited to this situation, since all the materials selected in this thesis for the conveying trials are cohesionless bulk solids.

Internal and effective friction angle can be measured by a Jenike direct shear tester as shown in Figure 5.7. The tester includes a shear cell of circular shape, a gravity vertical loading system which applies a normal force on the top of the shear cell, a driven loading stem which moves horizontally and generates the shearing action. The shear force is measured by a load cell and recorded by a chart recorder.

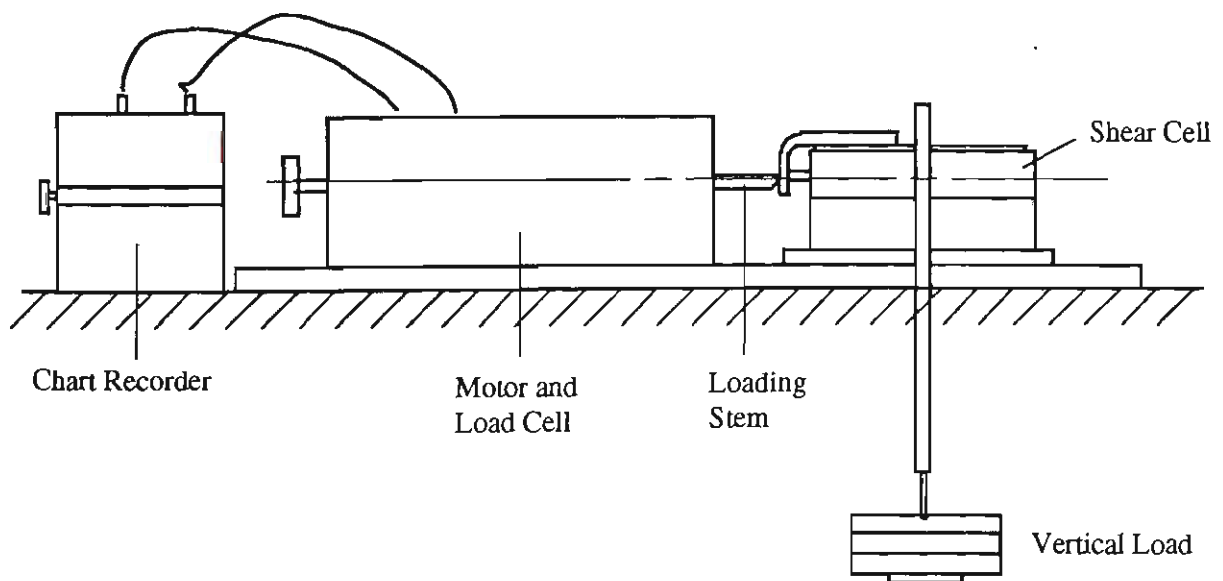


Figure 5.7 Jenike direct shear tester.

The test procedure is summarised below:

- (i) Turn on the Jenike shear tester and chart recorder, then calibrate the chart recorder.
- (ii) Undertake preconsolidation of the sample, i.e.
 - Put the shear cell rings with a mould ring on the frame of the tester and fill with the sample (do not press down on the sample).
 - Place the twisting top on the mould ring, apply weight W on the twisting top by a weight hanger and then twist the top for a given number of times.
 - Take the hanger with weight and mould ring off, scrape off the excess sample flush with the rings.
- (iii) Undertake consolidation of the sample (running a test), i.e.
 - Place the cover of the shear cell on the top ring, add shear weight V by the hanger and then turn on the force actuator.
 - Check the chart recorded results, turn off the force actuator after run the test full time.
 - Repeat from step (ii) onwards adjusting preconsolidation weights and twists until the correct result is obtained, i.e. chart flattens out.
 - Turn off the force actuator, take off the shear weight and put on shearing weight V' , V'' and V''' , respectively.
 - Write down the first height, i.e. where it flattens out, S and corresponding second height, i.e. where the top of the peak is in the chart recorder, S' , S'' and S''' .

- Draw a straight line passing through points (V', S') , (V'', S'') and (V''', S''') and a semi-Mohr circle tangential to the straight line and passing through the point (V, S) , as shown in Figure 5.8.

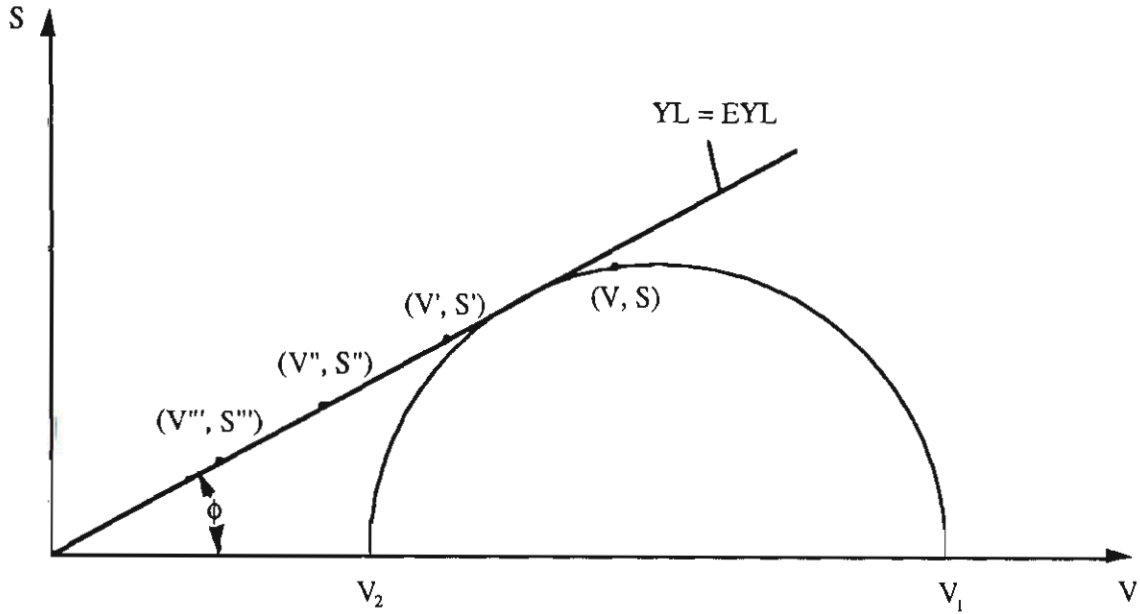


Figure 5.8 Typical measured yield locus.

This straight line is the yield locus of the bulk material and the slope of the yield locus defines the internal friction angle ϕ . If the material is cohesionless, the line will pass through the origin of the normal force and shear force axes, the angle between yield locus and V axis also is the effective friction angle δ . The semi-Mohr circle defines the major and minor principle forces V_1 and V_2 , see Figure 5.8. In order to obtain better results, it usually is necessary to repeat from step (ii) onwards using adjusted shear weights.

5.4.2 Wall Friction Angle

As shown in Figure 5.9, a direct shearing test is carried out by applying a normal force V and shearing force S on the shear ring. Failure occurs on the boundary of the bulk solid and wall as soon as S gets to a particular value. Repeat the shearing test for the sample with the same initial void ratio but with a range of constant V values. A wall yield locus (WYL for short) is obtained on the σ_n - τ_n coordinate system, as shown in Figure 5.10. The wall yield locus is another Coulomb friction line and is often in the form of a convex-

upward curved line. For a cohesionless material, the curve passes through the origin of the σ_n - τ_n coordinate system. The angle ϕ_w between the curve and σ_n -coordinate is called the wall friction angle.

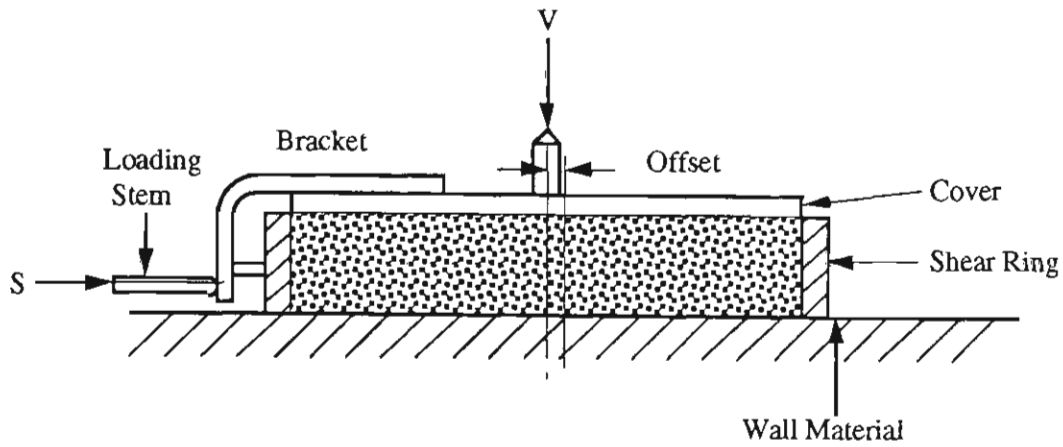


Figure 5.9 Arrangement for wall yield locus test.

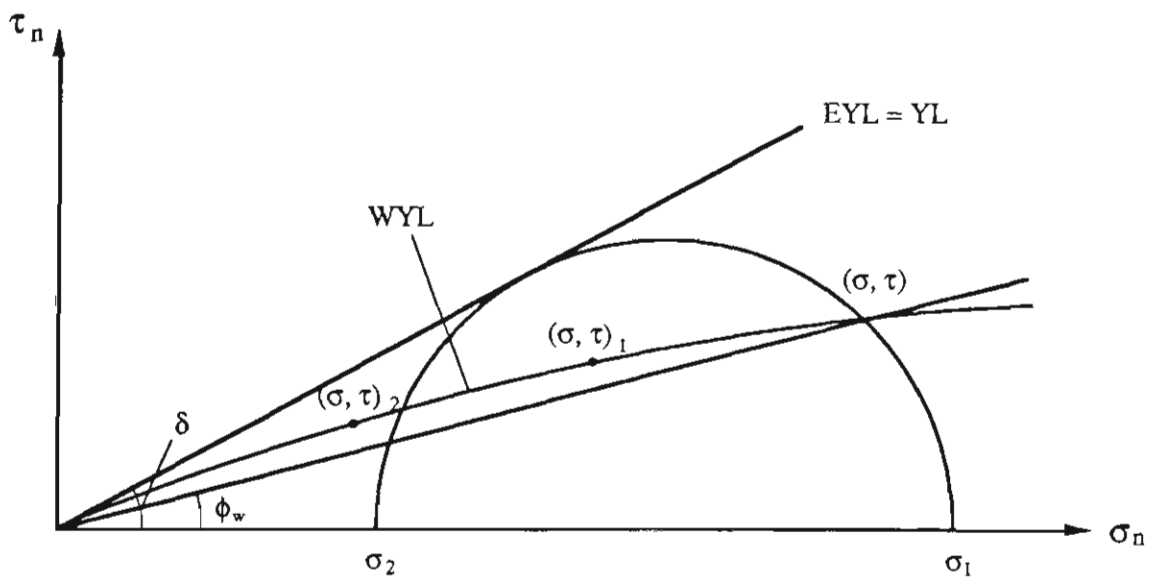


Figure 5.10 Wall yield locus.

Since the wall yield locus is usually represented by the curved line, the wall friction angle ϕ_w varies and is a function of the pressure at the wall. In practice, the following technique is used to determine the wall friction angle ϕ_w for a cohesionless material:

firstly, determine the value of the effective friction angle δ of the bulk material and the value of the major compressive stress σ_1 under a certain preconsolidation. Draw the EYL and tangential to the semi-Mohr circle passing through σ_1 , see Figure 5.10. Then draw a straight line from the origin to the point (σ, τ) which is the intersection of the semi-Mohr circle with the WYL. Finally, find the angle between the straight line and σ_n -coordinate. The Coulomb failure criterion can be written as follows for the boundary of bulk material and wall:

$$\tau = \sigma \tan \phi_w \quad (5.6)$$

where ϕ_w is the wall friction angle.

The wall friction angle can also be measured by the Jenike direct shear tester. The arrangement for the wall friction angle test is referred to in Figure 5.9. The test of the wall friction angle is much easier to be carried out than that of the internal friction angle. The measurement steps can be summarised as follows.

- (i) Turn on the Jenike shear tester and chart recorder, then calibrate the chart recorder.
- (ii) Set a material plate (i.e. wall) correctly and place the shear ring with a mould ring on it, then load the sample.
- (iii) Preconsolidate the sample with a given weight on a hanger (e.g. 18 lb including the hanger weight).
- (iv) Remove the weight hanger and mould ring, scrape off the excess sample so that it is flush with the shear ring.
- (v) Place the cover of the shear cell on the shear ring, then put the hanger on the cover, add 8 x 2 lb weights (normal forces V) on the hanger.

- (vi) Twist and lift the shear ring slightly so that it does not touch the plate (i.e. wall), turn on the loading stem advance.
- (vii) Observe the chart recorded results, while it rises to a peak, remove one 2 lb weight.
- (viii) When levels appear, remove another 2 lb weight until all 8 weights and the hanger have been removed, turn off the pusher and wind back the loading stem and shear ring to start.
- (ix) Take 10 readings of the shearing forces S and write them down.
- (x) Repeat from steps (vi) to (ix) until two similar results (shearing forces) are obtained.
- (xi) Draw the wall yield locus using the recorded normal forces and the corresponding average values of the two similar shear force results, as shown in Figure 5.11. The angle between the wall yield locus and normal force axis is the wall friction angle.

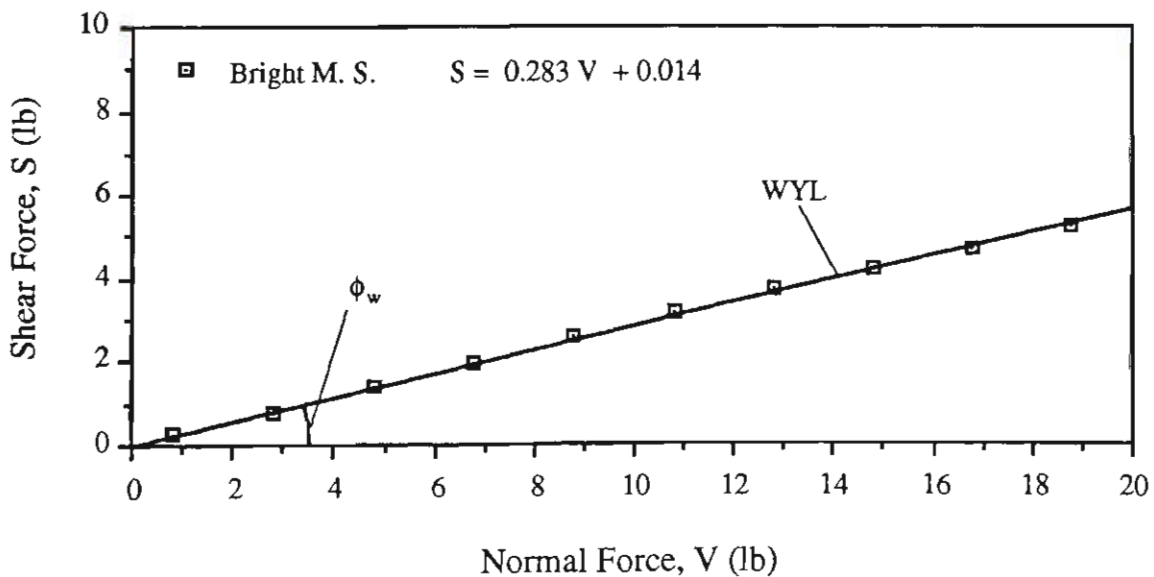


Figure 5.11 Wall yield locus for polystyrene chips.

5.5 Test Materials

Most bulk materials can be conveyed pneumatically in dilute-phase. However, a large number of materials are not suitable for dense-phase pneumatic conveying whilst others can be conveyed pneumatically in dense-phase only by the help of special apparatus (e.g. by pass, air knife, etc). Hence "conveyability" of bulk materials becomes an important design issue for dense-phase pneumatic conveying. Many researchers [28, 39, 41, 57, 58, 78] have carried out investigations into the suitability of bulk materials for dense-phase pneumatic conveying. Among them, Dixon's investigation [28] is used extensively by the researchers of low-velocity slug-flow pneumatic conveying.

Dixon [28] recognised that the fluidisation properties of a product have significant influences on its conveyability in dense-phase. Hence he classified the materials into four groups and generated the Dixon's diagram according to the fluidisation properties, refer to Figure 2.1. He then produced a theoretical approach for predicting the boundaries between the expected flow behaviours, based on equating gas slug velocity and single particle terminal velocity in vertical pipes.

According to the Dixon's slugging diagram for the 100 mm diameter pipe and his suggestion, materials in Group D appear to be the best candidate for natural slugging dense-phase pneumatic conveying. Hence to ensure the main test program of this research is successful, four types of material in Group D category are selected to undertake the low-velocity pneumatic conveying experiments. These materials are white plastic pellets, black plastic pellets, wheat and barley. Each material has nearly monosized particles size and similar particle shape. All these materials are found in following tests to have good conveyability in low-velocity pneumatic conveying. The major properties of the materials have been measured with the methods mentioned in the previous sections of this chapter. Table 5.1 lists the physical properties of these materials.

Table 5.1: Physical Properties of Test Material.

Bulk Solid	d (mm)	ρ_s (kgm ⁻³)	ρ_b (kgm ⁻³)	γ_s	γ_b	ϵ	ϕ_w^* (°)	ϕ (°)
White Plastic Pellets	3.12	865.1	493.7	0.865	0.494	0.430	15.15	44.70
Black Plastic Pellets	3.76	834.1	458.0	0.834	0.458	0.451	12.95	43.76
Wheat	3.47	1449.0	811.5	1.449	0.812	0.440	16.01	43.73
Barley	3.91	1350.0	721.7	1.350	0.722	0.465	14.20	31.07

* Wall material is bright mild steel.

CHAPTER 6
VELOCITY OF PARTICLE SLUG

6.1 Introduction

In pneumatic conveying systems, particles and conveying air are both moving entities. In order to describe and research flow pattern, velocities are used for the particles and conveying air. Both are very important parameters in the investigation of pneumatic conveying projects. They determine not only whether a bulk solid can be conveyed successfully in a pneumatic conveying system under given conditions (e.g. suspension, duning or plug/slug flow), but also whether the conveying system is operating efficiently and satisfactorily. There are many other reasons to carry out investigations into these velocities:

- Air velocity determines the conveying performance and total power consumption of a pneumatic conveying system.
- Transfer of energy from the air-stream to the particles takes place as a result of the drag force arising from relative or slip velocity (difference between the air velocity and particle velocity).
- Particle velocity determines the material output of pneumatic conveying. For low-velocity slug-flow pneumatic conveying, it also determines the total length of the pipe which is completely occupied by particles. Total pipeline pressure drop is dependent on this length.
- Particle velocity affects the inner stress state and distribution of particle slug during low-velocity pneumatic conveying.
- Particle velocity affects particle damage/attrition and pipeline wear, etc.

In pneumatic conveying, the air velocity is relatively simple to determine compared with the particle velocity. Hence, particle velocity has received much attentions in research. In the past years, many investigations [2, 38, 69, 71, 84, 85, 113] into particle velocity

have been completed and most of these have dealt with dilute-phase conveying. For low-velocity pneumatic conveying, only a few workers [69, 71, 84, 85] have investigated slug velocity, which reflects more the moving nature of the particles since the particles travel in the form of slugs. For example, Nicklin et al. [84] gave rise to the following form of correlation for vertical air-water system.

$$U_s = k_1(U_a - U_{mf}) + 0.35(gD)^{1/2} \quad (6.1)$$

where k_1 is a constant and is generally about 1.0 when the slugs have reached a stable size, U_a is the superficial air velocity, U_{mf} is the incipient fluidisation air velocity, g is the acceleration due to gravity and D is the pipe diameter.

As the behaviour of low-velocity pneumatic conveying is analogous to the behaviour of a gas-liquid system, it is accepted by most researchers that much of the theory for the latter can be applied to slug flow.

Legel and Schwedes [71] only measured the slug velocity of various materials and pipes and presented the measured results. No further work was undertaken for exploring the relationship between the slug velocity and its influential factors.

Konrad et al. [69] developed a third order equation model of slug velocity for horizontal slug-flow by using two phase theory. However, there exists some weaknesses in the model. Firstly, the model is too complex to be solved easily. Secondly, many assumptions are involved in the development of the model, such as the packed bed model of slug are doubtful. Thirdly, the model was found by the author's experiments in this research to be inaccurate.

For this reason, the work in this chapter deals with measuring various slug velocities by using the cross correlation function analysis technique while materials flow through a horizontal pipe. Then further work is carried out to develop a simple empirical model for predicting slug velocity based on the measured results.

6.2 Definitions of Velocity

Before undertaking the velocity investigation, velocities for describing different terms are firstly defined to avoid confusion.

6.2.1 Velocities for Fluid Medium

The fluid medium in pneumatic conveying is air. Air velocity and superficial air velocity are frequently used to describe the speed of the air. The air velocity is the actual velocity of conveying air in a pipe. Due to the variation of the air velocity at a cross section of pipe, mean air velocity is often employed to represent the air velocity. If there is only air flowing at a given flow-rate through a pipe, the mean air velocity at a cross section of the pipe can be determined easily from:

$$U_{ra} = \frac{m_f}{\rho_a A} \quad (6.2)$$

where U_{ra} is the air velocity, m_f is the mass flow-rate of air, ρ_a is the air density, A is the cross sectional area of the pipe.

However during pneumatic conveying, part of the space of the pipe is occupied by conveyed particles. If the voidage is known as ϵ (i.e. the volume ratio of the air to pipe in a certain length) in the conveying pipe, the actual mean air velocity is found to be

$$U_{ra} = \frac{m_f}{\rho_a \epsilon A} \quad (6.3)$$

Due to the variation of ϵ along the pipeline, the determination of the actual air velocity is complicated and extremely difficult. For this reason, superficial air velocity is introduced to the research of pneumatic conveying to represent the motion of air. The superficial air velocity is defined by the following equation,

$$U_a = \frac{m_f}{\rho_a A} \quad (6.4)$$

From this definition, it is found that the superficial air velocity is analogous to air velocity without particles flowing in the pipe for the same flow-rate of air.

6.2.2 Velocities for Particulate Medium

Particle velocity is often used to describing the motion of the particulate medium in pneumatic conveying. Strictly speaking, particle velocity indicates the actual moving speed of a particle. However, the motion of each particle is very complex and random in pneumatic conveying. Even in dilute-phase conveying, determining the motion and velocity of the particle at the time becomes almost impossible. In order to simplify the research into particle velocity, mean particle velocity generally is accepted by researchers. Many factors affect particle velocity (e.g. superficial air velocity, air and particle properties, etc.), hence the research into particle velocity is rather difficult, particularly on a theoretical basis.

When conveyed in the form of slugs during low-velocity pneumatic conveying, particles appear to be bound together. Obviously, slug velocity mainly reflects the particle motion in low-velocity pneumatic conveying. Hence it is reasonable to select slug velocity to describe the motion characteristics for the particulate medium in low-velocity pneumatic conveying. Since the velocities of the particles contained in a slug are not completely same, the slug velocity is defined in this study as the mean velocity of all the particles contained in the slug, that is

$$U_s = \frac{n_1 u_{p1} + n_2 u_{p2} + \cdots + n_k u_{pk}}{n_1 + n_2 + \cdots + n_k} \quad (6.5)$$

where $u_{p1}, u_{p2}, \dots, u_{pk}$ are the velocities of the particles in different parts of the slug and n_1, n_2, \dots, n_k are the numbers of the particles which have the particle velocities of $u_{p1}, u_{p2}, \dots, u_{pk}$.

Note that due to the compressibility of air, both air velocity (or superficial air velocity) and particle velocity (or slug velocity for low-velocity pneumatic conveying) vary along the length of the pipeline during pneumatic conveying.

According to the visual studies of particle motion in a slug, the slug can be divided into three sections, as shown in Figure 6.1.

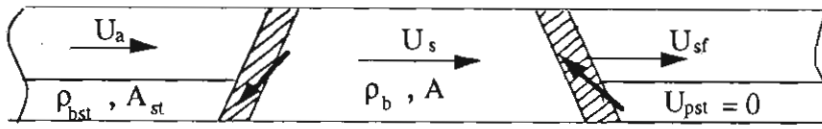


Figure 6.1 Slug flowing in a horizontal pipe.

For a steady flowing slug, most of particles are included in the middle part of the slug, these particles are basically fixed relative to each other and all move with the same velocity.

The front and back areas are the transition sections of the slug. In the front face, particles are collected from the stationary bed and join in the slug, the velocities of the particles increase from zero to a certain value. In the back face, the slug deposits particles to the pipe, the velocities of the particles in this area decrease from a given value to zero. Hence, the motions of the particles in these two transition sections are complex due to the variation of the moving speed and direction of the particles.

If the average velocities of the particles at the front and back areas are known as U_{pf} and U_{pb} , Equation (6.5) is simplified as follows:

$$U_s = \frac{n_p U_{pm} + n_f U_{pf} + n_b U_{pb}}{n_p + n_f + n_b} \quad (6.6)$$

where U_{pm} is the particle velocity at the middle part of the slug, n_p is the number of the particles which have velocity U_p , and n_f , n_b are the numbers of the particles staying at the front and back sections of the slug. Normally $n_p \gg n_f + n_b$, thus the slug velocity is close to the particle velocity in the middle part of the slug.

While a particle slug is moving forward, particles will join into the slug from the stationary bed. The front surface of the slug grows continuously and the front surface appears to move at a higher velocity than the average particle velocity. Similarly, the back surface of the slug obtains a higher back surface velocity due to the particles leaving the slug continuously. If the slug and stationary bed have the same bulk density of ρ_b , and if the same quantity of particles are collected from and deposited to the stationary bed, the relationship between the surface velocity and slug velocity can be derived from a mass balance as:

$$U_{sf} = U_{sb} = U_s \left(1 - \frac{A_{st}}{A} \right)^{-1} \quad (6.7)$$

Some researchers, such as Konrad et. al. [69], defined the slug velocity as the surface velocity in their investigations.

6.3 Experimental Determination of Slug Velocity

In order to obtain some practical knowledge about slug velocity, experiments have been conducted under various conveying conditions. The actual velocities of slugs have been measured from the experiments.

There are several ways for measuring particle velocity in pneumatic conveying. Among these, the cross correlation function analysis technique is often selected by many investigators. This method does not need extra apparatus and instruments and can obtain high accuracy of measurement. The measurement of slug velocity for low-velocity pneumatic conveying by using the cross correlation function analysis technique is discussed in the following section.

6.3.1 Principle and Method of Slug Velocity Measurement

Figure 6.2 shows two continuous-time waveforms, say $x(t)$ and $y(t)$. In order to describe the general dependence of one on the other, the cross correlation function is defined:

$$R_{xy}(\tau_d) = \lim_{T \rightarrow \infty} \frac{1}{T} \int_0^T x(t) y(t + \tau_d) dt \quad (6.8)$$

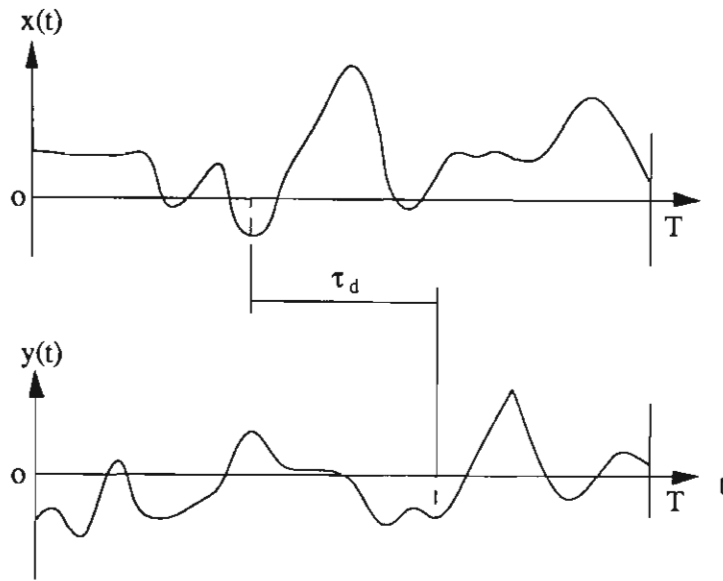


Figure 6.2 Time history records.

A typical plot of the cross correlation function versus time displacement for a pair of time history records is illustrated in Figure 6.3. When $R_{xy}(t) = 0$, $x(t)$ and $y(t)$ are said to be uncorrelated. The plot will sometimes display peaks which indicate the existence of correlation between $x(t)$ and $y(t)$ for a specific time delay (τ_p), see Figure 6.3.

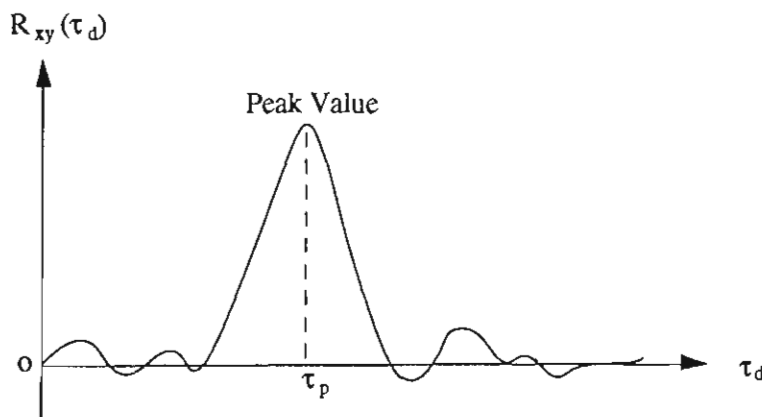


Figure 6.3 Typical cross-correlation plot.

According to this, if two correlated signals are obtained, the time delay between the signals can be established by noting the time displacement associated with an observed peak in the cross-correlation function graph. It is this principle that is applied to

measuring particle (or slug) velocity in a pneumatic conveying system. The following discusses the application of the cross correlation function and the basic method of measurement of particle slug velocity.

Figure 6.4 shows a low-velocity pneumatic conveying pipeline. While a particle slug passes point 1, the circumstances around point 1 (e.g. charge, capacitance, wall pressure, etc.) will change due to the slug appearing at that point. A short time τ_p later, the particle slug moves to a downstream point (e.g. point 2 in Figure 6.4). Affected by the slug, the circumstances there will certainly change too. If the distance between point 1 and 2 is close enough, the conditions of the particle slug will not change greatly while the slug moves from point 1 to point 2. The circumstances around point 1 and 2 have similar variations caused by the same slug. According to this, two sensors are installed at point 1 and 2 to receive the signals that reflect the variations of the circumstances. The received signal from point 1 correlates with the signal received from point 2 after the transit time (τ_p). Hence the transit time (τ_p) can be determined by calculating the cross correlation function of these two signals.

As the distance between point 1 and 2 can be designated as L_d , the slug velocity is

$$U_s = \frac{L_d}{\tau_p} \quad (6.9)$$

Signals that have been used frequently in pneumatic conveying systems include light, charge, capacitance, sound, and sometimes air pressure. For low-velocity pneumatic conveying, wall pressures generated by a slug flowing from one point to the other obviously would be similar. Hence in this study the cross correlation of wall pressure signals is selected to determine slug velocity.

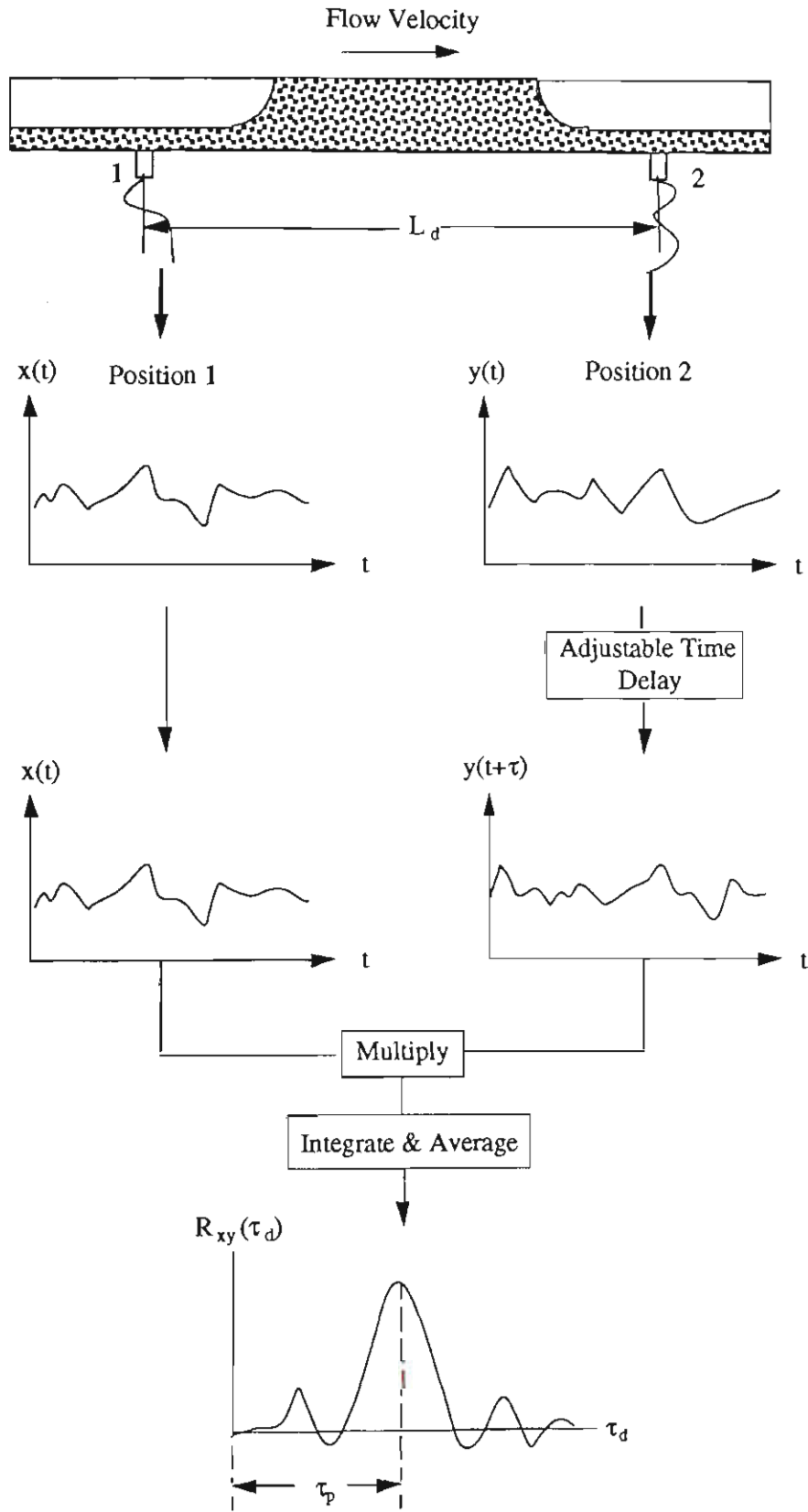


Figure 6.4 Correlated signals taken by two neighbouring sensors.

6.3.2 Calculation of Cross Correlation Function

Practical engineering signals are usually very complex and even random, such as the fluctuating air pressure during low-velocity pneumatic conveying. It is difficult or impossible to correlate these signals with time sequence. Hence the calculation of the cross correlation function is not practical for most engineering signals from the definition of cross correlation function, i.e. Equation (6.8). With the help of computer and wide applications of fast Fourier transform (FFT), a digital method [122] was developed to process and analyse various complex signals.

As signals measured by the sensors are continuous time records, the first step of digital signal processing is to digitise these continuous analogue signals (i.e. discrete time sequences) through an A/D converter. This first step is called sampling work. In this research, the sampling work is completed by the PC based quick data acquisition system. The features of the system have been introduced in Chapter 4. Various continuous signals (e.g. pressure, differential pressure, mass of material, etc.) sampled by the system are saved into the memory of the computer as an array.

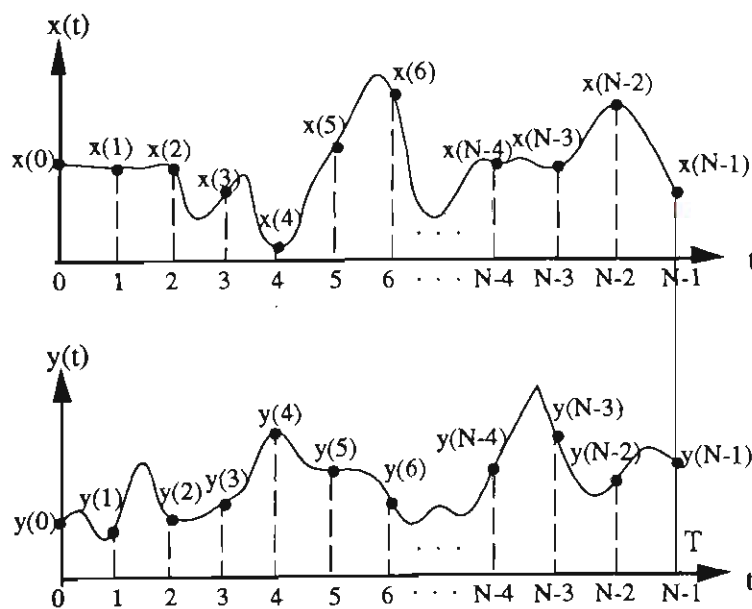


Figure 6.5 Discrete sequences sampled from continuous time signals.

As shown in Figure 6.5, the continuous signals $x(t)$ and $y(t)$ are sampled to discrete sequences $\{x(n)\}$ and $\{y(n)\}$ by an A/D converter,

$$\{x(n)\} = \{x(0), x(1), x(2), \dots, x(N-1)\}$$

and $\{y(n)\} = \{y(0), y(1), y(2), \dots, y(N-1)\}.$

where $x(n)$, $y(n)$ are the samples of $x(t)$ and $y(t)$ at $t = nT_s$, $n = 0, 1, 2, \dots, N-1$, $1/T_s$ is the sampling rate (frequency). Note it is better if $N = 2^r$, where r is an integer.

After the first step, various methods of digital processing and analysis can be then undertaken by a computer according to a given program, e.g. correlation analysis, power spectral density analysis, etc.

There are two algorithms for cross correlation function. One is a direct method which calculates the cross correlation function from the definition. As N ($N = 2^r$) values have been sampled respectively from the continuous signals $x(t)$ and $y(t)$, the estimate of the cross correlation function at time delay $\tau_d (= nT_s)$ can be obtained by the following equation,

$$\hat{R}_{xy}(n) = \hat{R}_{xy}(nT_s) = \sum_{i=0}^{N-n-1} x(i) y(i+n) \quad (6.10)$$

$$n = 1, 2, 3, \dots, m \quad (m < N)$$

where n is the number of the time delay, m is the maximum number of the time delay, $\hat{R}_{xy}(n)$ is the estimate of $R_{xy}(\tau_d)$ at the time delay $\tau_d (= nT_s)$, since there is a limit to the number of sampled data. More samples obtained from the $x(t)$ and $y(t)$ give a more accurate estimate of the cross correlation function.

Another way is an indirect method based on carrying out a reverse Fourier transform to the cross spectral density, as the cross spectral density and cross correlation function are a Fourier transform pair, that is

$$\begin{aligned}
 S_{xy}(f) &= \int_{-\infty}^{\infty} R_{xy}(\tau_d) e^{-j2\pi f \tau_d} d\tau_d \\
 R_{xy}(\tau_d) &= \int_{-\infty}^{\infty} S_{xy}(f) e^{j2\pi f \tau_d} df
 \end{aligned}
 \tag{6.11}$$

Equation (6.11) is usually called the "Wiener-Khinchine theorem" [122]. For discrete signals, it can be obtained in place of Equation (6.11),

$$\begin{aligned}
 \hat{S}_{xy}(f) &= T_s \sum_{n=-\infty}^{\infty} R_{xy}(n) e^{-j2\pi n f T_s} \\
 R_{xy}(n) &= \int_{-1/T_s}^{1/T_s} \hat{S}_{xy}(f) e^{j2\pi n f T_s} df
 \end{aligned}
 \tag{6.12}$$

Further, the cross spectral density can be obtained by calculating the following equation,

$$\hat{S}_{xy}(f_k) = \frac{2T_s}{N} X_k * Y_k, \quad k = 0, 1, 2, \dots, \frac{N}{2} - 1
 \tag{6.13}$$

where $X_k = \frac{X_T(f_k)}{T_s}$ and $Y_k = \frac{Y_T(f_k)}{T_s}$, $X_T(f_k)$ and $Y_T(f_k)$ are the limited Fourier transforms of the discrete signals $\{x(n)\}$ and $\{y(n)\}$. They are defined as

$$X_T(f_k) = T_s \sum_{n=0}^{N-1} x(n) e^{-j2\pi n f_k T_s}
 \tag{6.14}$$

$$Y_T(f_k) = T_s \sum_{n=0}^{N-1} y(n) e^{-j2\pi n f_k T_s}
 \tag{6.15}$$

Because $X_T(f_k)$ and $Y_T(f_k)$ can be obtained easily and quickly from the sequences $\{x(n)\}$ and $\{y(n)\}$ by FFT, this method is more efficient and quicker for calculating cross correlation function, particularly if a large number of data are recorded. Hence this indirect algorithm is applied to this research. The procedures can be summed up as follows.

- (i) Change the original sequences $\{x(n)\}$ and $\{y(n)\}$, $n = 0, 1, 2, \dots, N-1$, to the sequences $\{x'(n)\}$ and $\{y'(n)\}$, $n = 0, 1, 2, \dots, 2N-1$, by adding N zeroes into the original sequences, which is mathematically required for calculating the cross spectral density.

- (ii) Calculate X_k and Y_k of the sequences $\{x'(n)\}$ and $\{y'(n)\}$ by FFT program, i.e. Equations (6.14) and (6.15).
- (iii) Calculate the estimate of the cross spectral density $\hat{S}_{xy}(f_k)$ by using Equation (6.13).
- (iv) Calculate the reverse Fourier transform $\hat{S}_{xy}(f_k)$ by Equation (6.12).
- (v) Multiply the reverse Fourier transform by $N/(N-r)$ and eliminate the latter half of the result to obtain the modified estimate of cross correlation function $\hat{R}_{xy}(n)$, see Figure 6.6.

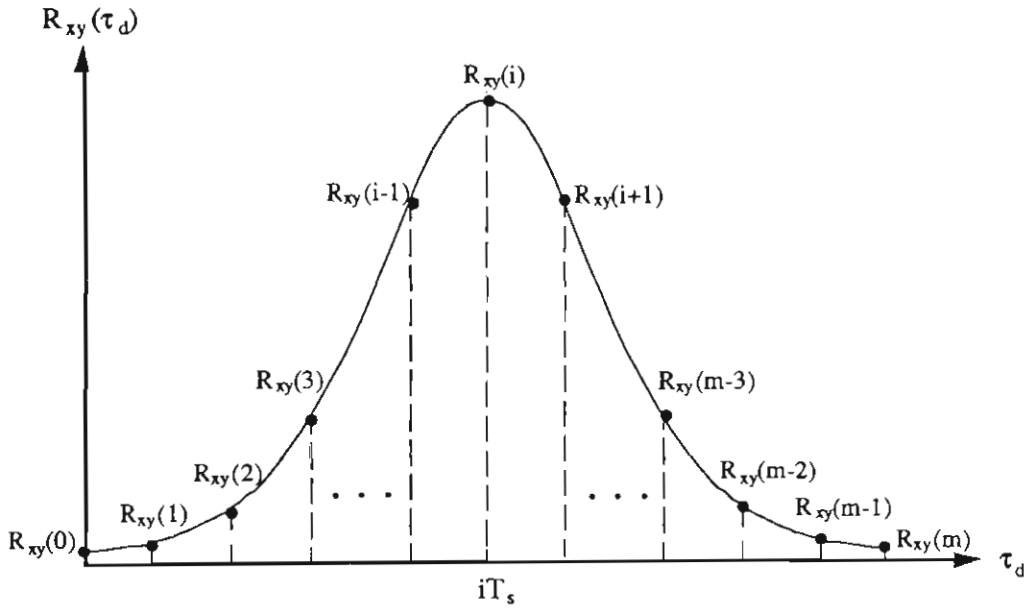


Figure 6.6 Discrete cross correlation function.

6.3.3 Resolution of Velocity

Figure 6.6 shows that the peak value of the cross correlation function $R_{xy}(\tau_d)$ occurs at the time delay $\tau_p = iT_s$. Therefore the peak value is $R_{xy}(i)$ which is one of the samples of $R_{xy}(\tau_d)$. Replacing τ_p in Equation (6.9) with iT_s , the velocity is $U_s = \frac{L_d}{iT_s}$, where i is an

integer.

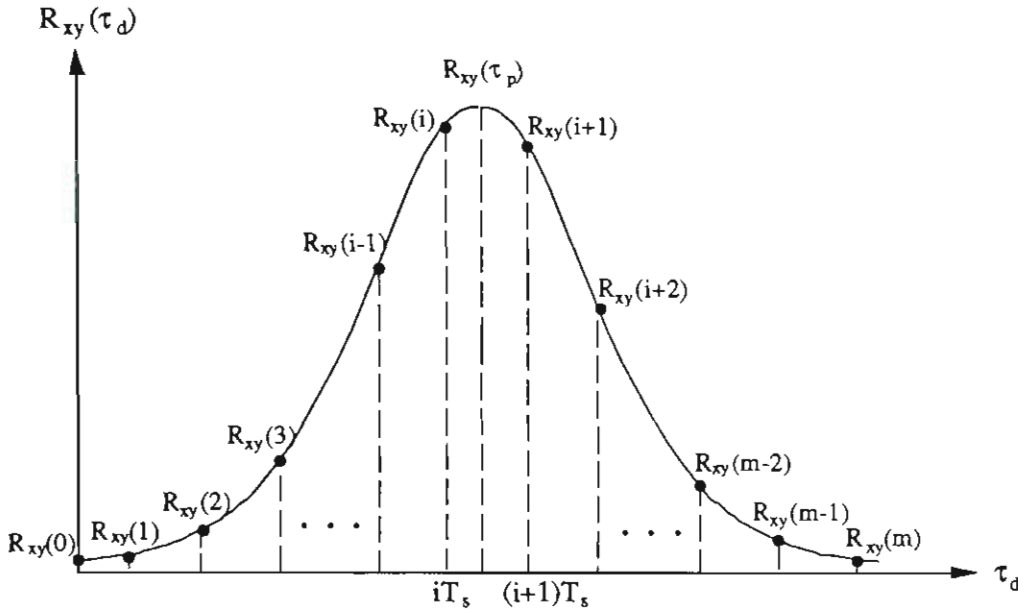


Figure 6.7 Discrete cross correlation function with the peak value not at sampling point.

However, it must be noted that in most cases the maximum $R_{xy}(\tau_d)$ occurs between two sampling points, e.g. $iT_s < \tau_p < (i+1)T_s$, as shown in Figure 6.7. In this case, the real maximum value of $R_{xy}(\tau_d)$ is lost in the calculation, generally the values neighbouring the real maximum $R_{xy}(\tau_d)$, i.e. $R_{xy}(i)$ or $R_{xy}(i+1)$ are chosen from the sequence of $\{R_{xy}(n)\}$ to be the maximum value of the cross correlation function of $R_{xy}(\tau_d)$. Based on this selection, the velocity is

$$U_{si} = \frac{L_d}{iT_s} = \frac{f L_d}{i} \quad (6.16)$$

or

$$U_{si+1} = \frac{L_d}{(i+1)T_s} = \frac{f L_d}{i+1} \quad (6.17)$$

Certainly both U_{si} and U_{si+1} are approximate values of U_s ($U_{si} > U_s > U_{si+1}$). Obviously the accuracy is dependent on the velocity resolution, i.e. the difference between U_{si} and U_{si+1} . Higher velocity resolution will give more accurate measurement of the velocity. However, it is limited by the scanning frequency (f) and sensor spacing (L_d). The following is a derivation of a relationship between these two:

Let U_r represent the velocity resolution, then

$$U_r = U_{si} - U_{si+1} \quad (6.18)$$

Replacing U_{si} and U_{si+1} in Equation (6.18) with Equations (6.16) and (6.17), then

$$U_r = \frac{f L_d}{i} - \frac{f L_d}{i+1} = f L_d \left(\frac{1}{i} - \frac{1}{i+1} \right)$$

or $f L_d = i(i+1)U_r \quad (6.19)$

As $i = \frac{f L}{U_{si}}$, the Equation (6.19) can be written as

$$f L_d = \frac{f L_d}{U_{si}} \left(\frac{f L_d}{U_{si}} + 1 \right) U_r \quad (6.20)$$

Dividing by $(f L_d)$ and rearranging Equation (6.20),

$$U_r = \frac{U_{si} U_{si+1}}{f L_d} \quad (6.21)$$

If the value of U_r is small enough compared with the real velocity U_s , the product $U_{si} \cdot U_{si+1}$ is approximately equal to U_s^2 , thus Equation (6.21) can be simplified as:

$$U_r \approx \frac{U_s^2}{f L_d} \quad (6.22)$$

From Equation (6.22) it can be found that the velocity resolution is inversely proportional to the sampling frequency of a data acquisition system and the distance between two sensors. If the accuracy of the velocity measurement needs to be improved (i.e. high velocity resolution is required), the sampling frequency f or distance L_d or both must be increased. However, it is a general requirement that the two points for installing the sensors in a pipe should be put as close as possible to ensure signal similarity. Therefore, the data acquisition system is expected to have a high sampling rate in the tests of velocity measurement. For example, assume that the sampling rate of a data acquisition system is fixed at 40 Hz (for four channels) which is the maximum scanning speed of the quick data system used in this research, the velocity of a moving object is 5 ms^{-1} which is a typical particle slug velocity and the required resolution is 5% of the velocity to be

measured, i.e. $U_r = 0.25 \text{ ms}^{-1}$, then according to Equation (6.22), the minimum distance between the two transducers is

$$L_d \approx \frac{U_s^2}{f U_r} = \frac{5^2}{40 \times 0.25} = 2.5(\text{m})$$

In other words, if the distance for installing the transducers is less than 2.5 m, the error in measurement will exceed 5%.

If the scanning speed is increased to 100 Hz, the two transducers can be put closer together:

$$L_d \approx \frac{U_s^2}{f U_r} = \frac{5^2}{100 \times 0.25} = 1.0(\text{m})$$

6.4 Experimental Results of Slug Velocity

Numerous experiments are conducted on the low-velocity pneumatic conveying test rig. Two wall pressure transducers, from which the signals are used to carry out the analysis of cross correlation function, are installed 2.49 m apart. The scanning speed of the quick data acquisition system is selected as high as possible. Hence the accuracy of measurement is sufficient for the low-velocity pneumatic conveying tests as most of the slug velocities measured in this project are less than 6 ms^{-1} . The experiments are undertaken in several groups. Each group relates to a constant mass flow rate of solids, but different mass flow-rates of air. Different groups have different mass flow-rates of solids so that the experiments can cover a wide range of conveying conditions. Refer to Chapter 4 for the details of the test program and procedures.

According to the calculation method introduced in Section 6.3.2, various slug velocities are obtained, see Appendix A, by calculating the cross correlation functions of the correlated wall pressure signals taken from the experiments which include various materials and conveying conditions. Figure 6.8 shows the plot of an actual cross correlation function calculated according to the experimental signals.

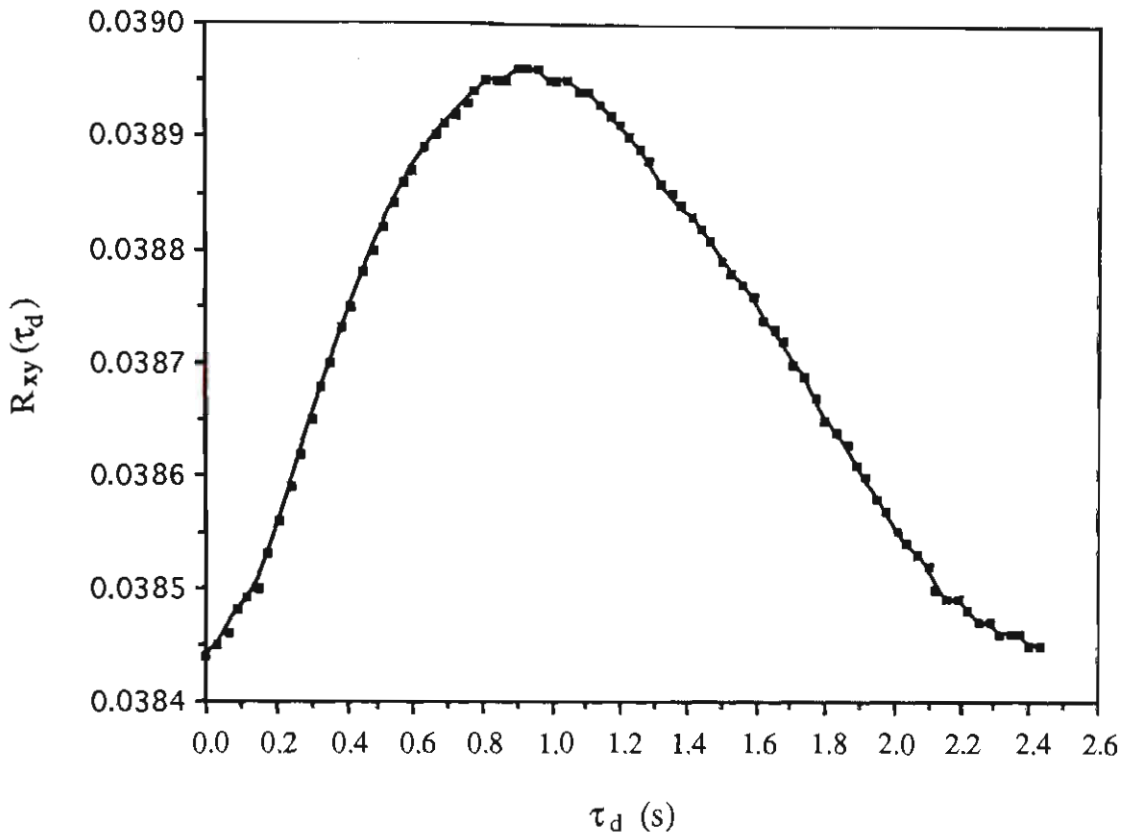


Figure 6.8 Graph of an actual cross correlation function, obtained from the experiment where $m_f = 0.0498 \text{ kgs}^{-1}$ and $m_s = 0.840 \text{ kgs}^{-1}$.

Since mass flow-rates of air and solids are the most important factors affecting the performance of pneumatic conveying, the measured slug velocities are presented against these factors and superficial air velocity.

6.4.1 Presentation of Results vs Mass Flow-Rate of Air

Figures 6.9 to 6.12 show the plots of slug velocity versus mass flow-rate of air for white plastic pellets, black plastic pellets, wheat and barley.

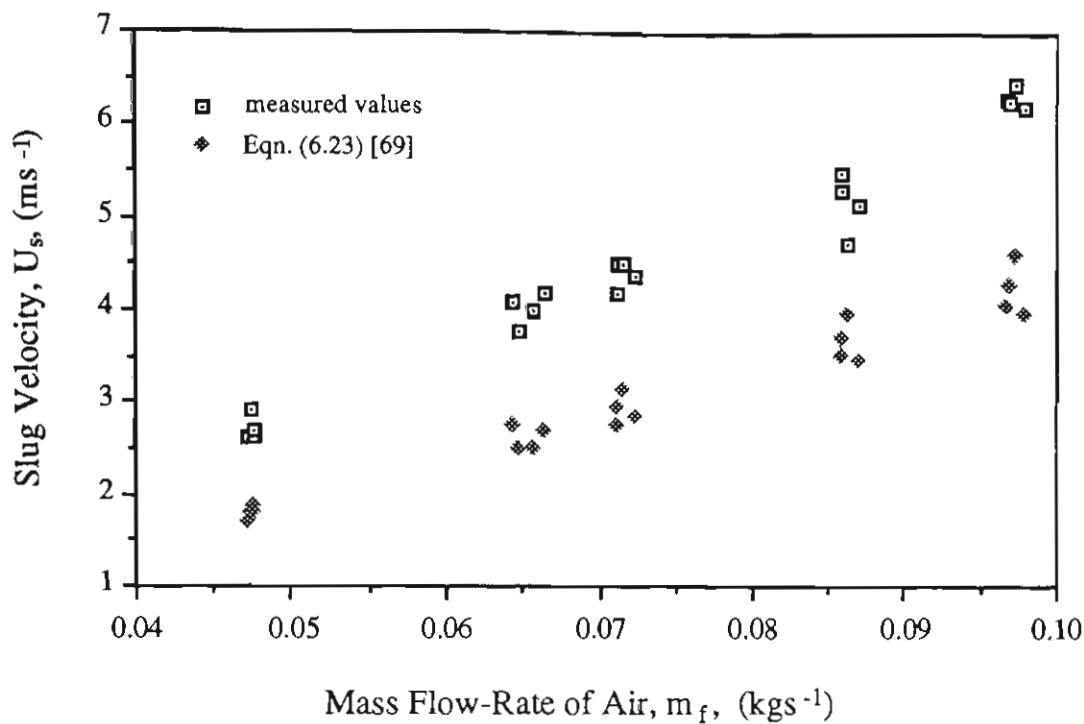


Figure 6.9 Slug velocity vs mass flow-rate of air for white plastic pellets.

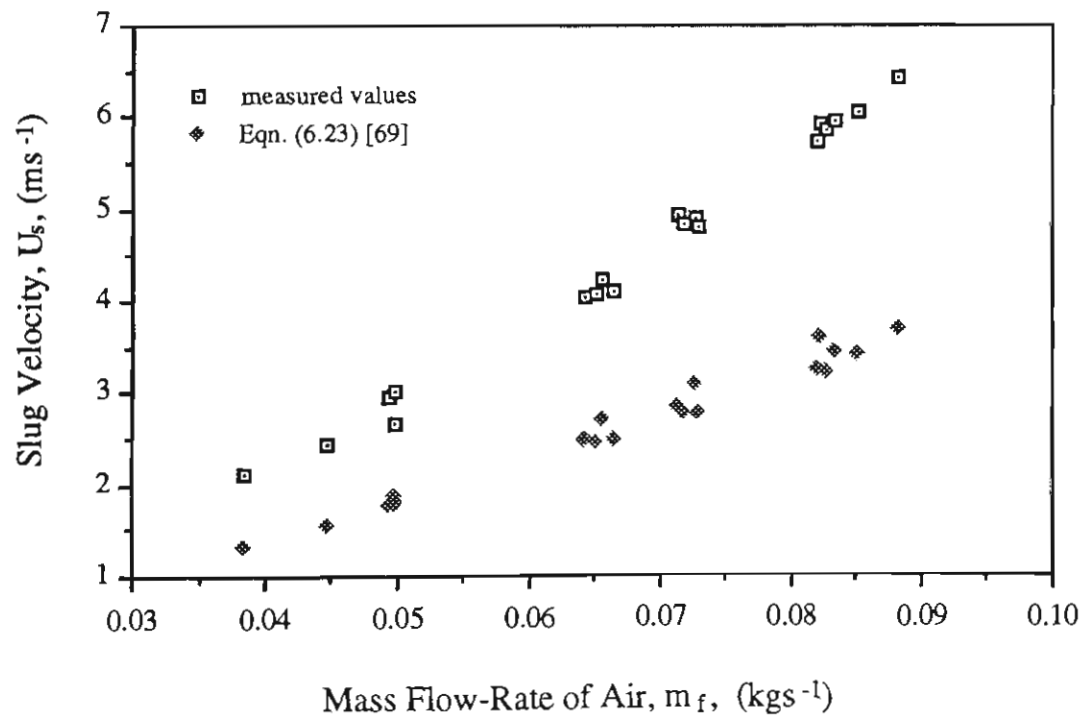


Figure 6.10 Slug velocity vs mass flow-rate of air for black plastic pellets.

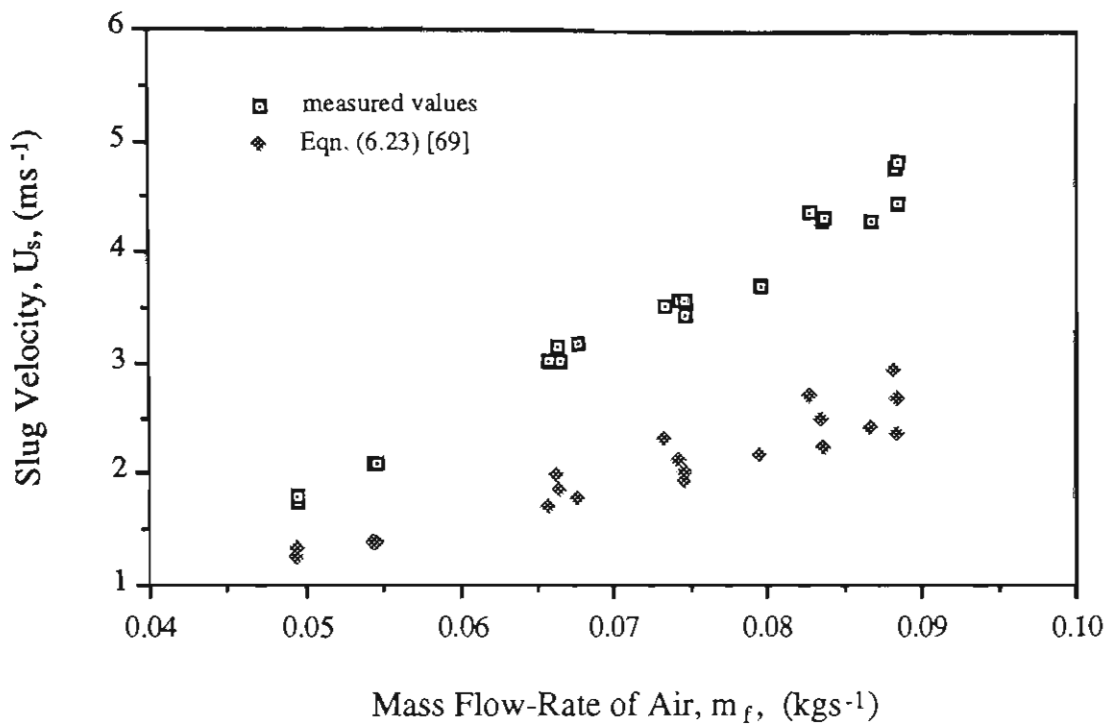


Figure 6.11 Slug velocity vs mass flow-rate of air for wheat.

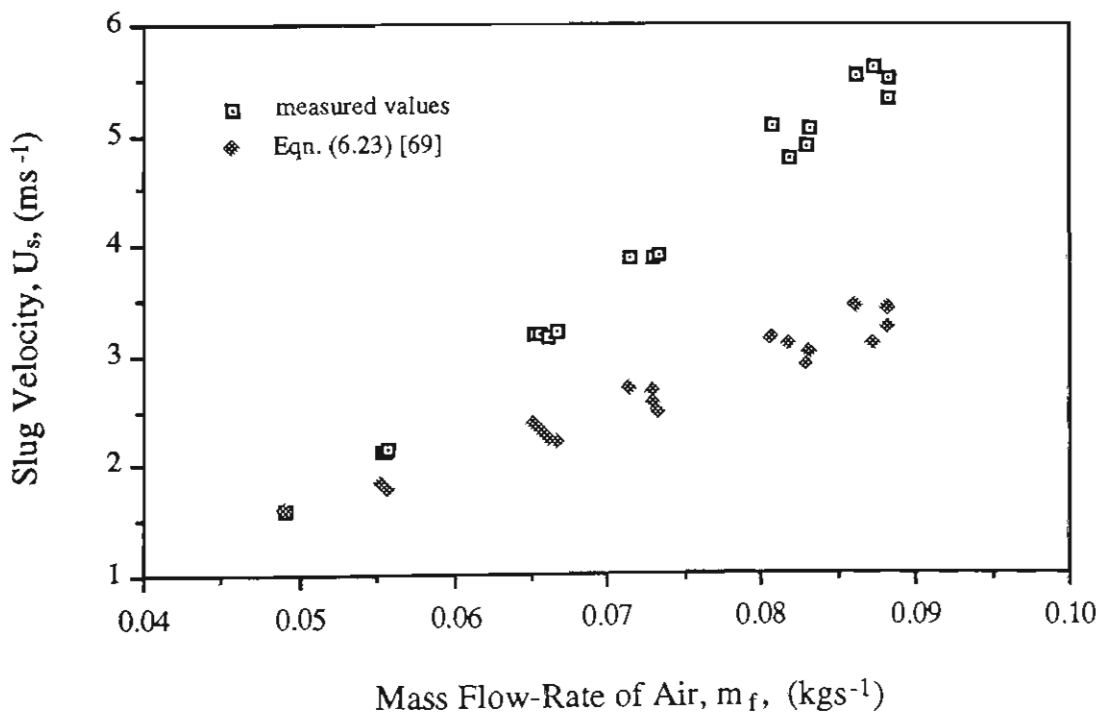


Figure 6.12 Slug velocity vs mass flow-rate of air for barley.

Konrad et al. [69] presented the following third order equation of U_s for horizontal slug-flow:

$$U_s^3 + U_s^2 \left(-\frac{(a+f_K)}{b\rho_a} - 2(U_a+U_p) - \frac{m_s}{\rho_b A} \right) + U_s \left(\frac{a(U_a+U_p)}{b\rho_a} + (U_a+U_p)^2 - \frac{2g\rho_b\mu_w}{b\rho_a} \right. \\ \left. + \frac{m_s(a+2f_K)}{\rho_b A b\rho_a} + \frac{m_s}{\rho_b A} 2(U_a+U_p) \right) - \frac{m_s}{\rho_b A} \left(\frac{a(U_a+U_p)}{b\rho_a} + (U_a+U_p)^2 - \frac{2g\rho_b\mu_w}{b\rho_a} \right) = 0 \quad (6.23)$$

where $f_K = \frac{2.168\rho_b\mu_w\lambda\sqrt{g}}{\sqrt{D}}$ is a constant. Equation (6.23) includes the parameters of the conveying conditions, physical properties of the conveyed material and pipeline diameter. Therefore, if these conditions are given, the slug velocity can be predicted by solving Equation (6.23). It should be noted that Equation (6.23) has three roots. The only root that is valid lies in the range $(U_a+U_f) > U_s > 2m_s/(\rho_b A)$.

Using Equation (6.23), the values of slug velocity are calculated for given experimental conditions and superimposed onto the above graphs for comparison. The results show that the slug velocities predicted by Equation (6.23) are always much lower than the measured values. For example, wheat was conveyed through the 52 m long pipeline in the low-velocity pneumatic conveying test rig. When $m_f = 0.0742 \text{ kgs}^{-1}$ and $m_s = 1.439 \text{ kgs}^{-1}$, the slug velocity was measured as 3.58 ms^{-1} at the point 15.85 m from the end of the pipeline, refer to Figure 6.11, whereas the slug velocity at the corresponding point was predicted as 2.13 ms^{-1} by Equation (6.23). Two possible reasons are listed below:

1. Care must be taken by investigators to apply Ergun's equation [32] to the particle slugs in low-velocity pneumatic conveying, as the equation can only calculate the pressure drop in fixed beds with a relatively narrow range of bulk voidages. Since the particle slugs are in the fluidised state during slug-flow, refer to Chapter 3, the application of Ergun's equation to this type of flow is not suitable.
2. Determination of the stress transmission coefficient λ in Equation (6.23) may be another problem. Konrad et al. [69] developed prediction equations for λ based on

the premise that stress failures occur at both the pipe wall and inside the bulk material, similar to the case of solids flowing in silos and hoppers. However, this premise is found in Chapter 7 to be incorrect for the slugs flowing in a pipe with rigid and parallel walls.

6.4.2 Presentation of Results vs Mass Flow-Rate of Solids

Figures 6.13 to 6.16 display the plots of slug velocity against mass flow-rate of solids for different test materials. It can be seen easily that the slug velocity is relatively independent of the mass flow-rate of solids. That is, the slug velocity is not affected significantly by the mass flow-rate of solids (i.e. for a given superficial air velocity). The variation of the flow-rate of solids only changes the number of the slugs contained in a certain length of a pipe at a specific time while the superficial air velocity maintains a constant.

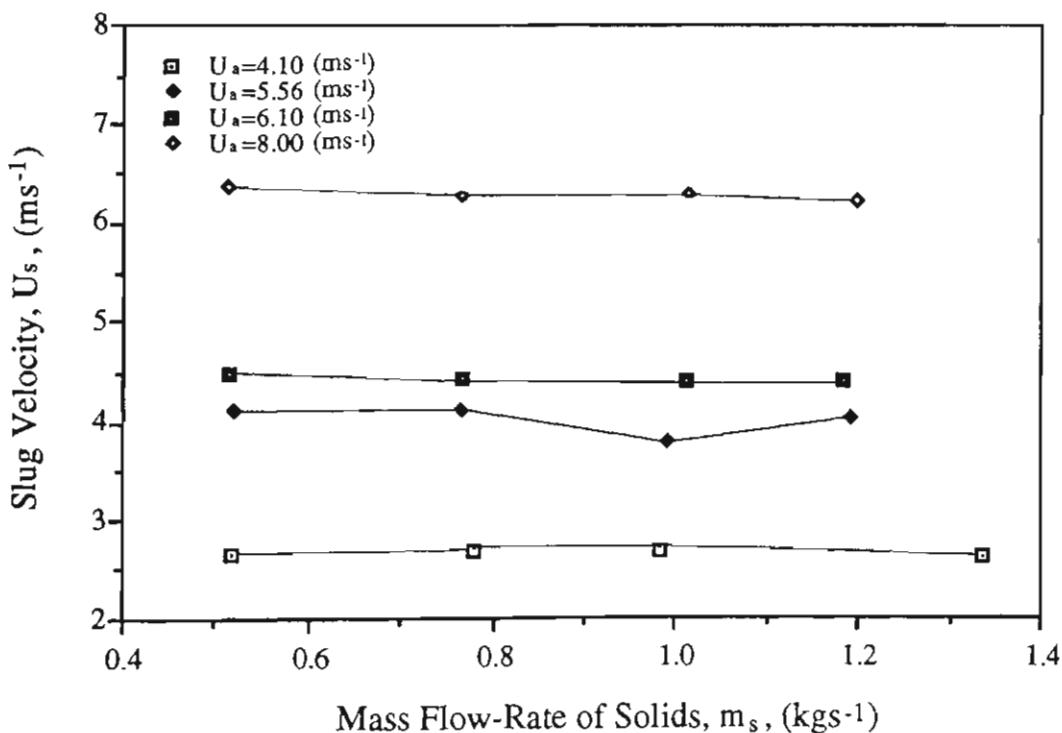


Figure 6.13 Slug velocity vs mass flow-rate of solids for white plastic pellets, carried out in the 105 mm ID mild steel pipeline.

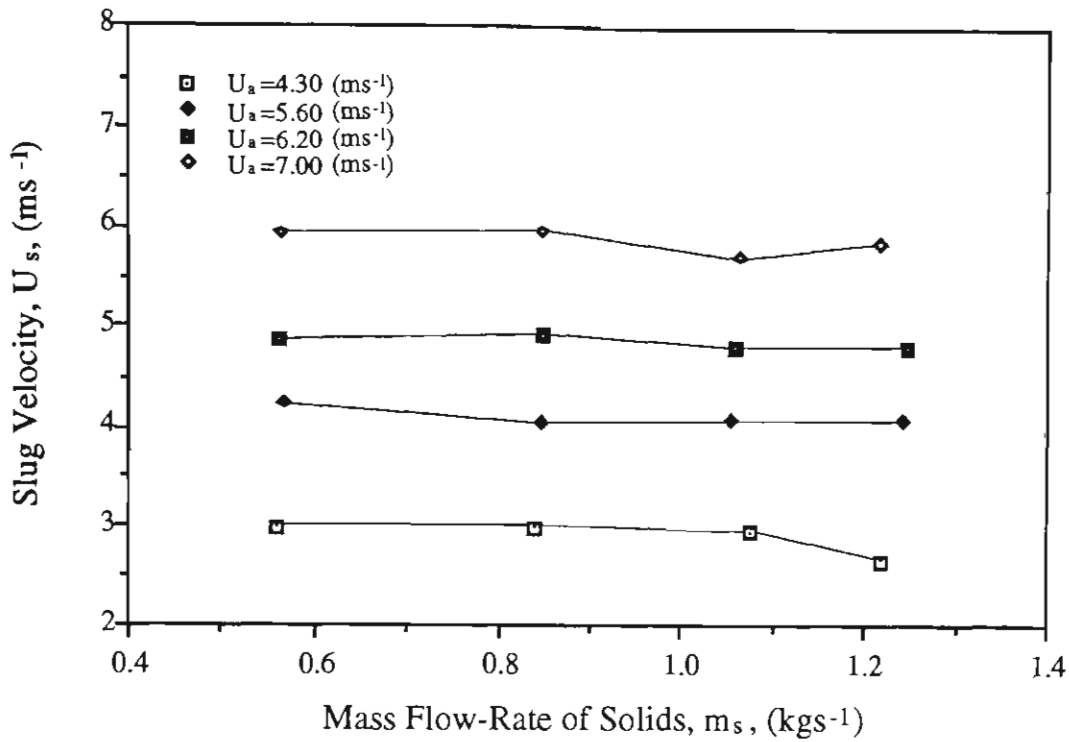


Figure 6.14 Slug velocity vs mass flow-rate of solids for black plastic pellets, carried out in the 105 mm ID mild steel pipeline.

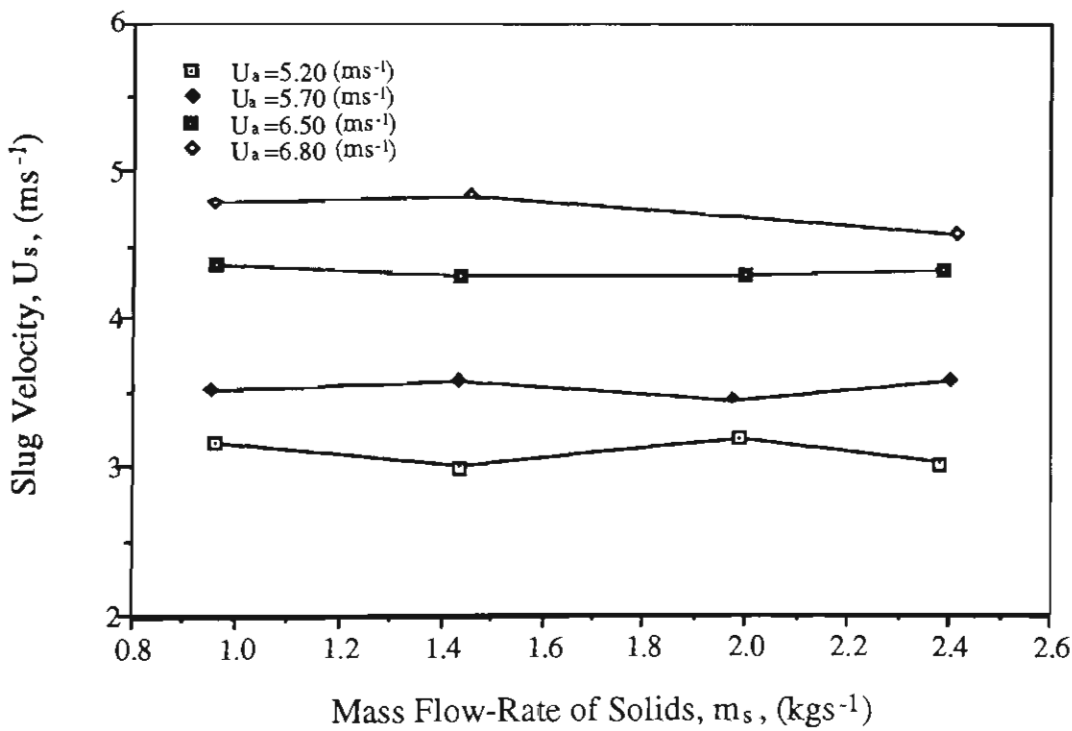


Figure 6.15 Slug velocity vs mass flow-rate of solids for wheat, carried out in the 105 mm ID mild steel pipeline.

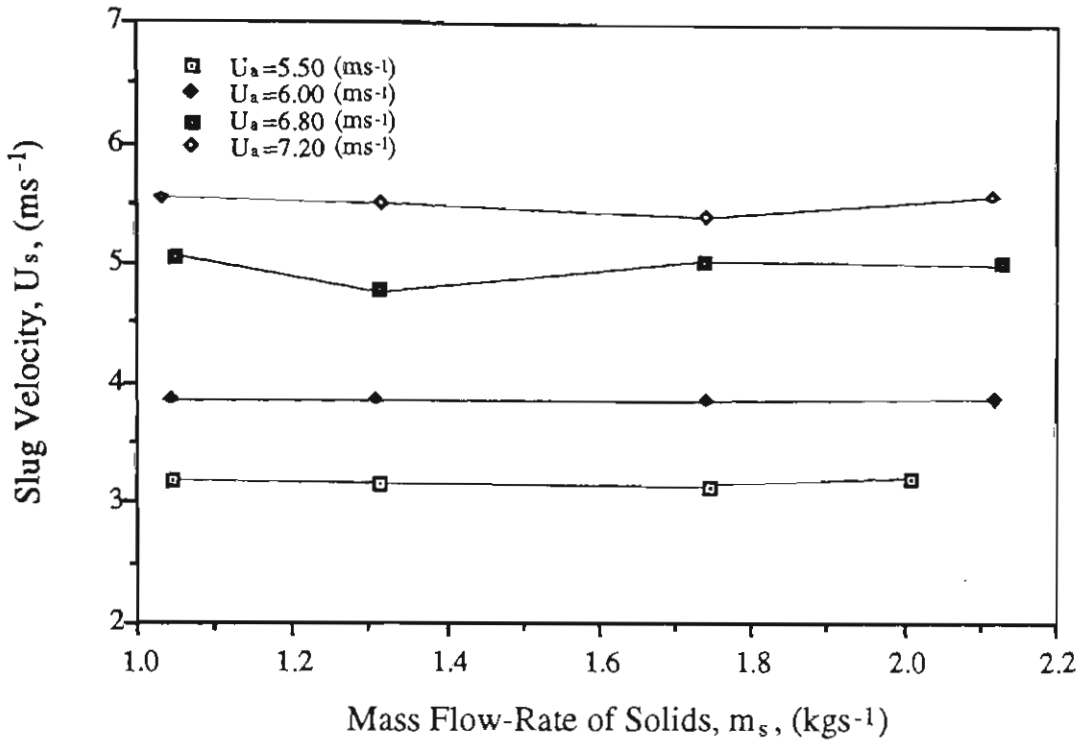


Figure 6.16 Slug velocity vs mass flow-rate of solids for barley, carried out in the 105 mm ID mild steel pipeline.

6.4.3 Presentation of Results vs Superficial Air Velocity

Figures 6.17 to 6.20 present the plots of slug velocity versus superficial air velocity for each different test material. The slug velocity depends strongly on the superficial air velocity. In the range of experimental superficial air velocity, the slug velocity appears to vary linearly. It should be noted that for each test material, the line does not pass through the origin given in Figures 6.17 to 6.20. This indicates the minimum air velocity that is necessary to initiate the motion of a particle slug in a horizontal pipe. This feature also was described by Legel and Schwedes [71] in their investigation.

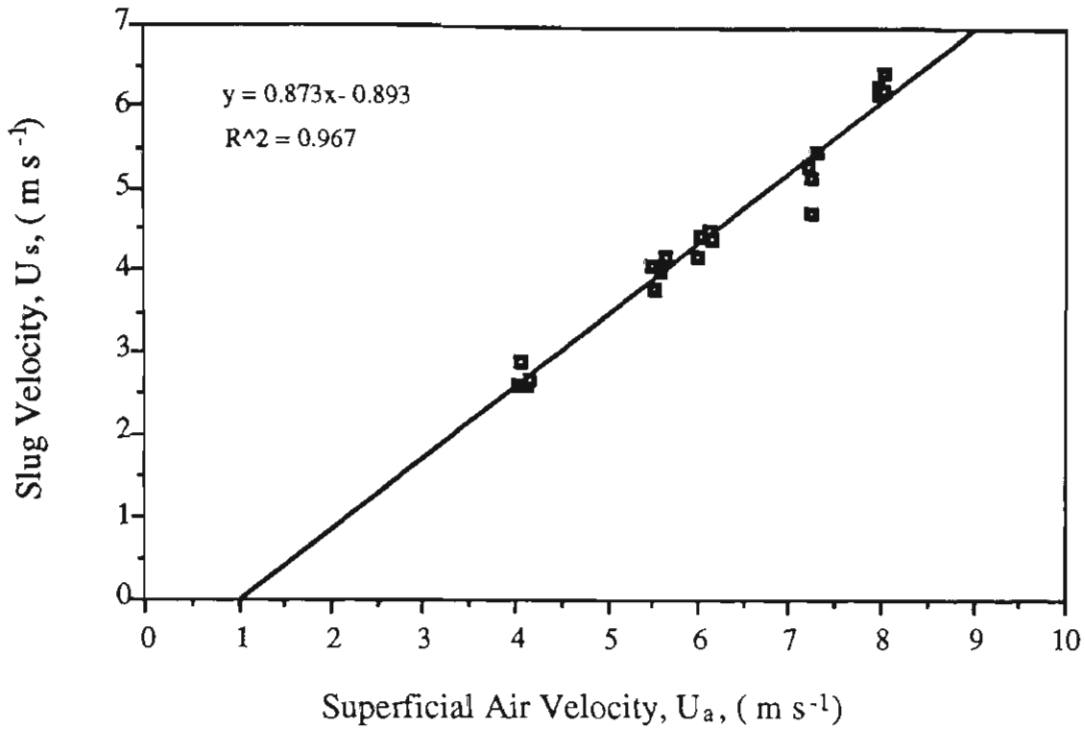


Figure 6.17 Slug velocity vs superficial air velocity for white plastic pellets, carried out in the 105 mm ID mild steel pipeline.

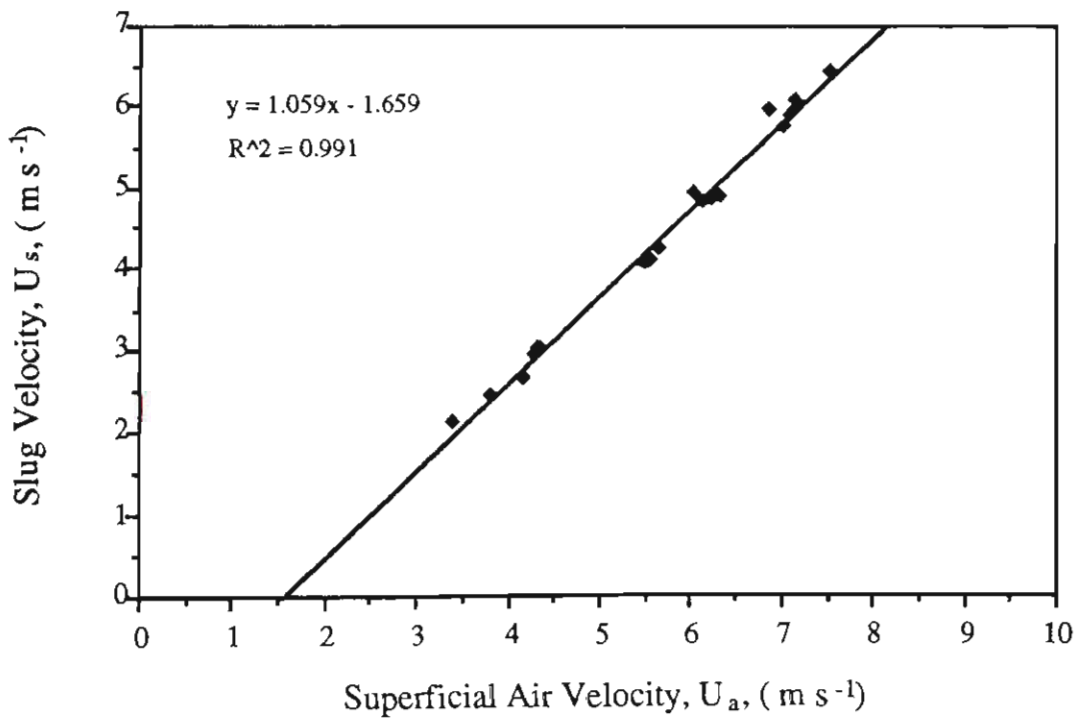


Figure 6.18 Slug velocity vs superficial air velocity for black plastic pellets, carried out in the 105 mm ID mild steel pipeline.

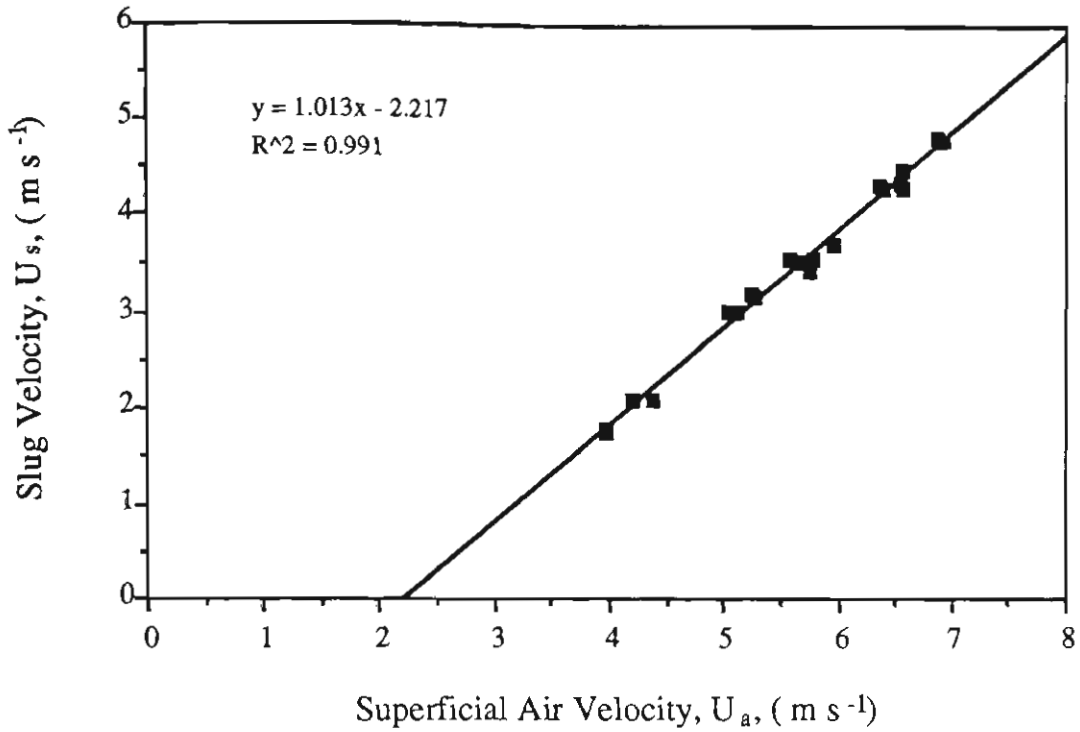


Figure 6.19 Slug velocity vs superficial air velocity for wheat, carried out in the 105 mm ID mild steel pipeline.

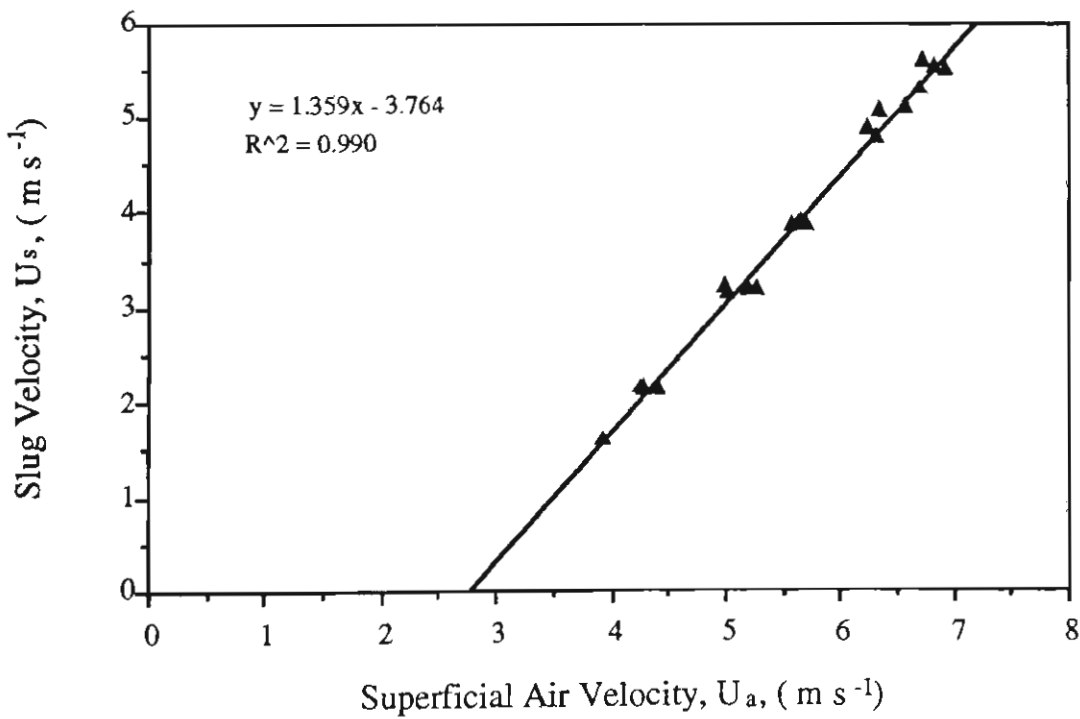


Figure 6.20 Slug velocity vs superficial air velocity for barley, carried out in the 105 mm ID mild steel pipeline.

6.5 Empirical Correlation for Slug Velocity

Since the prediction of slug velocity is not satisfactory according to Konrad's equation (i.e. Equation (6.23)), it is necessary to develop an empirical correlation of slug velocity based on the measured slug velocities and the relevant data at present. The following work is undertaken for this purpose.

6.5.1 Linear Model of Slug Velocity

It has been known that in the range of experimental superficial air velocity, the data for each material can be represented by an approximate linear correlation, hence a linear model of the slug velocity with superficial air velocity can be assumed firstly as:

$$U_s = K U_a + \text{constant}$$

(6.24)

where K is the slope of the line.

Due to the existence of a minimum air velocity, the linear model can be modified further as following,

$$U_s = K(U_a - U_{amin})$$

(6.25)

The lines of best fit are obtained by least-squares and shown in Figures 6.17 to 20. Table 6.1 lists the experimental values of the slope (K) and minimum air velocity (U_{amin}). The square of the correlation coefficient of each line is also listed in the table to show the goodness of fit.

Table 6.1: K , U_{amin} and γ^2 for lines of various test materials

Item	Plastic Pellets (White)	Plastic Pellets (Black)	Wheat	Barley
K	0.873	1.059	1.013	1.359
$U_{amin} \text{ (ms}^{-1}\text{)}$	1.023	1.566	2.189	2.770
γ^2	0.966	0.991	0.991	0.990

Obviously, for the experiments conducted in a 105 mm ID mild steel pipeline, different materials have different linear equations (i.e. different K and U_{amin}) to express the relationship between the slug velocity and superficial air velocity. This indicates that K and U_{amin} in the linear model of Equation (6.25) must be functions of material properties. Since material flow occurs in a pipe, the wall frictional force is certainly a major factor that affects slug velocity, i.e. the wall friction angle (ϕ_w) should be included in the functions. Therefore, $K = f(\epsilon, d, \rho_s, \phi, \phi_w)$ and $U_{amin} = f(\epsilon, d, \rho_s, \phi, \phi_w)$. It should be noted that the bulk density of material is excluded from the functions. The reason is that $\rho_b = (1 - \epsilon)\rho_s$. The mass flow-rate of solids (m_s) is also excluded from the model of slug velocity since it was found to have little effect on slug velocity.

6.5.2 Regression Slope for Linear Model

An expression for K in Equation (6.25) is assumed initially as follows,

$$K_i = \epsilon_i^{x_1} d_i^{x_2} \gamma_{si}^{x_3} \tan\phi_{wi}^{x_4} \tan\phi_i^{x_5}, \quad i=1,2,\dots, n \quad (6.26)$$

where ϵ is the bulk voidage of slug, d is the particle diameter and γ_s is the particle specific weight which is applied to Equation (6.26) to represent the effect of the particle density (ρ_s). The purpose of using γ_s instead of ρ_s is to obtain smaller difference between every two factors in Equation (6.26) so that a better regression can be achieved. ϕ_w is the wall friction angle, ϕ is the internal friction angle, x_1, x_2, x_3, x_4 and x_5 are coefficients, which are obtained by the method of least squares, n is the number of the test materials.

Therefore, a deviation function is generated as follows:

$$F(x) = \sum_{i=1}^n (\epsilon_i^{x_1} d_i^{x_2} \gamma_{si}^{x_3} \tan\phi_{wi}^{x_4} \tan\phi_i^{x_5} - K_i)^2 \quad (6.27)$$

The optimal coefficients x_1, x_2, x_3, x_4 and x_5 are obtained by minimizing the above function. Table 6.2 lists the coefficients calculated by using the optimization program "MDOD" [123].

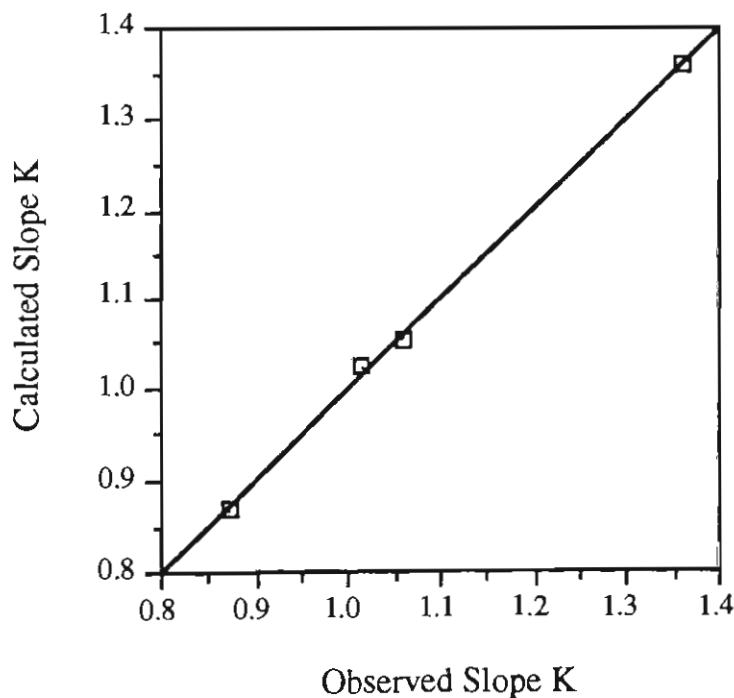
Table 6.2: Optimal coefficients

x_1	x_2	x_3	x_4	x_5
1.	1.	0.0013	0.333	-0.333

From this table, it is found that the effect of the particle specific weight term is not significant since the index x_3 is very small (near to zero). To simplify the model, the term of the particle specific weight is taken out from Equation (6.26), and the expression of the slope K is simplified as follows:

$$K = \epsilon d (\tan \phi_w / \tan \phi)^{\frac{1}{3}} \quad (6.28)$$

The goodness of fit of the regression model is shown in Figure 6.21.

Figure 6.21 Goodness of fit of K correlation.

It should be noted that while undertaking the regression calculation, the unit of millimetre is selected for the particle diameter. Hence the unit of millimetre for particle diameter should be used in Equations (6.28).

6.5.3 Dimensional Analysis

An expression for the slope K of the linear relationship between slug velocity and superficial air velocity which is a function of bulk voidage (ϵ), particle diameter (d), internal frictional angle (ϕ) and wall frictional angle (ϕ_w) has been developed by using the least square method based on the experimental data. However, it should be pointed out that all the data are based on the experiments carried out in the 105 mm ID mild steel horizontal pipeline. Hence, the data cannot provide information on the effect of pipe diameter on the slope K . Further investigations should be undertaken for different pipe diameters. However, limited by finance, time and measurement technique, etc., it seems impossible to construct a large number of pneumatic conveying test rigs with different diameter pipelines. To explore the influence of pipe diameter on slope K , dimensional analysis is employed in this investigation.

Since K is the slope of a linear model, it should be a parameter without unit. However, the present expression of K , see Equation (6.28), has the unit of length since the particle diameter exists in this equation. To taken into account the influence of pipe diameter, (i.e. pipe diameter is included in the expression of K), the following expression of K is proposed

$$K = c_d \frac{\epsilon d}{D} \left(\frac{\tan \phi_w}{\tan \phi} \right)^{\frac{1}{3}} \quad (6.29)$$

where c_d is a dimensionless coefficient.

Obviously the coefficient c_d can be determined by inserting the known slope K , physical properties of material and pipe diameter into Equation (6.29). For example, for the white plastic pellets flowing through the 105 mm ID mild steel pipeline in dense phase, the following values can be given:

$K = 0.873$, $\epsilon = 0.430$, $d = 3.12$ mm, $\tan \phi_w = 0.271$, $\tan \phi = 0.990$ and $D = 105$ mm. Therefore,

$$0.873 = c_d \frac{0.430 \times 3.12}{105} \left(\frac{0.271}{0.990} \right)^{\frac{1}{3}} \quad (6.30)$$

That is $c_d = 105$. The same value of c_d is obtained for the other test materials.

Hence for different pipe diameters, the slope K can be represented by:

$$K = 105 \cdot \frac{\epsilon d}{D} \left(\frac{\tan \phi_w}{\tan \phi} \right)^{\frac{1}{3}} \quad (6.31)$$

Therefore, the following correlation of slug velocity that best fits the experimental data can be obtained:

$$U_s = 105 \frac{\epsilon d}{D} \sqrt[3]{\frac{\tan \phi_w}{\tan \phi}} (U_a - U_{amin}) \quad (6.32)$$

6.5.4 Minimum Air Velocity

The experimental results and investigations of other researchers [71, 103] show a minimum air velocity exists in low-velocity pneumatic conveying. Only when the air velocity exceeds this critical value, does the particle slug start to move along the pipe. For vertical low-velocity pneumatic conveying, the minimum air velocity should be equal to or slightly higher than its incipient fluidisation velocity since slug-flow is regarded as an aggregative fluidisation system. An equation has been developed for the determination of the incipient fluidisation velocity by Richardson and Zaki [92]. An idea similar to that of Richardson and Zaki [92] probably can be applied to determine the minimum air velocity for a horizontal pipe, i.e. by using an expression for the relation between pressure drop and superficial velocity for a fixed bed and letting the pressure drop equal the frictional force caused by the buoyant weight of the particles, as shown in Figure 6.22.

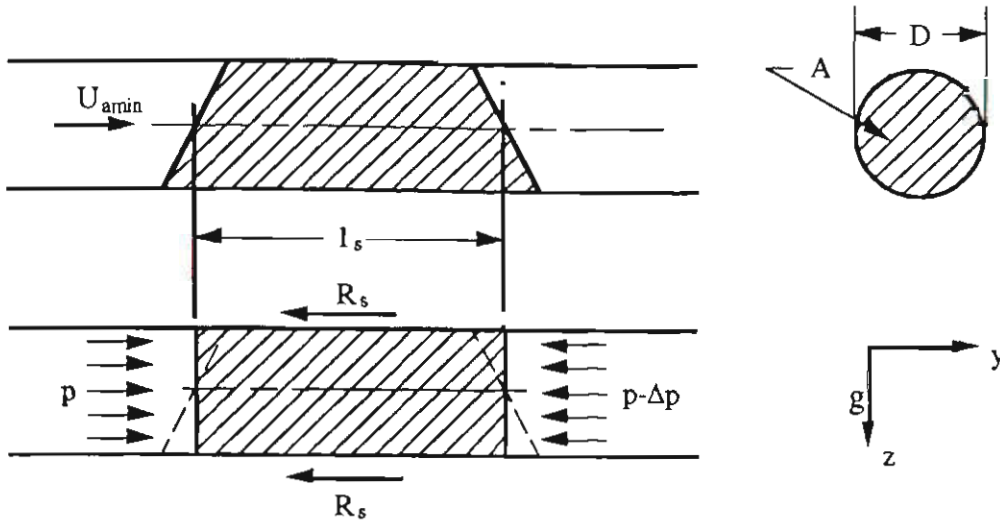


Figure 6.22 Idealised slug with acting forces at initial motion.

Thus,

$$\frac{\Delta p}{l_s} A l_s = R_s \quad (6.33)$$

Neglecting the buoyancy of air, Equation (6.33) becomes

$$\frac{\Delta p}{l_s} = 2\rho_b g \tan \phi_w \quad (6.34)$$

The correct selection of a suitable expression for the relation between the pressure drop and superficial velocity for a fixed bed will have a great influence on the predicted results of the minimum velocity. For example, for fluid flow at low Reynold's number (which is referred to as viscous flow), Carman [18] developed the following equation for the pressure gradient in a fixed bed:

$$\frac{\Delta p}{H_b} = \frac{k36(1-\epsilon)^2 \eta U_a}{\epsilon^3 d^2} \quad (6.35)$$

where, $k = \text{constant} \approx 5$. According to other experiments [22], the value of k was found to be dependent on particle diameter and contained in the range 4.65 to 5.34.

However, for turbulent flow through granular beds (i.e. at high Reynold's number), over a relatively narrow range of fixed bed voidages, Ergun [31, 32] carried out extensive research and suggested that during turbulent flow, the pressure loss across the bed is due to not only viscous energy loss but also kinetic energy loss. Based on the work of Carman [18], accounting for kinetic effects, Ergun [31, 32] developed the following initial equation for turbulent flow.

$$\frac{\Delta p}{H_b} = \frac{k36(1-\epsilon)^2 \eta U_a}{\epsilon^3 d^2} + \frac{\beta(1-\epsilon) \rho_a S_v U_a^2}{8\epsilon^3} \quad (6.36)$$

where β is a dimensionless coefficient and can be determined experimentally.

The first term of Equation (6.36) is the pressure loss due to viscous effects (viz. Equation (6.39)) and the second term defines the kinetic energy loss. Ergun [31] pointed out that the relative importance of the viscosity and kinetic terms is dependent on the range of Reynold's number. For example, for $Re = 0.1$, viscous forces account for 99.8% of the pressure and the second term is approximately zero, whereas for complete turbulent flow, $Re = 3000$ for instance, kinetic effects become more important and account for 96%. For turbulent flow, Equation (6.36) is in the following form,

$$\frac{\Delta p}{H_b} = \frac{150\eta(1-\epsilon)^2 U_a}{d^2 \epsilon^3} + \frac{1.75\rho_a(1-\epsilon) U_a^2}{d \epsilon^3} \quad (6.37)$$

Between these two values, flow is transitionary and both terms are significant. For these reasons, the flow type must be taken into account while selecting an expression for the relation between the pressure drop and superficial velocity for a fixed bed.

Assuming that the flow is a complete turbulent flow, prediction of the minimum air velocity can be obtained by substituting $\Delta p/l_s$ from Equation (6.34) into Equation (6.37), that is

$$\frac{150\eta(1-\epsilon)^2 U_{a\min}}{d^2 \epsilon^3} + \frac{1.75\rho_a(1-\epsilon) U_{a\min}^2}{d \epsilon^3} = 2\rho_b g \tan\phi_w \quad (6.38)$$

For the test materials white plastic pellets, black plastic pellets, wheat and barley, the calculated minimum velocities from Equation (6.38) are 0.616 ms^{-1} , 0.684 ms^{-1} , 0.953 ms^{-1} and 1.015 ms^{-1} , respectively. These values are much lower than the ones obtained from the linear regression of experimental data, see Table 6.1.

Assuming that the flow is viscous, substituting $\Delta p/l_s$ from Equation (6.34) into Equation (6.35), then

$$\frac{k36(1-\epsilon)^2\eta U_{a\min}}{d^2\epsilon^3} = 2\rho_b g \tan\phi_w \quad (6.39)$$

If $k = 5.0$, the minimum air velocities are found to be 1.902 ms^{-1} , 2.609 ms^{-1} , 4.554 ms^{-1} and 5.860 ms^{-1} for white plastic pellets, black plastic pellets, wheat and barley, respectively. These values are higher than the corresponding values listed in Table 6.1. One interesting fact is that all the calculated values are approximately twice the values listed in Table 6.1.

According to the assumption of complete turbulent flow or laminar flow, the calculation cannot obtain satisfactory results. This indicates that the air flow is neither complete viscous flow nor complete turbulent flow in the slug at initial motion. That is, the type of flow must be transitional.

In a vertical fixed bed, the air flows through the material uniformly across the cross section of the bed (i.e. due to an even distribution of voids). However, in a horizontal particle slug, as shown in Figure 6.22, affected by particle weight, the bulk voidage of the bed at the upper part of the pipe will be greater than that at the lower part. Hence it is easier for the air to pass through the upper part of the pipe and results in a variation of flow-rate across the cross section of the pipe. Sometimes channelling may occur at the top part of the pipe due to low wall friction, resulting in a high proportion of the air flowing through channels, so that only a small amount of air flows through the particle bed. Hence the different types of flow (i.e. laminar and turbulent flow) may exist

simultaneously at a cross section of the pipe. In addition, from the experimental values of minimum air velocity listed in Table 6.1, the air flow is also found to be in the transition from viscosity to turbulent flow. For example, at initial motion of a slug of white plastic pellets, the minimum air velocity is about 1 ms^{-1} and $\text{Re} \approx 220$. Hence it is more reasonable to assume that the total pressure loss is composed of both laminar flow and turbulent flow pressure losses. It is difficult to estimate accurately the actual proportion of viscous and turbulent flow in the slug. However it should be noted that the values predicted by Equation (6.39) are approximately twice the values listed in Table 6.2. Hence, it may be assumed that the two terms in Equation (6.36) have the same effect on pressure loss. That is, the pressure loss across the slug is assumed approximately twice the viscous or kinetic effect. That is,

$$\frac{\Delta p}{l_s} = \frac{k36(1-\epsilon)^2 \eta U_a}{\epsilon^3 d^2} + \frac{\beta(1-\epsilon) \rho_a S_v U_a^2}{8\epsilon^3} = 2 \frac{k36(1-\epsilon)^2 \eta U_a}{\epsilon^3 d^2} \quad (6.40)$$

Combining Equations (6.34) and (6.40) results in the following expression for the minimum superficial air velocity.

$$U_{\text{amin}} = \frac{\rho_s g \tan \phi_w \epsilon^3 d^2}{36k(1-\epsilon)\eta} \quad (6.41)$$

If $k \approx 5.0$, then according to Equation (6.41), the minimum superficial air velocities for white plastic pellets, black plastic pellets, wheat and barley are calculated as 0.951 ms^{-1} , 1.355 ms^{-1} , 2.266 ms^{-1} and 2.935 ms^{-1} , respectively. Compared with the corresponding values listed in Table 6.1, agreement generally is quite good. Considering the possible variation in the value of k mentioned earlier (i.e. between 4.7 and 5.3), better agreements are possible.

CHAPTER 7

WALL PRESSURE AND STRESS TRANSMISSION COEFFICIENT

7.1 Introduction

The pressure which is exerted on the wall of a silo by a bulk material (i.e. the wall pressure) has been studied by numerous investigators [7, 8, 9, 43, 55, 56, 106, 107, 108]. The term "silo" will be used here to describe all types of containing structures, e.g. bins, hoppers, conveying pipes, bunkers and chutes etc. There are many reasons to further this area of study. For example, whether the bulk material contained in a silo flows or not, the bulk material exerts pressure on various parts of the silo wall and the values of wall pressure are a major design parameter to determine the strength of the wall. Another example is that during low-velocity pneumatic conveying, the wall pressure generates the major resistance force to particle slugs.

Within the vertical part of a silo with a circular cross section, wall pressure is well represented by the Janssen formula:

$$\sigma_w = \frac{\rho_b D}{4\mu_w} \left(1 - e^{-\frac{4\lambda\mu_w}{D}x}\right) \quad (7.1)$$

The case of a bulk material flowing in the form of slugs through a conveying pipe (particularly a vertical pipe) is very similar to the case of a bulk material flowing in the vertical part of the silo. Therefore, based on Janssen's method, a formula for the wall pressure is derived for vertical slug-flow pneumatic conveying, refer to Appendix D:

$$\sigma_w = \lambda \sigma_f \left(1 - e^{-\frac{4\mu_w \lambda}{D}x}\right) \quad (7.2)$$

Equation (7.2) obviously is similar to Equation (7.1). A formula of the wall pressure was developed for horizontal slug-flow in Chapter 3, see Equation (3.18). For ease of reference, it is quoted here again:

$$\sigma_w = \lambda [(\sigma_b - \sigma_f) e^{-\frac{4\mu_w \lambda}{D}x} + \sigma_f] \quad (7.3)$$

In Equations (7.2) and (7.3), σ_w is the wall pressure. σ_f is the pressure on the front surface of a slug, which is generated by the slug collecting the particles and σ_b is the

pressure on the back surface of the slug, which is caused by the slug depositing particles. λ is the stress transmission coefficient which has been defined in Chapter 3 (refer to Section 3.4.1).

Although the general relationships between wall pressure and surface stress have been demonstrated by Equations (7.2) and (7.3), it must be noted that wall pressure cannot be predicted for low-velocity slug-flow pneumatic conveying from these equations, since the front and back stress σ_f , σ_b , as well as the stress transmission coefficient λ in these equations, are still unknown. Another reason is that many factors cannot be taken into account properly while developing these equations. For example, bulk materials may arch randomly, with the result that wall pressure increases sharply in the arched area. Also the material may collapse or deform in some area of a slug so that the wall pressure is rearranged. Hence further experimental work is needed to assist in the investigation of the wall pressure of slug flow pneumatic conveying. For this purpose, wall pressure measurement techniques and corresponding instrumentation have been developed and installed in specific points in the pipeline system of the low velocity pneumatic conveying test rig. As soon as the particle slug flows through these measuring points, wall pressures exerted by the slug can be obtained directly by measurement. To fully understand the effect of conveying conditions and particle properties on wall pressure, experiments are conducted with various conveying conditions and materials. The test results are presented later in this chapter.

From Equations (7.2) and (7.3), it can be seen that the stress transmission coefficient λ , which is defined as the ratio of radial stress to axial stress in Chapter 3, plays an important role in the analysis of wall pressure. It was applied firstly by Janssen to "silo" research about one hundred years ago. However, even up till now, many "silo" investigators still feel confused about its values. For low-velocity pneumatic conveying, less information about the stress transmission coefficient is presented. After measuring wall pressures in this research, some data for λ in the low-velocity pneumatic conveying

are obtained. Also a semi-empirical expression for λ is presented based on the data for the slugs flowing in a pipe with rigid and parallel walls.

7.2 Wall Pressure Measurement

7.2.1 Method of Wall Pressure Measurement

Measurement of wall pressure in silos has been carried out by many investigators over the past years (e.g. Jenike [55], Walker [107] and Borcz [8, 9], etc.). A general method is to install a pressure transducer that has a flat sensitive surface on the wall of a silo. The sensitive surface of the transducer must be flush with the wall, as shown in Figure 7.1(a).

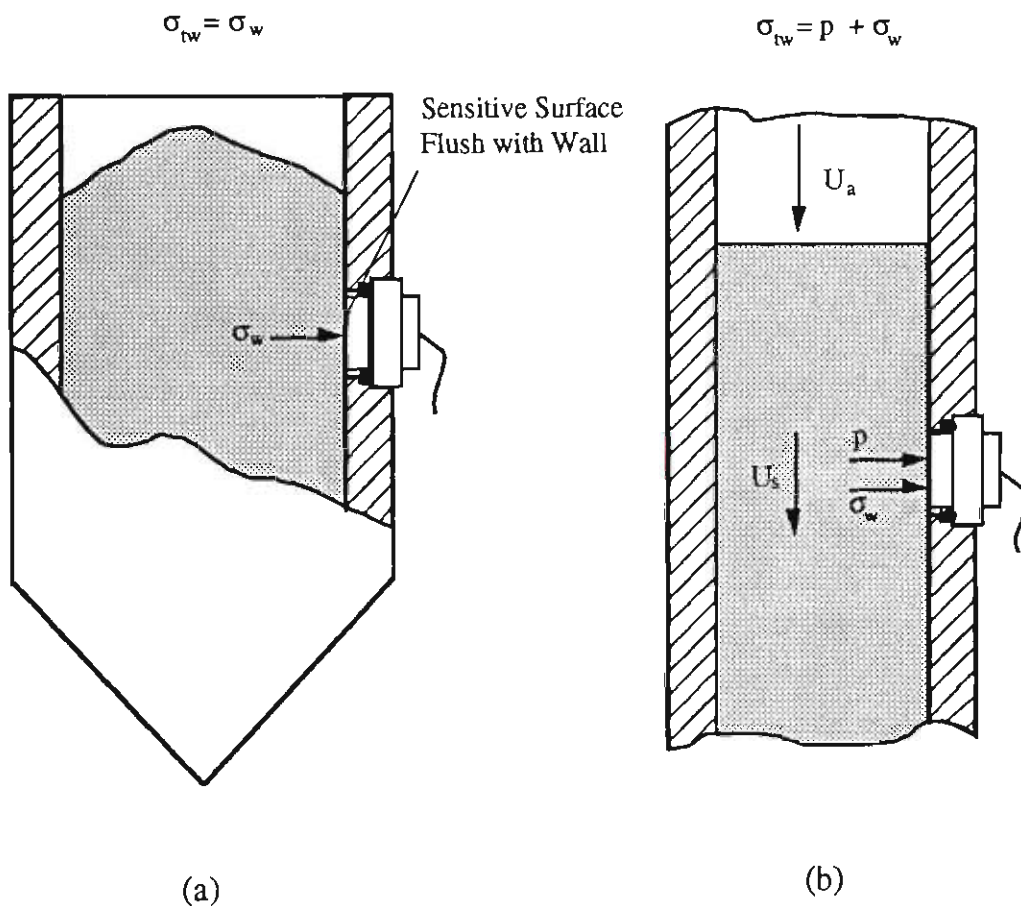


Figure 7.1 Pressures acting on the sensitive surfaces of transducers.

When bulk material is loaded into the silo, the sensitive surface of the transducer senses the pressure exerted by the bulk material. However, until now, no measurement has been

carried out for the wall pressure which is exerted by moving particle slugs during low-velocity pneumatic conveying. Unlike the case in the silo where only the bulk material exerts the pressure on the wall, in low-velocity pneumatic conveying both particle slugs and conveying air exert pressure on the wall of pipe, see Figure 7.1(b). That is, the pressure sensed by the transducer shown in Figure 7.1(b) represents a combined signal. Hence the conventional method for measuring the wall pressure of a silo cannot be applied directly to slug-flow pneumatic conveying. A special method is necessary to obtain the wall pressure from the combined signal in slug-flow pneumatic conveying. A wall pressure measuring assembly developed for measuring the wall pressure in low-velocity pneumatic conveying is shown in Figure 4.10. It mainly consists of two types of pressure transducer (i.e. the type-A and -B designated in this paper). The type-A is a normal static air pressure transducer and type-B is a flat sensitive surface pressure transducer shown in Figure 7.1. The type-A and -B transducers are installed at the same cross section of pipe. Note that the sensitive surface of the type-B transducer is installed flush with the inner pipe wall. The total values of the static air pressure and wall pressure can be measured by the type-B transducer, and at the same time, the type-A transducer records the static air pressure only. Providing the static air pressure keeps constant at the identical cross section of the pipe, the wall pressure can be obtained by subtracting the static air pressure measured by the type-A transducer from the total pressure measured by the type-B transducer.

7.2.2 Installation of Transducers

Since the wall pressure is obtained by processing a combined signal in low-velocity slug-flow pneumatic conveying, two types of pressure transducer are installed correctly to ensure mutual operation. The installation of each type of transducer is shown in Figure 4.10 and Figure 4.11. The following lists some special requirements for the correct installation of the transducers.

(a) Position requirement:

Air pressure in pneumatic conveying varies along the length of pipe, but is nearly constant across a cross section of pipe. To ensure that the air pressure can be eliminated totally, type-A and -B transducers are installed at an identical cross section, as shown in Figure 7.2(a).

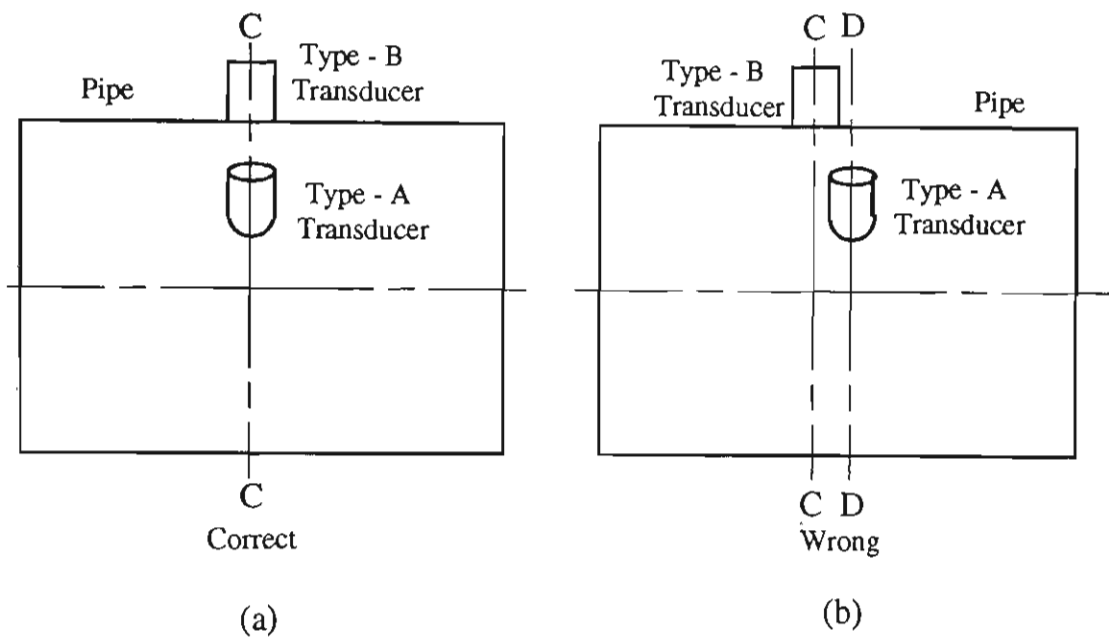


Figure 7.2 Location requirement of pressure transducers.

(b) Flush requirement:

Moving particles come in direct contact with the sensitive surface of the type-B transducer during slug-flow. The type-B transducer must be mounted as flush as possible with the wall of pipe to avoid restricting the moving particles and producing extra pressures on the sensitive surface of the transducer, as shown in Figure 7.3.

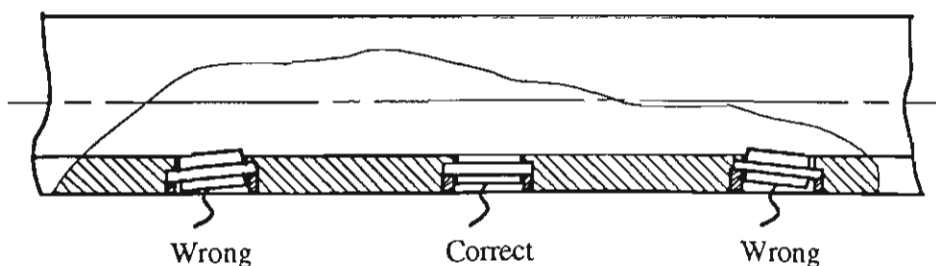


Figure 7.3 Type-B transducer installed flush with pipe wall.

7.2.3 Test Procedures and Special Requirements

Wall pressure measurements are taken during various low-velocity pneumatic conveying experiments. The experiments are completed according to the procedure described in Chapter 4, refer to Section 4.6 for details. As the wall pressure measurement is based on the mutual operation of two pressure transducers, further special procedures are required for the experiments and subsequent data processing.

7.2.3.1 Re-calibration of Transducers

It is known generally that each transducer must be calibrated to obtain a calibration factor. The calibration factor should not change over a short period of time, so that the calibration work is not necessary for each experiment. Normally, the calibration work is undertaken periodically (e.g. every 2 or 3 days depending on the frequency of work) and also before commencing the project. However, both type-A and -B pressure transducers should be calibrated frequently to obtain their calibration factors as accurately as possible (i.e. due to changes in environmental conditions). For example, the calibration factor of the type-B transducer will drift due to the sensitive surface being heated by direct contact of the slugs, whereas the calibration factor of the type-A transducer will be affected less by temperature. Hence it is recommended that type-A and -B transducers be calibrated before starting each group of tests. This work is designated as re-calibration of transducer. Calibration methods and steps for different types of transducers were described previously in Chapter 4, refer to Section 4.6.2 for details.

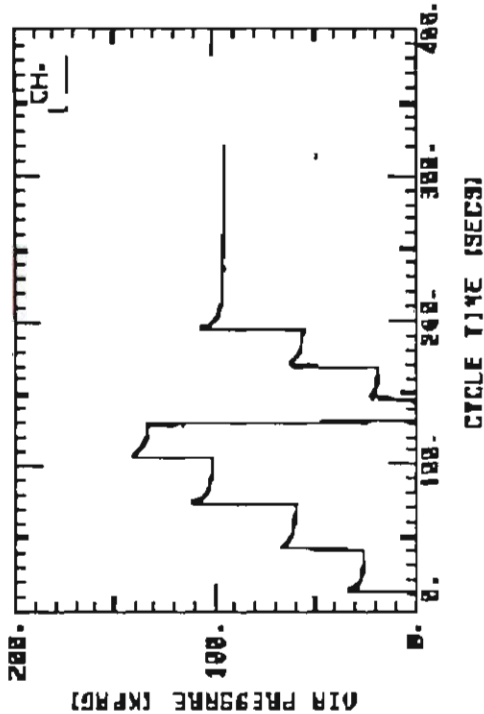
7.2.3.2 Check Test

In order to confirm that air pressure is eliminated totally during wall pressure measurement, a check test is conducted after the re-calibration of transducers. The steps of the check test are listed below:

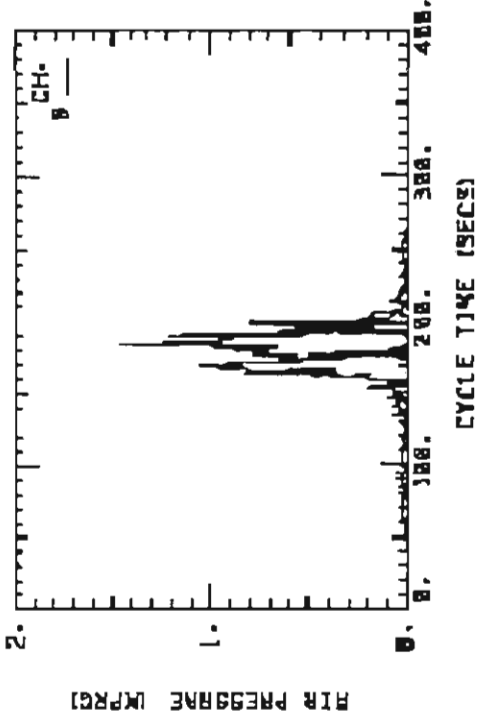
- (i) Remove all material from the pipeline of the low-velocity pneumatic conveying test rig, then block the pipeline at the feed end by using a steel plate and close the back pressure valve (refer to Figure 4.1).
- (ii) Open the air supply valve, blow air into the pipeline until a designated pressure (e.g. 50 kPag) is reached, then close the air supply valve.
- (iii) Maintain the pressure for a certain length of time.
- (iv) Open the air supply valve and blow more air into the pipeline to get a higher level of pressure (e.g. 100 kPag).
- (v) Repeat steps (iii) and (iv) until the highest possible experimental pressure (e.g. 300 kPag) is reached.
- (vi) By actuating the back pressure valve, decrease the pressure step by step to zero.
- (vii) Record and process all the data by computer (i.e subtract the pressure measured by type-A transducer from the pressure measured by the type-B transducer).

TEST DATE: 23/10/92

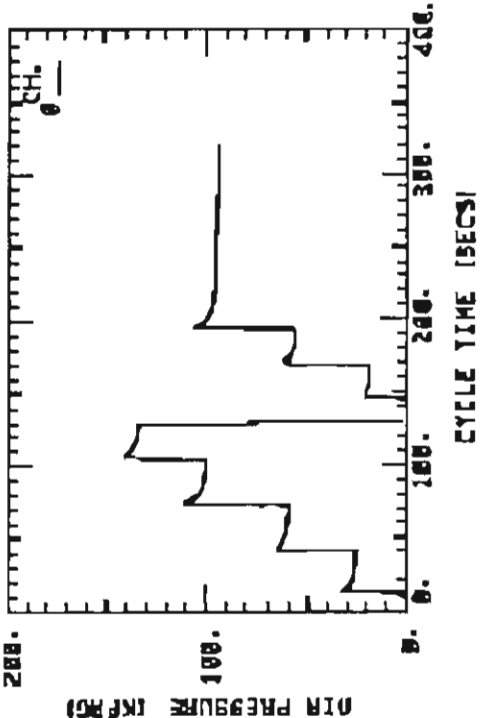
EXPERIMENT NO. 170 - 1



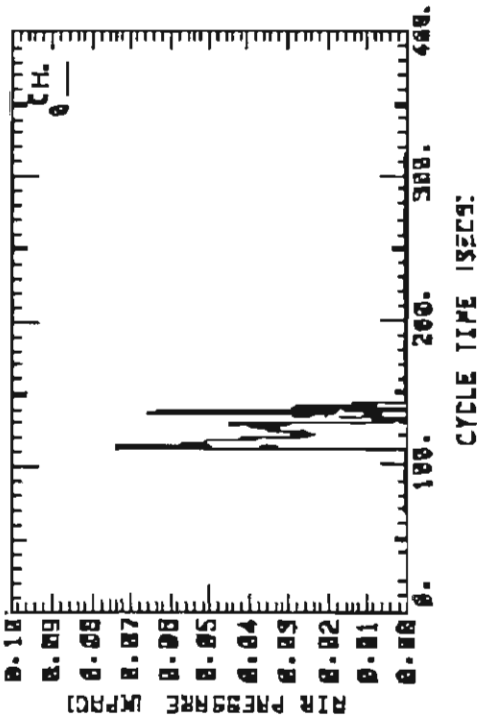
(a)



(b)



(c)



(d)

Figure 7.4 Typical graphs of the pressures and processed results from check tests.

Typical plots from the check tests are presented in Figure 7.4. Figures 7.4(a) and 7.4(b) display the graphs of the air pressure measured by type-B and -A transducers respectively in one check test. Figures 7.4(c) and 7.4(d) demonstrate the processed results, i.e. the pressure differences. Figure 7.4(c) shows that the pressure difference is equal to or near zero over the full range of pressures. This indicates that the test system is accurate and the air pressure can be eliminated successfully from the total pressure. Therefore wall pressure measurement can progress. It is believed that the average processed pressure difference should be less than ten percent of the estimate of wall pressure for using this measurement technique. Figure 7.4(d) shows the case that the pressure difference is too large and test system cannot ensure that the air pressure can be eliminated satisfactorily from the total pressure. Therefore the wall pressure measurement must be stopped (e.g. re-checking or re-installing the relevant transducers and seals, re-calibrating the transducers, etc.).

7.2.3.3 Improvement of Phase Difference of Signals

For two time-variable signals, even though the two signals have the same amplitude, the difference of the two signals will not be zero due to the existence of phase difference, as shown in Figure 7.5.

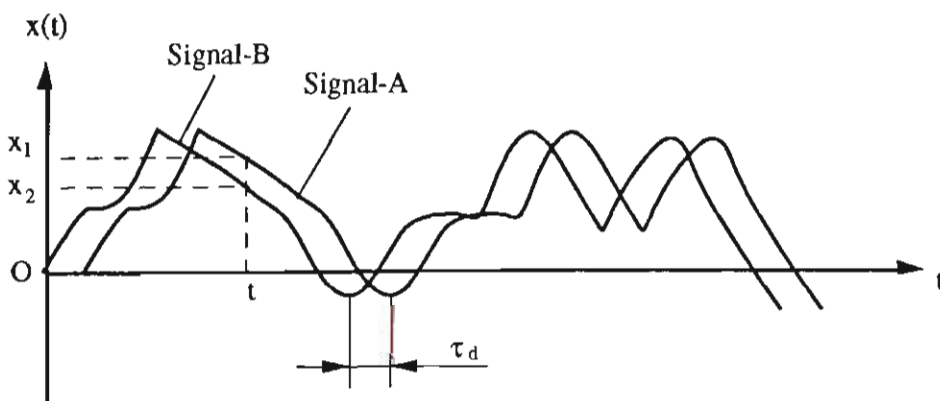


Figure 7.5 Phase difference of signals.

Theoretically, the pressure signals measured respectively by type-A and -B transducers (Signal-A and -B for short in the following) should have same the phase but different

amplitudes if the transducers are installed correctly at an identical cross section of a pipe. However, due to the resistance of the porous plastic, which is fitted in the static air pressure tapping to prevent particles penetrating/blocking the transducer, refer to Figure 4.10, the pressure signal taken after the porous plastic (i.e. Signal-A) will be delayed by a short time after the real time signal (i.e. Signal-B). That is, a small phase difference exists between Signal-A and -B, as shown in Figure 7.5. Thereafter, measurement error will be caused by this phase difference in the wall pressure measurement. To reduce the error, the phase difference must be decreased. Practical experience shows that the permeability of the porous plastic has a significant influence on the phase difference.

During a pneumatic conveying test, the fine particles in the pipe will enter the porous plastic and reduce its permeability or sometimes even block the porous plastics totally (i.e. after several runs). To ensure good permeability of the porous plastic, it is recommended that new porous plastics be used for each wall pressure measurement test.

In addition, the signals are scanned sequentially by a data acquisition system in this research. This also generates a phase difference of signals. For example, if the sampling rate of the data acquisition system is set to 1 Hz for 4 channels, then the time interval of the scan is 0.25 seconds. Providing that type-B transducer is connected to the channel 1 of the data acquisition system and the type-A transducer is connected to the channel 2, then the pressure signal sampled by the type-A transducer will be sampled 0.25 seconds after the pressure signal is scanned by the type-B transducer. If the type-A transducer is connected to channel 3, Signal-A will be delayed by 0.5 seconds after Signal-B. For this reason, it is required that the signals coming from the type-A and -B transducers should be connected to the neighbouring channels of the data acquisition system. Obviously, enhancing the sampling rate of the data acquisition system is another way to reduce the phase difference.

7.2.4 Data Processing

The continuous Signal-A and -B are sampled as two discrete sequences by the data acquisition system:

$$\text{A:} \quad x(t_0), x(t_1), x(t_2), x(t_3), \dots, x(t_{N-1})$$

$$\text{B:} \quad y(t_0), y(t_1), y(t_2), y(t_3), \dots, y(t_{N-1})$$

where N is the total scan number, which $N = 2^r$, and r is an integer.

Each element of the sequences represents the value of the signals at a particular time. Now, letting $z(t_i) = y(t_i) - x(t_i)$ and $i = 0, 1, 2, \dots, N-1$, the following sequence is obtained:

$$\text{C:} \quad z(t_0), z(t_1), z(t_2), z(t_3), \dots, z(t_{N-1})$$

The sequence C represents the values of the wall pressure signal exerted by slugs in a vertical slug-flow. For horizontal slug-flow, it represents the values of total wall pressure. This operation can be carried out easily by a computer. The sample values of the wall pressure are set to zero if they are found negative during computing (i.e. negative wall pressure is impossible).

7.3 Experimental Results

According to the above method, wall pressure data are obtained for various low-velocity pneumatic conveying experiments, see Appendix A. Figure 7.6 shows the wall pressures (see Figure 7.6(a)) and air pressures (see Figure 7.6(b)) for the black plastic pellets conveyed through the 52 m x 105 mm ID pipeline.

EXPERIMENT NO. 167 - 7

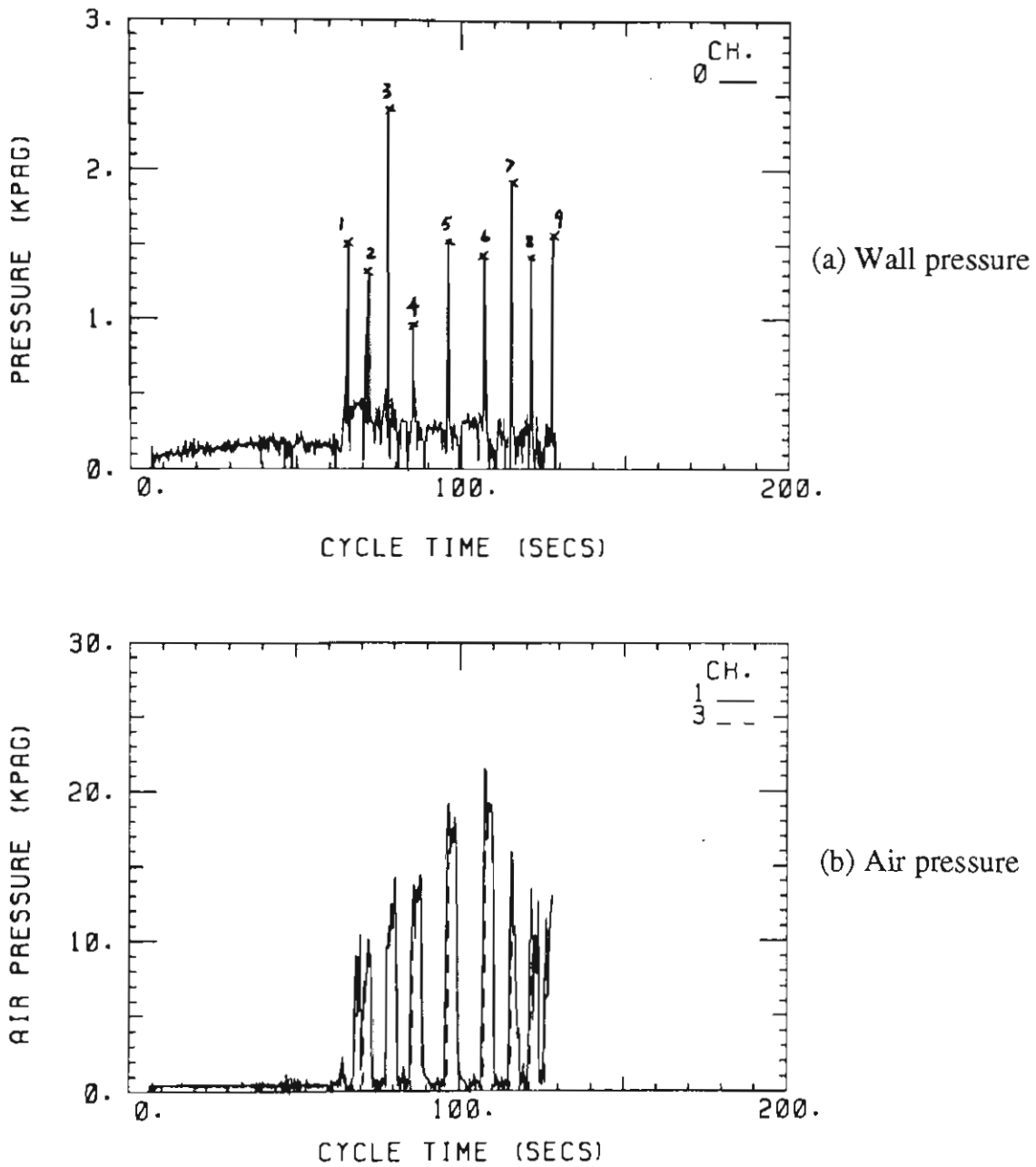


Figure 7.6 Plots of wall pressure and air pressure for black plastic pellets,

$$m_f = 0.0643 \text{ kgs}^{-1}, m_s = 0.849 \text{ kgs}^{-1}.$$

The fluctuations in signal and peaks are quite obvious in plots (a) and (b). Each peak indicates a particle slug flowing in the pipe. The peaks in Figure 7.6(a) basically correspond to the peaks in Figure 7.6(b). It is found in some other tests that occasionally a peak appears in the air pressure plot, while no peak occurs in the wall pressure plot.

This indicates that a slug forms at a downstream point of the test point of the wall pressure, as shown in Figure 7.7

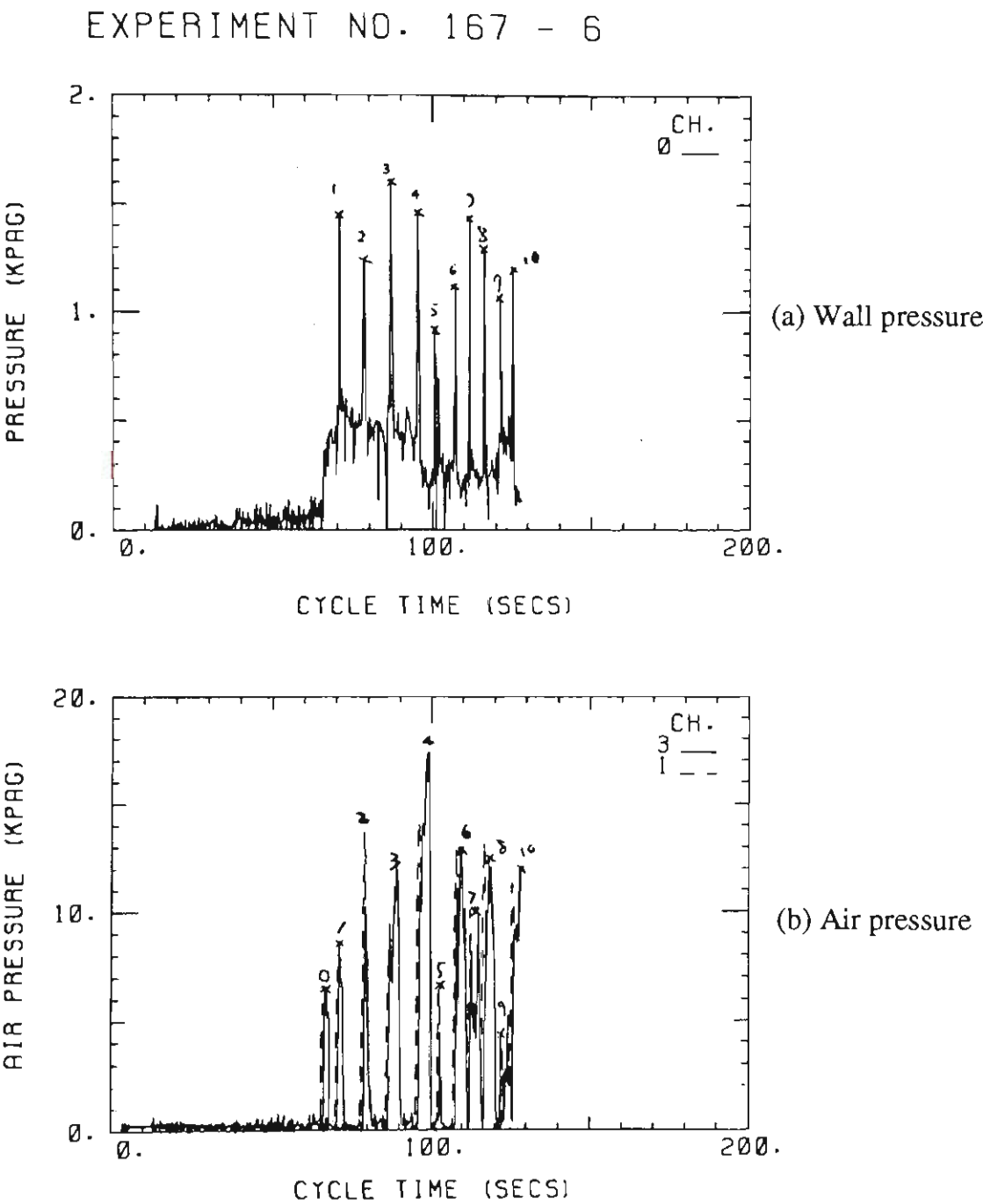


Figure 7.7 Plots of wall pressure and air pressures for black plastic pellets,
 $m_f = 0.0498 \text{ kgs}^{-1}$, $m_s = 0.840 \text{ kgs}^{-1}$.

Figures 7.6 and 7.7 also show that the location of each peak is same in the two plots, but the pressure decay rate after each peak is slower in plot (b) than plot (a). The reason is that the peak of wall pressure only appears when the slug passes through the test point,

i.e. the wall pressure "disappears" as soon as the slug leaves the test point. However, the air pressure still is evident until the slug arrives at the end of the pipe or the slug collapses. Hence the peak of the air pressure lasts for a longer time. Further discussions on this aspect are contained in the next chapter.

It can also be observed clearly from the wall pressure plots that different slugs cause different values of wall pressure (i.e. the wall pressure peaks have different heights), refer to Figures (7.6) and (7.7). Hence an average value of all these wall pressures is used to represent the wall pressure obtained during a test which is undertaken under a given conveying condition. For horizontal slug-flow, since the type-B transducer is located on the bottom of the pipe of the low-velocity pneumatic conveying test rig, that part of the measured value exceeding $\sigma_w = \rho_b g D$ is considered as the wall pressure. Otherwise the value is the wall pressure caused by the weight of the slug or stationary bed. Figures 7.8 to 7.11 present the average wall pressure of each test plotted against the mass flow-rate of air. These plots show that wall pressure increases linearly as mass flow-rate of air increases in low-velocity pneumatic conveying.

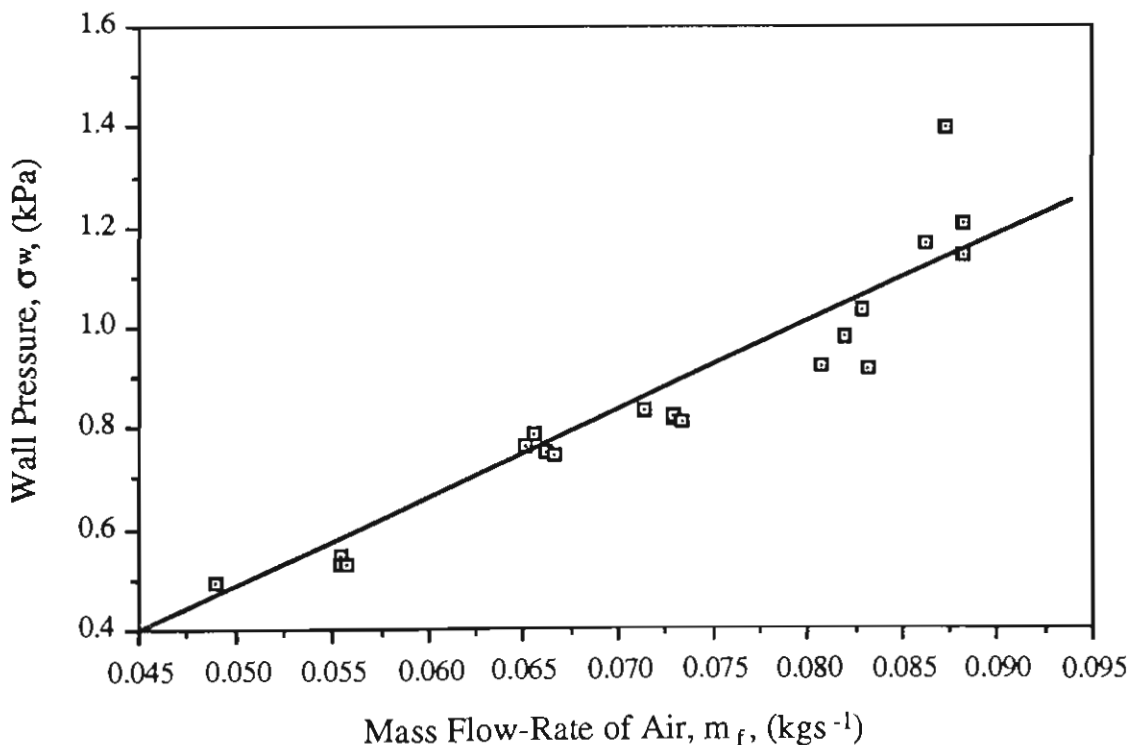


Figure 7.8 Wall pressure versus mass flow-rate of air for white plastic pellets.

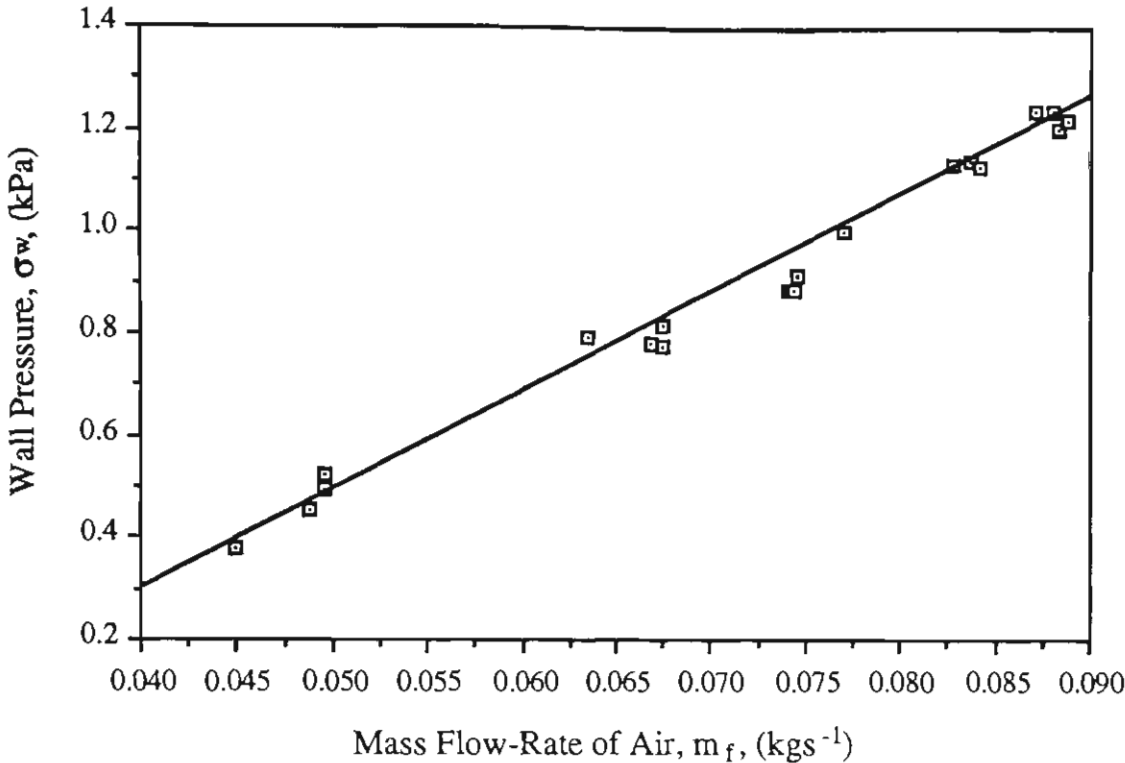


Figure 7.9 Wall pressure versus mass flow-rate of air for black plastic pellets.

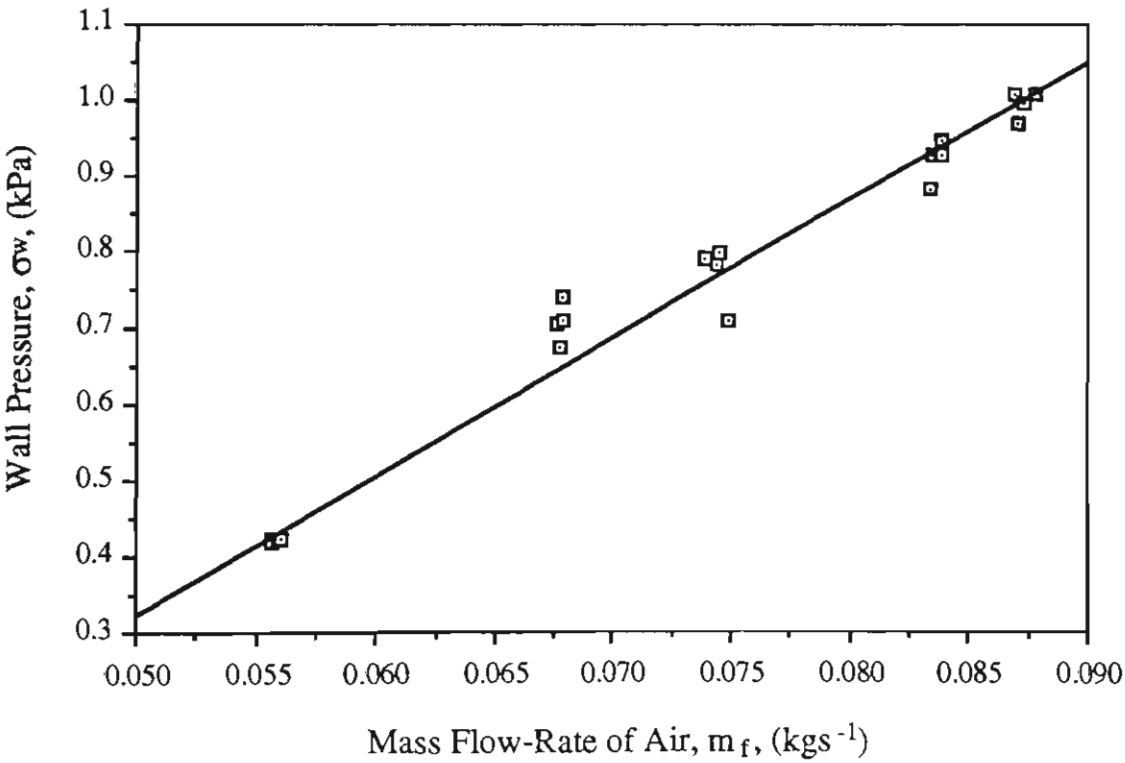


Figure 7.10 Wall pressure versus mass flow-rate of air for wheat.

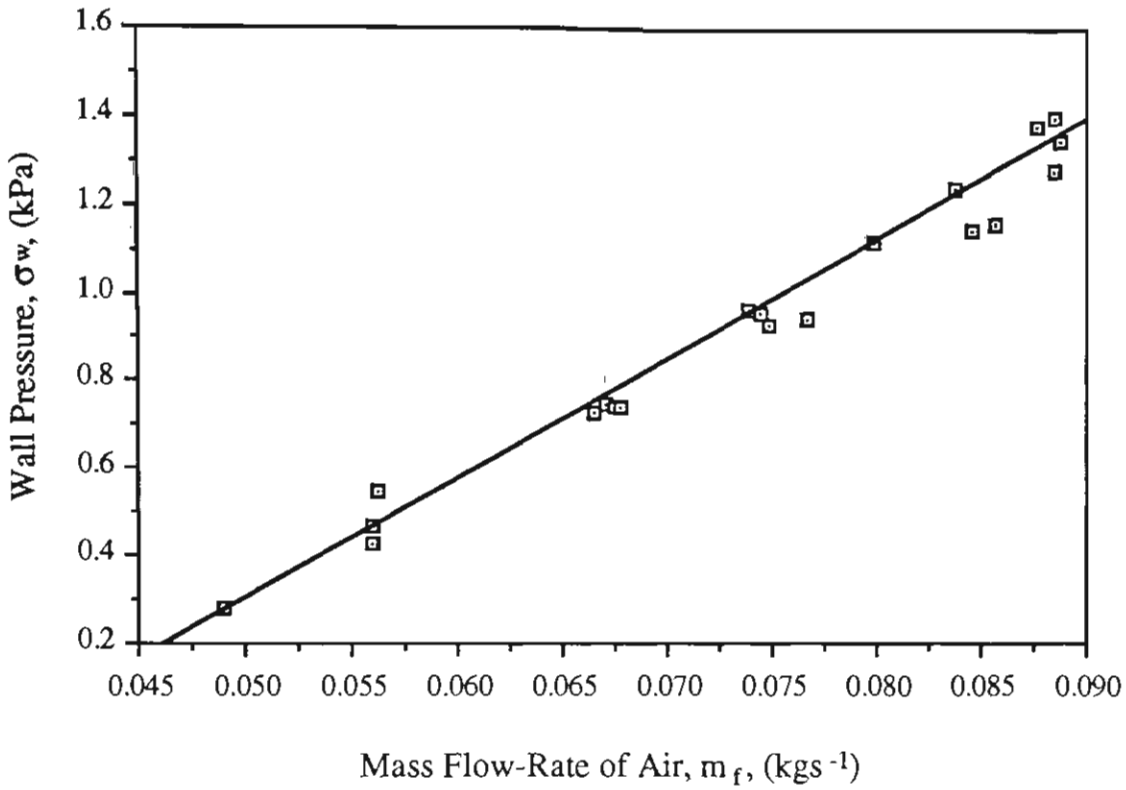


Figure 7.11 Wall pressure versus mass flow-rate of air for barley.

The stress transmission coefficient (λ) is a parameter relevant to wall pressure. Since the stress transmission coefficient in a slug is approximately equal to the ratio of the average wall pressure to the frontal stress of the slug in low-velocity pneumatic conveying, i.e. $\lambda \approx \frac{\sigma_{wm}}{\sigma_f}$, see Section 3.5.2, it is possible to obtain the approximate values of λ after the wall pressure data have been measured.

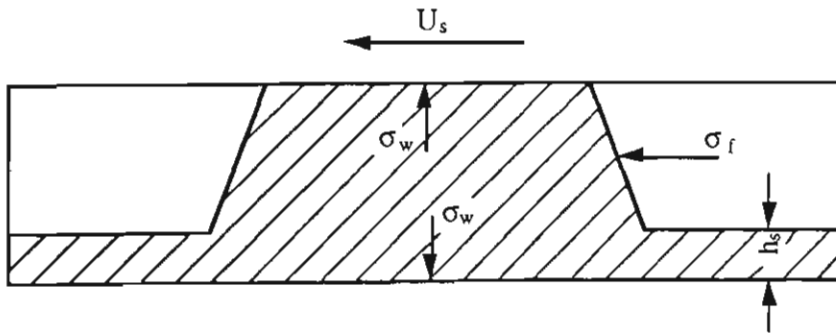


Figure 7.12 Stresses acting on a particle slug.

Besides the wall pressure, the slug velocity (U_s) and stationary bed thickness (h_s) as shown in Figure 7.12, are also needed to determine λ , since $\sigma_f = \alpha \rho_b U_s^2$. In fact, U_s and

h_s have been measured already in this research for different conveying tests. The results of the slug velocities have been shown in Chapter 6. The results of the stationary bed thickness and corresponding α are presented in Chapter 8. Hence λ can be calculated. For example, when wheat ($\rho_b = 811.5 \text{ kgm}^{-3}$) is conveyed under the conveying conditions of $m_f = 0.0495 \text{ kgs}^{-1}$ and $m_s = 0.967 \text{ kgs}^{-1}$, the average wall pressure, slug velocity, cross sectional area ratio of stationary bed to pipe are measured as: $\sigma_{wm} = 0.334 \text{ kPa}$, $U_s = 1.747 \text{ ms}^{-1}$ and $\alpha = 0.256$, therefore,

$$\sigma_f = \alpha \rho_b U_s^2 = 0.256 \times 811.5 \times 1.747^2 = 634.0 \text{ Pa} = 0.634 \text{ kPa}$$

and
$$\lambda = \frac{\sigma_{wm}}{\sigma_f} = \frac{0.334}{0.634} = 0.527$$

Table 7.1 lists the values of the stress transmission coefficient and corresponding operating conditions for wheat.

Table 7.1: Experimental wall pressure and stress transmission coefficient for wheat.

Exp. No.	52 m pipeline					96 m pipeline				
	m_f (kgs ⁻¹)	m_s (kgs ⁻¹)	σ_{wm} (kPa)	σ_f (kPa)	λ	m_f (kgs ⁻¹)	m_s (kgs ⁻¹)	σ_{wm} (kPa)	σ_f (kPa)	λ
1	0.0495	0.967	0.334	0.634	0.527	0.0557	1.159	0.420	0.768	0.547
2	0.0663	0.959	0.671	1.158	0.579	0.0676	1.157	0.702	1.193	0.588
3	0.0733	0.957	0.726	1.346	0.539	0.0749	1.161	0.706	1.310	0.539
4	0.0828	0.961	0.896	1.656	0.541	0.0838	1.168	0.926	1.688	0.601
5	0.0882	0.962	0.978	1.729	0.566	0.0870	1.162	0.969	1.712	0.587
6	0.0495	1.450	0.341	0.622	0.548	0.0559	1.494	0.423	0.762	0.555
7	0.0665	1.439	0.639	1.101	0.580	0.0678	1.494	0.737	1.223	0.603
8	0.0742	1.439	0.785	1.333	0.589	0.0754	1.496	0.796	1.364	0.584
9	0.0836	1.439	0.892	1.604	0.556	0.0833	1.497	0.882	1.529	0.577
10	0.0885	1.461	0.997	1.762	0.566	0.0869	1.493	1.007	1.623	0.622
11	0.0545	1.945	0.442	0.760	0.582	0.0560	1.960	0.423	0.728	0.515
12	0.0676	1.986	0.711	1.234	0.576	0.0678	1.957	0.707	1.191	0.594
13	0.0747	1.977	0.746	1.300	0.573	0.0739	1.968	0.788	1.346	0.585
14	0.0796	1.997	0.814	1.423	0.572	0.0838	1.969	0.948	1.524	0.622
15	0.0868	1.996	0.909	1.597	0.569	0.0878	1.964	1.008	1.703	0.592
16	0.0543	2.300	0.403	0.773	0.521	0.0556	2.387	0.423	0.828	0.511
17	0.0657	2.383	0.663	1.130	0.587	0.0677	2.402	0.673	1.190	0.566
18	0.0747	2.403	0.780	1.364	0.572	0.0744	2.374	0.781	1.357	0.576
19	0.0838	2.388	0.952	1.688	0.564	0.0835	2.373	0.928	1.535	0.605
20	0.0885	2.415	1.028	1.747	0.588	0.0873	2.375	0.996	1.709	0.583

From the values of λ listed in Table 7.1, it can be seen that for a given granular material, the stress transmission coefficient is approximately constant and for wheat obtains an average value of 0.572, despite the different conveying conditions and pipe lengths. This

indicates that the stress transmission coefficient is a function of the physical properties of the bulk material and pipe. The test results also obtain similar findings, see Appendix A. Table 7.2 lists the average values of λ obtained from experiment and the necessary calculations for each test material.

Table 7.2: Stress transmission coefficient λ for different test materials

Material	Plastic pellets (white)	Plastic pellets (white)	Wheat	Barley
λ	0.756	0.806	0.572	0.655

7.4 Strength of Particulate Medium

After obtaining the experimental values of stress transmission coefficient (λ), the next stage of the investigation is to correlate λ with the relevant influential factors. To achieve this, first of all it is necessary to explore some aspects of the strength of particulate material.

Applying the knowledge of the flow properties of bulk material introduced in Chapter 5, the strength of the bulk material, prepared to a specific degree of consolidation can be represented on a shear-compressive stress diagram by a yield locus (YL) together with a wall yield locus (WYL), which represent the limiting stress conditions that can be sustained by a plane wall bounding the bulk material, refer to Section 5.4.

Figure 7.13(a) shows an element P within a semi-infinite homogeneous bulk material and adjacent to a vertical plane wall. Suppose that the bulk material is in a static state initially, the stresses at the element P can be represented by a Mohr circle with the centre at C_0 lying completely below the yield locus and wall yield locus of the material, as shown in Figure 7.13(b). Points A and B on the Mohr circle C_0 represent the stresses acting on the horizontal and vertical planes passing through the element P, see Figure 7.13(a). As can be seen from Figure 7.13(b), the normal stress acting on the vertical plane (σ_x) is less than the normal stress acting on the horizontal plane (σ_z). This state of stress is called the

active case. If $\sigma_x > \sigma_z$, then the state of stress is called the passive case. σ_1 and σ_2 in Figure 7.13(b) are the major and minor principle stresses. In Figure 7.13(b), the yield locus and wall yield locus are straight lines passing through the origin of the σ_n - τ_n coordinate system. This case is true for clean, dry and cohesionless particulate materials. ϕ and ϕ_w are the internal friction angle and wall friction angle of the bulk material, respectively.

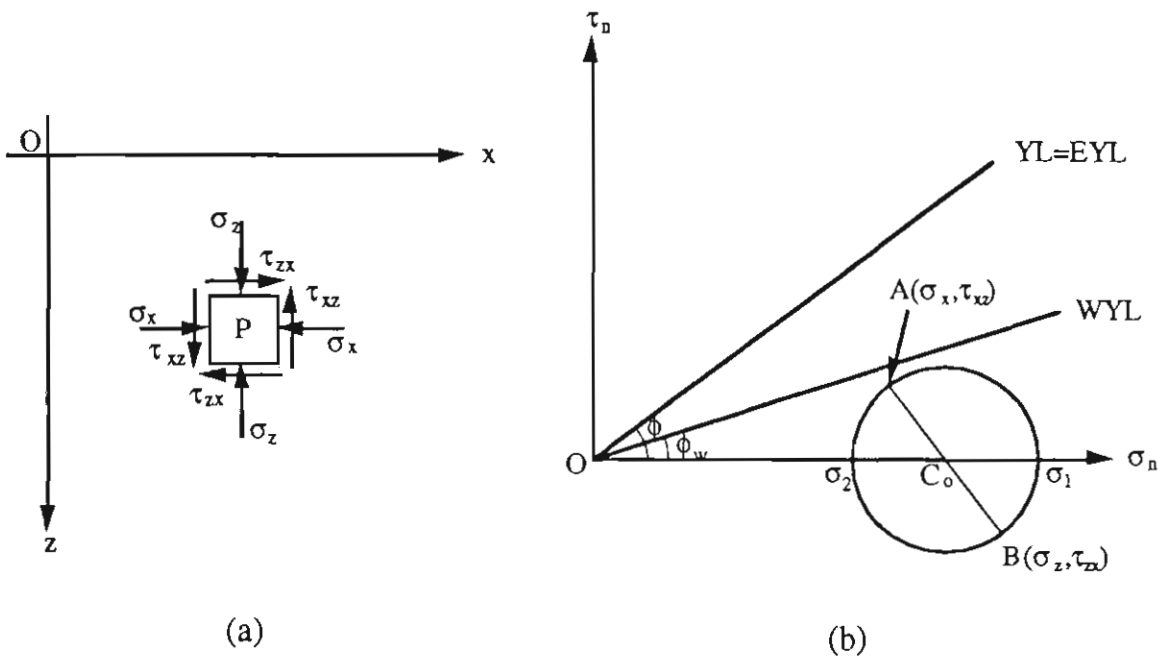


Figure 7.13 Stresses on element P in particulate medium and Mohr circle representation.

Suppose now that the state of stress at the element P begins to change in such a way that the major stress σ_1 remains unchanged but the minor stress σ_2 is reduced. The effect is shown by the series of Mohr circles in Figure 7.14 with the corresponding minor stresses σ_2 , σ'_2 and σ''_2 . Points A, A₁ and A₂ shown in Figure 7.14 represent the corresponding stresses acting on the vertical plane passing through the element P shown in Figure 7.13(a). During the procedure of the expansion of the Mohr circle, three states of the particulate medium are included. The first is the static state of the particulate medium, i.e. all the particles are stationary. At this time, the Mohr circle lies completely under the wall yield locus, see Mohr circle C_o in Figure 7.14.

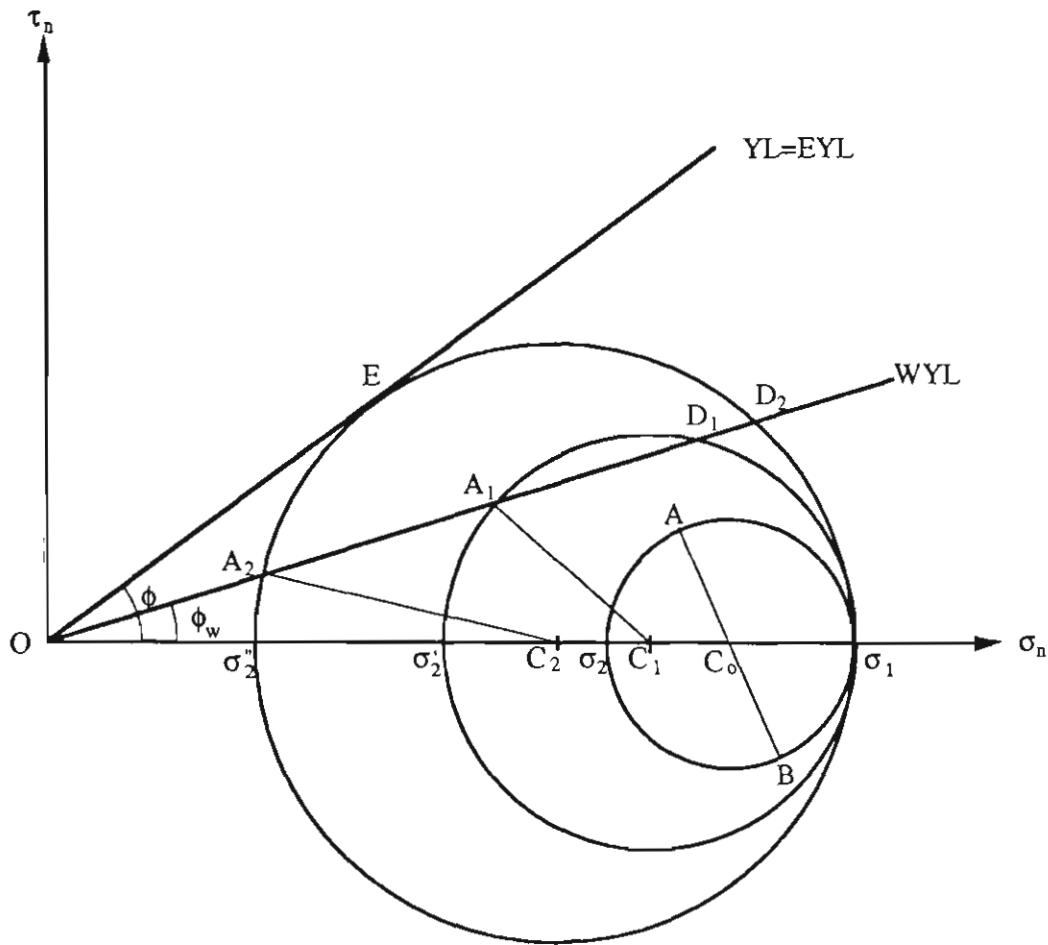


Figure 7.14 Possible state of stress at element P represented by a series of Mohr circles.

The second state of the particulate medium is that the Mohr circle touches the wall yield locus or is over it, but still lies completely under the yield locus, as shown in Figure 7.14 with centre at C_1 . In this state shearing occurs at the boundary between the particulate medium and wall, however, due to the Mohr circle C_1 being below the yield locus (called the Mohr failure envelope), the particles in the particulate medium are fixed relative to each other. Hence the particulate medium will slip as a rigid body along the wall plane. The points representing the plane of the wall lies at A_1 or D_1 . This state probably can be called a rigid movement state of particulate medium.

If the Mohr circle continues to expand until it is tangential to the Mohr failure envelope, where σ_2 gets its minimum value σ_2'' for the active stress state: no state of stress (nor Mohr circle) may exist above the Mohr failure envelope, such as that shown in Figure

7.14 with centre at C_2 . This is the third state of the particulate medium. In this state, the failure (flowing) of the material occurs, i.e. relative movement exists between the particles. The failure occurring at the active stress state is called active failure. The particles adjacent to the wall plane also slip along the wall and A_2 or D_2 represent the plane of the wall. The state of stress acting at the point E in Figure 7.14 is the theoretical limiting state of stress on the failure plane at failure.

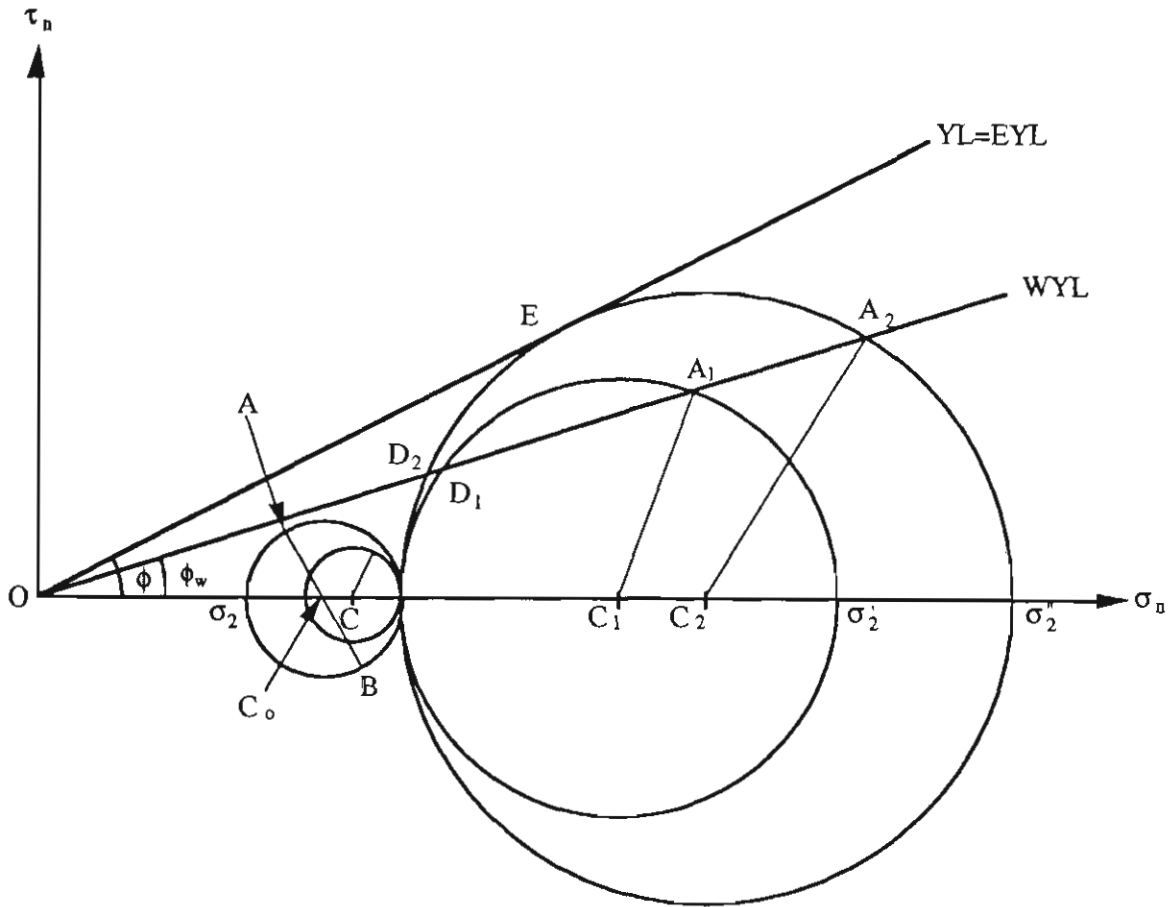


Figure 7.15 Possible states of stress at element P in passive stress state.

The above discussion involves the active stress case. If still maintaining the major stress σ_1 , the stress state now is changed by increasing the major stress σ_2 . The circles representing possible states of stress at element P are shown in Figure 7.15. With σ_2 increasing, the circle passes through the element circle $\sigma_2 = \sigma_1$ to the limiting case where the failure of the particulate medium occurs with σ'_2 and σ''_2 , as shown in Figure 7.15 with the centre at C_2 . σ''_2 is the maximum value in passive case. This failure is called

passive failure. The particles adjacent to the wall also slip along the wall plane and A_2 or D_2 represent the plane of the wall.

7.5 Stress Transmission Coefficient

Stress transmission coefficient exhibits the relationship of normal stress on two mutually vertical planes. Its value is affected by the state, strength and some physical properties of bulk material. The following stress analyses attempt to develop a general expression for λ .

7.5.1 Stress Transmission Coefficient in Pipe

As this research is concerned with low-velocity pneumatic conveying, the investigation starts with a particle slug flowing in a pipe. For convenience, the pipe is considered vertical, as shown in Figure 7.16.

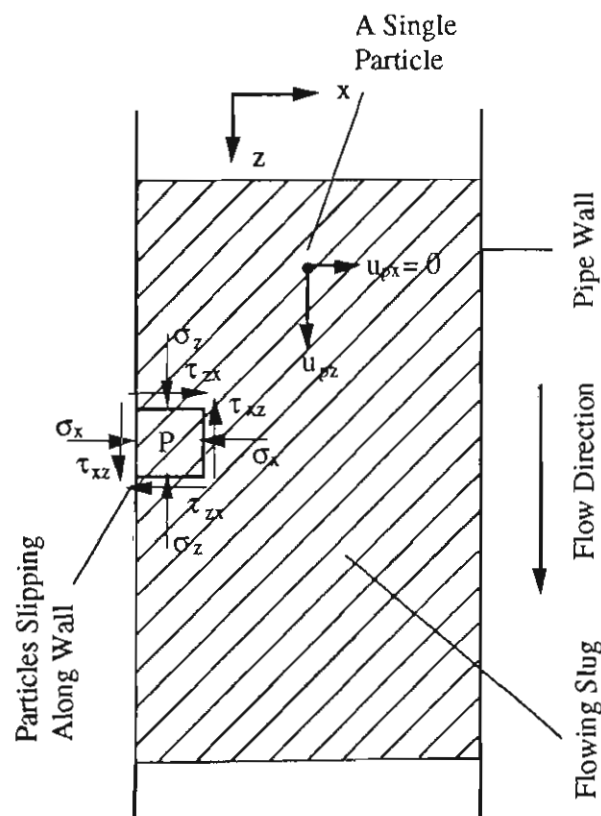


Figure 7.16 Particles flowing in a vertical pipe.

(axial) stress (σ_z) of the element P. Hence, the stress transmission coefficient in the vertical pipe will be σ_x/σ_z . As $\sigma_x < \sigma_z$, the stress state of the element P is the active case. The stress transmission coefficient at active case is written as λ_A which can be determined from the principles of geometry.

Draw a tangent line OF to the Mohr circle C and let it pass through the origin of σ_n - τ_n coordinate system, see Figure 7.17. The angle between the straight line OF and σ_n -coordinate is ϕ_s defined here as the static internal friction angle since any particle in the slug remains stationary relative to the adjacent particles at this stage. As the bulk material slips along the pipe wall, $\phi_w \leq \phi_s \leq \phi$.

Applying the sine rule to triangle OAC in Figure 7.17:

$$\sigma_x = P_s - r \cos(\omega - \phi_w) \quad (7.4)$$

$$\sigma_z = P_s + r \cos(\omega - \phi_w) \quad (7.5)$$

$$\frac{P_s}{\sin(\pi - \omega)} = \frac{r}{\sin \phi_w} \quad (7.6)$$

From the triangle OEC:

$$P_s = \frac{r}{\sin \phi_s} \quad (7.7)$$

Substituting P_s in Equations (7.4) and (7.5) with Equation (7.7), and eliminating r ,

$$\lambda_A = \frac{\sigma_x}{\sigma_z} = \frac{1 - \sin \phi_s \cos(\omega - \phi_w)}{1 + \sin \phi_s \cos(\omega - \phi_w)} \quad (7.8)$$

Also substituting P_s in Equation (7.6) with Equation (7.7) and eliminating r ,

$$\sin \omega = \sin \phi_w / \sin \phi_s \quad (7.9)$$

Note that all the above equations apply to the active case of stress state. For the passive case of stress state, the stress transmission coefficient λ_P is obtained similarly, provided σ_x and σ_z are interchanged in Figure 7.17. The final result is

$$\lambda_P = \frac{\sigma_x}{\sigma_z} = \frac{1 + \sin \phi_s \cos(\omega + \phi_w)}{1 - \sin \phi_s \cos(\omega + \phi_w)} \quad (7.10)$$

From Equations (7.8) and (7.10), it can be found that for a given bulk material, the stress transmission coefficient is determined only by its static internal friction angle and wall friction angle while the material flows in the pipe with rigid and parallel wall. Obviously $\lambda_P > \lambda_A$.

Note that although Equations (7.8), (7.9) and (7.10) are developed for the stress transmission coefficient in a vertical pipe, no special nature of the vertical pipe has been used during the development of the equations. Hence it is reasonable to assume that the equations are also suitable for the stress transmission coefficient in a horizontal pipe. Certainly for the horizontal pipe, the pressure due to weight must be excluded from this coefficient.

7.5.2 Discussion on Stress Transmission Coefficient

From Equations (7.8), (7.9) and (7.10), it can be seen clearly that stress transmission coefficient (λ) is a function of static internal friction angle (ϕ_s) and wall friction angle (ϕ_w). As the wall friction angle is normally a constant for a given bulk material and pipe, the following discussion is focused on the variation of λ with different ϕ_s .

Discussion 1: Wall friction angle $\phi_w = 0$.

This case occurs at the static state of the bulk material supported by a plane. Looking at Figure 7.16, if the pipe has a bottom, the material will be supported by the bottom and has no trend of slipping along the wall. Therefore, the wall friction angle is equal to zero. The bulk material contained in a silo or hopper with the outlet gate closed is analogous to

this case. The λ in this case is called static stress transmission coefficient, symbolled as λ_o . From Figure 7.16, as $\phi_w = 0$, there will be no shearing stress on the vertical and horizontal planes of the element P. This means the normal stress σ_x and σ_z is equal to principle stress σ_1 and σ_2 of the element. Hence the static stress transmission coefficient actually exhibits the relationship between the principle stresses. Substituting $\phi_w = 0$ into Equations (7.8), (7.9) and (7.10), λ_o is given as:

$$\text{For active case} \quad \lambda_o = \frac{\sigma_1}{\sigma_2} = \frac{1 - \sin \phi_s}{1 + \sin \phi_s} \quad (7.11)$$

$$\text{For passive case} \quad \lambda_o = \frac{\sigma_1}{\sigma_2} = \frac{1 + \sin \phi_s}{1 - \sin \phi_s} \quad (7.12)$$

It can be easily found from Equations (7.11) and (7.12) that λ_o decreases in the active case and increases in the passive case while increasing the static internal friction angle (ϕ_s). If ϕ_s increases to the internal friction angle ϕ , λ_o will obtain its minimum value in active case, whereas λ_o will reach the maximum value in the passive case. That is

$$\lambda_{o\min} = \frac{1 - \sin \phi}{1 + \sin \phi} \quad (7.13)$$

$$\lambda_{o\max} = \frac{1 + \sin \phi}{1 - \sin \phi} \quad (7.14)$$

where $\lambda_{o\min}$ and $\lambda_{o\max}$ are the minimum and maximum static stress transmission coefficients.

During the initial filling of material into a silo or hopper with the outlet gate closed, the minimum static stress transmission coefficient is available. Taking white plastic pellets for example, the internal and wall friction angles are 15.15° and 44.7° , respectively, hence the minimum stress transmission coefficient is

$$\lambda_{o\min} = \frac{1 - \sin 44.7^\circ}{1 + \sin 44.7^\circ} = 0.174$$

Discussion 2: Wall friction angle $\phi_w \neq 0$

Increasing the static internal friction angle (ϕ_s), see Equation (7.9), the value of ω decreases, then from Equation (7.10) it can be found that the stress transmission coefficient (λ) increases for the passive stress state. As soon as ϕ_s reaches to the internal friction angle ϕ , λ obtains a maximum value. At this stage, the passive failure occurs in the bulk material. This is so called the third state of the bulk material. Replacing ϕ_s with ϕ , the maximum stress transmission λ_{\max} can be

$$\lambda_{\max} = \frac{1 + \sin\phi \cos(\omega + \phi_w)}{1 - \sin\phi \cos(\omega + \phi_w)} \quad (7.15)$$

where $\sin \omega = \sin \phi_w / \sin \phi$.

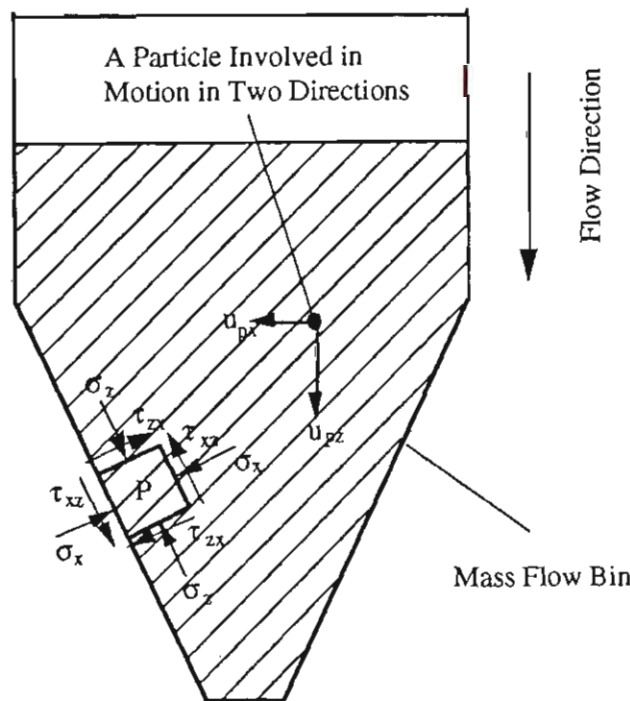


Figure 7.18 Particles moving in a silo.

The feature of the third state of the material is that the particles of the material start to flow (i.e. there is relative movement between the particles). If the particles are adjacent to a wall, they also slip along the wall plane. This case can be seen when bulk material flows in the convergent part of a silo, as shown in Figure 7.18. During the flow of the material,

due to the contraction of the cross sectional area of the silo, the deformation of particles will accompany the downward movement of the particles to allow the flow to continue. That is, the particles must move laterally in the silo as they flow down, resulting in relative movement between the particles.

The particles arching in a slug also exhibit the third state of the material, hence the arching area of the slug will give the maximum value of the stress transmission coefficient. That is why a slug sometimes can exert a very high pressure on a pipe wall. In wall pressure measurement, such extremely high wall pressures are excluded from the average calculation.

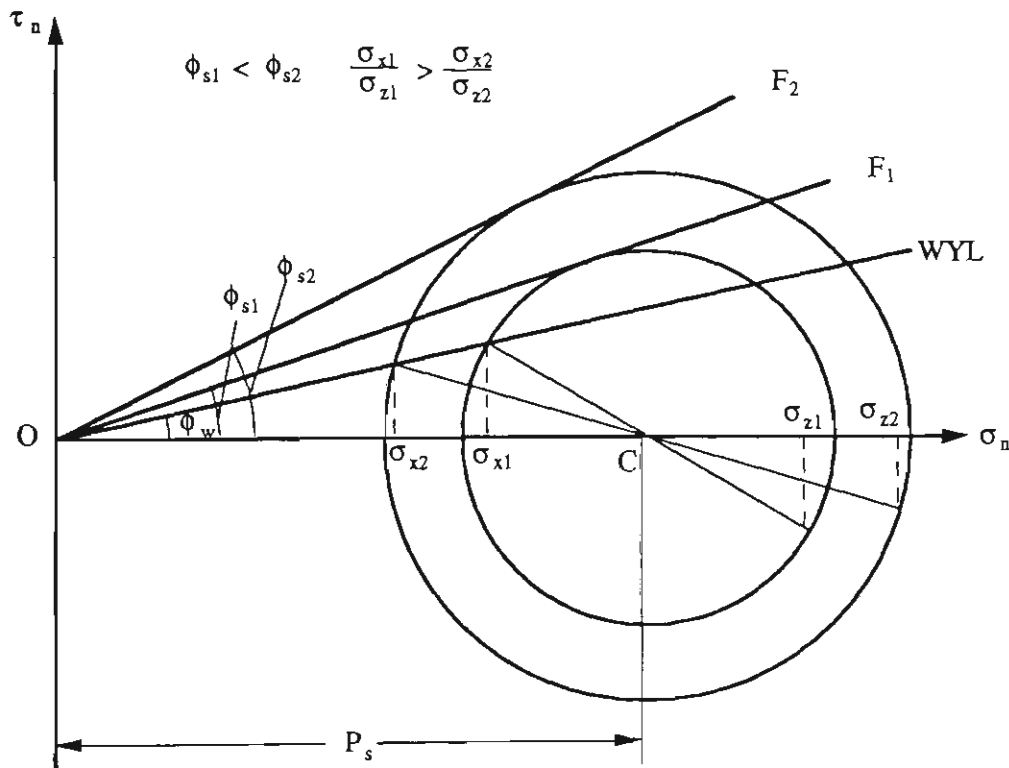


Figure 7.19 Variation trend of stress transmission coefficient in active case.

If the stress state is in active case, while ϕ_s increases, it is difficult to decide the variation trend of λ from Equation (7.8). However, it can be seen easily from the strength diagram shown in Figure 7.19 that the stress transmission coefficient decreases.

Similarly, the active failure occurs while ϕ_s rises to ϕ , the stress transmission coefficient λ reaches its minimum value. Replacing ϕ_s in Equation (7.8) with ϕ , the minimum λ can be

$$\lambda_{\min} = \frac{1 - \sin\phi \cos(\omega - \phi_w)}{1 + \sin\phi \cos(\omega - \phi_w)} \quad (7.16)$$

where $\sin\omega = \sin\phi_w / \sin\phi$.

This case can be found in the particles flowing in the expansion part of a silo.

From the discussion, it is known that the λ at active failure and passive failure are the extreme values which are determined by internal and wall friction angles. Generally speaking, the internal friction angle ϕ or wall friction angle ϕ_w are constant for a given material and wall, hence λ at active failure and passive failure (i.e. λ_{\min} and λ_{\max}) are determined uniquely. For example, ω is calculated as 21.82° for white plastic pellets, so that λ_{\min} and λ_{\max} are

$$\lambda_{\min} = \frac{1 - \sin 44.7^\circ \cos(21.82^\circ - 15.15^\circ)}{1 + \sin 44.7^\circ \cos(21.82^\circ - 15.15^\circ)} = 0.178$$

$$\lambda_{\max} = \frac{1 + \sin 44.7^\circ \cos(21.82^\circ + 15.15^\circ)}{1 - \sin 44.7^\circ \cos(21.82^\circ + 15.15^\circ)} = 3.566$$

That is, all possible stress transmission coefficients are contained in the range of $0.178 \leq \lambda \leq 3.566$ for the white plastic pellets.

7.6 Correlation of Static Internal Friction Angle

Equations have been developed and discussed in the previous section for the stress transmission coefficient λ . However, the value of λ is dependent on the static internal friction angle (ϕ_s) as given in Equations (7.8), (7.9) and (7.10). Hence, a relationship between ϕ_s and its influential factors also needs to be investigated.

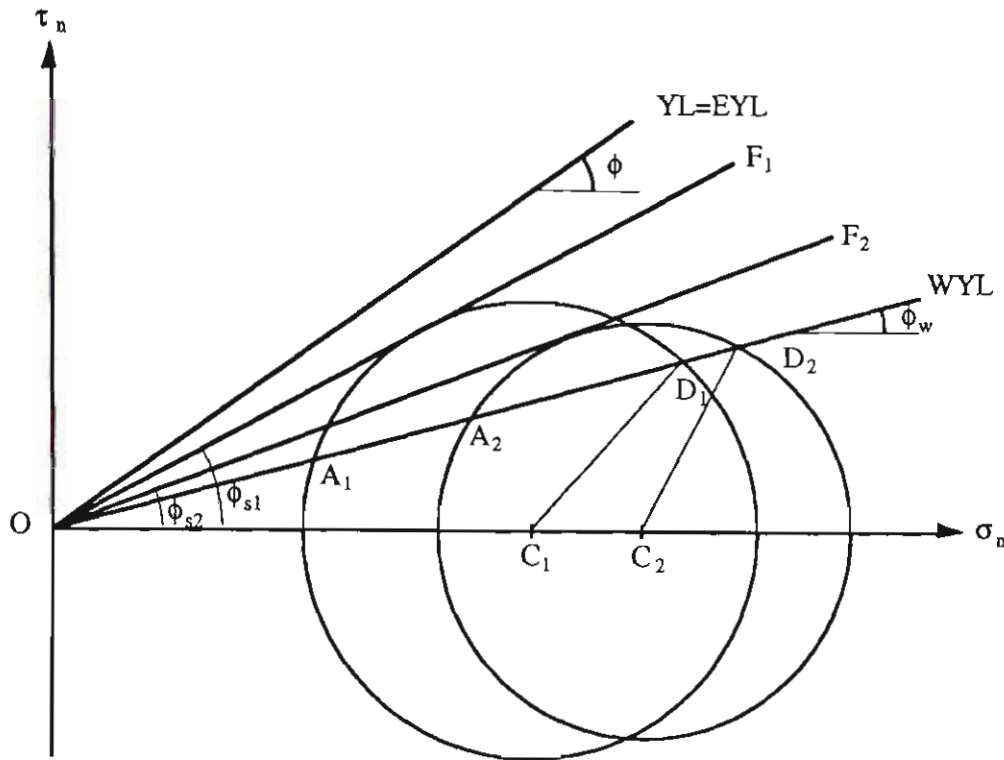


Figure 7.20 Possible Mohr circles representing the stress state of a particle slug.

As shown in Figure 7.20, while a bulk material flows in the form of slugs in a pipe, there are an infinite number of possible Mohr circles representing the stress state of the slug located between the YL and WYL of the material. For example, the stress states represented by the Mohr circles C_1 and C_2 satisfy the criteria of the slug flowing in the pipe, i.e. the particles of the slug slip along the pipe wall, but there is no relative movement between the particles. By drawing tangent line OF_1 to the Mohr circle C_1 and tangent line OF_2 to the Mohr circle C_2 through the origin of the coordinate system, two different static internal friction angles are obtained as ϕ_{s1} and ϕ_{s2} . It appears difficult to know exactly the actual static internal friction angle. However, there always exists a unique Mohr circle which represents the actual stress state of the slug. Due to the uncertainty of the actual "location" of Mohr circle of the slug, it seems impossible to predict the internal static friction angle from theory. Hence, an empirical correlation is sought.

From the results of λ listed in Table 7.2, static internal friction angles can be calculated by using Equations (7.8) and (7.9) or (7.10) for the test material. It is also noted that all the stress transmission coefficients for the materials are less than 1. This means that the stress state of slugs should be in the active stress case during slug-flow. Hence Equation (7.10) will not be useful for this calculation.

For example, the experimental λ of white plastic pellets is 0.756. Substituting this value and the data of the internal and wall friction angle of the white plastic pellets into Equations (7.8) and (7.9) gives

$$\sin \omega = \sin 15.15^\circ / \sin \phi_s \quad (7.17)$$

$$\frac{1 - \sin \phi_s \cos(\omega - 15.15^\circ)}{1 + \sin \phi_s \cos(\omega - 15.15^\circ)} = 0.756 \quad (7.18)$$

Solving Equations (7.17) and (7.18), the value of the static internal friction angle ϕ_s is 15.75° for the white plastic pellets when they flow in the form of slugs in a pipe.

Table 7.3 lists the calculated static internal friction angles of each test material.

Table 7.3: Static internal friction angles for test materials

Material	Plastic pellets (white)	Plastic pellets (white)	Wheat	Barley
ϕ_s	15.75°	13.40°	20.08°	16.81°

Based on the data listed in Table 7.3, an expression for static internal friction angle can be regressed. Similar to the internal friction angle, the static internal friction angle also is one of the flow properties of material. Therefore, its value is only relevant to the material and should have nothing to do with the size of the material and the external factors such as the size and shape of a pipe, conveying conditions, etc. Also, as the expression of ϕ_s is to be regressed for the material in the second state, i.e. the particles of the material slip along the wall but keep fixed relative to each other, ϕ_s will be relevant to the flow property of the wall friction angle instead of the internal friction angle. Hence ϕ_s should

be a function of the bulk voidage, density (or specific weight), and wall friction angle of material, that is $\phi_s = f(\epsilon, \gamma_s, \phi_w)$. The bulk density of the material is not included into the function as it is governed by ϵ and γ_s . An appropriate model for regression is assumed as follows,

$$\phi_{si} = x_1(1 - \epsilon_i)^{x_2} \gamma_{si}^{x_3} \phi_{wi}^{x_4}, \quad i=1,2,\dots, n \quad (7.19)$$

where x_1, x_2, x_3 , and x_4 are the coefficients to be determined, n is the number of the test materials.

Applying the method of least squares with the limit of $\phi_s < \phi$, the coefficients are obtained and listed in Table 7.4.

Table 7.4: Coefficient of best fit.

x_1	x_2	x_3	x_4
1.33	0.33	0.33	1.00

Therefore, ϕ_s is best fitted by the following function:

$$\phi_s = \frac{4}{3} \phi_w [(1 - \epsilon) \gamma_s]^{\frac{1}{3}} \quad (7.20)$$

As $\gamma_b = (1 - \epsilon) \gamma_s$, Equation (7.20) can be written as

$$\phi_s = \frac{4}{3} \phi_w \gamma_b^{\frac{1}{3}} \quad (7.21)$$

where γ_b is the bulk specific weight with respect to water at 4 °C.

The goodness of fit is show in Figure 7.21.

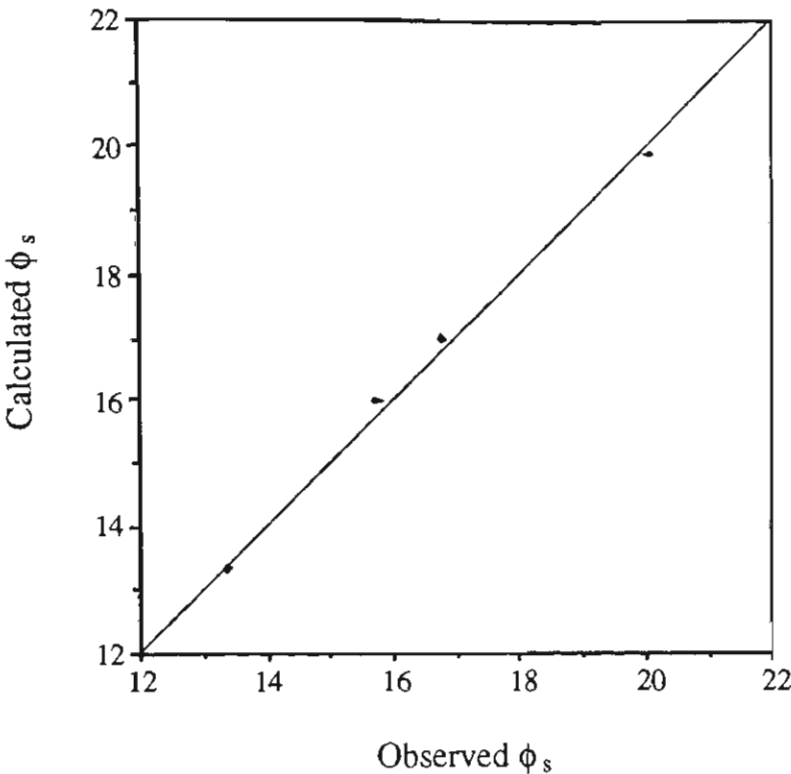


Figure 7.21 Goodness of fit.

CHAPTER 8

TOTAL HORIZONTAL PIPELINE PRESSURE DROP

8.1 Introduction

The accurate prediction of total pipeline pressure drop is one of the most important aspects of research in pneumatic conveying systems. For example, if a pneumatic conveying system is to be designed or upgraded to ensure satisfactory and efficient operation, accurate information on conveying performance (i.e. the relationship between total pipeline pressure drop and its influential factors) must be obtained. Generally, the factors affecting the total pipeline pressure drop mainly include the physical properties of the material, pipeline configurations and conveying conditions. Hence the development of a model which is a function of the physical properties, pipeline configurations and conveying conditions for the total pipeline pressure drop becomes the ultimate aim of many researchers of pneumatic conveying. Numerous predicting models have been developed for various pneumatic conveying systems. Most of these are confined to dilute-phase conveying. Unfortunately, only a few were developed for dense-phase conveying, and these models are still far from reliable due to the complexity and variability of the dense-phase conveying. For this reason, developing a more accurate and efficient model for low-velocity pneumatic conveying is the main ultimate goal of this research. As the pressure gradient across a single slug and the relevant factors affecting the pressure gradient such as slug velocity, wall pressure and stress transmission coefficient, etc. have been studied in previous chapters, the work in this chapter correlates the total pipeline pressure drop with the single slug pressure drop and other relevant factors to lead to the final model. The model should be a function of the physical properties of the material to be handled, conveying conditions and pipeline configurations. In order to complete the correlation work successfully and to achieve the ultimate goal of this research, the following extra investigations also are carried out.

A low-velocity pneumatic conveying system normally includes several slugs and air gaps flowing along the pipeline. Each slug length constitutes the total slug length that affects the total pipeline pressure drop. In addition, some other geometrical parameters such as

stationary bed thickness also influence the pressure drop. Therefore, the relationship between the geometrical parameters reflecting the nature of the flow pattern and conveying conditions is studied firstly based on numerous experiments and analyses of the experimental signals. As a result of this study, the flow pattern also can be understood more clearly and quantitatively.

The effects of pipeline configuration (i.e. the diameter and length of pipe, type and location of bends, etc.) on the total pipeline pressure drop then are investigated.

After these investigations, the model for predicting the total horizontal pipeline pressure drop is developed. Based on this model, a prediction procedure is recommended based on computer iteration.

Finally, comparisons are made between the predicted results and experimental results to examine the accuracy of the developed model.

8.2 Geometrical Parameters of Low-Velocity Pneumatic Conveying

Visual studies of slug flow geometry have been made by many researchers [16, 48, 69, 71, 105] for low-velocity pneumatic conveying. For example, a detailed description of the flow pattern was presented by Konrad et al. [69], see Section 3.2 in Chapter 3. In this research, the observations made during the numerous experiments of low-velocity pneumatic conveying of various types of granular material agree to this description. However, quantitative studies and analyses are rarely found for the flow pattern and its relations with the pipeline pressure drop and conveying conditions. The work in this section will provide some assistance for this purpose by presenting experimental data and analyses.

In order to describe flow pattern quantitatively, it is expected to know which geometrical parameters basically reflect the main aspects of the flow. It is believed that the parameters should at least include the slug length (l_s) and air gap length (l_g), slug diameter which is

normally equal to the inner diameter of pipe (D) for a full bore slug, stationary bed thickness (h_s) and the size and shape of the front and back head of slug which are here described by the angles (β_f) and (β_b), as shown in Figure 8.1. The radial size of air gap is determined by the inner diameter of pipe and the stationary bed thickness.

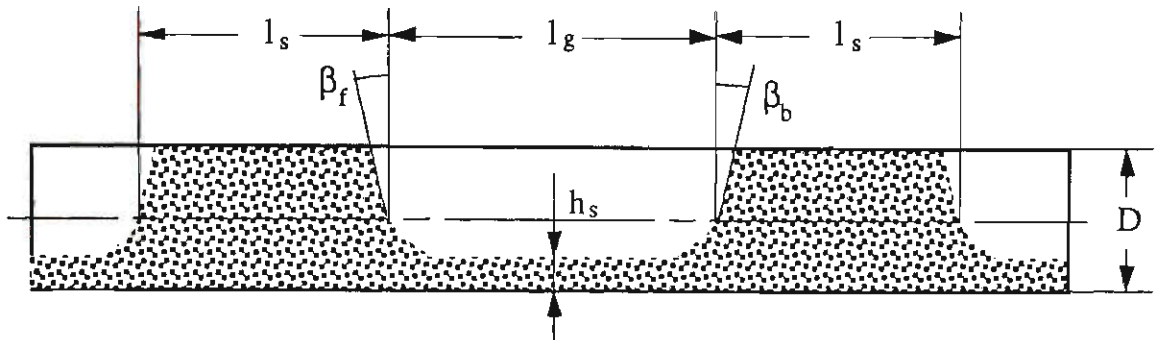


Figure 8.1 Geometrical parameters of slug-flow.

Of the above geometrical parameters, the shape and size of the head of slug (or air gap) are rather complex and unstable. The head of the slug only takes up a relatively small part of the slug so that its influence on the pressure drop will not be significant, thus the study of the head of slug will be ignored. Therefore, all the lengths indicate the size at the central axis of pipe.

As the radial sizes of slug and air gap are limited by the diameter of pipe, more attention is given to the investigation of the lengths of slug and air gap as well as the stationary bed thickness.

8.2.1 Air Gap Length

During low-velocity pneumatic conveying, granular particles are conveyed in the form of slugs, meanwhile most of the conveying air flows as air slugs (i.e. air gaps). The air gaps are axisymmetric in vertical slug-flow and asymmetric in horizontal slug-flow. It has been analysed in Chapter 3 that the air gaps are formed by the extra air for fluidising a bulk solid. Also, due to the much higher mass flow-rate of air used in low-velocity

pneumatic conveying than in fluidisation, bubbles always expand to fill up the full diameter of the bed (pipe) and form air gaps.

Numerous experiments of low-velocity pneumatic conveying found that the air gaps change their length while altering conveying conditions. To record and exhibit the variations accurately, the data of the air gap lengths are achieved and presented in the following by analysis of various pressure signals. In order to understand the principle of the method, it is necessary to know the relationship between slug motion and the corresponding pressure wave form.

Figure 8.2 shows the different positions of two slugs (named as Slug 1 and Slug 2) in a horizontal pipe of a low-velocity pneumatic conveying system. With the motions of the slugs, the corresponding time history wave forms of wall and air pressures are shown in Figure 8.3. Note that the two slugs flowing in the pipe are l_g apart (i.e. the length of the air gap between the two slugs is l_g). The transducers taking wall pressure and static air pressure signals are installed at an identical cross-section of the pipe. Point A in Figure 8.2 shows the position of the cross-section which is at a distance l_A from the end of the pipe.

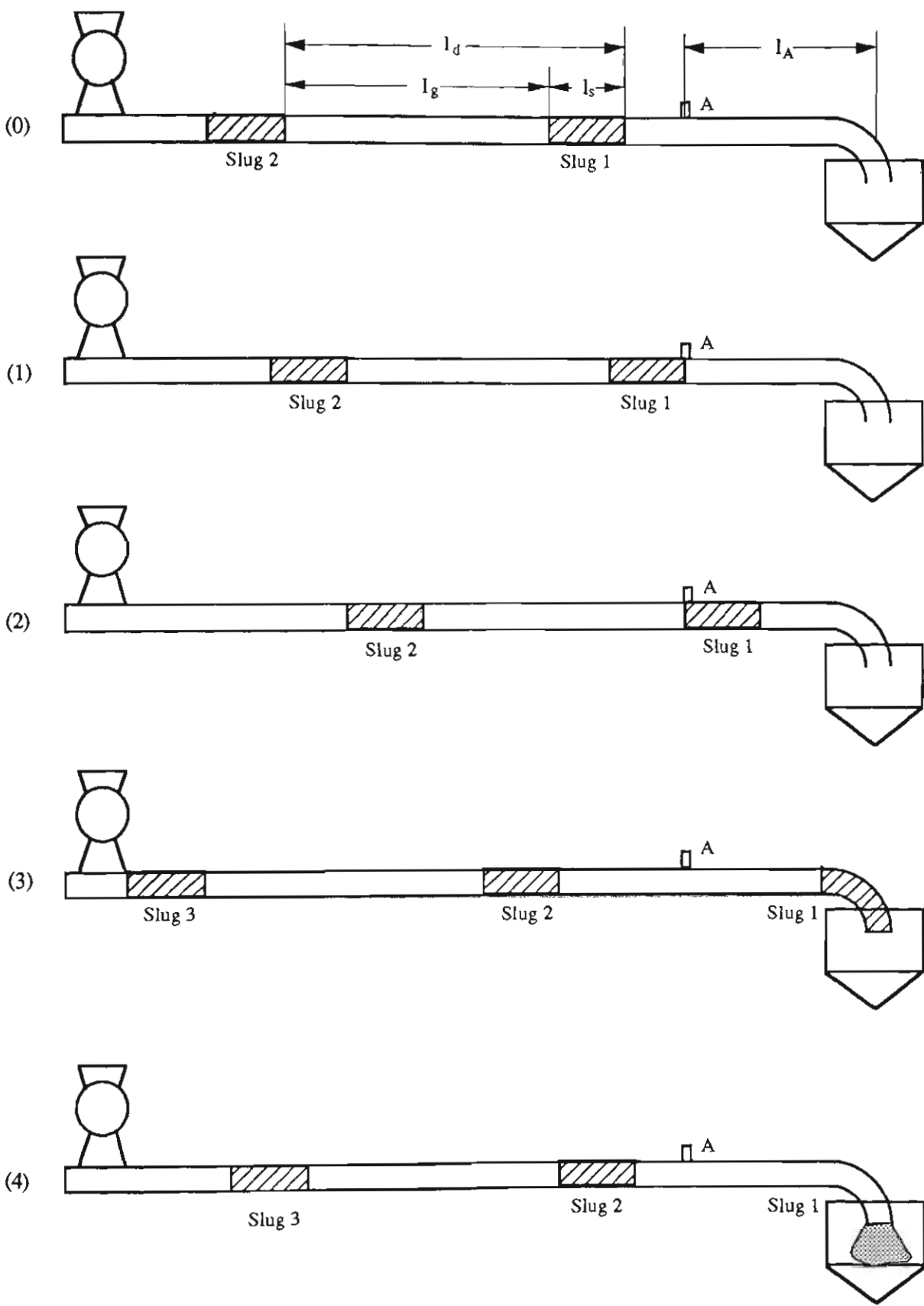


Figure 8.2 Various positions of slugs during low-velocity pneumatic conveying.

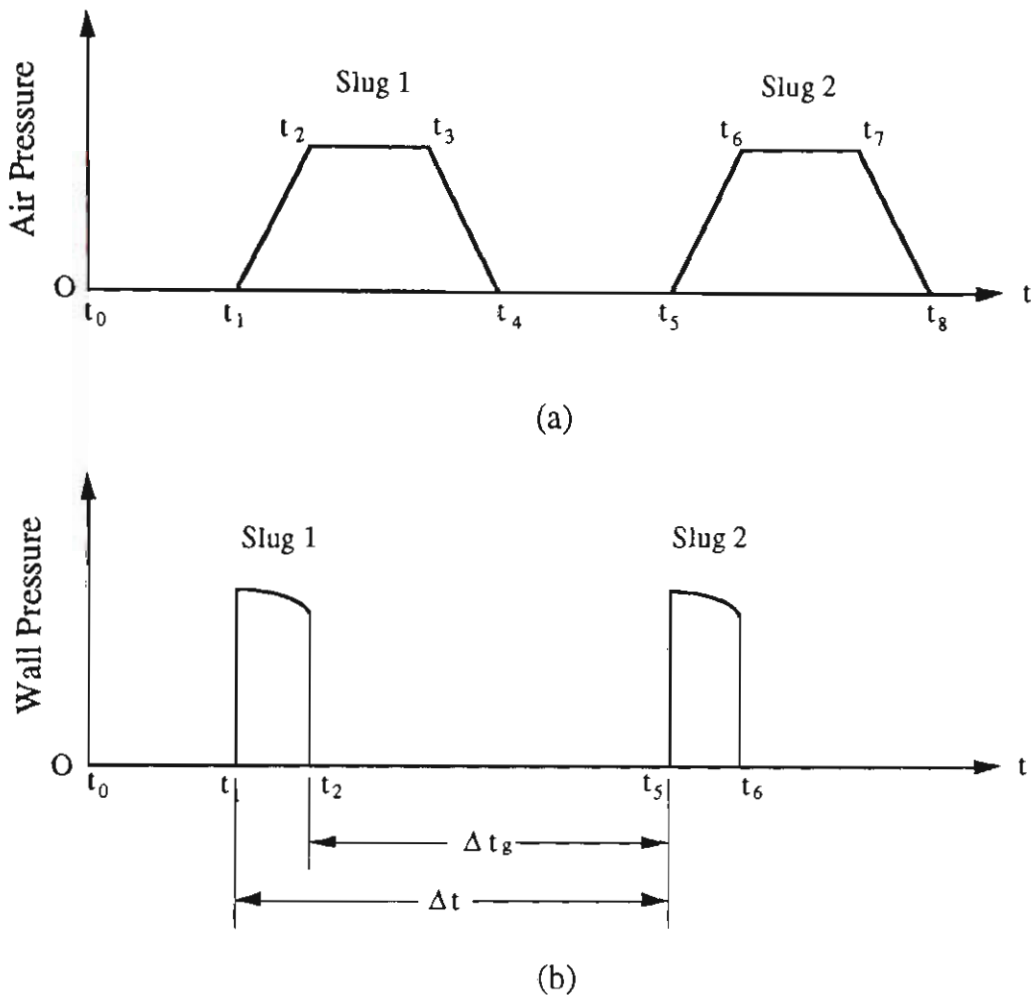


Figure 8.3 Time history records of static air and wall pressures.

Figure 8.2(0) shows the initial positions of the slugs. Because the transducers are located at the downstream of Slug 1 at this stage, neither the static air pressure nor wall pressure is sensed by the transducers if the pressure drop caused by the air alone is low enough to be neglected. Hence both the air and wall pressures are zero at this initial stage, see the time period from t_0 to t_1 in Figure 8.3(a) (i.e. the plot of the time history wave form of the static air pressure) and Figure 8.3(b) (i.e. the plot of the time history wave form of the wall pressure).

Figure 8.2(1) displays the positions of the slugs while Slug 1 just arrives at point A. The time at which Slug 1 arrives at the point is indicated as t_1 in Figure 8.3(a) and (b). From this time t_1 , the transducers begin to sense the static air and wall pressure signals. Then Slug 1 moves further forward, for example, until its end just leaves point A, as shown in

Figure 8.2(2). t_2 is used to indicate the "departure" time of Slug 1. During this process, both wall and air transducers can always receive time-variable signals with the variation of the positions of the slugs. From time t_1 to t_2 , the air pressure increases its value from zero to maximum as the air pressure is proportional to the length of the slug, however, the wall pressure gets a value which is equal to the transmission frontal stress ($\lambda\sigma_f$) immediately at time t_1 instead of zero and then varies exponentially according to the wall pressure distribution, refer to Chapter 3. When the whole Slug 1 has left point A, the wall pressure disappears, but the air pressure still maintains its maximum value if Slug 1 has not reached the end of the pipe.

Figure 8.2(3) and 8.2(4) show the positions of the slugs respectively when the head and end of Slug 1 have just arrived at the end of the pipe. Assuming $l_g > l_A + l_s$, then Slug 2 has not arrived yet at the test point A. During this period of time, i.e. from t_3 to t_4 shown in Figure 8.3(a) and (b), the air pressure reduces its value from the maximum to zero. With Slug 1 moving towards the end of the pipe, Slug 2 approaches point A.

After time t_4 , both the wall and air pressures are zero until Slug 2 reaches point A. As soon as Slug 2 arrives at the point, the pressure signals start to vary again and exhibit a similar time history wave form to the last one, as shown in Figure 8.3(a) and (b).

From Figures 8.3(a) and 8.3(b), it can be found that each peak of the wave forms corresponds to a slug passing through the test point, if $l_g > l_A + l_s$. The starting points of the peaks indicate the time that the slug just arrives at the test point. The end point of the peak of the wall pressure indicates the time that the slug leaves the test point, whereas the end point of the peak of the air pressure represents the time that the slug completely exits the pipe. This is why the peak of the air pressure lasts longer than the wall pressure does in the time coordinates of the plots. As the time that Slug 1 and Slug 2 arrive at the test point can be found from the plots of the air pressure or wall pressure to be t_1 and t_5 , respectively, the length of air gap can be calculated from:

$$l_g = U_s \Delta t - l_s \quad (8.1)$$

where $\Delta t = (t_5 - t_1)$.

If $l_s \ll l_g$ (which is true for most of the tests carried out in this thesis), then

$$l_g \approx U_s \Delta t \quad (8.2)$$

As the slug velocity has been measured and the interval time Δt can be obtained by checking the data files of pressure signals, the length of air gap can be determined approximately by Equation (8.2). This is the principle of the method for the determination of air gap length.

If an accurate value of the length of air gap is needed, the time history of Slug 1 leaving and Slug 2 reaching the test point can be examined only from the plot of the wall pressure to obtain t_2 and t_5 . The product of the slug velocity U_s and the interval time $\Delta t_g (= t_5 - t_2)$ will be the accurate length of air gap. That is

$$l_g = U_s \Delta t_g \quad (8.3)$$

Refer to Figure 7.6 for actual time history records of the static air and wall pressure for conveying black plastic pellets. The conveying is conducted in the low-velocity test rig with the 52 m pipeline. The conveying condition is given as $m_s = 0.849 \text{ kgs}^{-1}$, $m_f = 0.0643 \text{ kgs}^{-1}$. The sampling rate of the data acquisition system is selected as 4 Hz (i.e. 4 scans/second) for eight channels. From this figure, it can be seen that the time interval between neighbouring peaks is similar. This indicates that the distances between pairs of neighbouring slugs approximately equal for a given conveying condition, that is, the air gaps maintain an approximate length. However, it can also be seen that slight differences occur in some of these interval times. For example, the interval time between the peaks 4 and 5 is obviously larger than that between the peaks 1 and 2. This indicates that the air gap between slugs 4 and 5 is longer than that between slugs 1 and 2. If using the symbol

N_{sti} to represent the scan number corresponding with peak i , then it can be found that $N_{st1} = 278$, $N_{st2} = 299$, $N_{st4} = 346$ and $N_{st5} = 388$ from the recorded experimental data file. Therefore, the interval time

$$\Delta t_{12} = (N_{st2} - N_{st1})/f = (299 - 278)/4 = 5.25 \text{ (s)}$$

$$\Delta t_{45} = (N_{st5} - N_{st4})/f = (388 - 346)/4 = 10.5 \text{ (s)}$$

As the average slug velocity has been measured under this conveying condition as 4.032 ms^{-1} , then:

$$l_{g12} = 4.032 \times 5.25 = 21.168 \text{ (m)}$$

$$l_{g45} = 4.032 \times 10.5 = 42.336 \text{ (m)}$$

This means that an average value is necessary to express the air gap length for a given conveying condition. There are two ways to obtain the average length of air gap, one is to determine the starting and ending time of each pressure peak, calculate the length of each air gap by using Equation (8.3) and then find the average value. Another way is to establish the starting times of the first and last slugs t_f , t_l , count the total number of the slugs N_s and then calculate the average interval time from:

$$\Delta t_m = \frac{t_l - t_f}{N_s - 1} \quad (8.4)$$

The first method will be quite tedious, especially for a system including a large number of slugs. However, if an accurate value of average air gap length is required, this method is necessary. The second method can only calculate the average distance between the slugs but not the real air gap length.

In practice, the wall pressure wave form is employed to determine the length of air gap instead of the air pressure wave form. The reason is that the wall pressure wave form reflects more clearly a slug reaching and leaving the test point. Another reason is that if l_g

$< l_A + l_s$, refer to Figure 8.2(0), the peaks of the air pressure will join together and exhibit a continuous time history record so that the starting times of two neighbouring peaks can not be distinguished. For example, refer to the peaks 1 and 2 of the air pressure signal shown in Figure 7.6(b). Also sometimes although no slug passes through the test point, a peak of air pressure still appears on the plot when a slug forms downstream of the test point.

Figures 8.4 to 8.11 present results of average distances between neighbouring slugs which were determined by using Equation (8.4). For example, when black plastic pellets are conveyed through the 52 m long pipeline with $m_f = 0.0643 \text{ kgs}^{-1}$, $m_s = 0.849 \text{ kgs}^{-1}$, the average slug velocity are measured as 4.032 ms^{-1} . There are 9 wall pressure peaks in the full range of the test, refer to Figure 7.6(a). The starting times of the first and last peak (i.e. t_f and t_l) are at 69.5 s and 127 s, respectively. Hence, the average distance between the slugs is calculated as:

$$(l_g + l_s) = \frac{U_s(t_l - t_f)}{N_s - 1} = \frac{4.032(127 - 69.5)}{9 - 1} = 29.0 \text{ (m)}.$$

Due to $l_g \gg l_s$ in these tests, the distances are regarded as the approximate average length of air gap. The results are plotted against the mass flow-rate of solids and air.

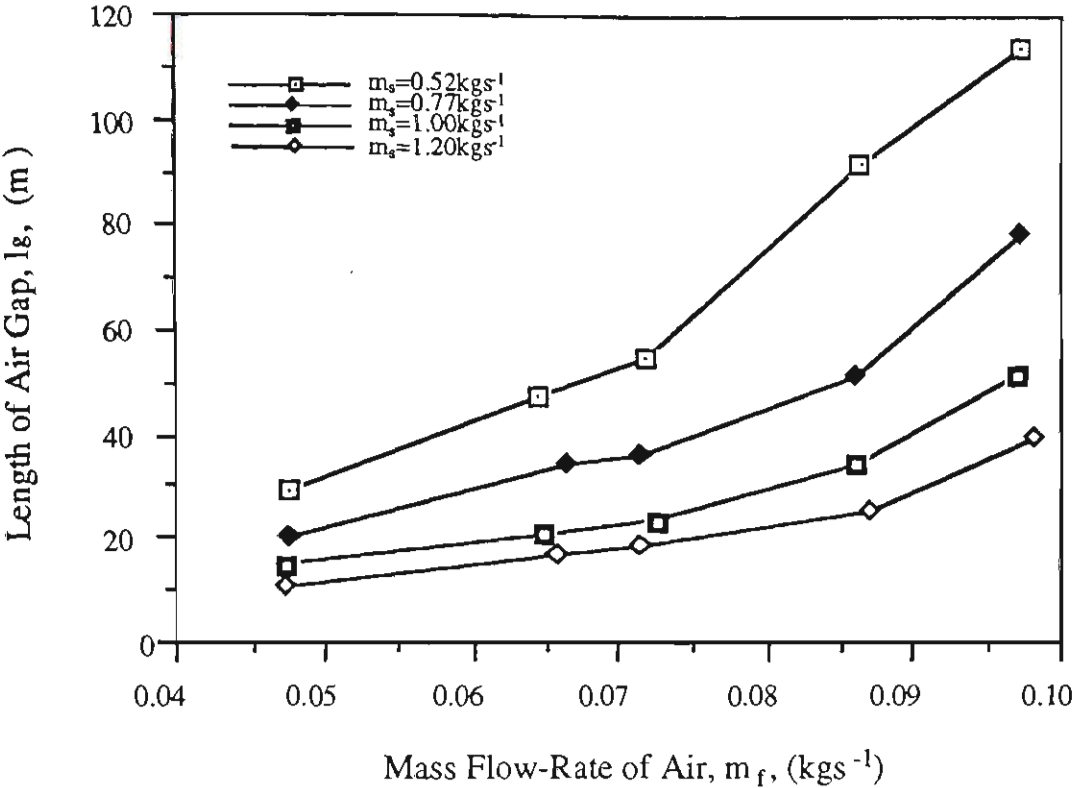


Figure 8.4 Plot of air gap length versus mass flow-rate of air for white plastic pellets.

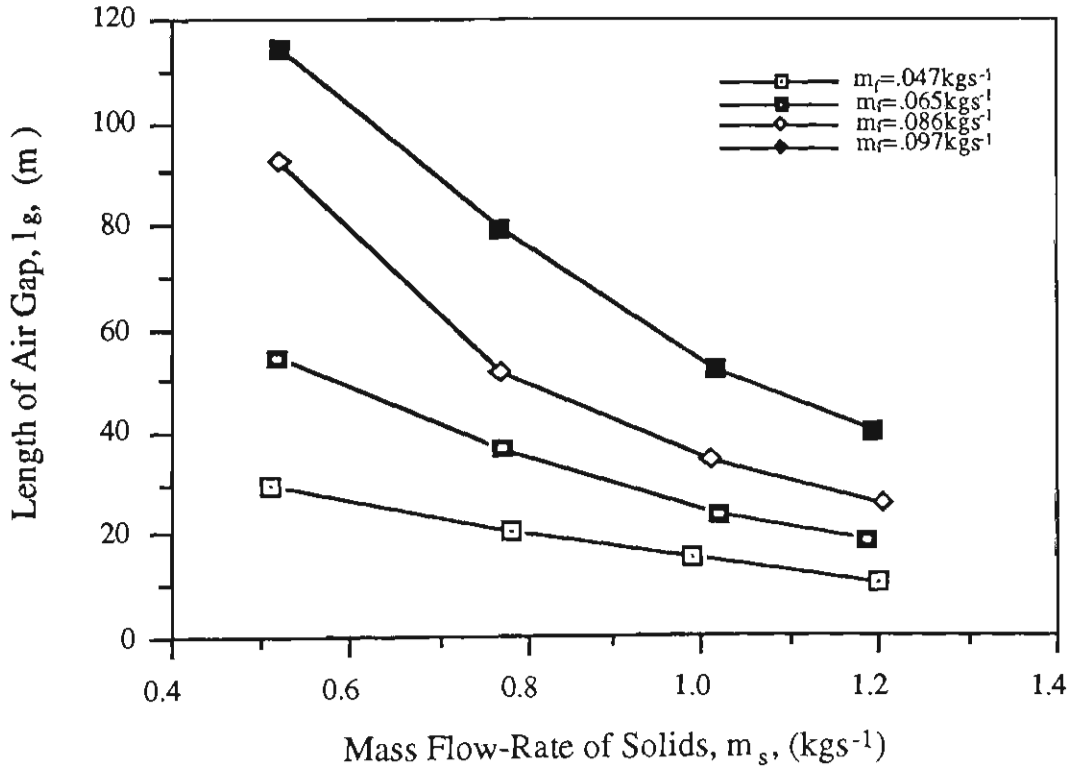


Figure 8.5 Plot of air gap length versus mass flow-rate of solids for white plastic pellets.

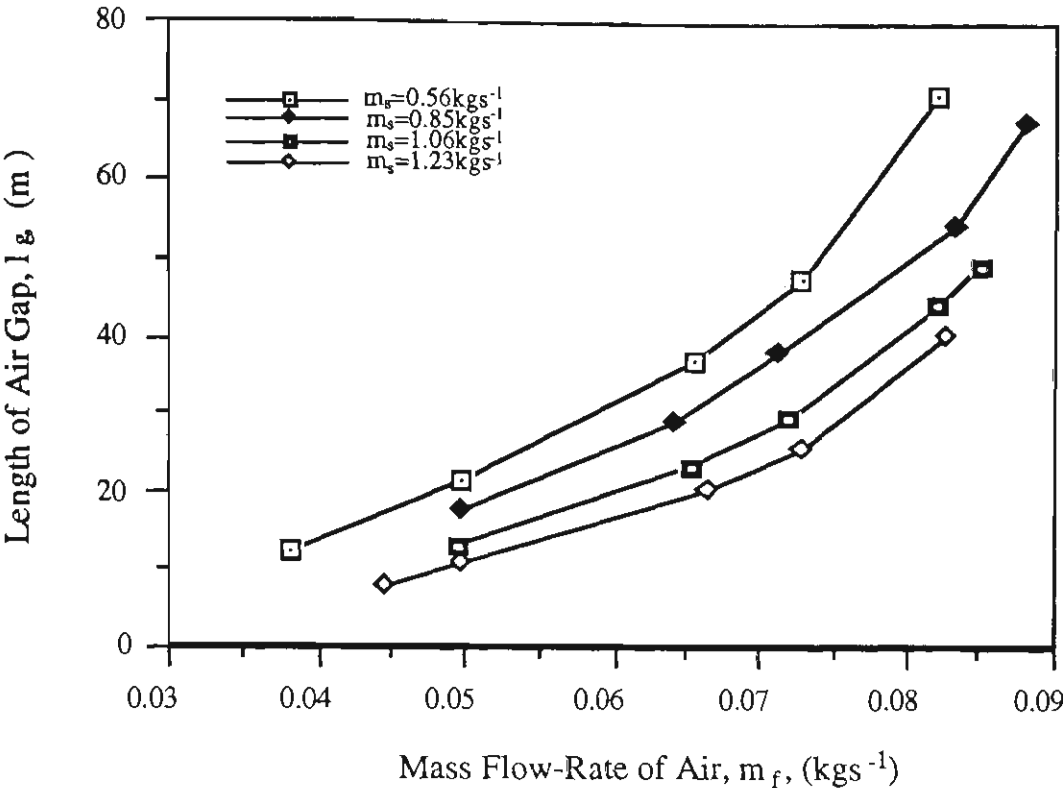


Figure 8.6 Plot of air gap length versus mass flow-rate of air for black plastic pellets.

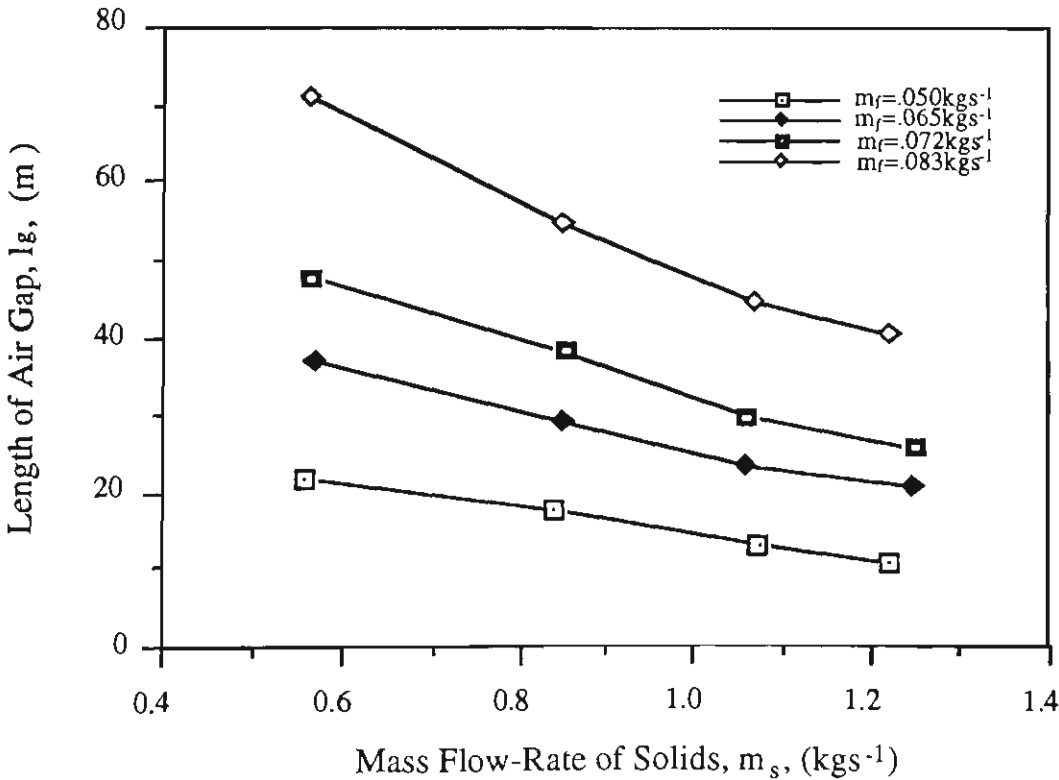


Figure 8.7 Plot of air gap length versus mass flow-rate of solids for black plastic pellets.

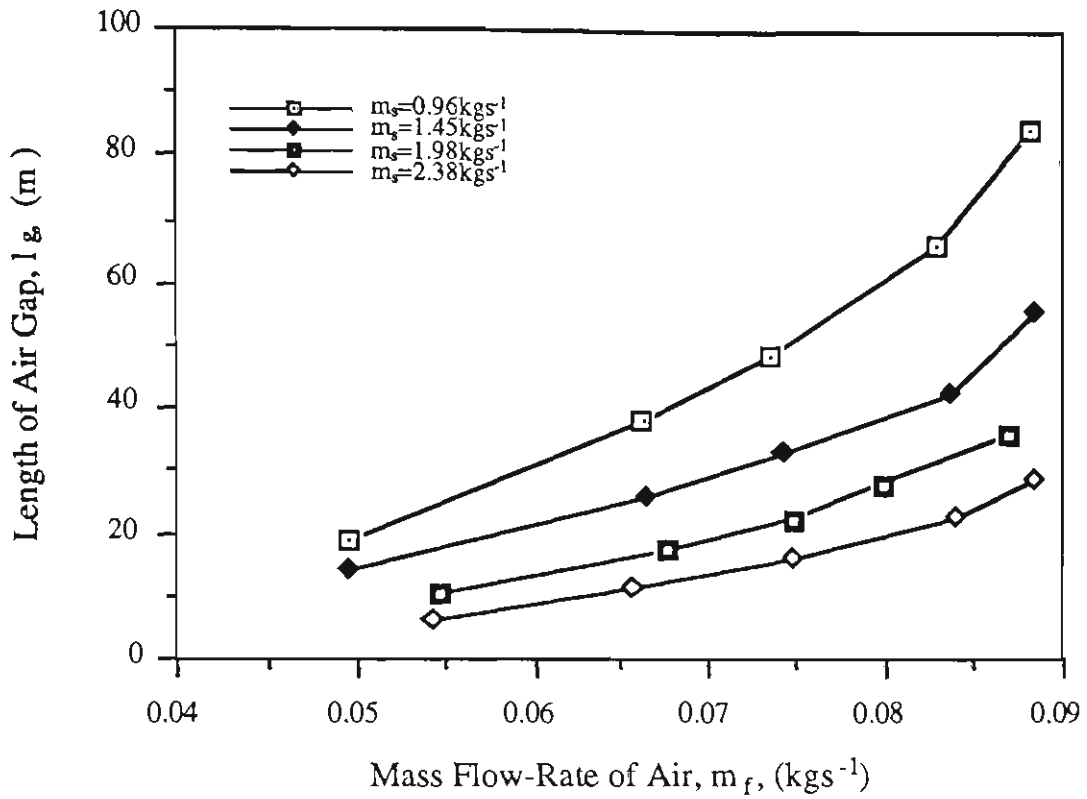


Figure 8.8 Plot of air gap length versus mass flow-rate of air for wheat.

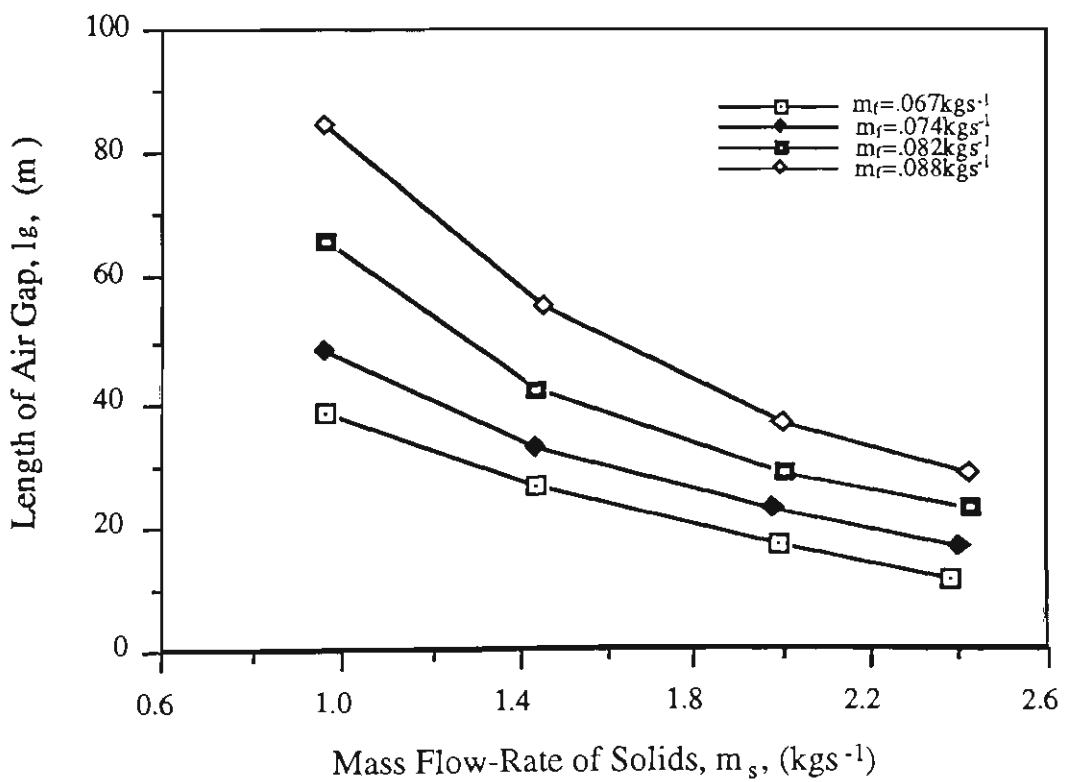


Figure 8.9 Plot of air gap length versus mass flow-rate of solids for wheat.

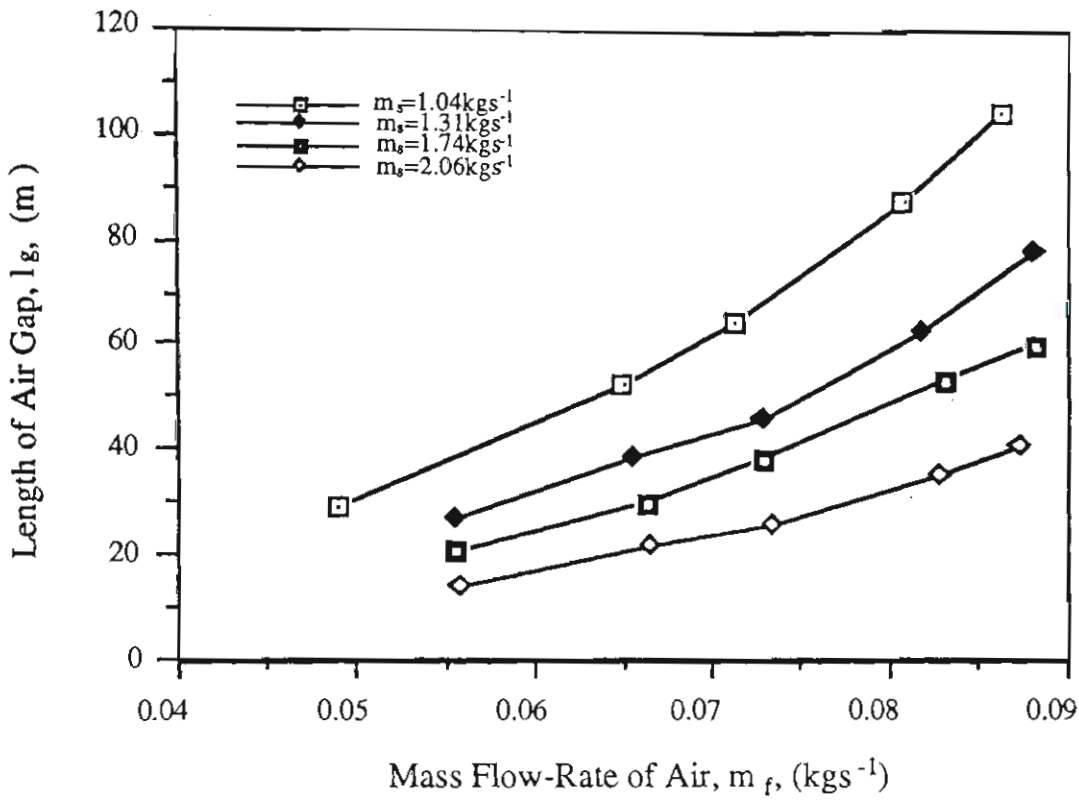


Figure 8.10 Plot of air gap length versus mass flow-rate of air for barley.

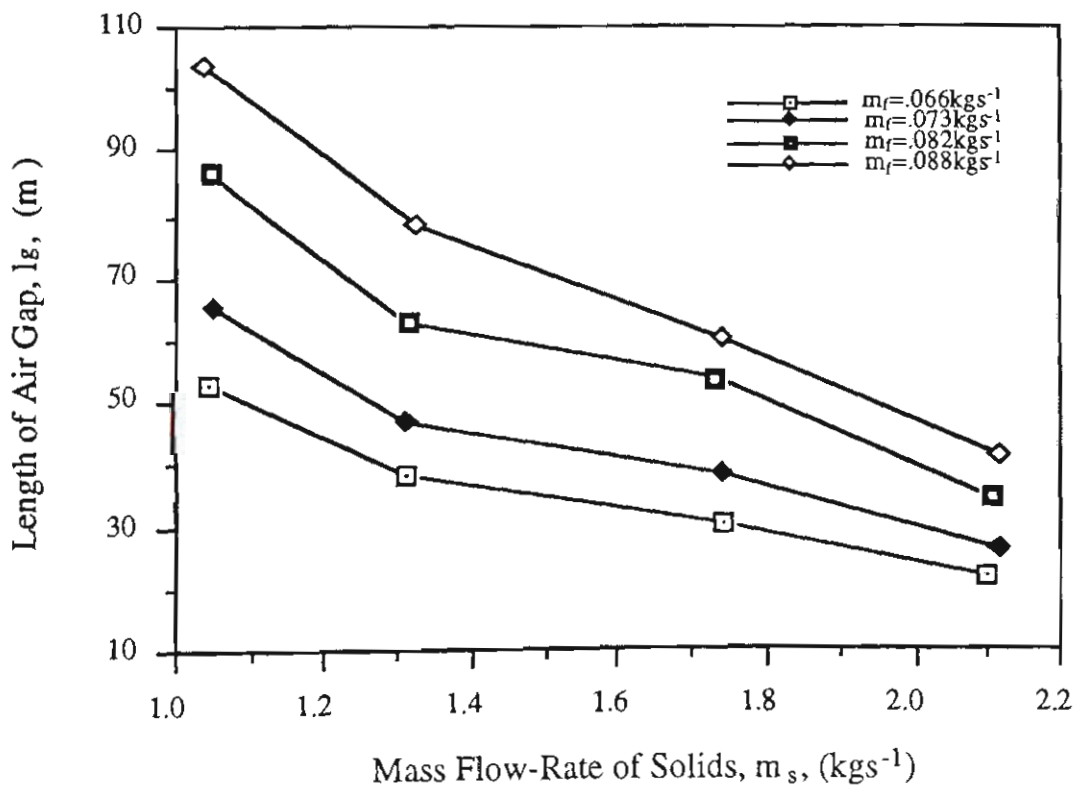


Figure 8.11 Plot of air gap length versus mass flow-rate of solids for barley.

From Figures 8.4 to 8.11, it can be seen for a given mass flow-rate of solids, the length of air gap increases with the mass flow-rate of air. The reason is that air gaps are formed by the extra air for "aerating" the material. For slug-flow conveying which has been aerated already, increasing the mass flow-rate of air simply increases the volume of the extra air for aerating the material in a given period of time. Since the diameter of air gap is limited by the pipe, the length of air gap must be increased. On the other hand, for a given mass flow-rate of air, increasing the mass flow-rate of solids decreases the length of air gap. In Chapter 6, it has been found that mass flow-rate of solids has little influence on slug velocity, refer to Section 6.5.2. In other words, the slug velocity remains approximately constant for a given mass flow-rate of air no matter how the mass flow-rate of solids changes. Hence if increasing the mass flow-rate of solids, but still keeping the mass flow-rate of air (i.e. slug velocity) constant, the number of the slugs included in a certain length of pipe obviously must increase to maintain the higher mass flow-rate of solids.

It can also be found from Figures 8.4 to 8.11 that under some conveying conditions, air gaps are longer than the length of pipe. For example, while black plastic pellets are conveyed through the 52 m long pipeline with $m_s = 0.57 \text{ kgs}^{-1}$, $m_f = 0.082 \text{ kgs}^{-1}$, the average air gap length is 71.15 m. This indicates that for certain periods of time there is no slug in the pipeline and the pressure drop approaches the air-only condition. In this case, the time history record of air pressure will display an discontinuous curve, refer to Figures 7.6(b)

8.2.2 Slug Length

Slug length is another major geometrical feature of the slug-flow pattern. Slug-flow pneumatic conveying normally includes several slugs flowing along the pipeline. All these slugs are observed to have approximately the same length, which is affected by the

mass flow-rate of air. It is also observed that the lengths of the slugs are very different for different types of material.

It appears that the method for analysing air gap length can also be applied to determine slug length. From the above analysis of the movement of slugs, it is known that the time a slug reaches and leaves a test point, say t_1 and t_2 , can be determined from the time history record of wall pressure, refer to Figures 8.2 and 8.3. Obviously, the product of the interval time $\Delta t = (t_2 - t_1)$ and the corresponding slug velocity U_s is the length of the slug, that is

$$l_s = \Delta t U_s = (t_2 - t_1) U_s \quad (8.5)$$

Unfortunately, limited by the resolution of the wall pressure signal, the results for slug length determined by Equation (8.5) are not satisfactory although quite good results have been achieved for air gap length by using the same method. The reason can be explained as follows.

Since all the signals are measured by the PC based data acquisition system, the accuracy of the determined slug or air gap length is dependent largely on the sampling rate of the data acquisition system. Since air gaps are much longer than material slugs (e.g. most of the slugs are observed to have a range of lengths from approximate 1.00 to 2.5 metres where the shortest air gaps were found to be ≈ 10 metres), determining the air gap and slug length by analysis of the pressure signal which has a fixed resolution, obviously the relative deviation of slug length will be much greater than that of air gap length. The different relative deviations for an air gap length and slug caused by signal resolution can be seen more clearly by the following calculation.

The longest slug and shortest air gap for white plastic pellets were obtained with $m_s = 1.2 \text{ kgs}^{-1}$, $m_f = 0.047 \text{ kgs}^{-1}$. That is, the minimum relative deviation for the slug and maximum relative deviation for the air gap most probably will be obtained under this

conveying condition. The slug velocity was measured as 2.632 ms^{-1} . The air gap length was calculated as 10.6 metres and the slug length was observed about 1.5 metres. Even though the wall pressure signals were sampled at the rate of 10 Hz, which is the highest possible sampling rate for obtaining a sufficient long time history record due to the memory limitations of the computer, the relative deviation for the slug is still too large to be accepted. That is, the maximum possible deviation of the length of air gap and slug can be 0.26 m (i.e. $2.632 \text{ ms}^{-1} \times 0.1 \text{ s}$). Therefore, the relative deviations will be 2.4 % for the air gap and 17 % for the slug.

Besides the length of single slug, the total slug length contained in the conveying pipeline is also an important parameter for the particle slug since slug-flow usually includes several slugs. In fact, it is the total slug length that determines the total pipeline pressure drop if the pressure gradient has been determined. Note that the total slug length used here indicates an average value, since low-velocity pneumatic conveying is a discontinuous flow of slugs. Although the data of each single slug length have not been obtained, it still is possible to calculate the total slug length for a given conveying condition. For example, the slug velocity (U_s) can be found according to the investigations in Chapter 6 when the mass flow-rate of air (m_f) is given. If the total length of pipeline is L_t , the time taken by a slug to travel across the pipeline will be

$$t_s = \frac{L_t}{U_s} \quad (8.6)$$

In addition, if the mass flow-rate of solids is known, the mass of particles entering the pipeline can be calculated mathematically during a certain period of time, i.e. it follows that the mass of the moving solids $M = (\text{mass flow rate of solids}) \times (\text{time})$. The number of particles moving in the pipeline is equal to that amount of the particles entering the pipeline during the time taken for the slug to travel across the pipeline, that is

$$M = m_s t_s = \frac{m_s L_t}{U_s} \quad (8.7)$$

As almost all the particles flow in the form of slugs and as these slugs have been assumed to have a loose-poured bulk density for granular material, therefore, the mass of particles also is

$$M = \rho_b V_s \quad (8.8)$$

where V is the volume of the particles moving in the pipeline and $V_s = A(1-\alpha)L_s$ in slug-flow pneumatic conveying if the total slug length is L_s .

Combining Equation (8.7) and Equation (8.8) and replacing V_s in Equation (8.8) with $A(1-\alpha)L_s$, then an equation for calculating the total length of slugs can be obtained:

$$L_s = \frac{m_s L_t}{A(1-\alpha)\rho_b U_s} \quad (8.9)$$

8.2.3 Stationary Bed Thickness

A stationary bed occurs only in the horizontal pipes of low-velocity pneumatic conveying. The formation of the stationary bed is due to the particle slugs delivering some quantities of particles to the horizontal pipe behind it while the particle slugs move forward. Hence, during the initial stages of low-velocity pneumatic conveying, the particle slugs formed at the entrance of the conveying pipeline often disappear before they arrive at the end of the pipeline. Only at the stable or equilibrium stage of conveying (i.e. stationary bed has covered the entire length of the pipeline), can the slugs move through the entire pipeline with an approximately constant volume. As the bottom of the pipe is occupied by the particles of the stationary bed, air gaps can not fill up the whole pipe area between two slugs and therefore display asymmetric bubbles in horizontal slug-flow. Through sight glass observations, stationary bed thickness is observed to vary for different conveying conditions and different materials.

It was found earlier that the existence of the stationary bed affects the movement and inner stress of the slug. While a slug picks up particles from the stationary bed in front of

it, stress will be generated in the front surface of the slug. That frontal stress will affect the distribution of inner stress of the slug and resist the motion of the slug. From momentum balance investigation, the value of the frontal stress is determined by the slug velocity U_s and the area ratio α , refer to Equation (3.28). Hence after completing the investigation into slug velocity, it is necessary to evaluate the size of stationary bed. The following section discusses the measurement of the thickness of stationary bed at various conveying conditions and also presents these experimental data.

8.2.3.1 Measurement of Stationary Bed Thickness

A cross section of horizontal pipe with a stationary bed is shown in Figure 8.12. The shaded area at the lower part of the pipe shows the stationary bed. The chord AB represents the top surface of the stationary bed which is observed to be basically a plane surface.

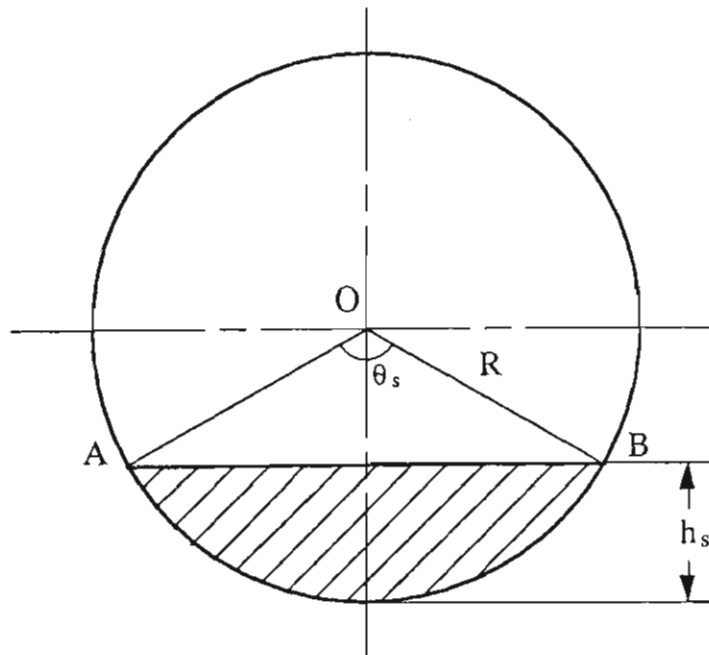


Figure 8.12 Cross section of stationary bed.

Stationary bed thickness here is indicated by the height h_s . If the thickness for a given diameter of pipe is known, according to trigonometry, the cross-sectional area of the stationary bed can be calculated by the following equations:

$$A_{st} = \frac{1}{2}(R^2\theta_s - \sin\theta_s) \quad (8.10)$$

Therefore, the cross-sectional area ratio of stationary bed to pipe is

$$\alpha = \frac{A_{st}}{A} = \frac{1}{2\pi}(\theta_s - \frac{\sin\theta_s}{R^2}) \quad (8.11)$$

where $\theta_s = 2\cos^{-1}(1 - \frac{h_s}{R})$.

In this research, the measurement of stationary bed thickness is obtained simply by taking photos of a stationary bed.

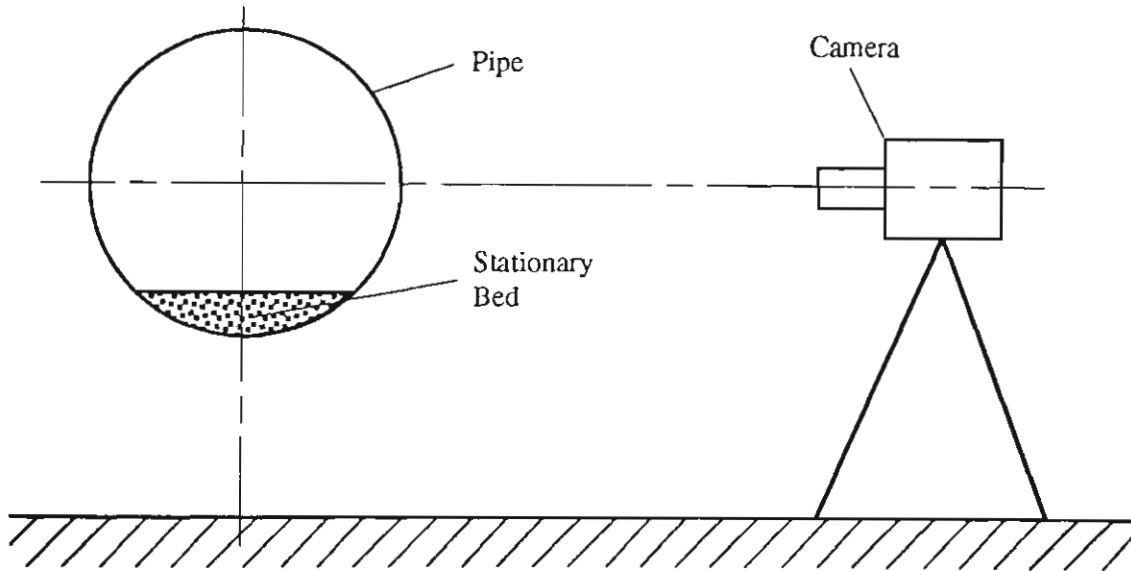


Figure 8.13 Measurement of stationary bed thickness with a camera.

As shown in Figure 8.13, an ordinary camera is fixed by a tripod next to a sight glass which is connected in the pipeline of the low-velocity pneumatic conveying test rig. Lateral pictures of the pipeline with stationary beds then can be recorded by taking photographs on the camera. Although the installation of the sight glass (i.e. due to the different material of the sight glass) will have some effect on the stationary bed, pressure and slug velocity, etc., these effects are regarded as insignificant, because the sight glass only occupies a very small part of the pipeline. In order to obtain proper pictures, the camera was installed with the axial line of its lens and the sight glass on the same level

surface. Generally speaking, there is no special requirement for the distance between the camera and sight glass as long as the sight glass is located properly in the viewfinder of the camera. However, in order to obtain large-scale photographs, This distance was minimised. Between the interval time of two neighbouring slugs, the stationary bed maintains a static and stable state. Hence, it was easy to obtain clear photographs, as shown in Figure 8.14.



Figure 8.14 A typical photograph of the stationary bed of barley for the experiment of $m_s = 1.32 \text{ kgs}^{-1}$, $m_f = 0.088 \text{ kgs}^{-1}$, conducted in the 96 m long pipeline.

After obtaining proper photographs, stationary bed thickness was obtained by a simple scaling technique. Due to the random performance of low-velocity pneumatic conveying, the stationary bed thickness was found to vary during each test. For this reason, as many photographs as possible were taken during the experiment so that a representative average value of stationary bed thickness are able to be obtained.

8.2.3.2 Results of Stationary Bed Thickness

According to the method described above, stationary bed thicknesses were obtained for low-velocity conveying of different types of material in the 105 mm ID pipeline under various conveying conditions. From these thickness data, the cross-sectional area of each stationary bed and the corresponding cross-sectional area ratio of stationary bed to pipe are calculated according to Equations (8.10) and (8.11), refer to Appendix A. To display the results, the cross-sectional area ratio of stationary bed to pipe are plotted against the slug velocity for the test materials, as shown in Figures 8.15, 8.16, 8.17 and 8.18.

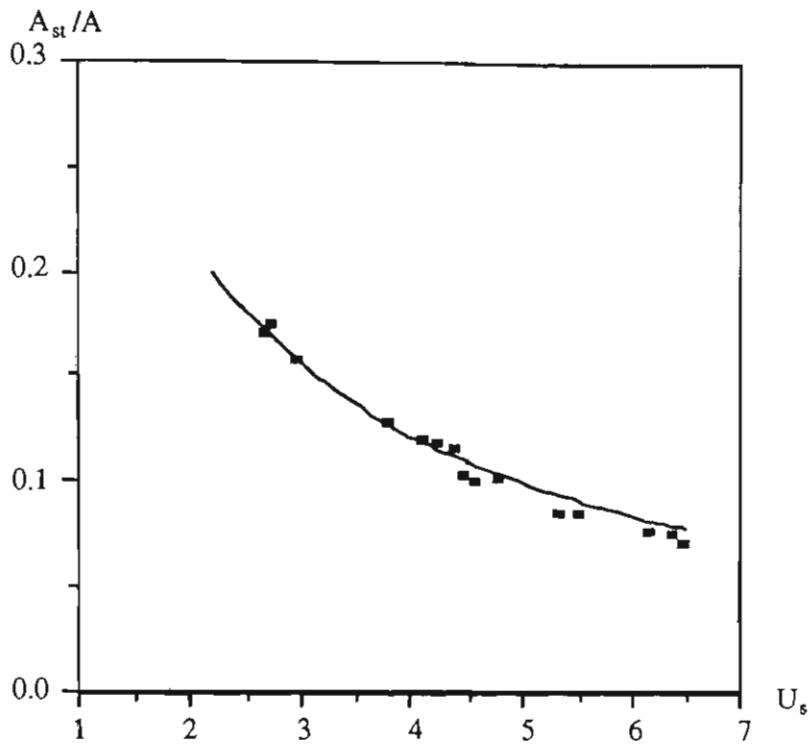


Figure 8.15 Cross-sectional area ratio of stationary bed to pipe versus slug velocity for white plastic pellets.

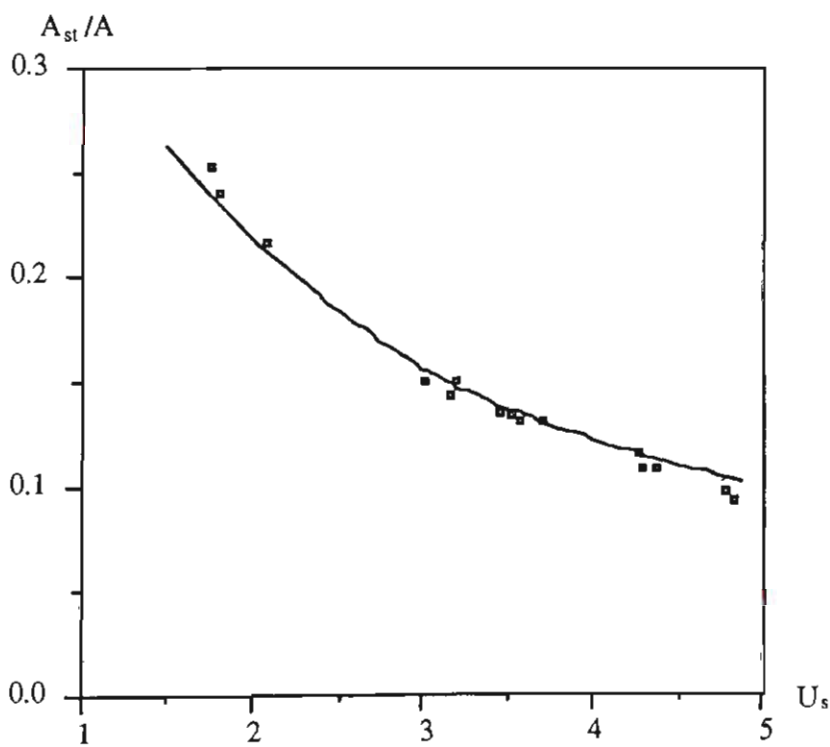


Figure 8.16 Cross-sectional area ratio of stationary bed to pipe versus slug velocity for black plastic pellets.

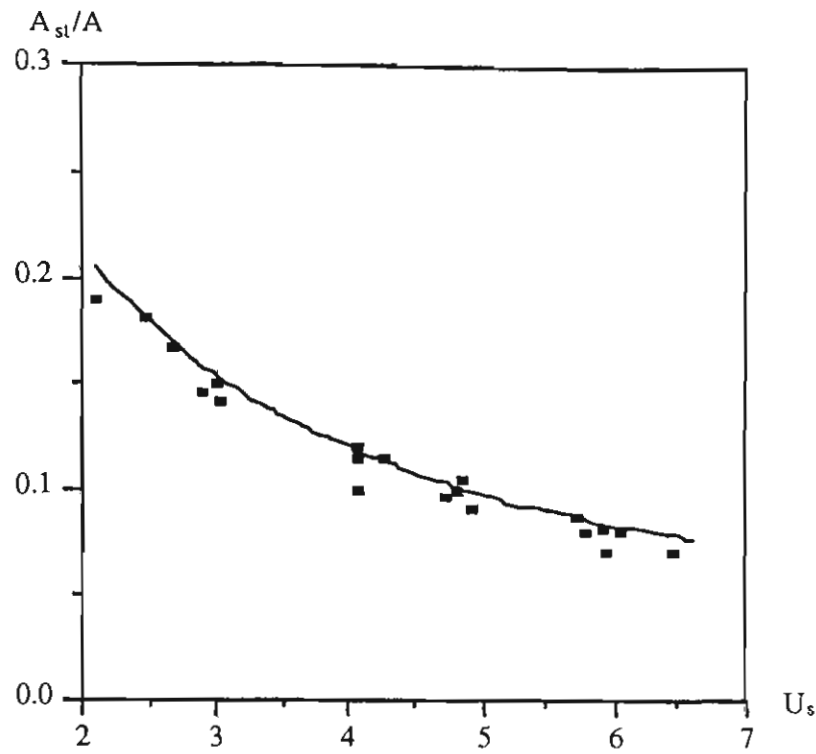


Figure 8.17 Cross-sectional area ratio of stationary bed to pipe versus slug velocity for wheat.

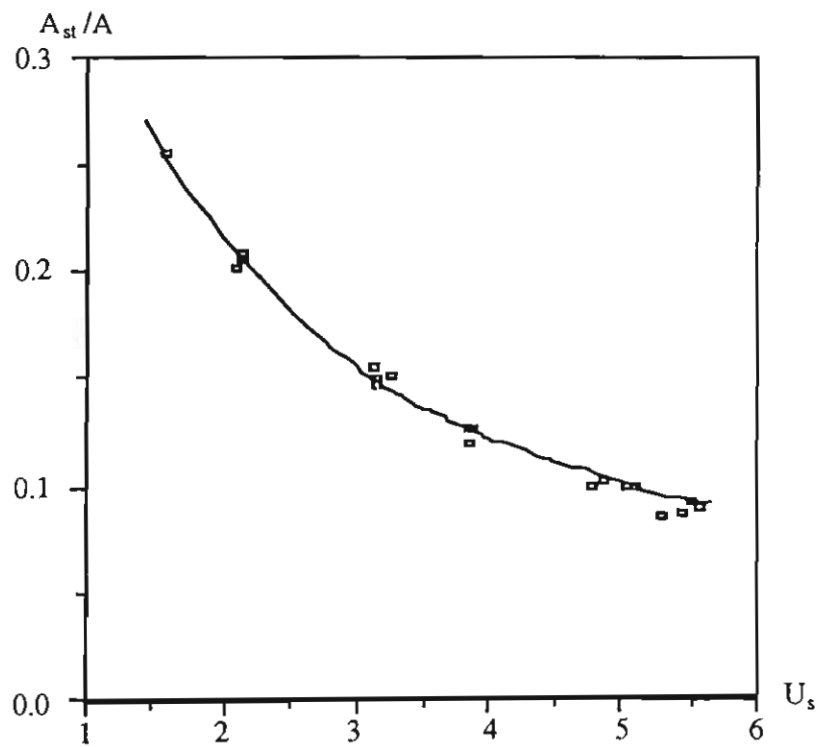


Figure 8.18 Cross-sectional area ratio of stationary bed to pipe versus slug velocity for barley.

The curves in the above plots are based on Equation (8.12) which was developed by Konrad et al. [69] for the estimation of the ratio of the two areas.

$$\alpha = \frac{A_{st}}{A} = \frac{1}{(1 + U_s/0.542\sqrt{gD})} \quad (8.12)$$

The plots show that the curves of Equation (8.12) fit the test data very well.

8.3 Pneumatic Conveying Characteristics

It has been known that conveying performance (i.e. the variation of the total pipeline pressure drop with conveying conditions) is very important for design or upgrading a pneumatic conveying system. While bulk material is conveyed in a given conveying system, the properties of the material and pipeline configuration of the system are regarded as constant. Hence the total pipeline pressure drop will depend completely on the conveying conditions. It is essential to use a convenient and workable technique to present clearly the relationship between the total pipeline pressure drop and conveying conditions.

One technique is shown in Figure 8.19, which is composed of a series of curves of constant mass flow-rate of solids (m_s) and referred to as the steady-state pipeline conveying characteristics. This clearly displays the variation of steady-state mass flow-rate of solids m_s (kgs^{-1}) with respect to the mass flow-rate of supplied air m_f (kgs^{-1}) and the total pipeline air pressure drop Δp_t (kPa). Based on the information given by steady-state pneumatic conveying characteristics (refer to Figure 8.19), it is easy to find out the pressure variation trend and select the proper operating condition for the system to be designed or upgraded.

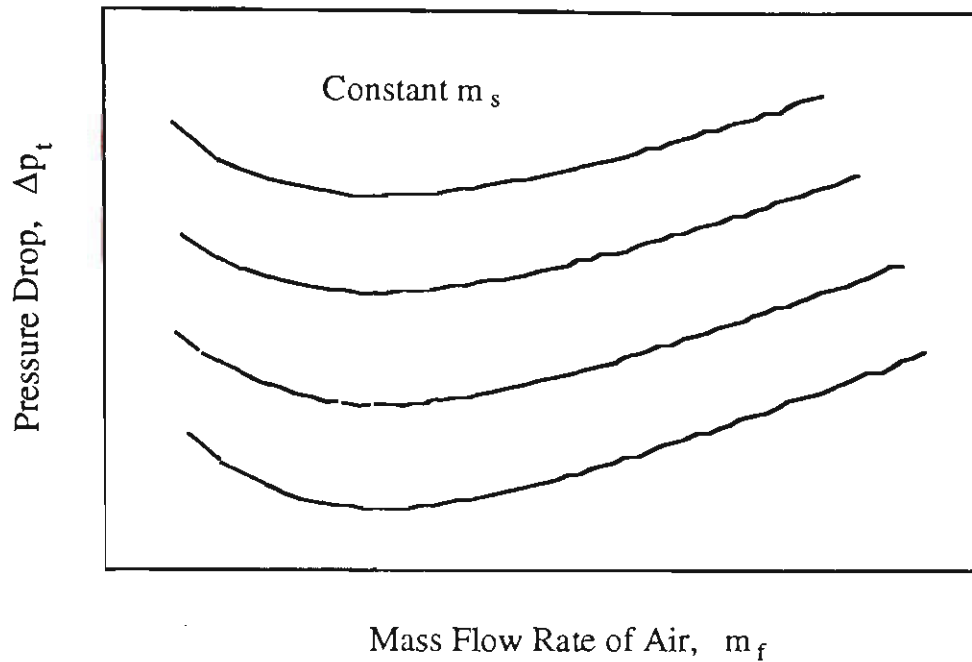


Figure 8.19 General form of steady state pneumatic conveying characteristics for a given material and pipeline.

If a pneumatic conveying system has been set up already, the characteristics of a given material can be obtained through conducting experiments. The method is outlined below (when a rotary valve is used as the material feeder of the system):

- (i) Undertake a group of pneumatic conveying tests which have a constant m_s (i.e. fixed rotor speed of the rotary valve), but various m_{fi} ($i = 1, 2, \dots, n$) from low to high.
- (ii) Measure the corresponding total pipeline pressure drop Δp_{ti} ($i = 1, 2, \dots, n$) of each test.
- (iii) Draw a curve of constant m_s on the m_f - Δp_t coordinate system with the measured data of m_{fi} and Δp_{ti} .
- (iv) Alter the rotor speed of the rotary valve to change the mass flow-rate of solids, repeat the above procedures to obtain more curves of constant m_s .

Figures 8.20 and 8.21 present typical experimental steady-state low-velocity conveying characteristics for black plastic pellets and wheat.

The experimental conveying characteristics show that the total pipeline pressure drop decreases as the air mass flow-rate increases for low-velocity pneumatic conveying. This trend is opposite to that in dilute-phase conveying. One reason is that more air mass flow-rate can aerate particle slugs better (e.g. less formation of arching in the slugs), so as to improve the inner stress state of the slugs and reduce the wall friction forces. Another reason is that slug velocity increases with air mass flow-rate, so that the total length of slug reduces for a given mass flow-rate of solids, refer to Equation (8.9). Since the particle slugs are in an aerated state during low-velocity pneumatic conveying, the pressure gradient in the slugs does not increase significantly and can be assumed as a constant. Hence the total pipeline pressure drop will decrease.

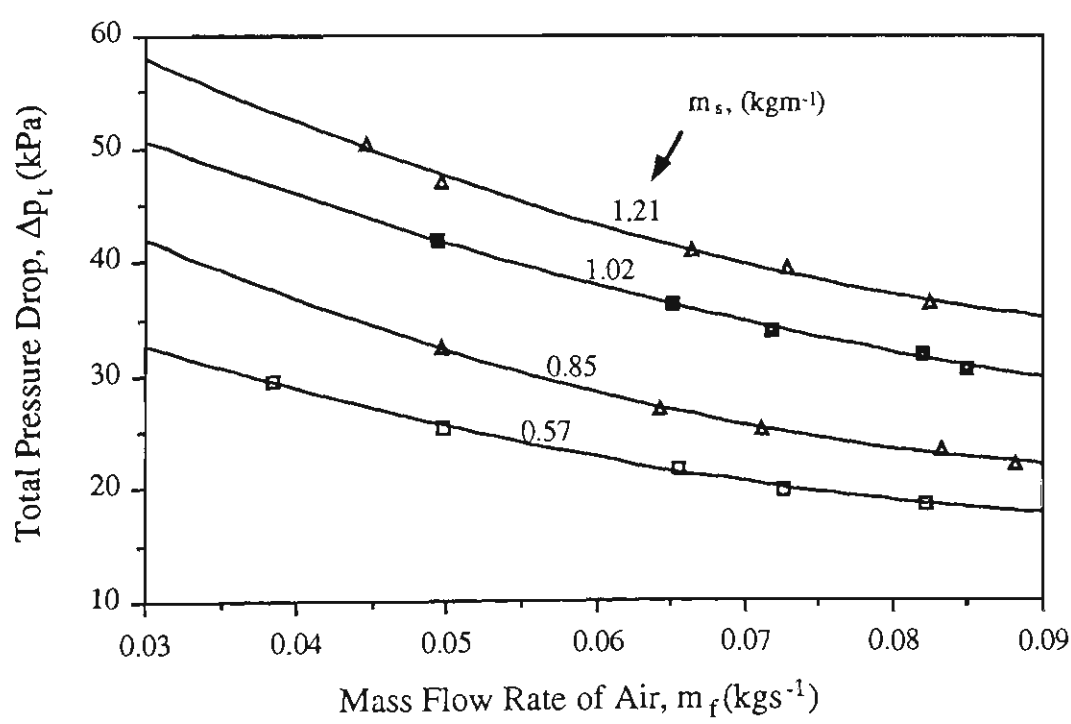


Figure 8.20 Experimental conveying characteristics of black plastic pellets conveyed in the 52 m long pipeline.

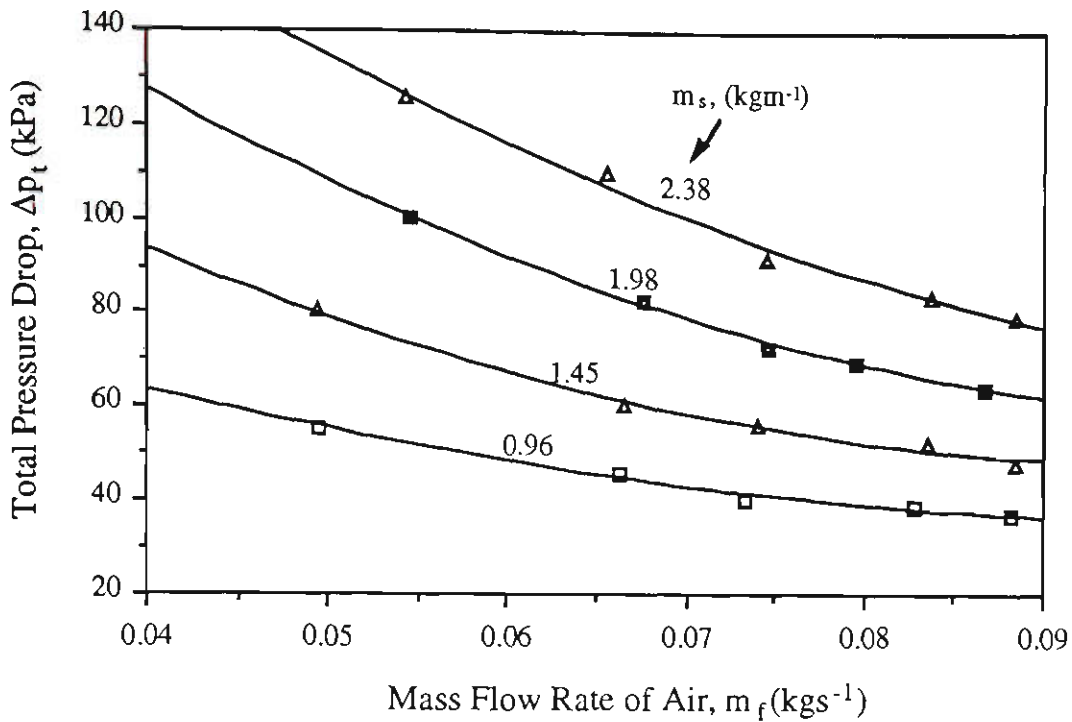


Figure 8.21 Experimental conveying characteristics of wheat conveyed in the 52 m long pipeline.

While carrying out the experiments to obtain the conveying characteristics, the air pressure distributions along the horizontal section of the pipeline also were obtained by using the air pressure transducers along the pipeline, refer to Figure B.1 in Appendix B. Some results, see Appendix A, are shown in Figures 8.22 to 8.25. The relevant conveying conditions are given in the top left-hand corner of each figure.

From Figures 8.22 to 8.25, it can be seen that the pipeline pressure exhibits an approximately linear distribution along the length of pipe (i.e. the pressure gradient is a constant), particularly at the lower values of mass flow-rate of solid. This conclusion supports the assumption made in Chapter 3 when carrying out the integration of Equation (3.9).

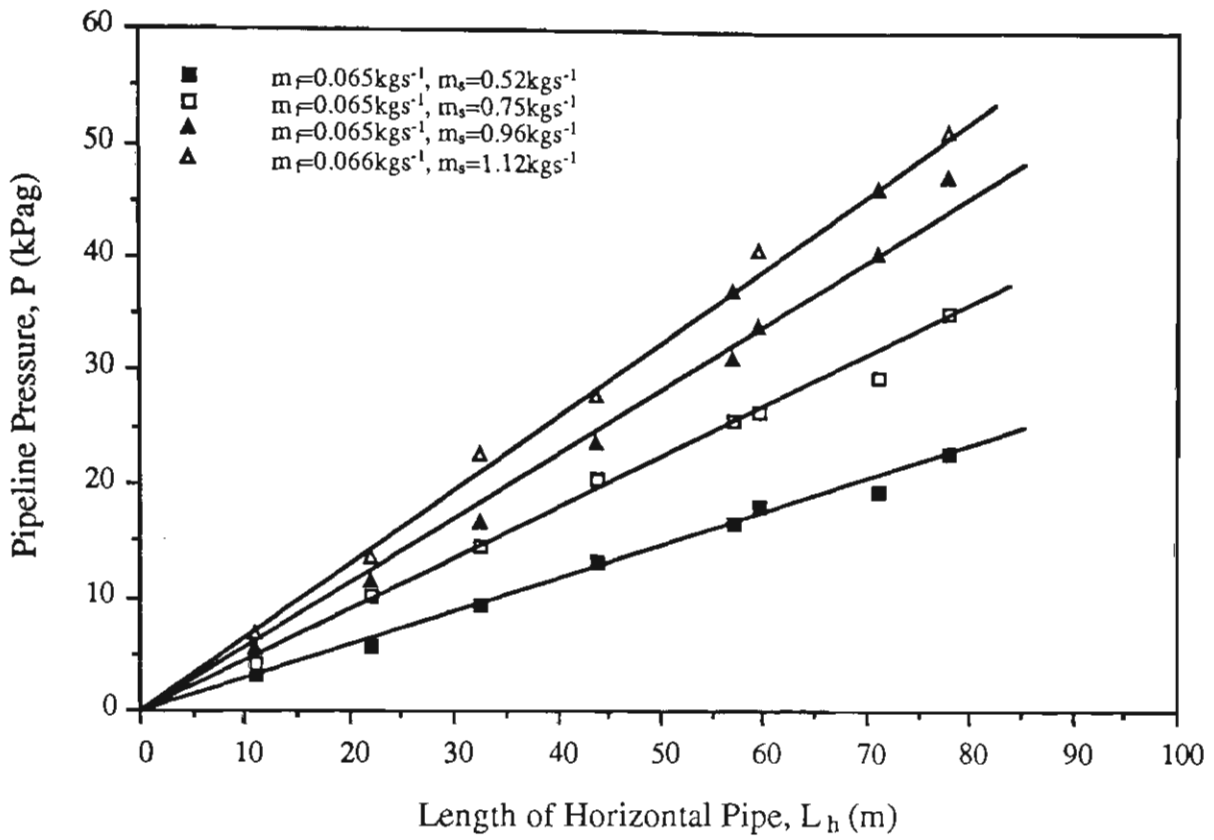


Figure 8.22 Pressure distribution along a horizontal pipe for white plastic pellets.

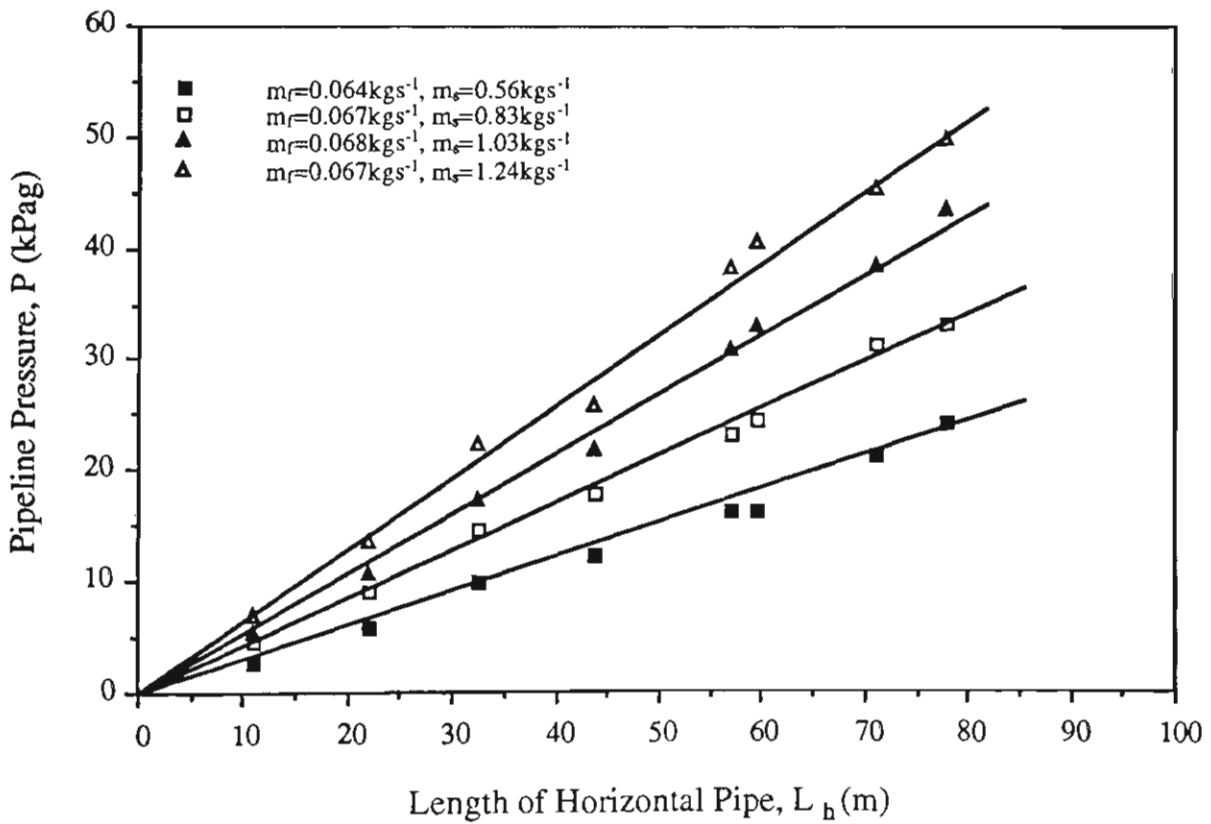


Figure 8.23 Pressure distribution along a horizontal pipe for black plastic pellets.

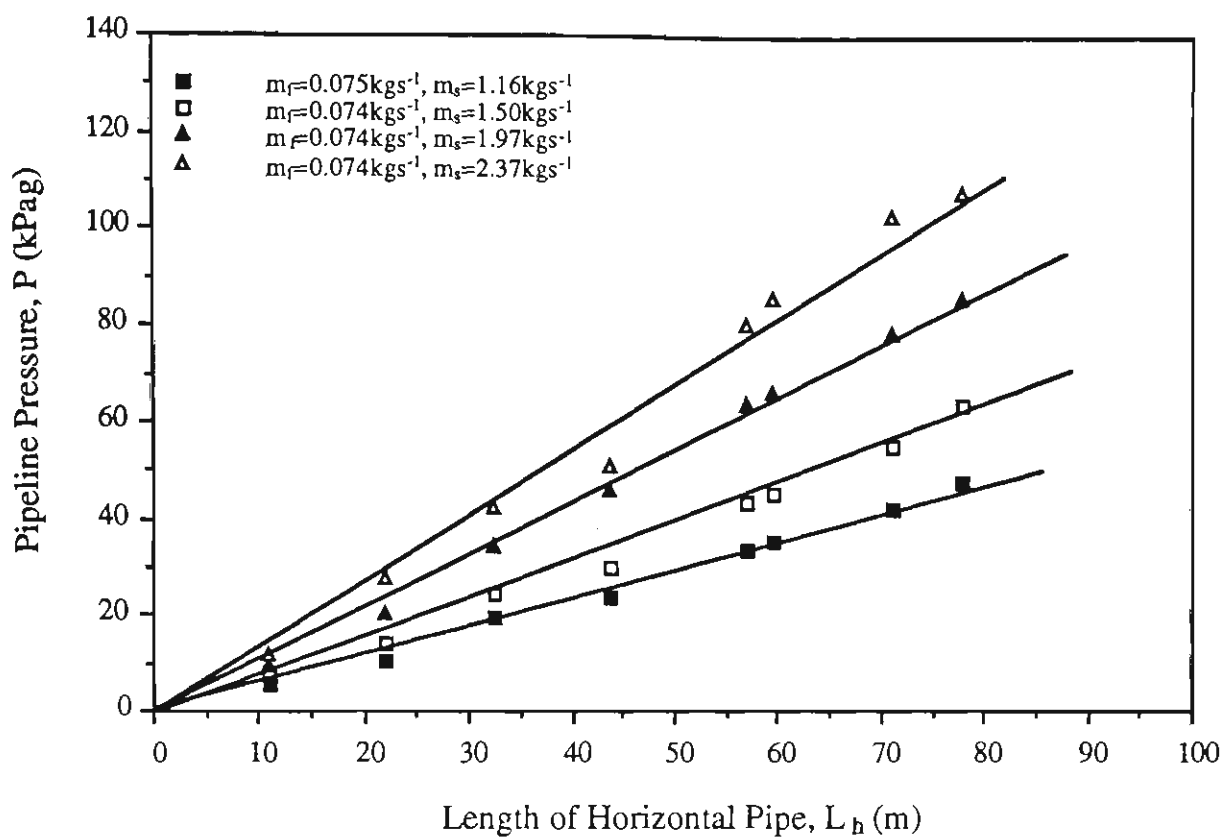


Figure 8.24 Pressure distribution along a horizontal pipe for wheat.

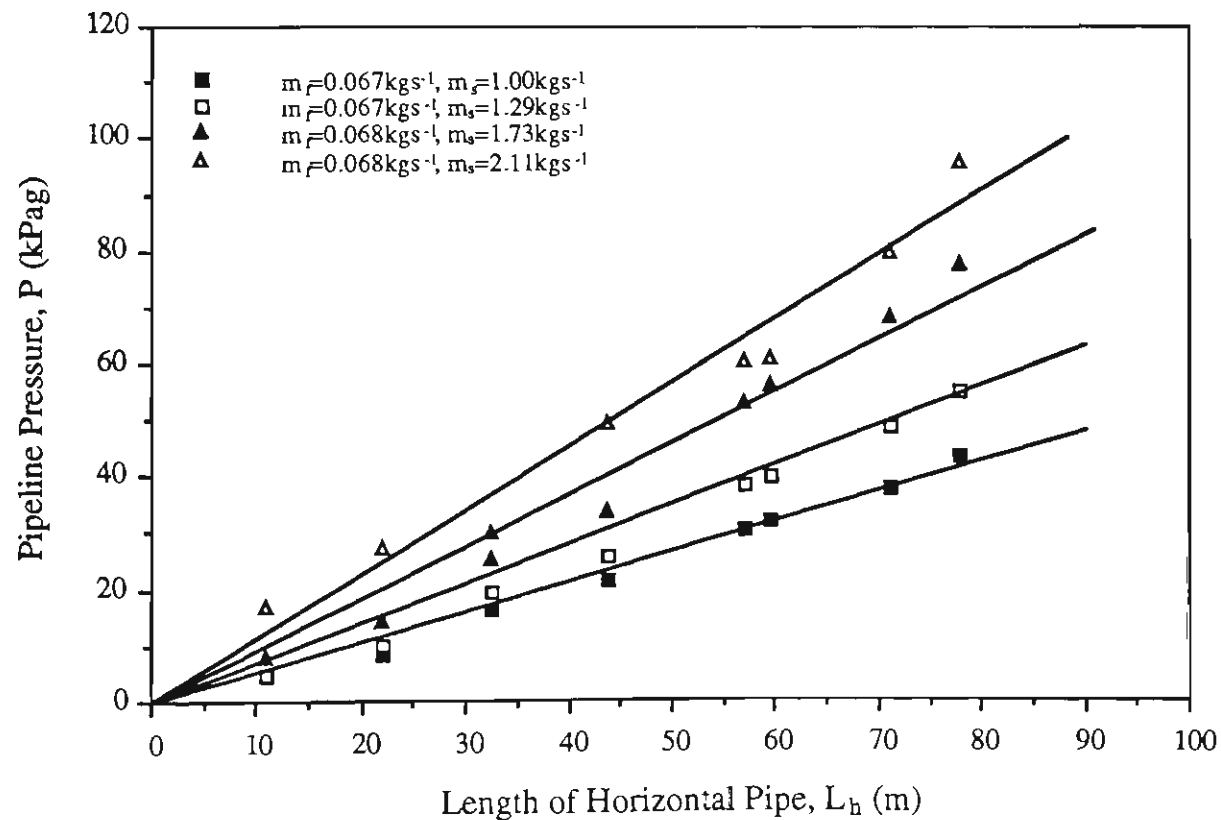


Figure 8.25 Pressure distribution along a horizontal pipe for barley.

8.4 Effect of Bends on Pressure Drop

Based on the author's experiences of dilute-phase conveying, bends have significant effects on the pipeline pressure drop. Also, the different sizes, types and locations of bends have different effects on the pressure drop. Many investigations (e.g. Bradley [11] and Klinzing [62], etc.) into bend effect have been carried out for dilute-phase conveying. However, due to the very different flow patterns and quite low velocities of air and material in low-velocity conveying, it is likely that the results of these dilute-phase investigations are not suitable for low-velocity pneumatic conveying. In order to determine the effect of bends on low-velocity pneumatic conveying, experiments were carried in the low-velocity pneumatic conveying test rig.

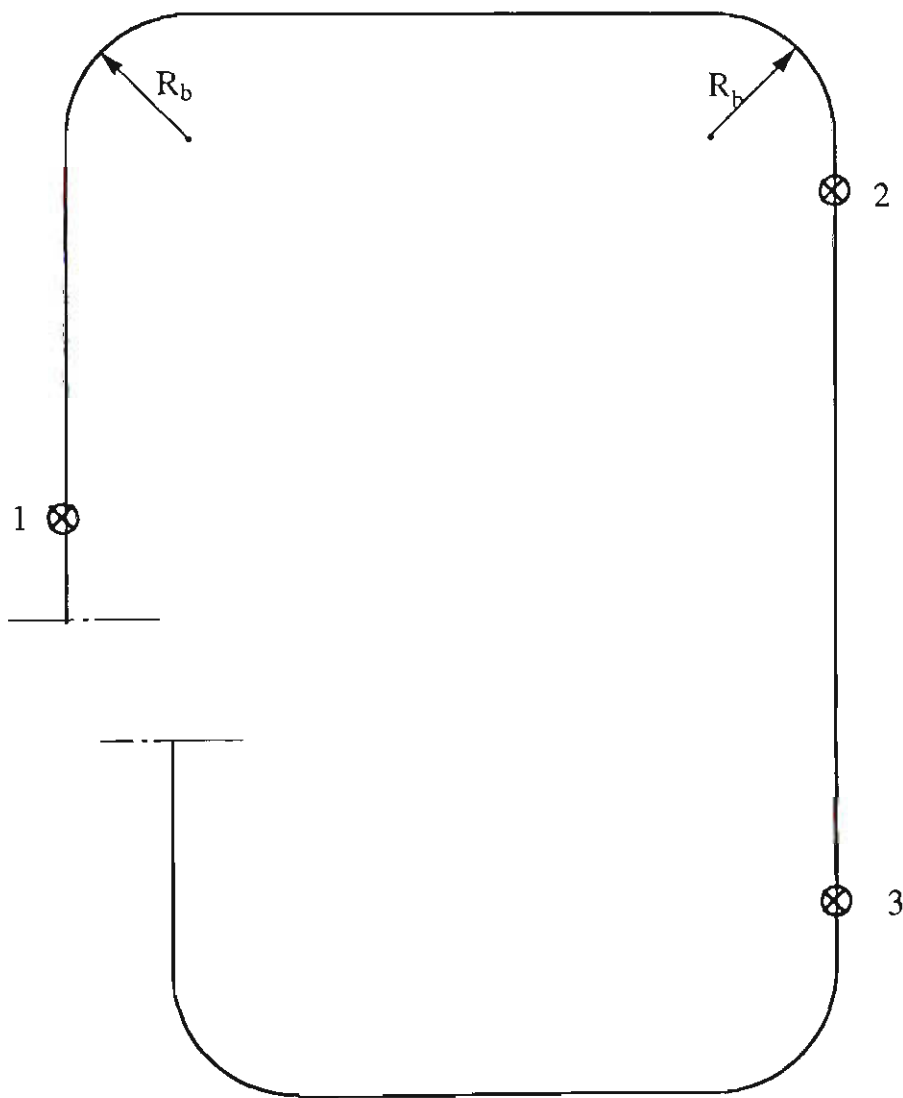


Figure 8.26 Arrangement of transducers for the investigation into bend effect.

Figure 8.26 shows part of the horizontal pipeline of the low-velocity pneumatic conveying test rig, where pressure transducers were installed at the positions indicated in the figure. The particles and air flowing from position 1 to 2 would pass through two bends each of 1.2 m radius. The pipeline is straight from position 2 to 3. The distance from position 1 to 2 (l_{12}) is 13.628 metres and from position 2 to 3 (l_{23}) 11.78 metres. Black and white plastic pellets were transported over a wide range of conveying conditions, but note that all the tests were limited in the range of low-velocity pneumatic conveying.

While operating the tests, the static air pressures at each position were measured. The pressure gradients between position 1 and 2, as well as position 2 and 3 then were calculated respectively (i.e. the values of the differential pressures Δp_{12} and Δp_{23} divided by the corresponding distance l_{12} and l_{23}). The pressure gradient Δp_{12} would include the effect of the two bends, but Δp_{23} would not. Comparing the values of $\frac{\Delta p_{12}}{l_{12}}$ with those of $\frac{\Delta p_{23}}{l_{23}}$, it was found that in most case the values of $\frac{\Delta p_{12}}{l_{12}}$ are slightly greater than the values of $\frac{\Delta p_{23}}{l_{23}}$, but still very close. This indicates that the effect of bends is not significant in low-velocity pneumatic conveying. To show the comparison, graphs are drawn by using $\frac{\Delta p_{12}}{l_{12}}$ and $\frac{\Delta p_{23}}{l_{23}}$ as horizontal and vertical coordinates, as shown in Figures 8.27 and 8.28. An explanation of the graphs is given below:

If a point lies on the 45° line, it means that the corresponding $\frac{\Delta p_{12}}{l_{12}}$ is exactly equal to $\frac{\Delta p_{23}}{l_{23}}$. A point lying underneath the 45° line indicates that $\frac{\Delta p_{12}}{l_{12}}$ is greater than $\frac{\Delta p_{23}}{l_{23}}$. The further the point is from the 45° line, the larger the difference between $\frac{\Delta p_{12}}{l_{12}}$ and $\frac{\Delta p_{23}}{l_{23}}$.

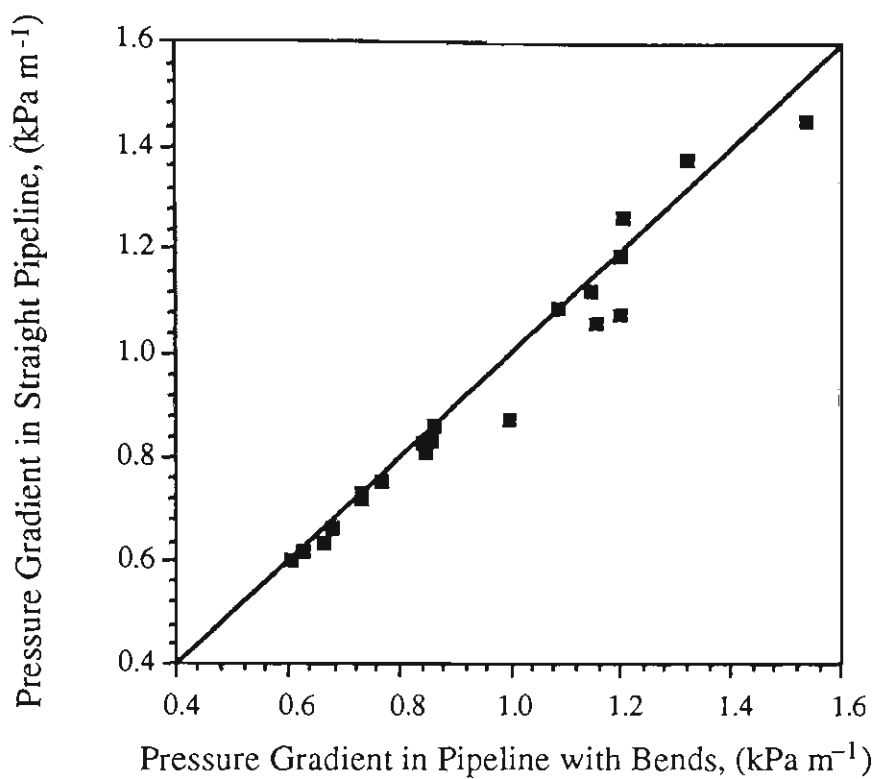


Figure 8.27 Comparison of pressure gradient for black plastic pellets.

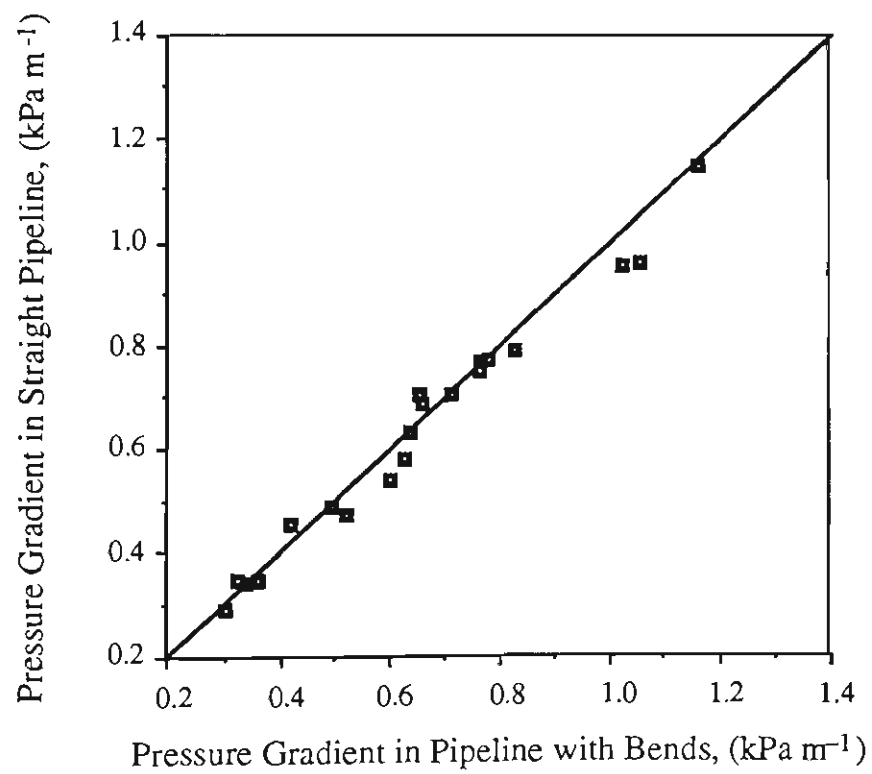


Figure 8.28 Comparison of pressure gradient for white plastic pellets.

From the figures, it can be seen that all the data points are contained in a very narrow range near the 45° line, particularly at lower pressure gradient. Also it is observed that most points lie under the 45° line. This means that the presence of the bends increases the pressure drop in low-velocity pneumatic conveying, but only slightly. Through an analysis of the pressure caused by a slug flowing through a pipeline with a bend, as shown in Figure 8.29, an explanation is given for the reason a bend only has a small effect on pressure in low-velocity pneumatic conveying.

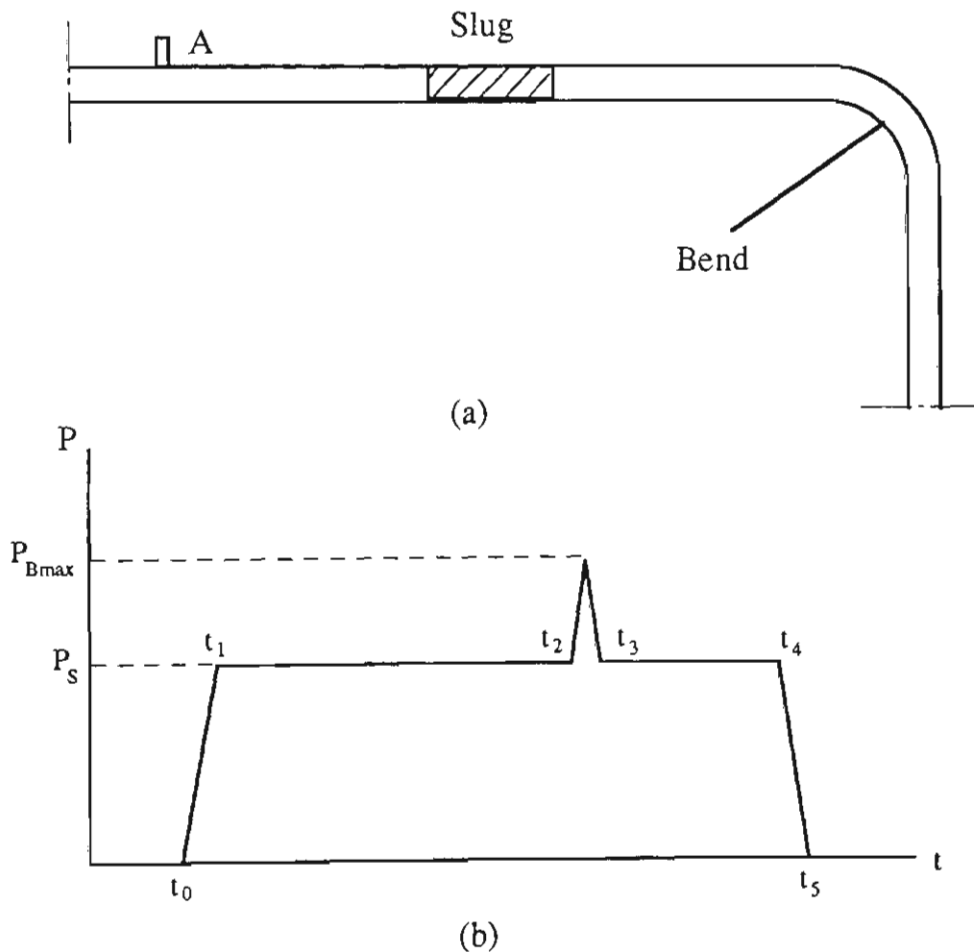


Figure 8.29 Slug flowing through pipeline with a bend and the corresponding idealised pressure wave form.

Firstly, the following assumptions are made to simplify the analysis:

- (i) Only one particle slug is moving along the pipeline.
- (ii) The slug maintains a constant size (i.e. it does not collapse during the flow).

- (iii) The pressure loss caused by the conveying air is neglected due to the low air velocity (i.e. all pressure loss is contributed by the slug).

If a pressure transducer is installed at a point which is l_A metres away from the end of the pipeline, see Figure 8.29(a), then a pressure time history can be recorded as shown in Figure 8.29(b). The figure shows the following pressure variations:

- (i) From t_0 to t_1 , the slug moves into the pipe downstream of the test point, the pressure at point A increases from zero to $P_S = \Delta p$, which is the pressure drop across the slug.
- (ii) From t_4 to t_5 , the slug exits from the pipe, the pressure at point A decreases from P_S to zero.
- (iii) From t_1 to t_2 and t_3 to t_4 , the slug flows in the straight section of the pipeline, the pressure at point A remains at P_S since only one slug is contained in the pipeline.
- (iv) From t_2 to t_3 , the slug passes through the bend, the pressure will rise to a value greater than P_S , say $P_{B\max}$, due to the extra resistance to flow.

The time that the slug enters and leaves the pipeline (i.e. $(t_1 - t_0)$ and $(t_5 - t_4)$) is very short and the pressure is equal to P_S if there is no bend in the pipeline (i.e. the pressure is equal to P_S from t_2 to t_3). If a bend exists in the pipeline, the average pressure at point A will be

$$P = \frac{P_S [(t_4 - t_1) - (t_3 - t_2)] + P_B (t_3 - t_2)}{(t_4 - t_1)}$$

that is $P = P_S + (P_B - P_S) \frac{t_3 - t_2}{t_4 - t_1}$ (8.13)

where P_B is the average pressure while the slug travels through the bend.

In Equation (8.13), as P_S is the pressure of point A without the bend, the term $(P_B - P_S) \frac{t_3 - t_2}{t_4 - t_1}$ indicates the effect of the bend on pressure. $(t_3 - t_2)$ represents the time that

the slug passes through the bend, and $(t_4 - t_1)$ represents the approximate time that the slug flows through the total pipeline. In most pneumatic conveying systems, the total pipeline length is always much greater than the total length of bends included in the pipeline, thus $(t_4 - t_1) \gg (t_3 - t_2)$, therefore the bends do not have a great effect on Δp_t even though P_B could be much greater than P_S .

8.5 Correlation of Horizontal Pipeline Pressure Drop

For a single horizontal slug of cohesionless material, Equation (3.14) was developed for the prediction of the pressure gradient of the slug. However, an actual low-velocity pneumatic conveying system normally has several slugs flowing along the pipeline. Since each slug undergoes the same variation in velocity while it flows from the high pressure end to the low pressure end, it is reasonable to assume that every slug flows through the pipeline with one average velocity. Hence all the moving particles in the pipeline can be treated as one long slug with a length L_s , which represents the sum of the length of all the individual slugs. The relationship between L_s and L_t is expressed by Equation (8.9).

If a system is totally composed of horizontal pipes and bends and neglecting the pressure loss caused by conveying air and bends, then the pressure gradient in the total length of slug can be obtained by replacing Δp and l_s in Equation (3.14) with the total horizontal pipeline pressure drop Δp_t and total length of slug L_s , respectively. That is

$$\frac{\Delta p_t}{L_s} = \frac{4\mu_w \lambda}{D} \sigma_f + 2\rho_b g \mu_w \quad (8.14)$$

Substituting Equation (8.9) and Equation (3.27) into Equation (8.14), then the total pressure drop in the horizontal pipeline is given by

$$\Delta p_t = \left(\frac{\alpha}{1-\alpha} \frac{2\lambda U_s^2}{gD} + \frac{1}{1-\alpha} \right) \frac{2g\mu_w m_s L_t}{A U_s} \quad (8.15)$$

Replacing α in Equation (8.15) with Equation (8.12) and letting $Fr = \frac{U_s^2}{gD}$, then

$$\Delta p_t = (1 + 1.084\lambda Fr^{0.5} + 0.542 Fr^{-0.5}) \frac{2g\mu_w m_s L_t}{A U_s} \quad (8.16)$$

where Fr is called the Froude number for the material.

Equation (8.16) shows that the total pipeline pressure drop is a function of the properties of the material, conveying condition and pipeline configuration. Although m_f and some parameters reflecting the particle properties are not in the equation, the slug velocity U_s and stress transmission coefficient λ in the equation are functions of m_f and particle properties. It must be pointed out that Equation (8.16) is developed under the assumption that a system is totally composed of horizontal pipes. If a system contains some vertical sections, then Equation (8.16) is only suitable for predicting the overall pressure drop of the horizontal section of pipeline. To avoid confusion and possible error, Δp_t and L_t in Equation (8.16) are replaced with Δp_{th} and L_{th} , respectively, that is

$$\Delta p_{th} = (1 + 1.084\lambda Fr^{0.5} + 0.542 Fr^{-0.5}) \frac{2g\mu_w m_s L_{th}}{A U_s} \quad (8.17)$$

where Δp_{th} is the overall horizontal pipeline pressure drop, L_{th} is the total length of horizontal pipeline.

Although the model can be used only to predict the pressure drops for horizontal pipelines, the predicted results still have great significance since most pipeline systems contain a significant proportion of horizontal piping.

By assuming a preliminary pipeline pressure drop for a low-velocity pneumatic conveying system, the mean slug velocity (U_s) and Froude number (Fr) in Equation (8.17) can be estimated for a given mass flow rate of air (m_f) and pipeline diameter (D). The determination of the value of the stress transmission coefficient (λ) was discussed earlier in Chapter 7, see Equations (7.8), (7.9) and (7.21). Therefore, for low-velocity

pneumatic conveying with a given mass flow-rate of solids (m_s), the pressure drop across the horizontal pipe of length (L_t) can be predicted by using computer iteration, refer to Appendix C for computer programme. The calculation procedure is listed as follows:

- (i) Calculate the stress transmission coefficient (λ), according to Equations (7.8), (7.9) and (7.21) in Chapter 7.
- (ii) Assume an initial value for the pipeline pressure drop (Δp_{ti}).
- (iii) Calculate the mean air density (ρ_a) and the mean superficial air velocity (U_a).
- (iv) Estimate the mean slug velocity (U_s) from Equations (6.32) and (6.41) in Chapter 6, and determine the Froude number of the conveyed material (Fr).
- (v) Substitute these values of U_s , Fr , and λ into Equation (8.17) to calculate the pressure drop.
- (vi) Revise the estimate of the pipeline pressure drop in (ii), and repeat from (iii) until convergence is obtained.

8.6 Comparison of Experimental and Predicted Results

To examine the accuracy of the developed model, pneumatic conveying characteristics of horizontal pipelines are predicted by using Equation (8.17) for conveying the various materials in the low-velocity pneumatic conveying test rig, as shown in Figures 8.30 to 8.37. The experimental results are superimposed onto each figure for comparison. The comparison shows that the agreement is very good, so that the prediction model is considered accurate and reliable.

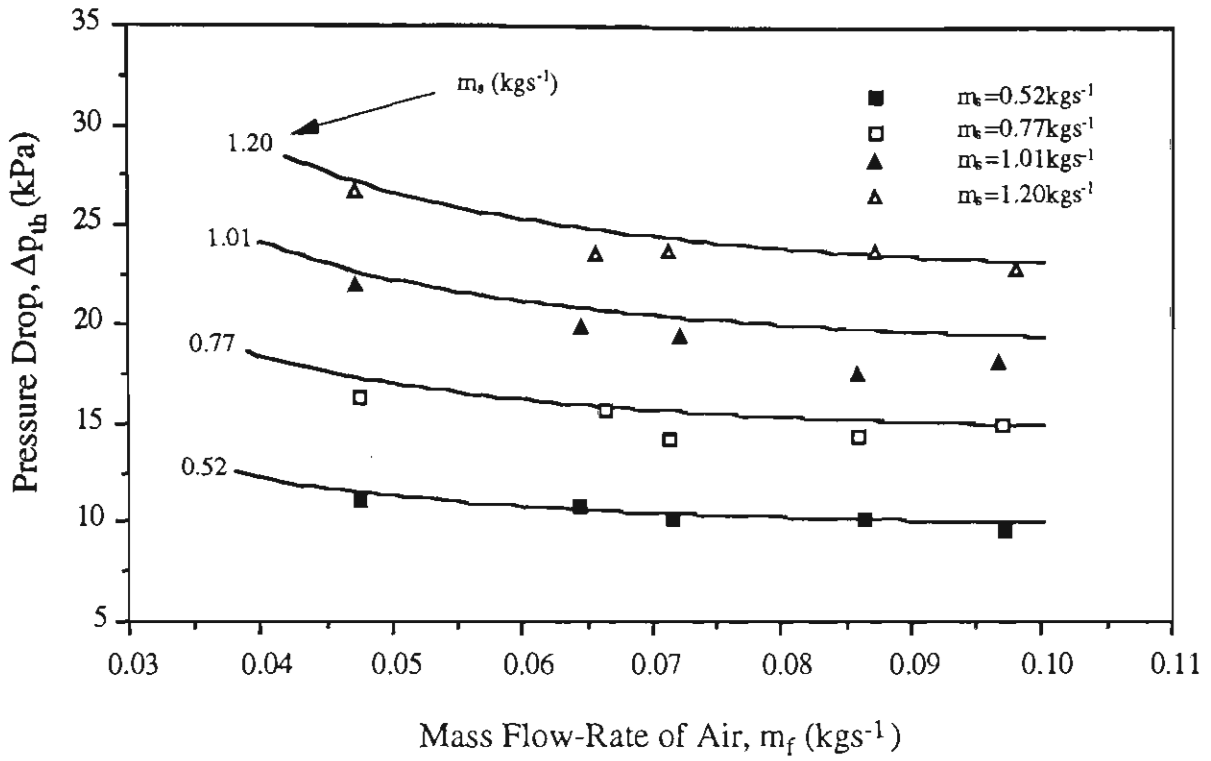


Figure 8.30 Predicted conveying characteristics of white plastic pellets in the horizontal pipe $L_{th} = 36$ m and $D = 0.105$ m, showing the curves of constant m_s .

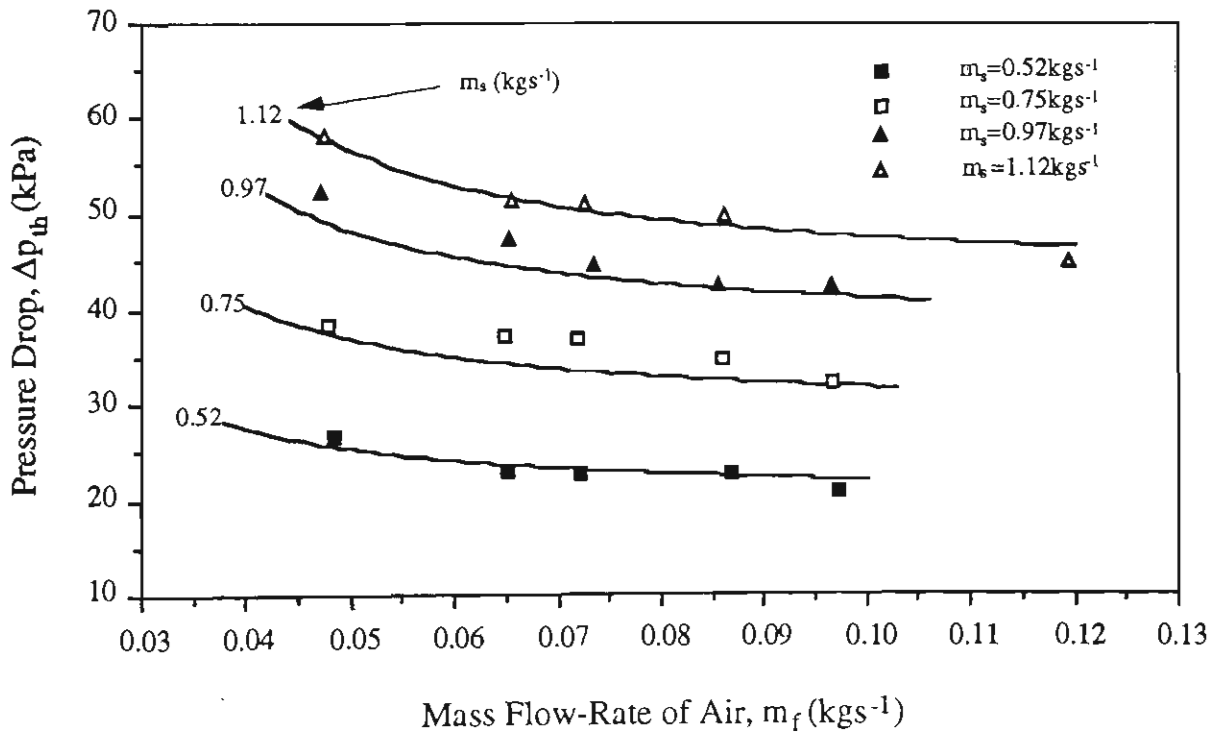


Figure 8.31 Predicted conveying characteristics of white plastic pellets in the horizontal pipe $L_{th} = 78$ m and $D = 0.105$ m, showing the curves of constant m_s .

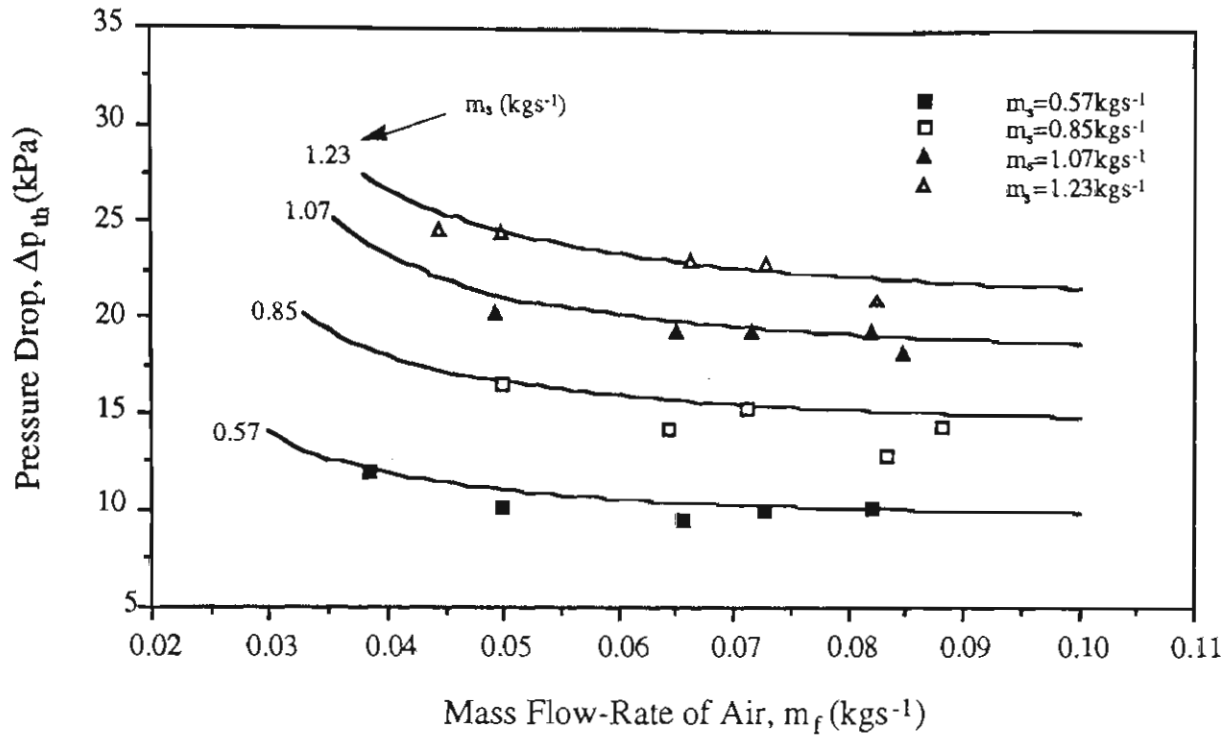


Figure 8.32 Predicted conveying characteristics of black plastic pellets in the horizontal pipe $L_{th} = 36$ m and $D = 0.105$ m, showing the curves of constant m_s .

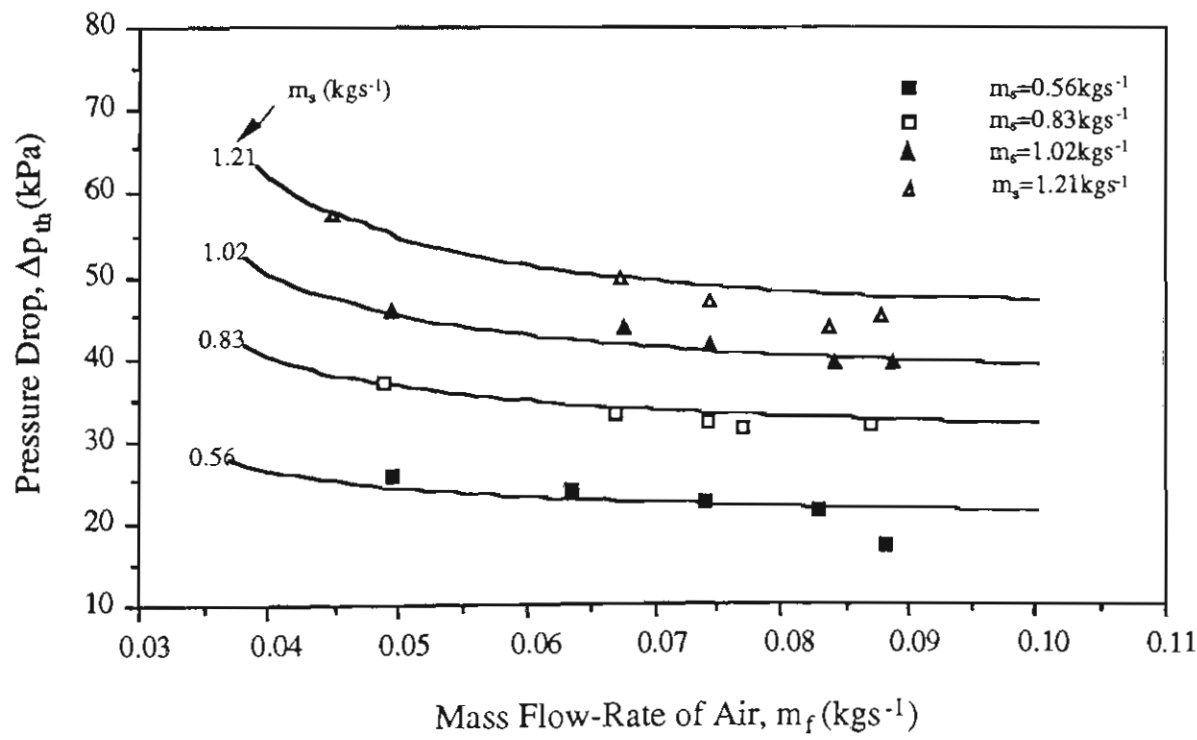


Figure 8.33 Predicted conveying characteristics of black plastic pellets in the horizontal pipe $L_{th} = 78$ m and $D = 0.105$ m, showing the curves of constant m_s .

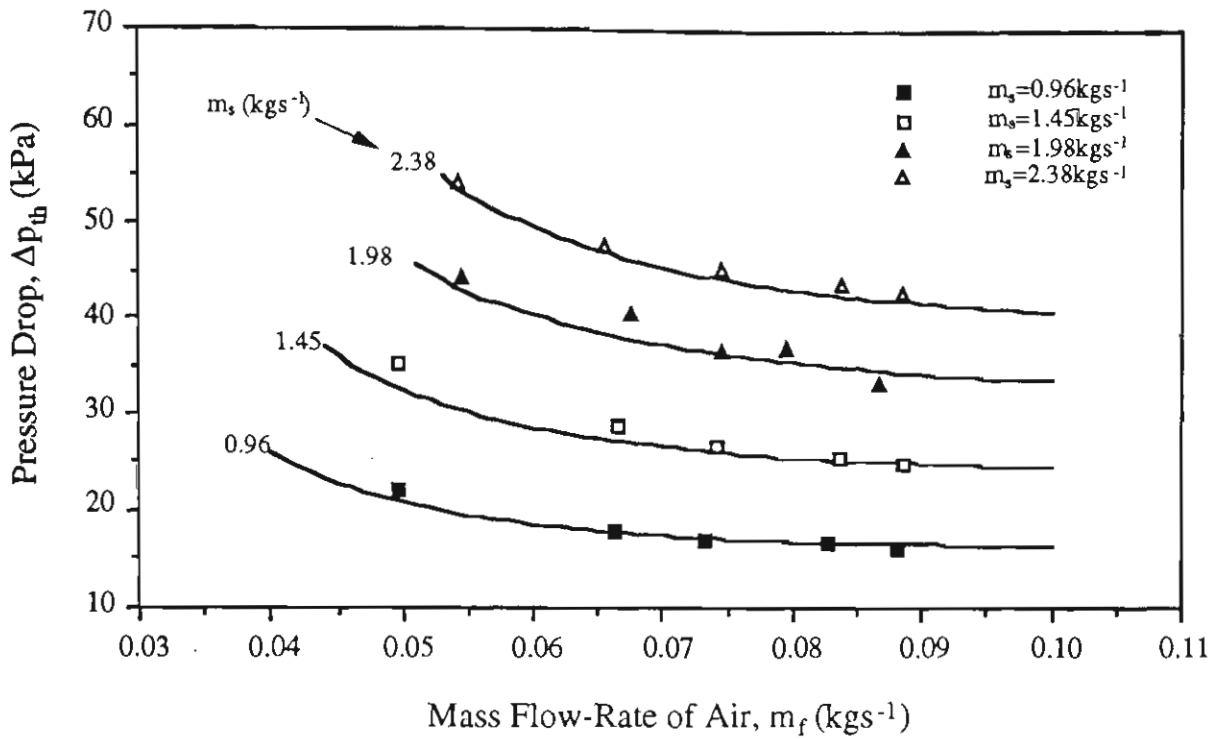


Figure 8.34 Predicted conveying characteristics of wheat in the horizontal pipe

$L_{th} = 36$ m and $D = 0.105$ m, showing the curves of constant m_s .

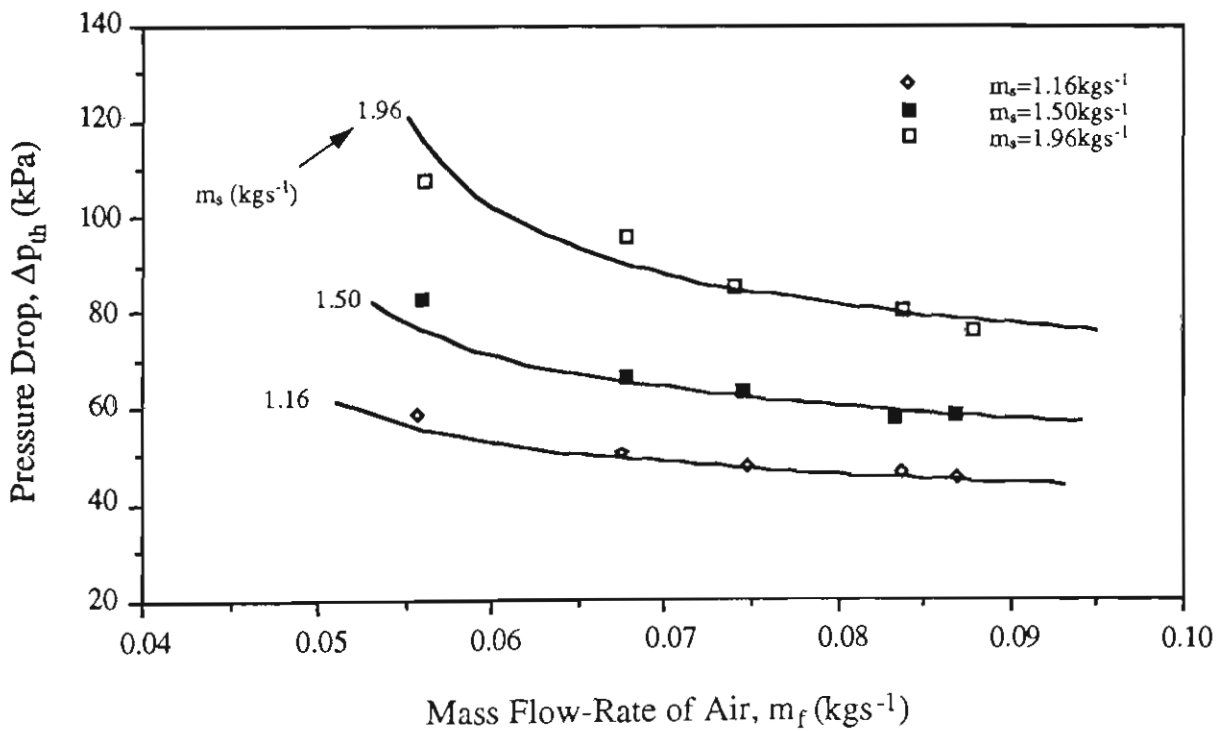


Figure 8.35 Predicted conveying characteristics of wheat in the horizontal pipe

$L_{th} = 78$ m and $D = 0.105$ m, showing the curves of constant m_s .

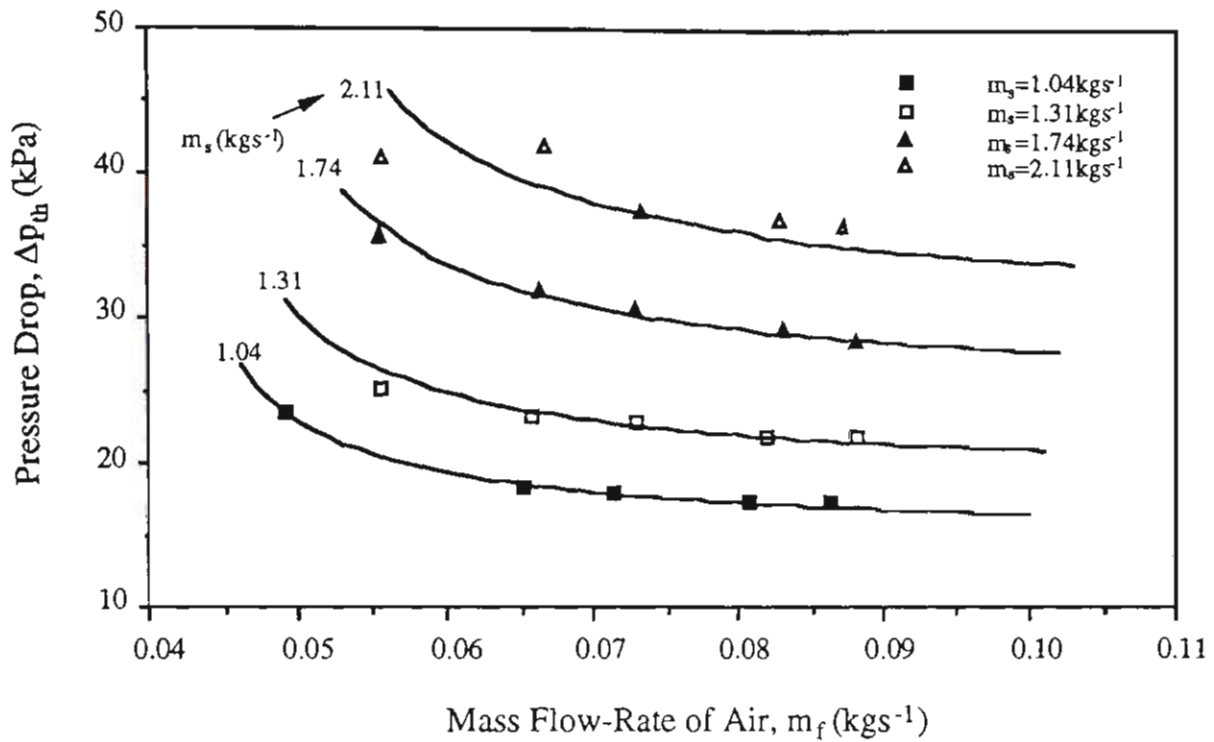


Figure 8.36 Predicted conveying characteristics of barley in the horizontal pipe

$L_{th} = 36$ m and $D = 0.105$ m, showing the curves of constant m_s .

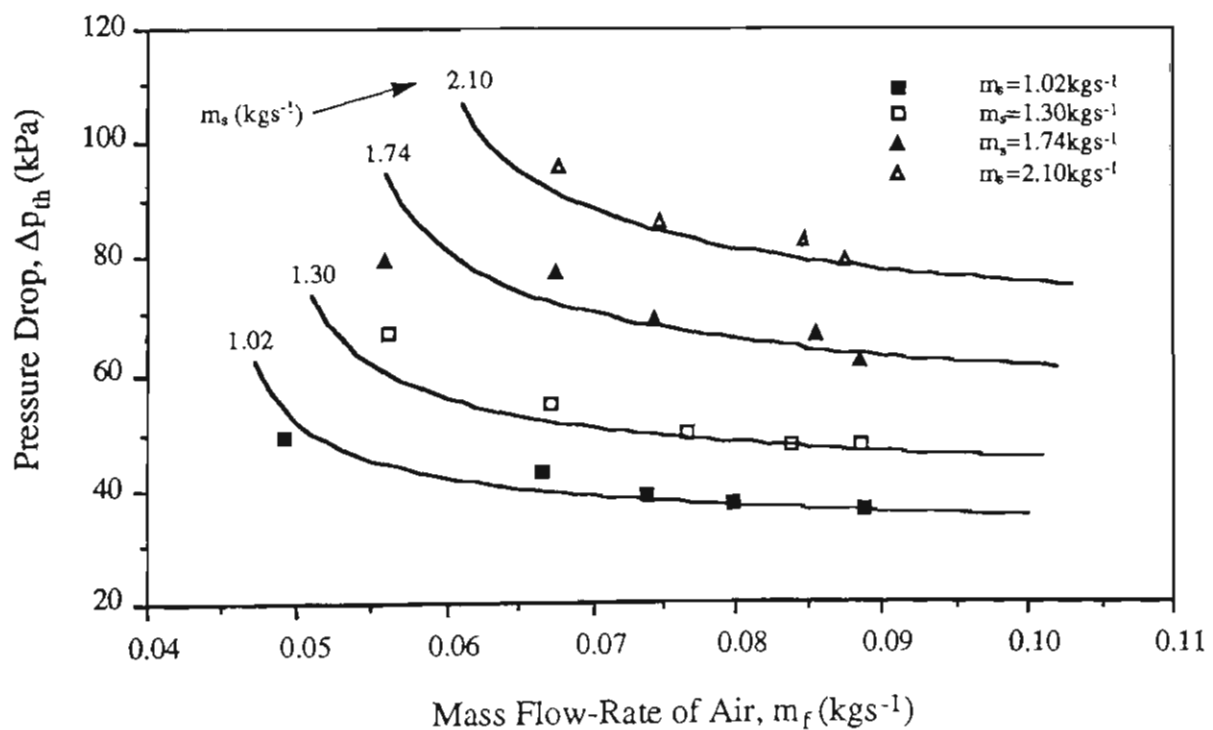


Figure 8.37 Predicted conveying characteristics of barley in the horizontal pipe

$L_{th} = 78$ m and $D = 0.105$ m, showing the curves of constant m_s .

CHAPTER 9

PRACTICAL APPLICATIONS

9.1 Introduction

A model for predicting pipeline pressure drop was developed in Chapter 8 for low-velocity pneumatic conveying. This model was found to have good accuracy in the prediction of the dense-phase pneumatic conveying characteristics of four different materials. To examine further the applicability of the models developed in this thesis to the industrial design and analysis of low-velocity conveying systems, this chapter addresses the following three areas of concern:

- Prediction of dense-phase pneumatic conveying characteristics for other materials and pipeline configurations.
- Determination of pressure distribution along the pipeline.
- Selection of economical conveying conditions for low-velocity pneumatic conveying systems.

Also, the suitability of the model to fine powders is investigated by conveying pneumatically the fine powder semolina in dense-phase. According to these experimental results, the model is modified to enable the accurate prediction of pressure drop for low-velocity pneumatic conveying of fine powders.

9.2 Prediction of Pneumatic Conveying Characteristics

Pneumatic conveying characteristics are very useful for designing a new system or upgrading an existing system. A traditional method [117] that is used to obtain the pneumatic conveying characteristics of an actual conveying system is to scale up the data obtained from experiments conducted on a pilot test rig. Using this method, the reliability of the scaled up pneumatic conveying characteristics will be limited by the conditions of the pilot test rig, the accuracy of the experimental data and the scale-up technology. Hence there may be doubt associated with the applicability of this method, particularly in

dense-phase conveying as the scale-up technology has not been proven yet for this type of conveying.

As the model developed in Chapter 8 is a function of material properties, pipeline configuration and conveying condition, it is possible that pneumatic conveying characteristics can be determined directly from the model for low-velocity pneumatic conveying (i.e. instead of conducting pilot plant experiments) if the conditions of the material and pipeline are known. The following sections provide examples of this application. It should be noted that all the work is conducted on the basis of the horizontal section of pipeline.

9.2.1 Test Materials

Polystyrene chips and black plastic pellets are very useful materials which have been applied to many fields of industries. These materials are also good candidates for pneumatic conveying. They have been transported successfully in dilute- and dense-phase by various pneumatic conveying systems in the Bulk Solids Handling Laboratory at the University of Wollongong. Based on the developed model, low-velocity pneumatic conveying characteristics of these materials are predicted for those conveying systems. Note that the pneumatic conveying characteristics of black plastic pellets were obtained previously by experiment and the model here will predict and compare the characteristics of black plastic pellets in a different test rig.

Representative properties of bulk material are often the particle diameter, particle and bulk density, internal and wall friction angle in pneumatic conveying. The definitions and measurement methods of these terms were introduced in Chapter 5. Using these methods, the following values are obtained for polystyrene chips:

Mean particle diameter, d	2.98	mm
Particle density, ρ_s	1039	kgm ⁻³

Bulk density (loosed), ρ_b	637	kgm ⁻³
Bulk voidage, ϵ	0.387	
Internal friction angle, ϕ	44.6	°
Wall friction angle (with respect to mild steel), ϕ_w	15.8	°

The properties of black plastic pellets were measured and listed previously in Table 5.1.

9.2.2 Test Rigs

Three different test rigs (called Rigs 1, 2 and 3) are employed to convey polystyrene chips and one rig (called Rig 4) for black plastic pellets. Details of the rigs are given below.

Rig 1 is the low-velocity pneumatic conveying test rig employed to conduct most of the experiments of this research, refer to Figure 4.1 for details. The low-velocity pneumatic conveying test rig has two arrangements for its pipeline system, in this application only the 96 m long pipeline arrangement is used for conveying polystyrene chips.

Rigs 2 and 3 employ an identical 156 mm ID mild steel pipeline system. The only difference between these rigs is that Rig 3 uses a ZGR-250 rotary valve feeder, whereas Rig 2 uses a 0.9 m³ blow tank. The main purpose of applying different material feeders to the one pipeline is to investigate the suitability of both feeders to polystyrene chips and also to achieve higher pressures and capacities in Rig 2. The use of different material feeders has little influence on pipeline conveying characteristics (i.e. as long as rotary valve air leakage is allowed for in the air flow calculations in Rig 1).

The pipeline layout of Rigs 2 and 3 is very similar to the low-velocity pneumatic conveying test rig with the 52 m long pipeline arrangement, refer to Figure 4.6. Hence, Rigs 2 and 3 have the same pipeline length and arrangement of bends as the low-velocity pneumatic conveying test rig with the 52 m pipeline arrangement. That is, Rigs 2 and 3

have a total pipeline length of 52 m, in which 45.5 m is horizontal pipe, and 6 bends of 1.2 m radius.

Rig 4 is composed of an 80.5 mm ID mild steel pipeline with a total length of 137 m and 8 bends of 0.254 m radius. The schematic layout is shown in Figure 9.1. A 0.9 m³ blow tank is used as material feeder. The blow tank is supported on the framework by load cells which monitor the mass of material delivered to the pipeline from the blow tank. After discharging from the blow tank, the material is lifted almost immediately to a height of 5.9 m by a vertical pipe and then transported horizontally to a 1.0 m³ receiving silo which is located just above the blow tank. The total length of the horizontal section of the pipeline is 127 m. The mass of material loaded in the silo also is measured by the load cells supporting the silo. The received material can be discharged into the blow tank by opening the outlet valve for the next transportation.

Major details on the above test rigs are summarised in Table 9.1.

Table 9.1: Conveying pipelines.

Test Rig	D (mm)	L_t (m)	L_{th} (m)	L_{th}^* (m)	NB*
Rig 1	105	96	89.5	78	10
Rigs 2 and 3	156	52	45.5	40	6
Rig 4	80.5	137	127.8	116	8

L_{th}^* Total horizontal pipeline length for calculation.

NB* Number of bends (for total pipeline).

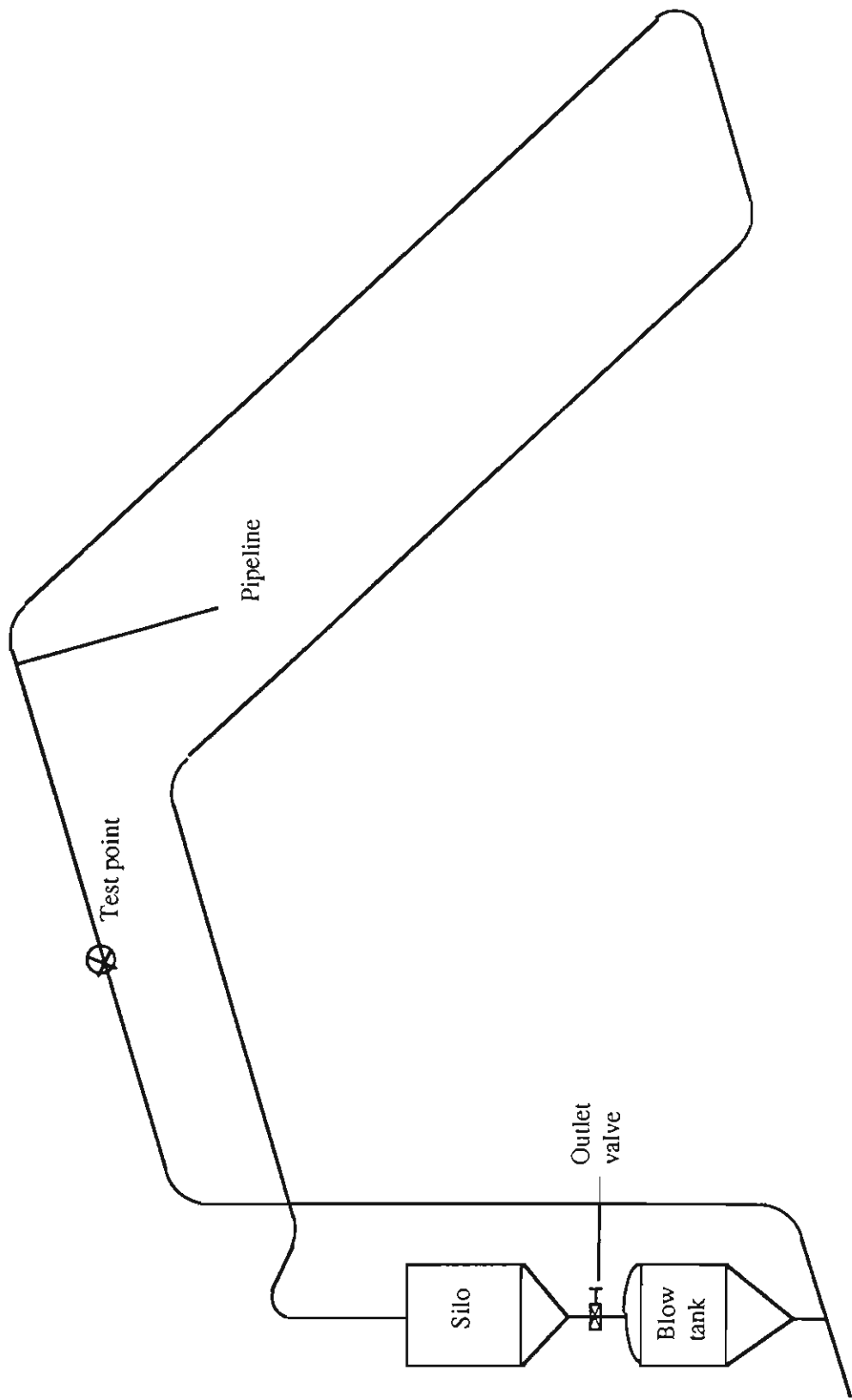


Figure 9.1 Pneumatic conveying test rig with 80.5 mm ID pipeline.

9.2.3 Test Results

Polystyrene chips and black plastic pellets are conveyed pneumatically in the above test rigs. A wide range of conveying conditions are selected for these tests, i.e. for a given mass flow-rate of solids, the air mass flow-rate is selected to convey the materials from dense-phase to dilute-phase. A large number of results are obtained. Tables 9.2 and 9.3 list the horizontal pipeline pressures and relevant parameters during dense-phase conveying.

Table 9.2: Steady-state dense-phase results for black plastic pellets.

Test Rig	Exp. No.	Speed* (rpm)	m_{ft} (kgs ⁻¹)	m_{fl} (kgs ⁻¹)	m_f (kgs ⁻¹)	m_s (kgs ⁻¹)	Δp_{th} (kPa)
4	1	-	.0293	-	.0293	.304	40.12.
	2	-	.0422	-	.0422	.332	40.08.
	8	-	.0319	-	.0319	.378	54.23.
	9	-	.0450	-	.0450	.415	47.81
	15	-	.0344	-	.0344	.454	59.01
	16	-	.0465	-	.0465	.497	54.50.
	22	-	.0350	-	.0350	.470	61.21
	23	-	.0470	-	.0470	.515	55.14
	29	-	.0352	-	.0352	.474	61.61
	30	-	.0469	-	.0469	.535	54.00

* Rotary valve speed.

Note that:

- Speed = rotary valve speed (applicable to Rigs 1 and 3 only),
- m_{ft} = total supplied mass flow rate of air,
- m_{fl} = rotary valve air leakage,
- m_f = actual mass flow rate of air in pipeline,
- m_s = mass flow rate of solids,
- Δp_{th} = total horizontal pipeline pressure drop.

Table 9.3: Steady-state dense-phase results for polystyrene chips.

Test Rig	Exp. No.	Speed* (rpm)	m_{ft} (kgs ⁻¹)	m_{fl} (kgs ⁻¹)	m_f (kgs ⁻¹)	m_s (kgs ⁻¹)	Δp_{th} (kPa)
1	4	20	.083	.027	.056	1.279	71.
	5	30	.084	.036	.048	1.714	111.
	6	42	.084	.037	.047	1.804	126.
	7	35	.085	.037	.048	1.764	118.
	10	35	.083	.038	.045	1.782	121.
	11	35	.104	.034	.070	1.900	102.
	15	27	.084	.033	.051	1.570	104.
	19	18	.084	.024	.060	1.150	68.
	21	18	.073	.027	.045	1.182	78.
2	57	-	.193	-	.193	8.57	107.
	58	-	.181	-	.181	8.82	109.
	59	-	.187	-	.187	8.28	101.
	60	-	.141	-	.141	6.49	91.
	64	-	.142	-	.142	6.87	105.
	65	-	.141	-	.141	7.04	102.
	66	-	.099	-	.099	4.67	87.
3	102	35	.090	.019	.071	1.95	41.5
	103	35	.109	.018	.091	2.00	37.8
	104	35	.108	.017	.091	2.00	37.0
	105	35	.128	.015	.128	2.10	33.4
	106	35	.150	.013	.137	2.10	28.0
	110	21	.080	.016	.064	1.43	34.0
	111	21	.097	.013	.084	1.43	26.0
	112	21	.118	.012	.106	1.45	22.3
	113	21	.135	.011	.124	1.47	22.4

9.2.4 Predicted Pneumatic Conveying Characteristics

According to the procedures recommended in Chapter 8, horizontal pipeline pressure drop can be predicted for a given mass flow-rate of air and solids. However, to obtain a pressure drop curve of a constant m_s , a group of pressure drop data with different mass

flow-rates of air are necessary. This work can be achieved by repeating the calculation of pipeline pressure drop. The calculation process is outlined in Figure 9.2. A computer program is developed for this purpose, see Appendix C.

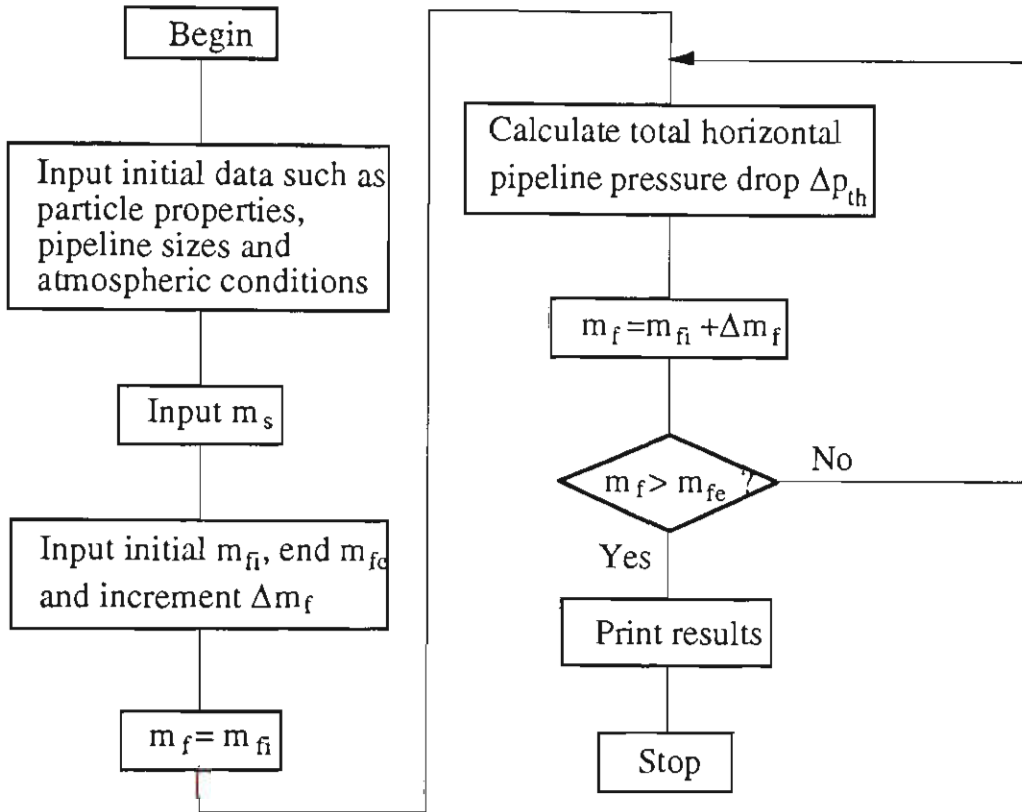


Figure 9.2 Procedure for determining pneumatic conveying characteristics.

Note that a slight adjustment is made for the model of slug velocity, i.e. Equation (6.32), involved in the computer program to obtain reliable predictions. That is, if the slug velocity calculated by Equation (6.32) is less than an empirical figure of 1.5 ms^{-1} , repeat the calculation by replacing the minimum air velocity with half of the value predicted by Equation (6.41). The reason for making this adjustment is explained below.

The studies in Chapter 6 show that the slug velocity is expressed linearly by the superficial air velocity in the experiments conducted in this project and there also exists a minimum superficial air velocity that is necessary to initiate the motion of a slug, as shown in Figure 9.3.

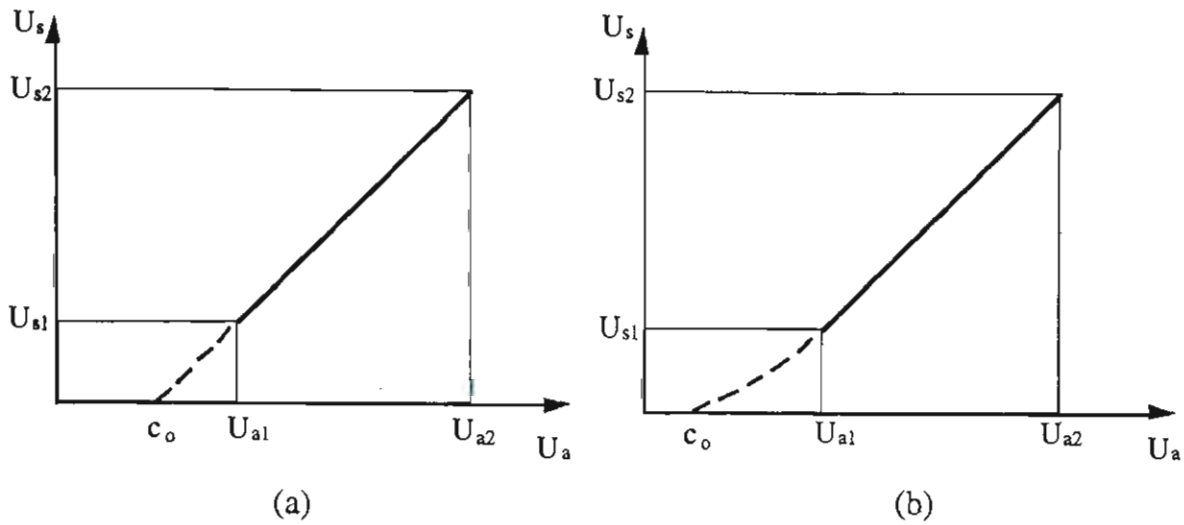


Figure 9.3 Relationship between slug velocity and superficial air velocity.

In Chapter 6, the minimum superficial air velocity of each test material was obtained by extending the straight line to intersect the U_a axis, see Figure 9.3(a). The model given by Equation (6.41) then was developed to fit this value. However, experience has shown that while the superficial air velocity is low, the relationship between slug velocity and superficial air velocity in practice is often expressed by a curve instead of a straight line, see Figure 9.3(b). The reason is that the configuration of particle slug (e.g. the bulk voidage of slug, the arrangement of particles, etc.) will change slightly while the superficial air velocity is reduced. This certainly affects the trend of slug velocity. It may be more convenient to call the minimum air velocity used presently as the nominal minimum air velocity. In most cases, the real minimum air velocity is lower than the nominal minimum air velocity as the bulk voidage of slug reduces slightly with the air velocity decreasing, see Figure 9.3(b). Limited by the ZGR-250 rotary valve (i.e. the air mass flow-rate used for the conveying experiments must be greater than a limit value, otherwise the rotary valve stops working), the real minimum superficial air velocity was not obtained from the experiments for each test material. Hence, the relationship between real minimum superficial air velocity and nominal minimum air velocity was not established. According to the author's experience, the slight adjustment described

previously to the model of slug velocity is able to satisfy the pressure prediction in the case of low air mass flow-rate.

The low-velocity pneumatic conveying characteristics of the horizontal pipelines of various test rigs are predicted by using the computer program and presented in Figures 9.4, 9.5 and 9.6. The experimental results of m_s are superimposed onto each figure for comparison.

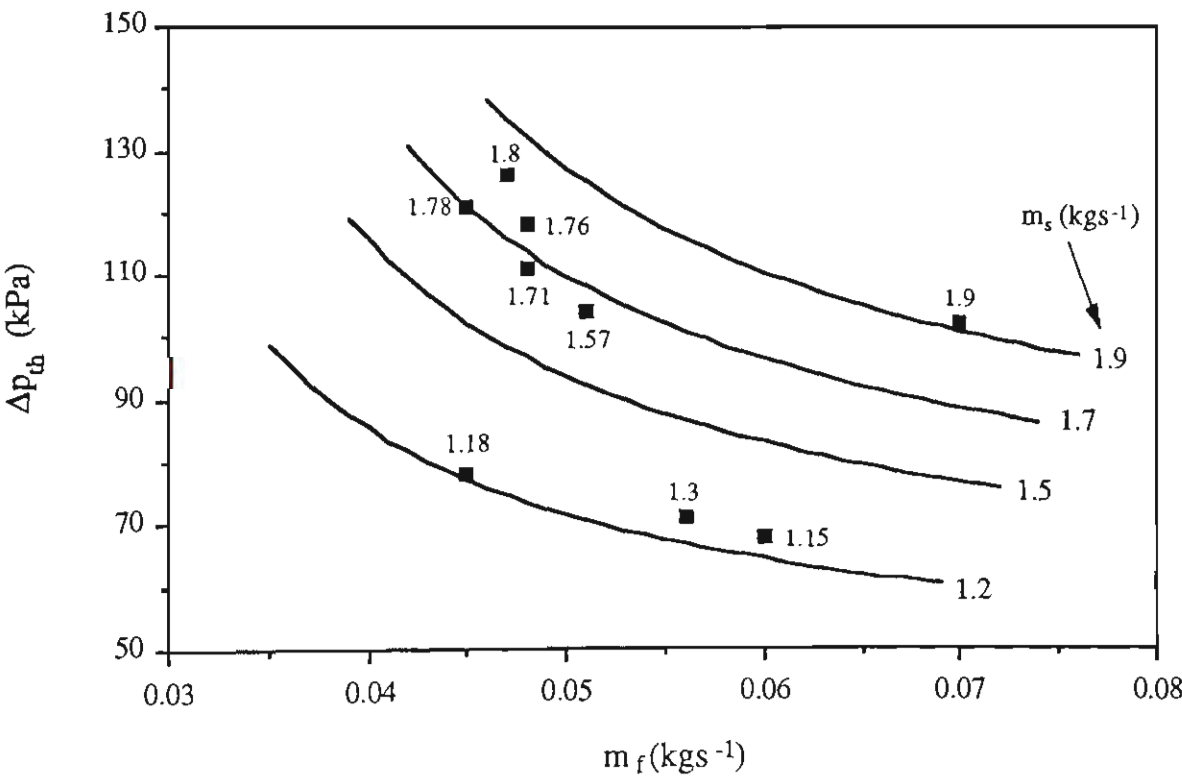


Figure 9.4 Predicted PCC of the horizontal pipeline of Rig 1 for conveying polystyrene chips, $L_{th} = 78$ m, $D = 105$ mm.

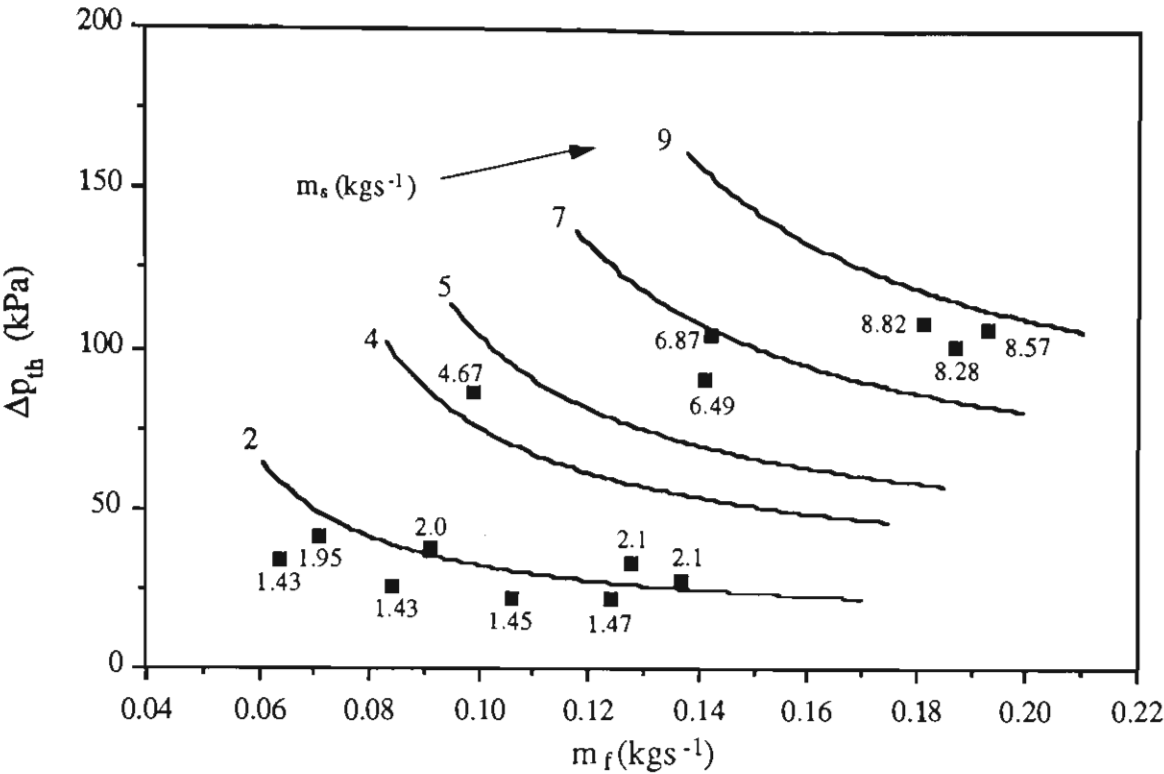


Figure 9.5 Predicted PCC of the horizontal pipeline of Rigs 2 and 3 for conveying polystyrene chips, $L_{th} = 40$ m, $D = 156$ mm.

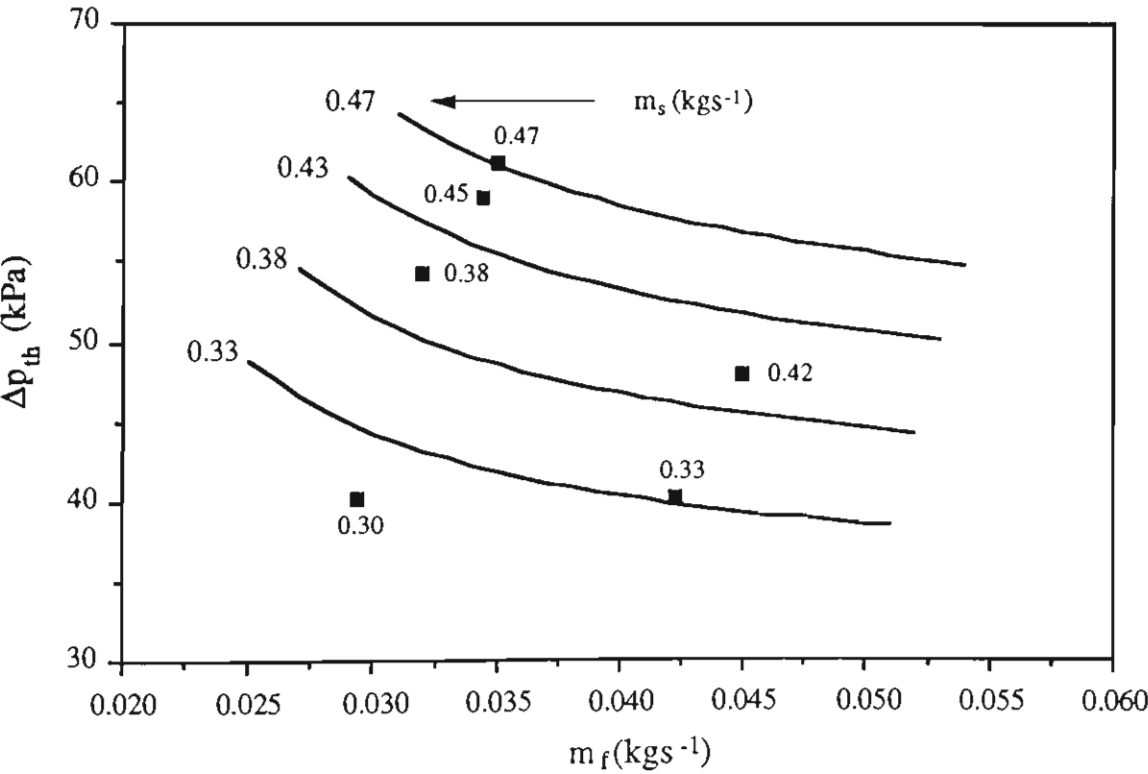


Figure 9.6 Predicted PCC of the horizontal pipeline of Rig 4 for conveying black plastic pellets, $L_{th} = 116$ m, $D = 80.5$ mm.

In order to display more clearly the accuracy of all the predictions, the predicted pressures are plotted against the experimental values, as shown in Figures 9.7, 9.8 and 9.9.

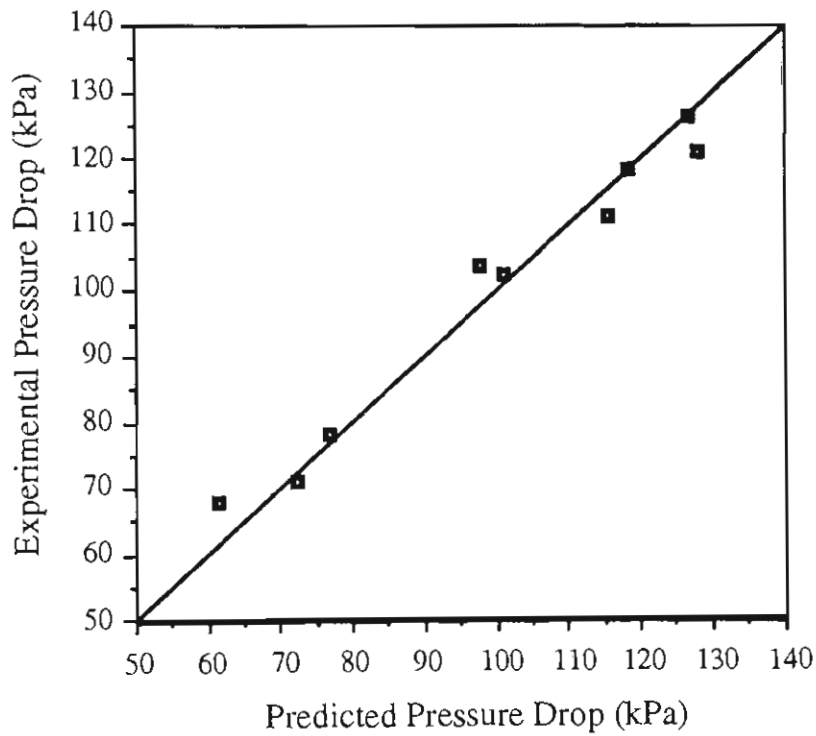


Figure 9.7 Predicted pressure drop compared with experimental pressure drop obtained on Rig 1 for polystyrene chips.

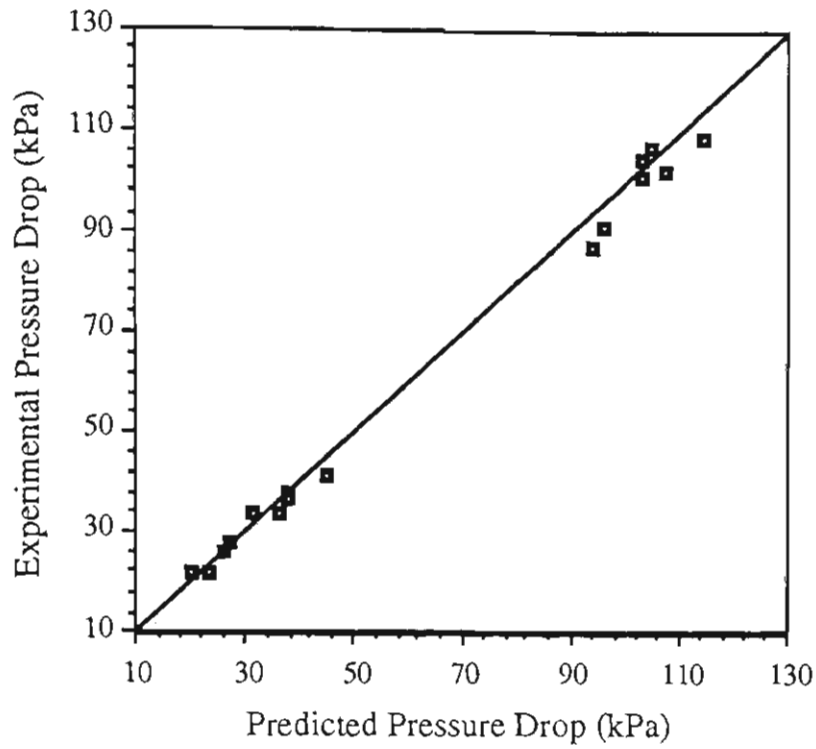


Figure 9.8 Predicted pressure drop compared with experimental pressure drop obtained on Rigs 2 and 3 for polystyrene chips.

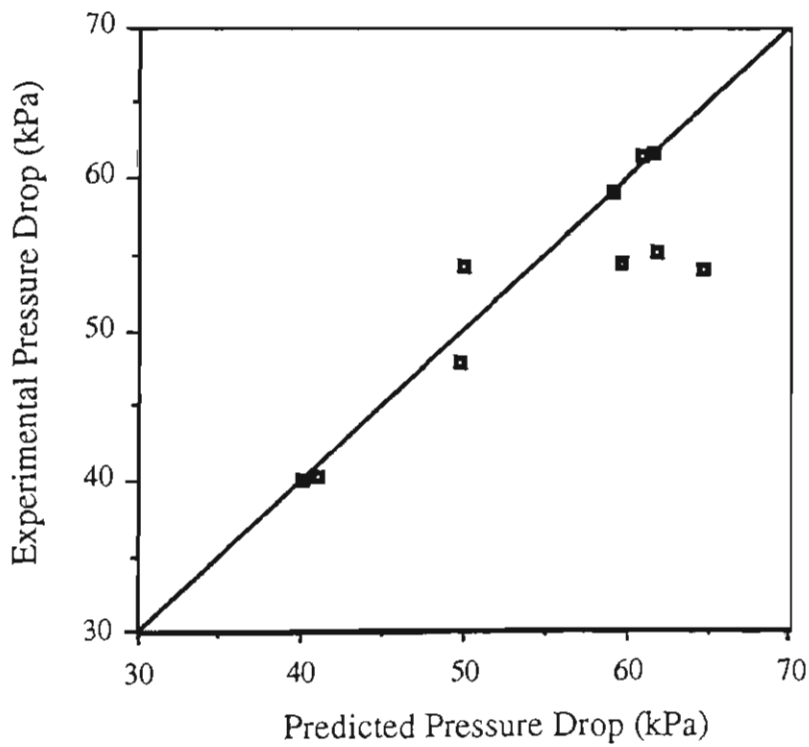


Figure 9.9 Predicted pressure drop compared with experimental pressure drop obtained on Rig 4 for black plastic pellets.

Considering the wide range of pipe sizes and conveying conditions, the above agreements are considered to be quite good. Note that three points in Figure 9.9 (i.e. corresponding to the experiment No. 16, 23 and 30 in Table 9.2) are further from the 45° line. That is, these predicted values of pressure drop are significantly larger than the experimental values. The reason is that the conveying under these conveying conditions is probably in transition area (i.e. not in complete dense phase slug-flow mode) since the high mass flow rates of air, refer to Table 9.2, were obtained in these experiments, resulting in large decrease of pressure drop. In the above work, all the predictions are carried out for a specific section of the pipeline. They only show that the model is correct when predicting pressure drops for a specific section of pipeline under various conveying conditions. The following section considers the situation when the model predicts the pressures at various points along a pipeline (i.e. a pressure profile).

9.3 Prediction of Pipeline Pressure Distribution

Pipeline pressure distribution is an important feature of pneumatic conveying systems. Another application of the model is the prediction of the pressure distribution for a given material and conveying condition. From Equation (8.17), it can be seen that it is not difficult to calculate the pressure distribution (i.e. the pressure of each point along pipeline) as long as the total horizontal pipeline length (L_{th}) in Equation (8.17) is replaced with different values. Figures 9.10 to 9.13 show the predicted and experimental pressure distributions under various conditions. The curves shown in the figures are drawn according to the calculated results.

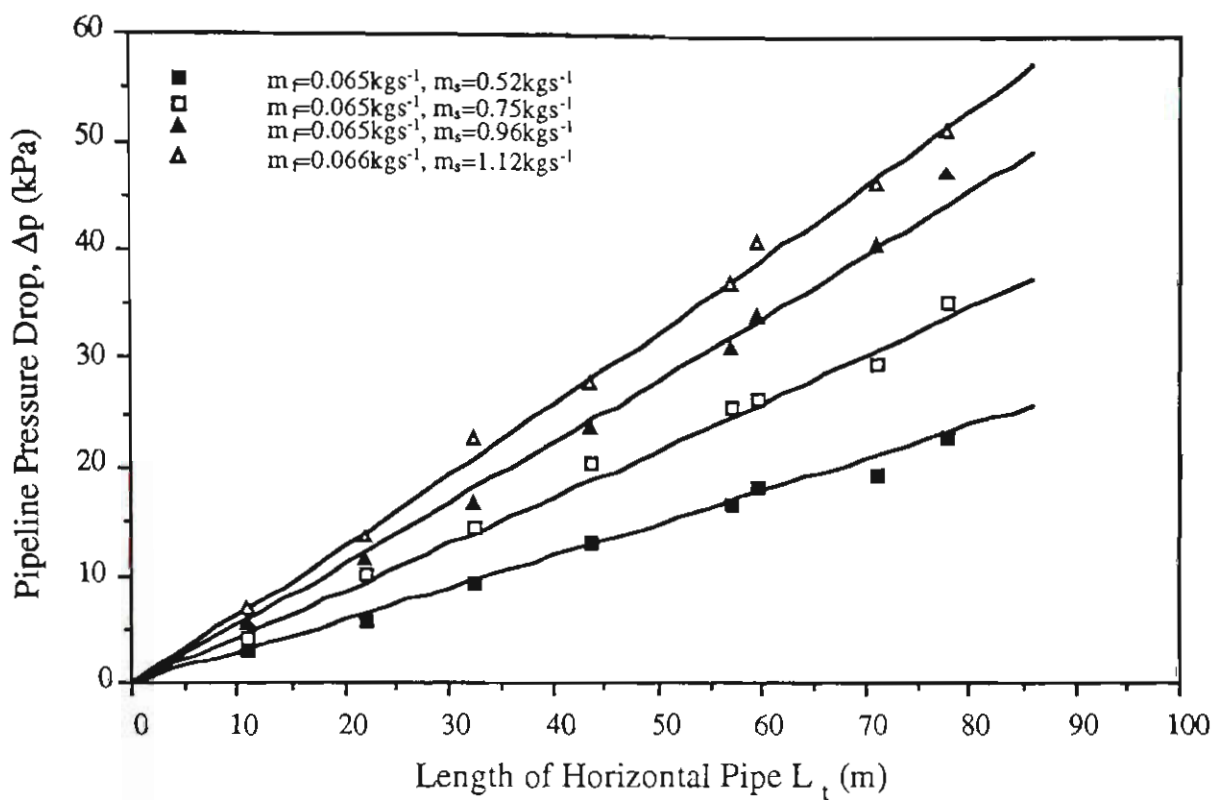


Figure 9.10 Pipeline pressure distribution for white plastic pellets and $D = 105$ mm.

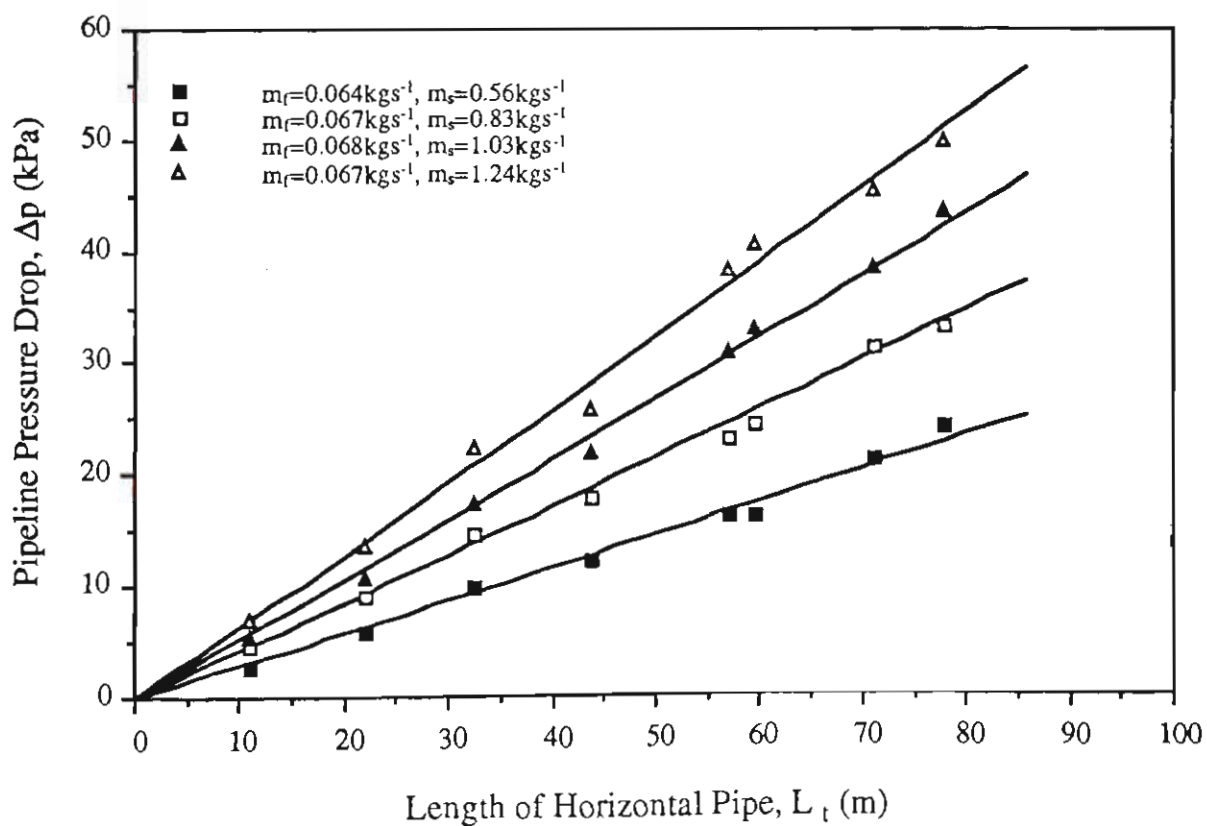


Figure 9.11 Pipeline pressure distribution for black plastic pellets and $D = 105$ mm.

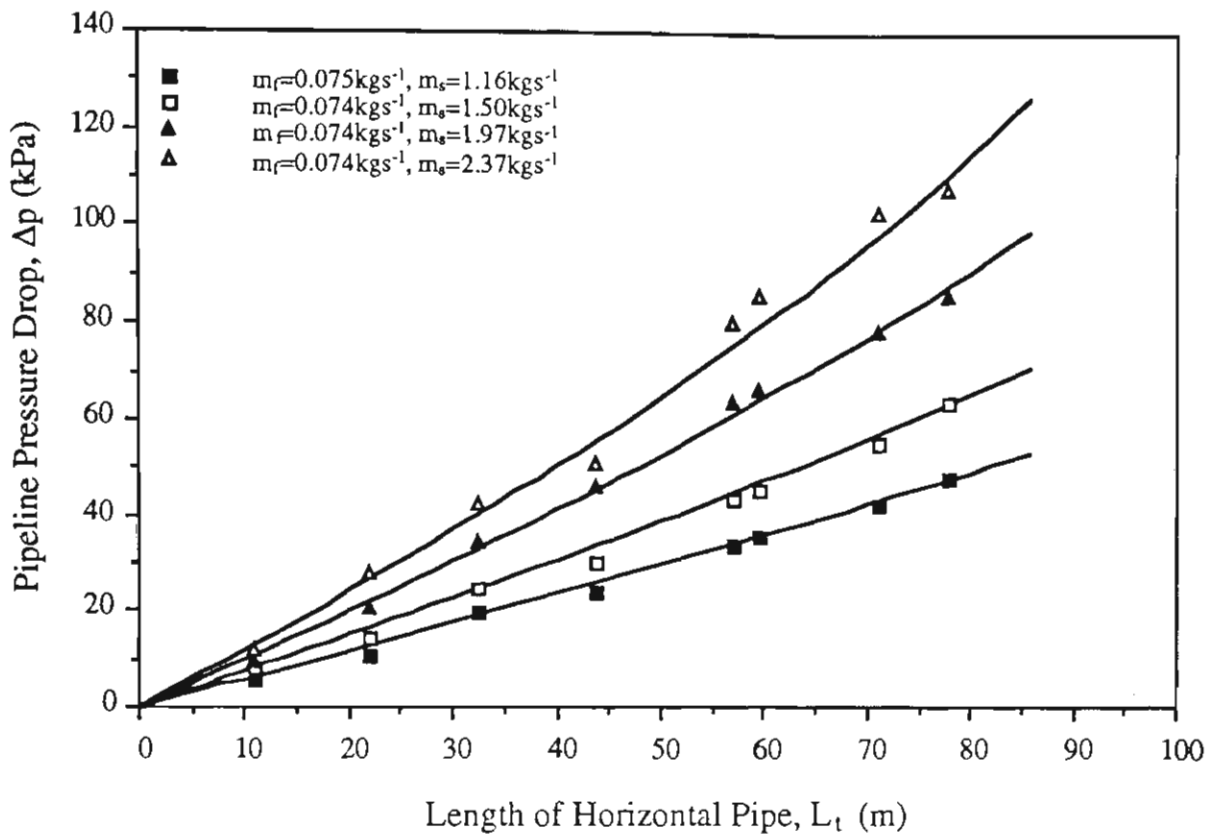


Figure 9.12 Pipeline pressure distribution for wheat and $D = 105$ mm.

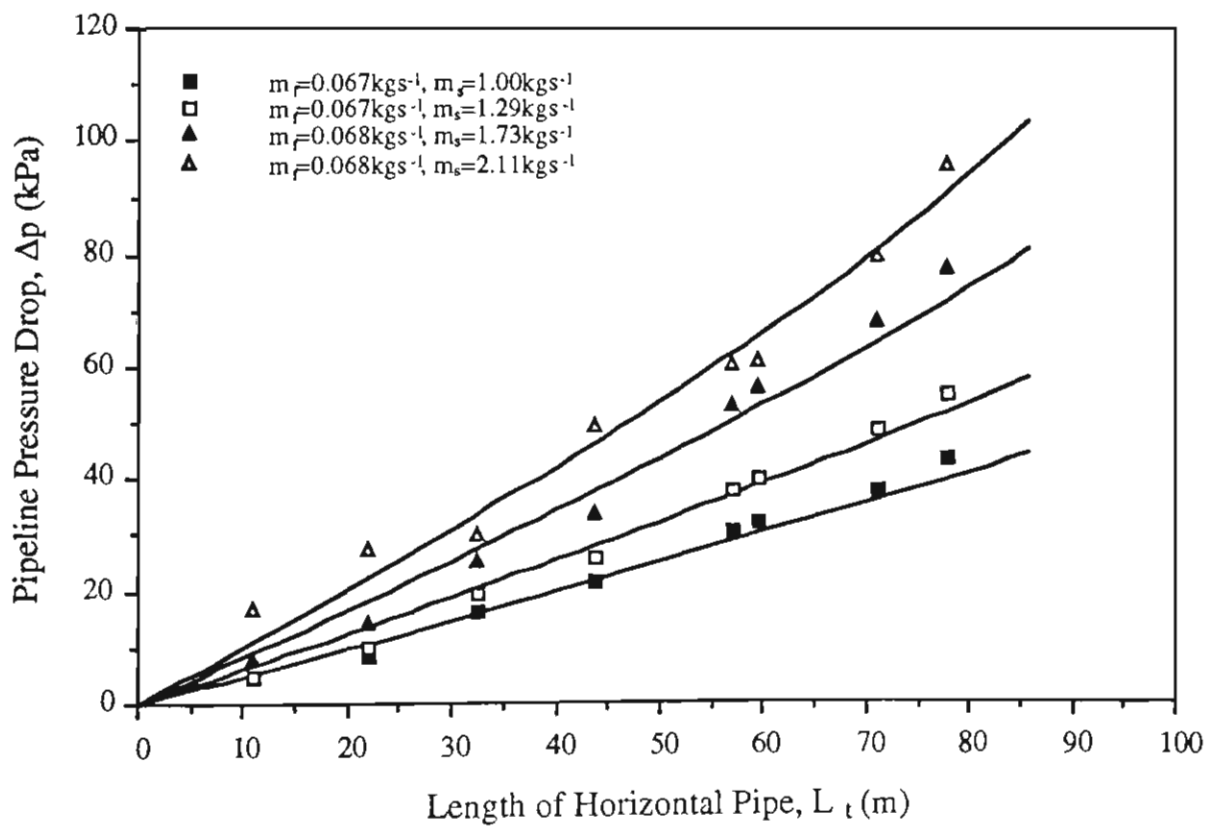


Figure 9.13 Pipeline pressure distribution for barley and $D = 105$ mm.

The calculated results obviously agree well with the experimental data. This demonstrates that the model is very successful in predicting the pressure drops and the pipeline pressures of various points along the pipelines.

It should be noted that a constant pressure gradient was assumed while developing the model, and the experiments basically agree with this assumption. However, the predicted pressure distributions are curves instead of straight lines, particularly at the high pressure section of the pipeline. The reason is explained as follows.

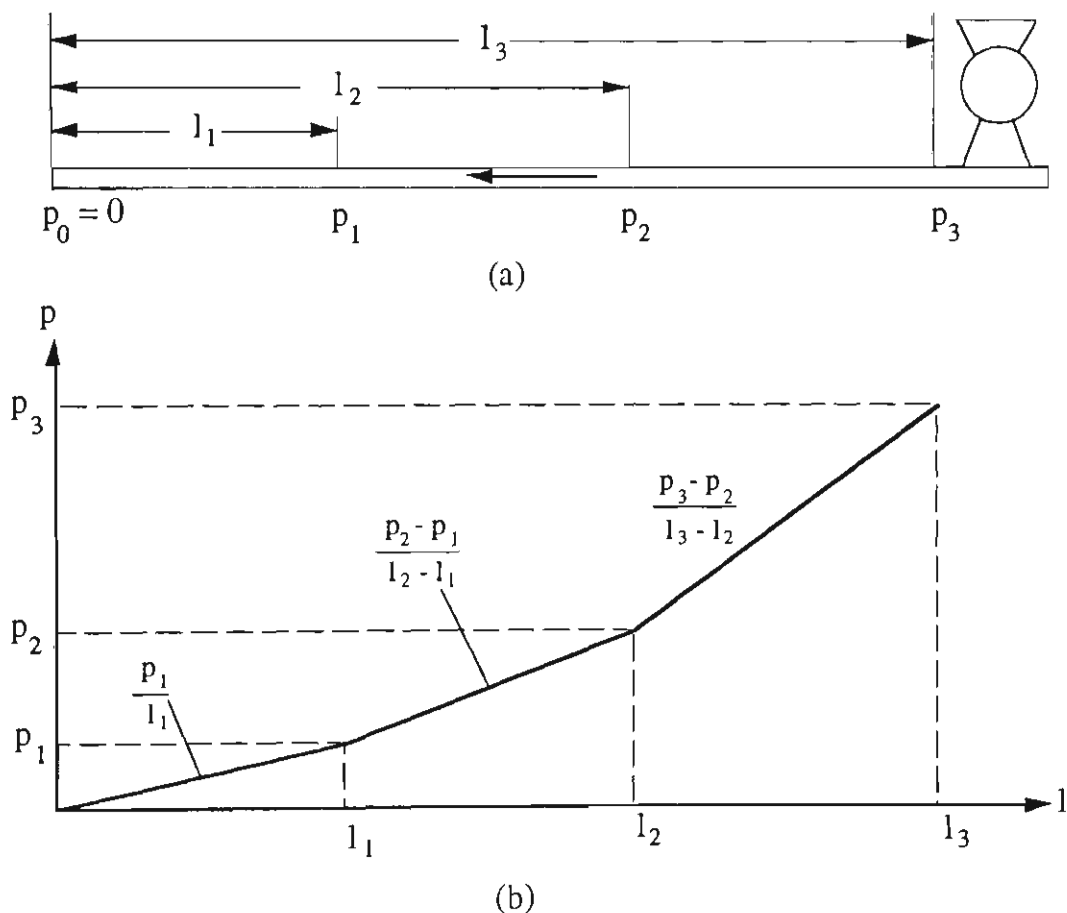


Figure 9.14 Variation of pressure gradient.

As shown in Figure 9.14(a), a pressure distribution is calculated by dividing a pipeline into many short pipes. To calculate the pressure p_1 , Equation (8.17) is applied to the pipe section with length l_1 , which has constant pressure gradient p_1/l_1 . Similarly, to calculate the pressure p_2 , Equation (8.17) is applied to the pipe section with length $(l_2 - l_1)$, which has constant pressure gradient $(p_2 - p_1)/(l_2 - l_1)$. During the calculation of p_1 and p_2 , mean

pressures and slug velocities (i.e. the values at the middle of l_1 and l_2-l_1) are applied to determine relevant variables such as slug length, slug stress, etc. in Equation (8.17). Therefore, p_1/l_1 will not be equal to $(p_2-p_1)/(l_2-l_1)$, resulting in a varying pressure gradient along the pipeline. By taking numerous intervals along the section of pipeline, this non-linear variation of pressure can be represented well by this technique, as show in Figures 9.10 to 9.13.

9.4 Determination of Economical Operating Point

Low-velocity slug-flow pneumatic conveying characteristic curves, e.g. Figures 8.30 to 8.37 and Figures 9.4 to 9.6, show that for a given m_s , Δp_t decreases with increasing m_f . Also, it can be seen that the pressure gradient increases quite sharply at low values of m_f . Theoretically, it is possible to operate at any point along the m_s curve. However, from an energy point of view, this may not be feasible. Since power consumption is a major concern in the application of pneumatic conveying systems, it is desirable to operate the slug-flow system at minimal energy. The following equation can be used to calculate the nominal power of the conveying system.

$$P_n = \Delta p_t \cdot A \cdot U_a \quad (9.1)$$

where Δp_t is the total pipeline pressure drop, A is the cross sectional area of pipe, U_a is the mean superficial air velocity.

As the U_a is not the actual air velocity at the point corresponding to Δp_t , the calculation value of Equation (9.1) is called the "nominal power" of the conveying system instead of the actual power. However, it will not affect the final result of the optimal calculation as the "nominal power" is directly proportional to the actual power.

Replacing Δp_t with Equation (8.16), then

$$P_n = (1 + 1.084\lambda Fr^{0.5} + 0.542 Fr^{-0.5}) \frac{2g\mu_w m_s L_t}{U_s} U_a \quad (9.2)$$

To minimise power consumption, Equation (9.2) is differentiated with respect to U_a and let equal to zero. That is,

$$K^2U_a^3-3K^2U_{amin}U_a^2+(3K^2U_{amin}^2-\frac{\sqrt{gD}}{1.084\lambda}KU_{amin}-\frac{gD}{2\lambda})U_a$$
$$-(K^2U_{amin}^3-\frac{\sqrt{gD}}{1.084\lambda}KU_{amin}^2+\frac{gD}{2\lambda}U_{amin})=0$$

(9.3)

where K is the slope in Equation (6.25). Three roots of solution can be obtained from Equation (9.3). Actual calculations have found that two roots are complex and obviously unrepresentative of a real system. The real root is the mean superficial air velocity which minimises energy consumption. From Equation (9.3), it can be seen that this "economical" superficial air velocity is representative of a given conveyed material and pipe diameter, it has nothing to do with the mass flow-rate of solids and pipeline length. Table 9.4 lists "economical" superficial air velocities for the test products flowing in a 105 mm ID mild steel horizontal pipe.

Table 9.4: Economical superficial air velocity.

Material	White plastic pellets	Black plastic pellets	Wheat	Barley
U_a (ms ⁻¹)	2.762	3.071	4.738	5.102

However, the corresponding "economical" value of m_f still is dependent on the mass flow rate of solids and pipe length (i.e. due to the air flow being compressible). After obtaining "economical" superficial air velocities, economical mass flow-rates of air can be easily calculated by using computer iteration for different mass flow rate of solids and pipe lengths. Figures 9.15 to 9.18 show economical operating curves shown on PCC graphs for various materials. From these figures, it can be found that materials with higher particle density (e.g. wheat) and smaller internal friction angle (e.g. barley) appear to need a larger mass flow-rate of air for economical conveying.

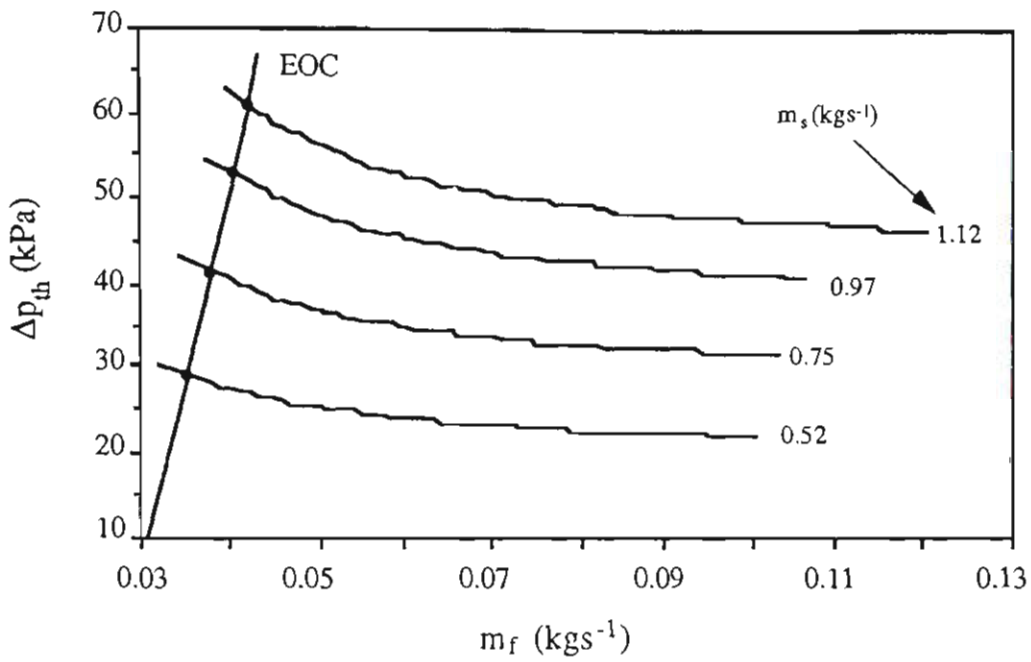


Figure 9.15 Economical operating curve of white plastic pellets shown on PCC graph for 36 m horizontal pipeline.

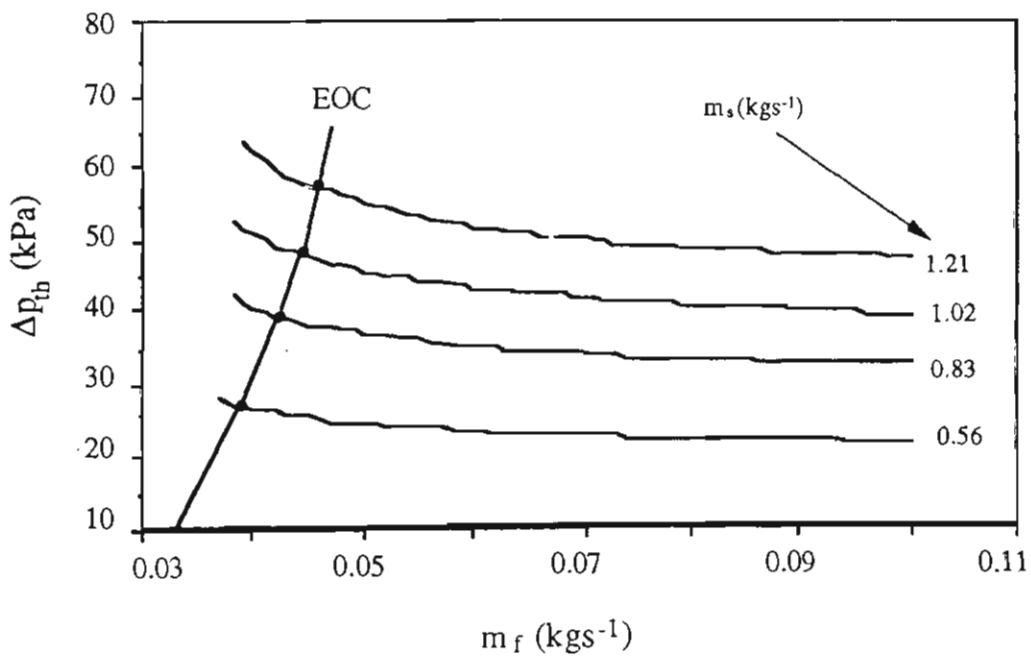


Figure 9.16 Economical operating curve of black plastic pellets shown on PCC graph for 36 m horizontal pipeline.

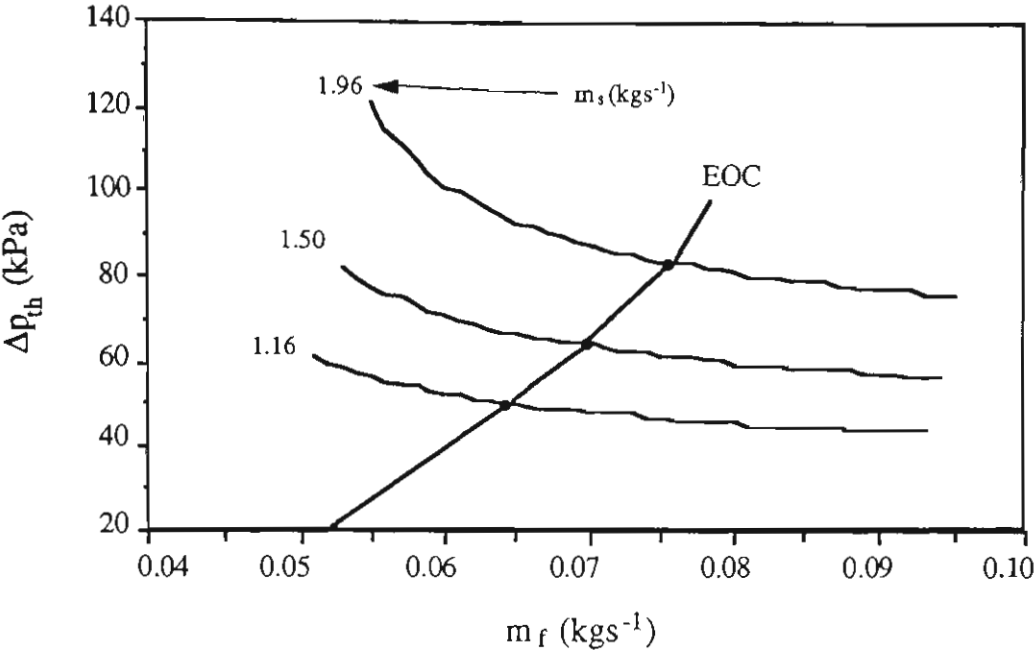


Figure 9.17 Economical operating curve of wheat shown on PCC graph for 78 m horizontal pipeline.

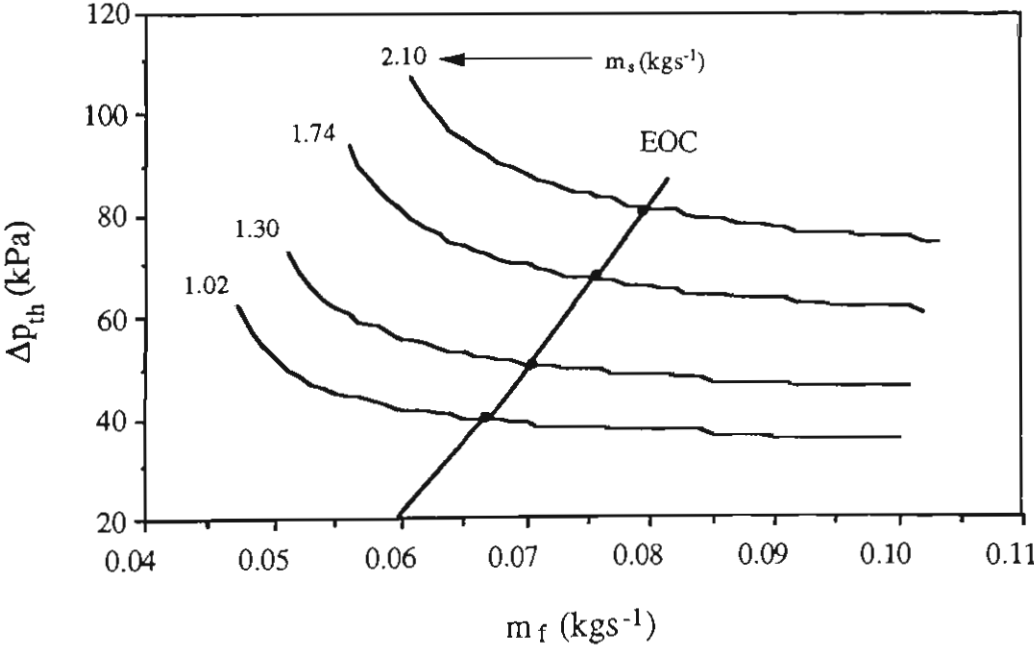


Figure 9.18 Economical operating curve of barley shown on PCC graph for 36 m horizontal pipeline.

A general procedure for the reliable design of low-velocity pneumatic conveying systems with economical power consumption is summarised below:

- (i) Measure the physical properties of the bulk material to be conveyed pneumatically, refer to Chapter 5.
- (ii) Determine the pipeline configuration, including the pipeline diameter, pipeline length, size, type and locations of bends, according to the provided conditions.
- (iii) Calculate the economical superficial air velocity by using Equation (9.3) for low-velocity pneumatic conveying.
- (iv) Determine the economical mass flow-rate of air for a given mass flow-rate of solids and the pipeline length by using computer iteration.
- (v) Use the pressure prediction procedure recommended in Chapter 8 to predict the total pipeline pressure drop according to the measured particle properties, the pipeline configuration and the calculated economical conveying conditions.
- (vi) Choose a suitable compressor for the system according to the predicted total pipeline pressure drop and required intake volume.

9.5 Application of Model to Fine Powders

The previously presented pressure prediction model was based on low-velocity experimental data obtained on various coarse granular materials. Hence, this model should be used only for the coarse granular materials at this stage. It would be premature to apply the model directly to fine powders, as these materials may have very different effects on some aspects of the performance of low-velocity pneumatic conveying. However, low-velocity pneumatic conveying of bulk materials, regardless of fine powders or coarse granules, always has a similar flow pattern and mechanism. Hence it should be possible to apply the model to fine powders (although some modifications to

some fundamental aspects such as slug velocity may be needed). To investigate these issue, some low-velocity pneumatic conveying experiments are carried out on a fine powder.

9.5.1 Test Material and Properties

Semolina is considered as a fine powder. According to the measurement methods introduced in Chapter 5, the physical properties of semolina are measured and listed below:

Median particle diameter, d	390	μm
Particle density, ρ_s	1459	kgm^{-3}
Bulk density (loose), ρ_b	736	kgm^{-3}
Bulk voidage, ϵ	0.496	
Internal friction angle, ϕ	30.8	$^\circ$
Wall friction angle (with respect to mild steel), ϕ_w	27.5	$^\circ$

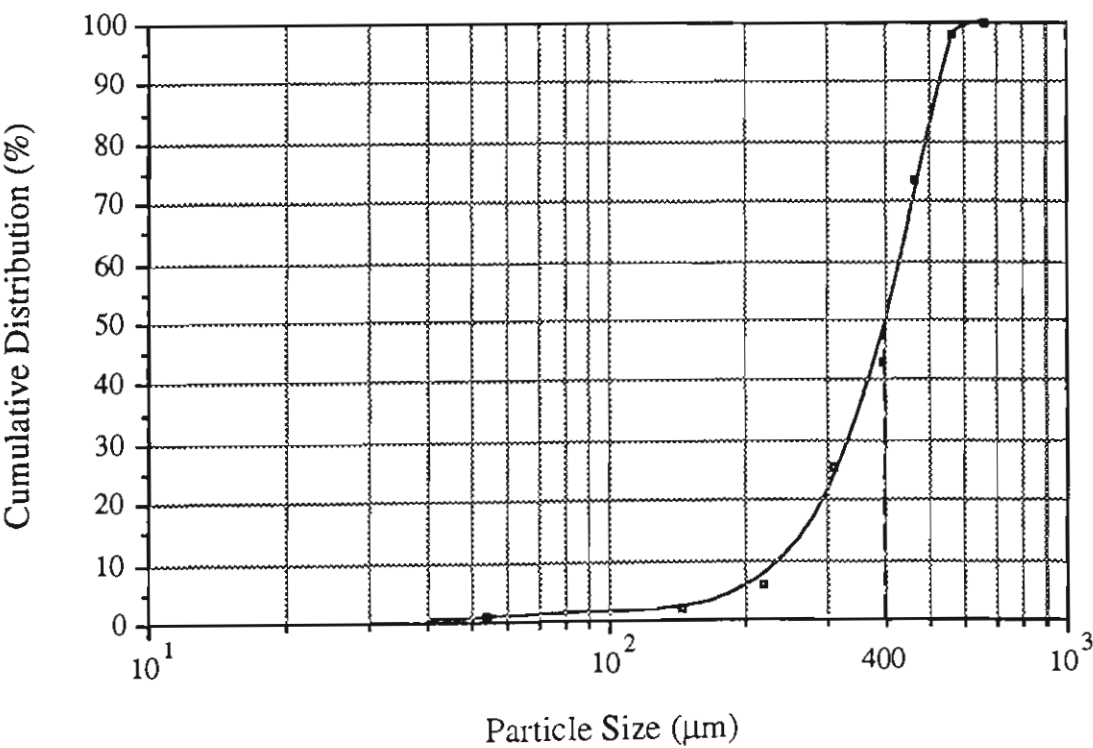


Figure 9.19 Particle size distribution of semolina.

Note that for fine powders, the particle size used here is the median particle diameter which is defined as the particle size which represents 50 % of the sample by mass. Mechanical sieving is employed to determine the size distribution. The measurement of the particle size is repeated two times to obtain an average value. One of the results is shown in Figure 9.19.

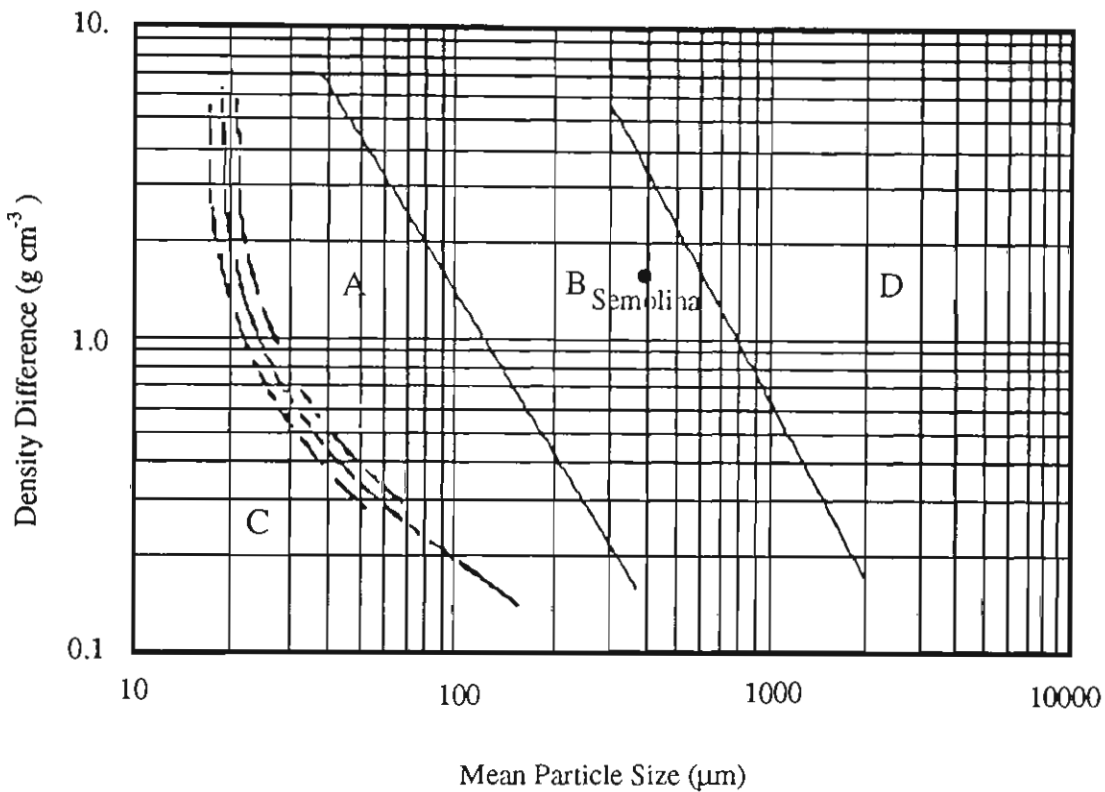


Figure 9.20 Semolina shown in Dixon's slugging diagram.

According to the measured properties of semolina, it belongs to Dixon [28] Group B, but is close to Group D, as shown in Figure 9.20. Hence it may be possible to convey semolina under low-velocity slug-flow conditions (to be confirmed by experiment).

9.5.2 Test Results

During the conveying tests, the semolina was found to be a good candidate for low-velocity pneumatic conveying. That is, while conveying semolina with an appropriate mass flow-rate of air, regular slugs formed naturally and reliably without the aid of any slug forming device. Compared with the conveying of the Group D granular materials

(e.g. plastic pellets, wheat, etc.), the semolina did appear more sensitive with regard to pipeline blockage. That is, there existed a minimum mass flow-rate of air for a given mass flow-rate of solids, at which pipeline blockage was easy to obtain.

From the experimental data, the low-velocity pneumatic conveying characteristics over 52 m are presented in Figure 9.21.

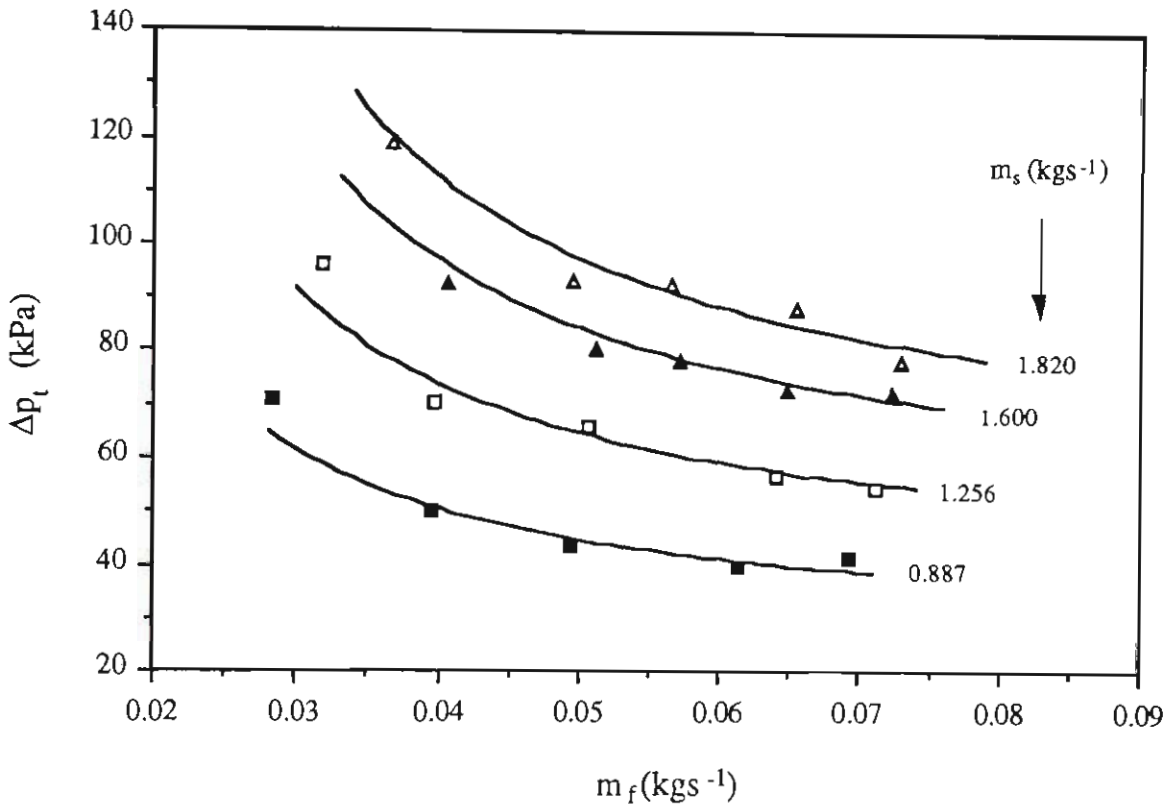


Figure 9.21 Low-velocity pneumatic conveying characteristics of 105 mm ID, 52 m mild steel pipeline for semolina.

Velocities also are measured for the semolina. As previous investigations (see Chapter 6) into low-velocity pneumatic conveying indicated that the mass flow-rate of solids only had little influence on particle velocity, the velocities of the semolina are measured only with different mass flow-rates of air. Note that the velocities determined by using the cross correlation function analysis technique relate to particle slugs rather than to individual particles. Figure 9.22 shows the plot of the slug velocity versus superficial air velocity.

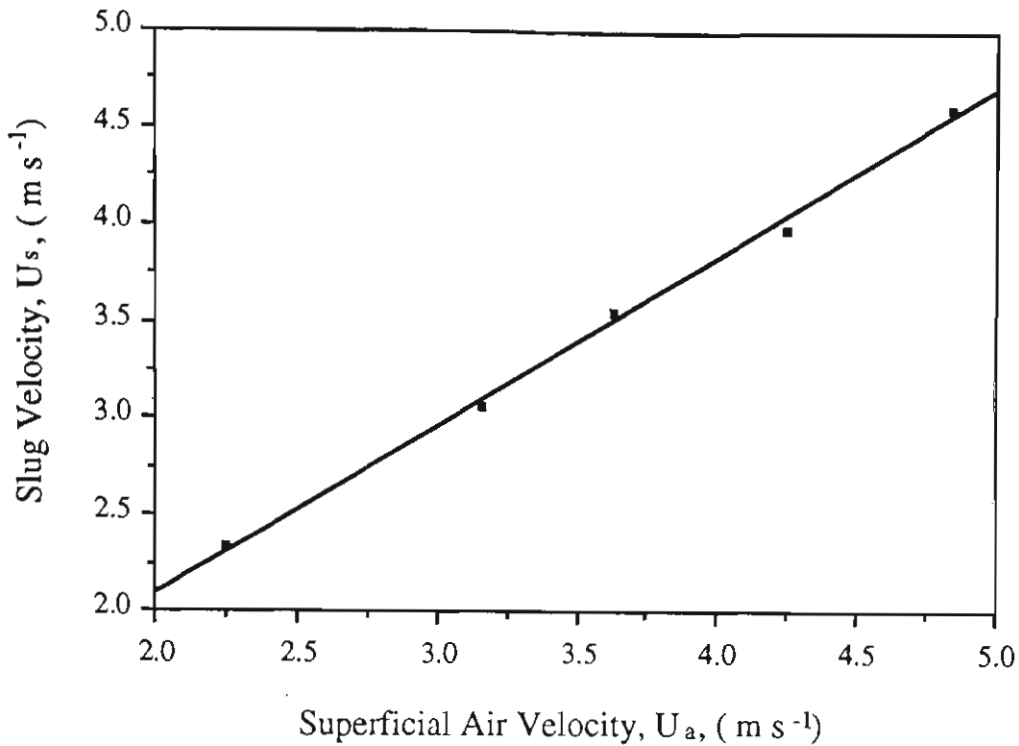


Figure 9.22 Plot of slug velocity versus superficial air velocity for semolina.

This figure shows clearly that in the range of experimental values of superficial air velocity, the slug velocity varies linearly with the superficial air velocity. Also it can be observed that their values are almost equal to each other.

9.5.3 Modification of Model and Predicted Results

At first, an attempt was made to apply the model directly to the fine powder semolina and the result was unsatisfactory. Through analysis, it was found that the model given by Equation (6.32), which is an empirical correlation of slug velocity with superficial air velocity based on coarse granular materials, is not suitable for fine powders. For example, inserting the value of the particle diameter of semolina into Equation (6.32), it can be found that the predicted slug velocity approaches zero. This does not agree with the actual observations during the experiments for conveying semolina. In fact, the slug velocity of semolina was measured to have a value almost equal to the superficial air velocity.

Chapter 6 presented the linear correlation of slug velocity given by Nicklin et al [84] based on an air-water system, refer to Equation (6.1). The slope of the correlation generally is about 1.0 when the slugs have reached a stable size.

As the behaviour of fine powder slug-flow would be more analogous to the behaviour of a gas-liquid system, the slope of Equation (6.32), which represents the variation rate of the slug velocity with respect to superficial air velocity, in fine powder slug-flow may be similar to that in air-water system. Also note that the slug velocity of semolina is approximately equal to the superficial air velocity, it is recommended that the slope in Equation (6.32) be replaced by the constant 1.0 for fine powders. However, two systems should have different expressions for initial air velocity (intercept). After this modification, the predicted results achieve a dramatic agreement with the experimental data, as shown in Figure 9.23. This indicates that most significant effect on the low-velocity performance of fine powders is the slug velocity.

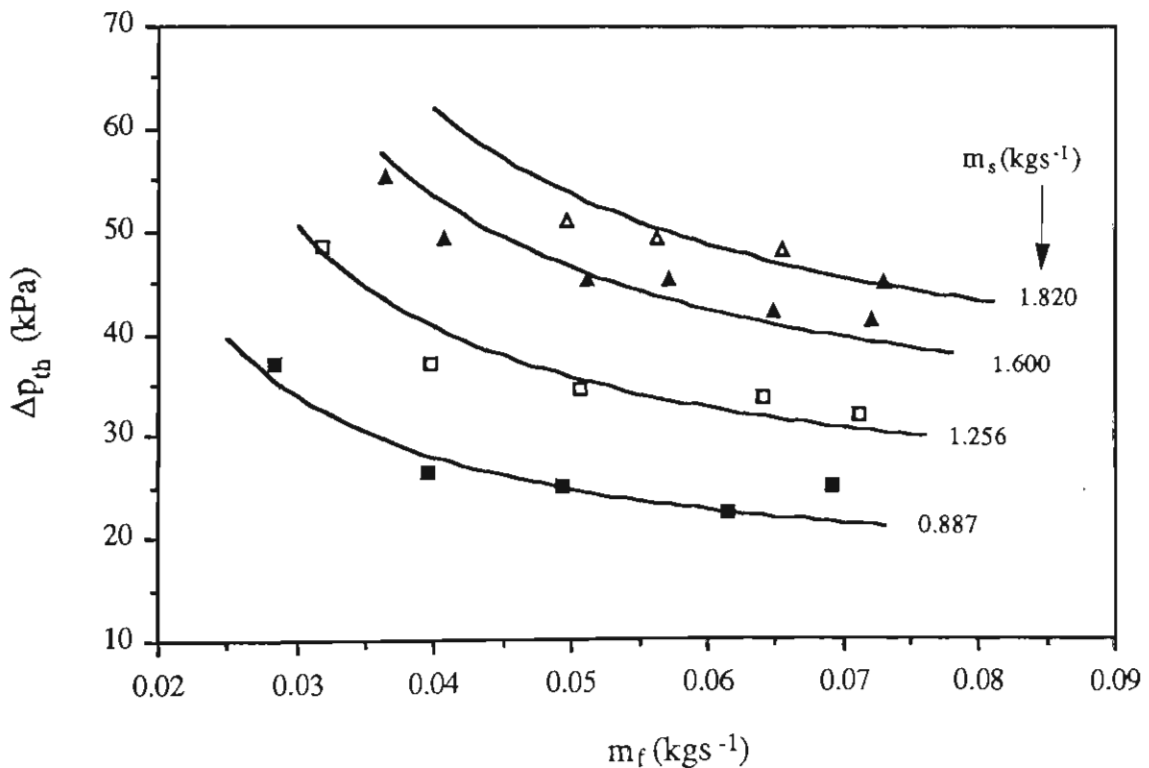


Figure 9.23 Predicted pneumatic conveying characteristics of semolina and 36 m horizontal pipeline by using modified model.

CHAPTER 10

CONCLUSIONS AND SUGGESTIONS FOR FURTHER WORK

10.1 Conclusions

This thesis was aimed at developing a model for predicting the total horizontal pipeline pressure drop for low-velocity pneumatic conveying. For this purpose, a theoretical analysis was carried out for the pressure gradient and stress state in a single slug, then numerous experiments were undertaken to investigate the slug velocity, wall pressure, stress transmission coefficient, etc. to establish empirical or semi-empirical correlations for these parameters. The relationship between the pressure drop across a single slug and the total pipeline pressure drop also was established. The following conclusions are based on the investigations and findings of thesis.

1 Flow pattern

- During low-velocity horizontal pneumatic conveying, particles are conveyed in the form of discrete slugs. Between each pair of slugs, the pipe usually is filled with an air gap and a stationary bed of particles. Each slug sweeps up the particles from the stationary bed in front of it and delivers about same the quantity of particles to the pipe behind it while travelling forward along the pipeline.
- Low-velocity pneumatic conveying is analogous to an aggregative fluidised bed model. Two particle phases exist in low-velocity pneumatic conveying. One is particle dense phase i.e. particle slugs, and the other is particle dilute-phase i.e. air gaps. These constitute the discontinuous flow pattern of low-velocity pneumatic conveying.
- The particle slugs are a special case of dense phase i.e. incipient fluidisation, in which the air flow-rate is at least equal to that required just to fluidise the material. The air gaps are formed by the excess air for fluidising the material. Therefore, for the low-velocity pneumatic conveying system of a given mass flow-rate of solids, increasing the mass flow-rate of air does not change the pressure gradient through the slugs in

theory and only increases the length of air gaps or forms a new air gap. The air gaps are axisymmetric for vertical slug-flow and asymmetric for horizontal slug-flow due to the presence of stationary bed.

- From the definition of incipient fluidisation it is known that the particle slugs have a conventional fixed-bed configuration (i.e. the particles in the slugs are fixed relative to each other) and a bulk density similar to the loose-poured condition.
- For a given mass flow-rate of solids, increasing the mass flow-rate of air increases the length of air gap, whereas for a given mass flow-rate of air, increasing the mass flow-rate of solids decreases the length of air gap.
- The experimental results on the cross sectional area ratio of stationary bed to pipe agree well with the predictions of Konrad et al. [69].

2 Stress in Slug

- Inter-particle normal stress in a moving slug varies as an exponential function along its length and is confined by the stress on the front and back surface of the slug, see Equation (3.18).
- The stress on the front and back surface of a slug is a function of the slug velocity and stationary bed thickness, see Equations (3.27) and (3.28). The stress on the front surface is nearly equal to the stress on the back surface of the slug since the average stationary bed thickness is approximately the same both in front of and behind the slug.
- The average axial normal stress in a slug is approximately equal to its frontal stress. Thus the stress transmission coefficient of a slug can be approximated by the ratio of the average radial stress to the frontal stress.

- The normal stress in a horizontal moving slug is in active state so that the value of stress transmission coefficient is determined by Equations (7.8), (7.9) and (7.21).

3 Slug Velocity

- Slug velocity appears to be independent of mass flow rate of solids, but varies linearly with superficial air velocity. A minimum air velocity exists for each material to initiate the motion of particle slug.
- The linear model of slug velocity for coarse granular materials can be expressed by Equation (6.32). For fine powders, the slope of the linear model of Equation (6.32) appears to be 1.0.
- Carman's equation [18] for fluid flowing through a fixed granular fixed bed and the suggestions of Ergun [31, 32] are combined to produce Equation (6.41) which provides a good estimate of the minimum air velocity.

4 Total Horizontal Pipeline Pressure Drop

- Pipeline pressure exhibits approximately a linear distribution along the length of pipe, particularly at low mass flow-rate of solids.
- Total pipeline pressure drop decreases as mass flow-rate of air increases for dense-phase conveying. This trend is opposite to that in dilute-phase conveying.
- The presence of bends increases the pipeline pressure drop, but the effect is not significant for low-velocity pneumatic conveying.
- For low-velocity pneumatic conveying, the minimum pressure drop point is not the minimum power consumption point. "Economical" superficial air velocity is representative of a given conveyed material and pipe diameter and has nothing to do with the mass flow-rate of solids and pipeline length.

10.2 Suggestions for Further Work

1 Pressure Drop in Vertical Pipe

The work completed in this thesis is concerned with developing a pressure prediction model for horizontal low-velocity pneumatic conveying since horizontal pipes are used extensively in all test rigs. However, the experiments in this thesis show that the pressure gradient in vertical slug-flow is much greater than that in horizontal slug-flow, so that the pressure drop in the vertical pipe often cannot be ignored. For example, the pressure drop over the 52 m long pipeline which contains a 6.5 m vertical lift was nearly twice as large as the pressure drop over the 36 m long horizontal section of the pipeline when conveying black plastic pellets, see Figures 8.20 and 8.32. Hence, investigations into slug-flow in vertical pipe are necessary so that a reliable prediction model is established for the vertical pipeline pressure drop.

2 Fine and Mixed Size Material

The work in this thesis concentrates on the investigation into low-velocity pneumatic conveying of coarse monosized granular materials. Fine and mixed size materials will exhibit different behaviour and performance in some aspects during pneumatic conveying. Although the model developed based on coarse granular material has been modified to suit the application for fine powders, only one type of fine powder semolina was tested. Experiments of conveying more fine powders in low-velocity are necessary. It also is necessary to clarify and define the concept of "fine powder" and "coarse granule" to establish the appropriate slope in Equation (6.32). The effect of mixed size materials on the pressure prediction model and the suitability of using a representing particle diameter also requires further investigation.

3 Boundaries of Low-Velocity Pneumatic Conveying

Pneumatic conveying characteristics show that there are two boundaries for low-velocity pneumatic conveying. The lower boundary represents the minimum air velocity required just to initiate the motion of particle slug. The higher boundary represents the transition from stable steady slug-flow to unstable flow. The estimation of each boundary is essential for the reliable design of low-velocity pneumatic conveying systems. In addition, further studies of the lower boundary (i.e. the minimum air velocity) will be helpful for the modification of the slug velocity model given by Equation (6.32), so as to predict more accurately the pressure drop at low mass flow-rates of air, refer to Section 9.2.4.

4 Flow Pattern

For dense phase pneumatic conveying, flow patterns define the problem that has to be solved in order to predict the pressure drop and the conveyability of the product. More contributions are necessary to describe numerically the flow pattern of low-velocity pneumatic conveying, e.g. develop models for defining the length of single slug and air gap and the shape of the air-particle interface between two slugs. Flow patterns of other types of dense phase conveying (e.g. fluidised dense phase, moving bed flow and dense phase plug-flow of cohesive products) also need to be investigated further.

CHAPTER 11

REFERENCES

1. Albright, C. W., Holden, J. H., Simons, H. H. and Schmitt, L. D., Pressure Drop in Flow of Dense Coal-Air Mixtures, *Industrial and Engineering Chemistry*, Vol. 43, No. 8, Aug. 1951, pp 1837 -1840.
2. Anthony, S., The Determination of Solids Velocity by Cross- Correlation of Pressure Signals in a Pneumatic Conveying Pipeline, BE Thesis, Dept. of Mechanical Engineering, University of Wollongong, 1991.
3. Arnold, P. C. and Wypych, P. W., The Development of Pneumatic Conveying in Australia, *Bulk Solids Handling*, Vol. 11, No. 1, 1991, pp 85 - 91.
4. Arnold, P. C., Reed, A. R. and Wypych, P. W., Advances in the Design of Pneumatic Transport Systems, *International Symposium on Reliable Flow of Particulate Solids II*, Aug. 23 - 25, 1993, Oslo, Norway, pp 453 - 475.
5. Aziz, Z. B. and Klinzing, G. E., Dense Phase Transfer: Plug Flow Around Bends, *Pneumatech 4*, Fourth International Conference on Pneumatic Conveying Technology, Mar. 1987, pp 1 - 18.
6. Barker, C. G. J. and Geldart, D., An Investigation into the Slugging Characteristics of Large Particles, *Powder Technology*, Vol. 19, 1978, pp 177 - 187.
7. Blair-fish, P. M. and Bransby, P. L., Flow Patterns and Wall Stresses in a Mass-Flow Bunker, *Journal of Engineering for Industry*, Transaction of ASME, Series B, Vol. 95, No. 1, 1973, pp 17 - 26.
8. Borcz, A. and Rahim, H. A., A New Method to Measure Pressure and Temperature in Silos, *Powder Handling and Processing*, Vol. 1, No. 4, 1989, pp 349 - 352.

9. Borcz, A. and Rahim, H. A., Pressure Measurements on Cement Silos, Powder Handling and Processing, Vol. 2, No. 3, 1990, pp 239 - 246.
10. Borzone, L. A. and Klinzing, G. E., Dense-Phase Transport : Vertical Plug Flow, Powder Technology, 53, 1987, pp 273 - 283.
11. Bradley, M. S. A. and Mills, D., Approaches to Dealing with the Problems of Energy Loss Due to Bends, 13th Annual Powder and Bulk Solids Conference, May 9 - 12, 1988, pp 705 - 715.
12. Bradley, M. S. A. and Reed, A. R., Advances in the Design of Pneumatic Conveying Systems, Bulk Solid Handling, Vol. 11, No. 1, Mar. 1991, pp 93 - 97.
13. Bradley, M. S. A., An Improved Method of Predicting Pressure Drop Along Pneumatic Conveying Pipelines, Third International Conference on Bulk Materials, Storage, Handling and Transportation, Jun. 1989, pp 282 - 288.
14. Briks, A. H., A Bulk Solid Classification System Based on Failure Property Mechanisms, 14th Annual Powder and Bulk Solids Conference, 1989, pp 3 - 10.
15. Brown, R. W., Dense Phase Conveying, Pneumotransport 3, Third International Conference on the Pneumatic Transport of Solids in Pipes, Apr. 7 - 9, 1976, England, A 4 - 33.
16. Butters, G., Plastic Pneumatic Conveying and Bulk Storage, Applied Science, London, 1981.
17. Chambers, A. J., Introduction to Pneumatic Conveying, ITC Bulk Materials Handling, Design and Operation of Pneumatic Conveying Systems, Short Course Notes, 3 - 5 July 1989, Dept. of Mechanical Engineering, University of Wollongong.

18. Carman, P. C., Fluid Flow Through Granular Beds, Transactions of the Institution of Chemical Engineers, Vol. 15, 1937, pp 150 - 166.
19. Chari, S. S., Pressure Drop in Horizontal Dense Phase Conveying of Air-Solid Mixtures, AIChE Symposium Series, Vol. 67, No. 116, 1971, pp 77 - 84.
20. Chen, T. Y., Walkwender, W. P. and Fan, L. T., Moving Bed Solids Flow Between Two Fluidised Beds, Powder Technology, 22, 1979, pp 89 -96.
21. Cheng, K. Q. and Chen, H. X., An Approach to Determining Moving Parameters of Pulse Plug Flow Type Pneumatic Conveying, Pneumatech 4, Fourth International Conference on Pneumatic Conveying Technology, Mar. 1987, pp 235 - 252.
22. Coulson, The Streamline Flow of Liquids Through Beds Composed of Spherical Particles, PhD thesis, University of London, 1935.
23. Daoud, K., Ginestet, A., Large, J., F. and Guigon, P., Performances of Dense Phase Plug Flow Pneumatic Conveyor and Characterisation on Flow Regime, International Symposium on Reliable Flow of Particulate Solids II, Aug. 23 - 25, 1993, Oslo, Norway, pp 677 - 684.
24. Davidson, J. F. and Harrison, D., Fluidisation, Academic Press, London and New York, 1971.
25. Dayam, J. and Levenspiel, O., The Residence-Time Distribution for Flow Models with Cross Flow between Plug-Flow Regions, AIChE Chemical Engineering Progress Symposium Series, No. 101, Vol. 66, pp 28 - 36.
26. Decamps, F., Dumont, G. and Goossens, W., Vertical Pneumatic Conveyor with a Fluidised Bed as Mixing Zone, Powder Technology, 5, 1971/1972, pp 299 - 306.

27. Dickson, A. J., Skews, B. W. and Marcus, R. D., Plug Phase Conveying, Pneumotransport 4, Fourth International Conference on the Pneumatic Transport of Solids in Pipes, Jun. 26 - 28, 1978, California, USA, D 6 - 73.
28. Dixon, G. The Impact of Powder Properties on Dense Phase Flow, Proceedings of International Conference on Pneumatic Conveying, Jan. 1979, London, UK.
29. Dixon, G., Fluidisation Theory Throws Light on Dense Phase Conveying Particle, Pneumatech 4, Fourth International Conference on Pneumatic Conveying Technology, March, 1987, pp 27 - 37.
30. Dixon, G., How do Different Powders Behave, Bulk Storage Movement Control, May/June, 1979, pp 81 - 88.
31. Ergun, S. and Orning, A. A., Fluid Flow Through Randomly Packed Columns and Fluidised Beds, Industrial and Engineering Chemistry, Vol. 41, No. 6, pp 1179 - 1184.
32. Ergun, S., Fluid Flow Through Packed Columns, Chemical Engineering Progress, Vol. 48, 1952, pp 89 - 94.
33. Esmailzadeh, E. K., Horizontal Pneumatic Transport at High Solids Loadings, Pneumotransport 3, Third International Conference on the Pneumatic Transport of Solids in Pipes, Apr. 7 - 9, 1976, England, D 3 - 33.
34. Flatt, W. and Blumer, P., Low Velocity Conveying, Pneumatech 1, First International Conference on Pneumatic Conveying Technology, May 3 - 5, 1982, Stratford-Upon-Avon, UK, pp 1 - 4.
35. Flatt, W., Latest Developments and Applications of High Density Pneumatic Conveying Systems, Pneumotransport 3, Third International Conference on the Pneumatic Transport of Solids in Pipes, Apr. 7 - 9, 1976, England, A 3 - 21.

36. Flatt, W., Low Velocity Pneumatic Conveying of Granulated and Pulverised Products, Criteria for Selecting the Optimal Pneumatic Conveying System, Pneumotransport 5, Fifth International Conference on the Pneumatic Transport of Solids in Pipes, Apr. 16 - 18, 1980, London, UK, pp 409 - 418.
37. Flatt, W., Today's Possibilities for Low Velocity Conveying of Carbon Black and Pigments with New Conveying Technology, International Conference on Pneumatic Conveying Technology, Sep. 4 - 6, 1984, Canterbury, UK, pp 1 - 18.
38. Francisco, J. and Cabrejos, I. M., Incipient Motion of Solid Particles in Pneumatic Conveying, M. Sc. Dissertation, University of Pittsburgh, 1991
39. Geldart, D., Types of Gas Fluidisation, Powder Technology, 7, 1973, pp 285 - 292.
40. Gerchow, F. J., Rotary Valve Selection for Pneumatic Conveying Systems, Bulk Solids Handling, Vol. 1, No. 1, Feb. 1981, pp 171 - 174.
41. Ginestet, A., Daoud, K., Largr, J. F., Guigon, P. and Jodlowski, C., Suitability of Bulk Products for Dense Phase Pneumatic Conveying, Pneumatech 4, Fourth International Conference on Pneumatic Conveying Technology, Mar. 1987, pp 27 - 37.
42. Gu, H. and Klinzing, G. E., Vertical Plug Flow of Cohesive Coal in 2- and 4-Inch Pipes, Powder Technology, 57, 1989, pp 59 -67.
43. Hancock, A. W. and Nedderman, R. M., Prediction of Stresses on Vertical Bunker Walls, Transactions of the Institution of Chemical Engineers, Vol. 52, No. 2, Apr. 1974, pp 170 -179.
44. Happel, J., Pressure Drop Due to Vapour Flow through Moving Beds, Industrial and Engineering Chemistry, Vol. 41, No. 6, pp 1161 - 1174.

45. Hariu, O. H. and Molstad, M. C., Pressure Drop in Vertical Tubes in Transport of Solids by Gases, *Industrial and Engineering Chemistry*, Vol. 41, No. 6, Jun. 1949, pp 1148 - 1160.
46. Hauser, G. and Sommer, K., Plug Flow Pneumatic Transport in Dilute and Dense Phase, *Bulk Solids Handling*, Vol. 2, No. 2, Jun. 1982, pp 9 - 15.
47. Hikita, T., Ikeda, M. and Asano, H., Upward Transportation of Particles in Dense Phase, *Fourth International Conference on Fluidisation*, 1983, Kasikojima, Japan, pp 219 - 232
48. Hitt, R. J., An Investigation into the Low Velocity Pneumatic Conveying of Bulk Solids, PhD dissertation, School of Mechanical Engineering, Thames Polytechnic, Jan. 1985.
49. Hitt, R. J., An Investigation into the Low Velocity Pneumatic Conveying of Bulk Solids, *Pneumatech 1*, First International Conference on Pneumatic Conveying Technology, May 3 - 5, 1982, Stratford-Upon-Avon, UK, pp 1 - 26
50. Hong, J. and Shen, Y., Characteristics in Horizontal Pneumatic Conveying at High Solids Loading and Low Gas Velocity, *International Symposium on Reliable Flow of Particulate Solids II*, Aug. 23 - 25, 1993, Oslo, Norway, pp 677 - 711.
51. Hongky, J. N., Design and Scale-Up Low Velocity Pneumatic Conveying Systems, BE Thesis, Dept. of Mechanical Engineering, University of Wollongong, 1990.
52. Hoppe, H., Heep, D. and Storf, R., Modern Rotary Valve Technology for Various Pneumatic Conveying Systems, *Bulk Solids Handling*, Vol. 5, No. 4, Aug. 1985, pp 161 - 165.

53. Hoppe, H., Modern, Economical Pneumatic Conveying Technologies for In-plant Quality Assurance, Pneumatech 4, Fourth International Conference on Pneumatic Conveying Technology, Mar. 1987, pp 253 - 266.
54. Huggett, M. R., Low Velocity - The Ultimate Dense Phase Conveyor, Powder Handling and Processing, Vol. 2, No. 3, 1990, pp 207 - 210.
55. Jenike, A. W. and Johanson, J. R., Bin Loads, Journal of the Structure Division, ASCE, Vol. 95, No. ST4, 1968, pp 1011 - 1041
56. Jenike, A. W. and Johanson, J. R., On the Theory of Bin Loads, Journal of Engineering for Industry, Transactions of ASME, Series B, Vol. 91, No. 2, May 1969, pp 339 - 344.
57. Jodlowski, C., Considerations on Two Phase Gas/Solid Flow at Low Velocities, Pneumatech 2, International Conference on Pneumatic Conveying Technology, Sep. 4 - 6, 1984, Canterbury, UK, pp 19 - 39.
58. Jones, M. G., Mills, D. and Mason, J. S., Pneumatic Conveying of High Bulk Density Products, Pneumatech 4, Fourth International Conference on Pneumatic Conveying Technology, Mar. 1987, pp 371 - 396.
59. Kadlec, R. H., The Behaviour of Slugging Gas-Fluidised Solid, PhD Dissertation, University of Michigan, 1961.
60. Kessel, S. R., Reed, A. R. and Mason, J. S., An Investigation into the Flow Behaviour in the Entrainment Section of a Rotary Valve Fed Pneumatic Conveying System, Pneumatech 1, First International Conference on Pneumatic Conveying Technology, May 3 - 5, 1982, Stratford-Upon-Avon, UK, pp 1 - 23.

61. Klintworth, J. and Marcus, R. D., A Review of Low-Velocity Pneumatic Conveying Systems, *Bulk Solids Handling*, Vol. 5, No. 4, Aug. 1985, pp 25 - 31.
62. Klinzing, G. E., A Comparison Pressure Losses in Bends Between Recent Data and Models for Gas-Solid Flow, *Canadian Journal of Chemical Engineering*, Vol. 58, 1980, pp 670 - 672.
63. Klinzing, G. E., Artificial Intelligence Approaches to Pneumatic Conveying Operations, *International Symposium on Reliable Flow of Particulate Solids II*, Aug. 23 - 25, 1993, Oslo, Norway, pp 481 - 499.
64. Konrad, K. and Totah, T. S., Vertical Pneumatic Conveying of Particle Plugs, *Canadian Journal of Chemical Engineering*, Vol. 67, Apr. 1989, pp 245 - 250.
65. Konrad, K., Dense-Phase Pneumatic Conveying through Long Pipelines: Effect of Significantly Compressible Air Flow on Pressure Drop, *Powder Technology*, 48 (1986), pp 193 - 203.
66. Konrad, K., An Exploratory Analysis of Dense Phase Pneumatic Conveying through Vertical Pipeline, *Journal of Pipelines* 6, 1987, pp 99 - 104.
67. Konrad, K., Dense Phase Pneumatic Conveying of Particles, PhD dissertation, Trinity College, University of Cambridge, 1980.
68. Konrad, K., Dense Phase Pneumatic Conveying: A Review, *Powder Technology*, 49, 1986, pp 1 - 35.
69. Konrad, K., Harrison, D., Nedderman, R. M. and Davidson, J. F., Prediction of the Pressure Drop for Horizontal Dense Phase Pneumatic Conveying of Particles, *Pneumotransport 5*, Fifth International Conference on the Pneumatic Transport of Solids in Pipes, Apr. 16 - 18, 1980, London, UK, pp 225 - 244.

70. Kunii, D. and Levenspid, O., *Fluidisation Engineering*, Wiley, New York, London, Sydney and Toronto, 1969.
71. Legel, D. and Schwedes, J., Investigation of Pneumatic Conveying of Plug of Cohesionless Bulk Solids in Horizontal Pipes, *Bulk Solids Handling*, Vol. 4, No. 2, Jun. 1984, pp 399 - 405.
72. Leung, L. S., Vertical Pneumatic Conveying: A Flow Regime Diagram and a Review of Choking Versus Non-Choking Systems, *Powder Technology*, Vol. 25, 1980, pp 185 - 190.
73. Leva, M., Fluid Flow through Packed Beds, *Chemical Engineering*, 56, May 1949, pp 115 - 117.
74. Leva, M., *Fluidisation*, MacGraw-Hill, New York, 1959.
75. Lewis, W. K. and Gilliland, E. R. and Baner, W. C., Characteristics of Fluidised Particles, *Industrial and Engineering Chemistry*, Vol. 41, No. 6, pp 1104 - 1117.
76. Li, H., The Fluid-Particle Flow Phase Diagram and Ideal Sealing State for a Vertical Moving Bed, *Powder Technology*, 67, 1991, pp 37 - 42.
77. Lippert, A., Pneumatic Conveyence at High Solids Concentrations, *Chemie-Ing-Techn.* 38, No. 3, pp 350 - 355.
78. Mainwaring, N. J. and Reed, A. R., An Appraisal of Dixon's Slugging Diagram for Assessing the Dense Phase Conveying Potential of Bulk Solid Materials, *Pneumatech 4*, Fourth International Conference on Pneumatic Conveying Technology, Mar. 1987, pp 221 - 234.

79. Mason, D. J., Cross, M., Patel, M. K. and Reed, A. R., Numerical Modelling of "Dense Phase" Pneumatic Conveying of Bulk Particulate Materials, 14th Annual Powder and Bulk Solids Conference, 1989, pp 449 - 460.
80. Matsen, J. M., A Phase Diagram for Gas-Particle Flow, Fluidisation IV, Fourth International Conference on Fluidisation, 1983, Kasikojima, Japan, pp 225 - 233.
81. Morikawa, Y. and Sakamoto, S., Flow Characteristics of Mixed Size Particles in Horizontal Pneumatic Conveying, Bulk Solids Handling, Vol. 5, No. 3, Jun. 1985, pp 61 - 65.
82. Morse, R. D., Fluidisation of Granular Solids (Fluid Mechanics and Quality), Industrial and Engineering Chemistry, Vol. 41, No. 6, pp 1117 - 1124.
83. Myler, C. A., Zaltash, A., Dhodapkar, S. and Klinzing, G. E., Phase Equilibrium in Horizontal Pneumatic Transport, Powder Technology, 57, 1989, pp 51 - 57.
84. Nicklin, D. J., Wilkes, J. O. and Davidson, J. F., Two-Phase Flow in Vertical Tubes, Transactions of the Institution of Chemical Engineers, Vol. 40, 1962, pp 61 - 68.
85. Ormiston, R. M., Mitchell, F. R. G. and Davidson, J. F., The Velocity of Slugs in Fluidised Beds, Transactions of the Institution of Chemical Engineers, Vol. 43, 1965, pp 209 - 216.
86. Owen, P. R., Pneumatic transport, Journal of Fluid Mechanics, Vol. 39, Part 2, 1969, pp 407 - 432.
87. Partridge, B. A. and Rowe, P. N., Analysis of Gas Flow in a Bubbling Fluidised Bed When Cloud Formation Occurs, Transactions of the Institution of Chemical Engineers, Vol. 44, 1966, T 349 - 358.

88. Perloff, W. H. and Baron, W., *Soil Mechanics, Principles and Applications*, 1976, Wiley, New York.
89. Rao, K. R. and Ramakrishnan, T., *Investigations into Dense Phase Pneumatic Conveying*, International Symposium on Reliable Flow of Particulate Solids II, Aug. 23 - 25, 1993, Oslo, Norway, pp 539 - 547.
90. Rao, M. M., Ramakrishnan, T. and David, P., *Numerical Study of Plug-Type Pneumatic Conveying*, Powder Handling and Processing, Vol. 3, No. 1, 1991, pp 57 - 60.
91. Richardson, J. F. and Mcleman, M., *Pneumatic Conveying - Part II, Solids Velocities and Pressure Gradients in One-Inch Horizontal Pipe*, Transactions of the Institution of Chemical Engineers, Vol. 38, 1960, pp 257 - 266.
92. Richardson, J. F. and Zaki, W. N., *Sedimentation and Fluidisation: Part I*, Transactions of the Institution of Chemical Engineers, Vol. 32, 1954, pp 35 - 53.
93. Rizk, F., *A Comparison Between Horizontal and Vertical Pneumatic Conveying Systems Considering the Optimal Operating Conditions*, Journal of Powder and Bulk Solids Technology 7, pp 5 - 11.
94. Sadler, A. M., *Gas-Solids Fluidising for Transport*, Chemical Engineering, 56, May 1949, pp 110 - 111.
95. Sandy, C. W., Daubert, T. E. and Jones, J. H., *Vertical Dense Phase Gas-Solid Transport*, AIChE Chemical Engineering Progress Symposium Series, No. 105, pp 133 - 142.
96. Saunders, J. H., Chao, B. T. and Soo, S. L., *Real Time Mass Flux Measurements of Gas-Solid Suspensions at Low Velocities*, Journal of Powder and Bulk Solids Technology, 6, Part 3, 1982, pp 17 - 21.

97. Shepherd, N. G. and Dickson, A. J., Dense Phase Conveying Wool Pulp, Pneumotransport 4, Fourth International Conference on the Pneumatic Transport of Solids in Pipes, Jun. 24 - 28, 1978, California, USA, D 5 - 61.
98. Stadler, H., Dense Phase Pneumatic Conveying, South African Mechanical Engineer, Vol. 26, Part 4, 1976, pp 168 - 173.
99. Streat, M. and Wilson, K. C., Comments on Moving-Bed Solids Flow Between Two Fluidised Beds, Powder Technology, Vol. 24, 1979, pp 271 - 272.
100. Tanaka, T., Yonemura, S. and Tsuji, Y., Discrete Particle Simulation of Dispersed Particulate Flows, International Symposium on Reliable Flow of Particulate Solids II, Aug. 23 - 25, 1993, Oslo, Norway, pp 373 - 383.
101. Tomita, Y., Yutani, S. and Jotaki, T., Pressure Drop in Vertical Pneumatic Transport Lines of Powdery Material at High Solids Loading, Powder Technology, 25, 1978, pp 101 - 107.
102. Trees, J., A Practical Investigation of the Flow of Particulate Solids through Sloping Pipes, Institution of Chemical Engineering Transaction, Vol. 40, 1962, pp 286 - 296.
103. Tsuji, Y., Morikawa, Y. and Honda, H., A Study on Blowing off A Stationary Plug of Coarse Particles in a Horizontal Pipe, Journal of Powder and Bulk Solids Technology, 3, Part 4, 1979, pp 30 - 35.
104. Tsuji, Y., Recent Studies of Pneumatic Conveying in Japan, Bulk Solids Handling, Vol. 3, No. 3, Sept. 1983, pp 147 - 153
105. Tsuji, Y., Tanaka, T. and Ishida, T., Graphic Simulation of Plug Conveying, Pneumatech 4, Fourth International Conference on Pneumatic Conveying Technology, Mar. 1987, pp 39 - 50.

106. Walker, D. M., An Approximate Theory for Pressures and Arching in Hoppers, *Chemical Engineering Science*, Vol. 21, 1966, pp 975 - 997.
107. Walker, D. M. and Blanchard, M. H., Pressures in Experimental Coal Hoppers, *Chemical Engineering Science*, Vol. 22, 1967, pp 1713 - 1745.
108. Walters, J. K., A Theoretical Analysis of Stresses in Silos with Vertical Walls, *Chemical Engineering Science*, Vol. 28, 1973, pp 13 - 21.
109. Wen, C. Y. and Simons, H. P., Flow Characteristics in Horizontal Fluidised Solids Transport, *AIChE Journal*, Vol. 5, No. 2, 1959, pp 263 - 267.
110. Werner, D., Influence of Particle Size Distribution During Pneumatic Dense Phase Conveying in Vertical and Horizontal Pipes, *Bulk Solids Handling*, Vol. 3, No. 2, Jun. 1983, pp 43 - 51.
111. Wilson, K. C. and Judge, D. G., New Techniques for the Scale-Up of Pilot-Plant Results to Coal Slurry Pipelines, *Journal of Powder and Bulk Solids Technology*, 4, Part 1, 1980, pp 15 - 22.
112. Wilson, K. C., Analysis of Slip of a Particulate Mass in a Horizontal Pipe, *Bulk Solids Handling*, Vol. 1, No. 2, May 1981, pp 67 - 71.
113. Wirth, K. E. and Molerus, O., Critical Solids Transport Velocity with Horizontal Pneumatic Conveying, *Journal of Powder and Bulk Solids Technology*, 9, Part 1, 1985, pp 17 - 24.
114. Wuertele, F. S., Dense Phase Pneumatic Conveying, Classification and Industry Standards, *Bulk Solids Handling*, Vol. 12, No. 1, Feb. 1992, pp 57 - 59.
115. Wypych, P. W. and Arnold, P. C., A Standardised-Test Procedure for Pneumatic Conveying Design, *Bulk Solids Handling*, Vol. 5, No. 4, Aug. 1985, pp 33 - 41.



116. Wypych, P. W. and Hauser, G., Design Considerations for Low-velocity Conveying Systems and Pipelines, Pneumatech 4, Fourth International Conference on Pneumatic Conveying Technology, Jun. 26 - 28, 1990, Glasgow, Scotland.
117. Wypych, P. W., On improving Scale-up Procedures for Pneumatic Conveying Design, Powder Technology, 50, 1987, pp 281 - 294.
118. Zenz, F. A. and Othmer, D. F., Fluidisation and Fluid-Particle Systems, Reinhold, New York, 1960.
119. Zheng, L., Zhang, Y. and Pan, X., Analysis of the Pressure Drop for Horizontal Plug Pneumatic Conveying of Particles, Bulk Solids Handling, Vol. 7, No. 6, Dec. 1987, pp 859 - 864.
120. Beijing University of Iron and Steel Technology, Pneumatic Conveying Equipment, Renming Jiaotong Press, Beijing, Dec. 1974.
121. Arnold, P. C. and Mclean, A. G., Seminar for Bulk Solids Storage and Flow - Some Recent Development, Powder Europa, 22 - 24 Jan. 1980, Rhein - Main - Halle, Wiesbaden.
122. Elliott, D. F., Handbook of Digital Signal Processing, Engineering Applications, Academic Press, 1987.
123. Pan, R., Private Communication, University of Wollongong, Wollongong, Australia.
124. Marcus, R. D., Pneumatic Conveying of Bulk Solids, Notes for a Short Course, The University of Newcastle, Newcastle, Australia, September 1983.

APPENDICES

A Experimental Data of Main Tests

Table A.1: Experimental values of major parameters for conveying white plastic pellets in 52 m long pipeline.

No.	m_f kgs ⁻¹	m_s kgs ⁻¹	Δp_t kPa	Δp_{th} kPa	U_a ms ⁻¹	U_s ms ⁻¹	σ_{wm} kPa	λ	α
1	0.0476	0.512	23.5	11.1	4.120	2.643	0.442	0.749	0.171
2	0.0644	0.524	22.8	10.8	5.480	4.095	0.767	0.758	0.122
3	0.0716	0.519	22.5	10.2	6.142	4.495	0.797	0.775	0.103
4	0.0863	0.521	19.2	10.2	7.226	4.743	0.943	0.840	0.101
5	0.0973	0.520	15.7	9.6	8.030	6.468	1.114	0.749	0.072
6	0.0476	0.780	31.5	16.3	4.172	2.697	0.452	0.723	0.174
7	0.0664	0.773	26.0	15.6	5.653	4.206	0.741	0.719	0.118
8	0.0713	0.768	25.3	14.2	6.027	4.423	0.802	0.742	0.101
9	0.0859	0.773	23.0	14.4	7.213	5.294	0.920	0.772	0.086
10	0.0970	0.773	25.5	14.9	8.017	6.256	1.135	0.772	0.076
11	0.0474	0.986	44.8	21.9	4.054	2.912	0.491	0.742	0.158
12	0.0647	1.004	37.4	19.9	5.521	3.778	0.750	0.824	0.129
13	0.0723	1.014	32.0	19.5	6.170	4.392	0.804	0.734	0.115
14	0.0859	1.011	25.9	17.5	7.314	5.509	0.971	0.762	0.085
15	0.0968	1.012	26.0	18.1	7.975	6.291	1.086	0.731	0.076
16	0.0473	1.200	53.0	26.8	4.025	2.632	0.417	0.713	-
17	0.0658	1.201	43.3	23.6	5.594	4.013	0.731	0.772	-
18	0.0713	1.184	38.7	23.7	6.003	4.185	0.792	0.796	-
19	0.0871	1.204	37.5	23.7	7.225	5.145	0.884	0.712	-
20	0.0980	1.195	34.9	22.9	7.974	6.209	1.123	0.734	-

Table A.2: Experimental values of major parameters for conveying white plastic pellets in 96 m long pipeline.

No.	m_f kg s^{-1}	m_s kg s^{-1}	Δp_t kPa	Δp_{th} kPa	U_a ms^{-1}	U_s ms^{-1}	σ_{wm} kPa	λ	α
1	0.0483	0.519	38.8	26.4	4.067	2.702	0.496	0.757	0.182
2	0.0650	0.519	36.2	22.7	5.405	4.150	0.760	0.744	0.120
3	0.0721	0.514	34.2	22.4	6.174	4.392	0.831	0.758	0.115
4	0.0867	0.520	30.0	22.4	7.211	4.743	0.917	0.764	0.108
5	0.0973	0.520	26.7	20.6	7.757	6.468	1.161	0.694	0.081
6	0.0479	0.765	58.4	39.5	3.964	2.603	0.546	0.772	0.205
7	0.0648	0.746	51.7	38.3	5.328	3.800	0.787	0.823	0.134
8	0.0719	0.751	49.1	38.0	5.937	4.423	0.812	0.750	0.112
9	0.0858	0.750	44.7	35.8	7.312	5.294	0.979	0.760	0.093
10	0.0968	0.757	42.4	33.5	8.224	6.291	1.206	0.761	0.081
11	0.0472	0.960	73.2	52.3	3.867	2.630	0.526	0.790	0.193
12	0.0653	0.958	64.3	47.2	5.552	4.013	0.751	0.767	0.123
13	0.0734	0.969	60.6	44.6	6.311	4.596	0.818	0.777	0.101
14	0.0857	0.969	56.3	42.3	7.402	5.510	0.910	0.723	0.084
15	0.0968	0.974	54.4	42.5	7.942	6.256	1.141	0.766	0.077
16	0.0476	1.115	79.1	57.9	3.972	2.611	0.527	0.738	0.207
17	0.0656	1.117	70.6	51.3	5.403	4.013	0.746	0.739	0.127
18	0.0727	1.119	67.3	51.1	6.391	4.492	0.805	0.754	0.107
19	0.0862	1.114	63.4	49.8	7.417	5.394	1.029	0.723	0.099
20	0.1195	1.116	55.7	43.1	9.781	8.002	1.396	0.736	0.060

Table A.3: Experimental values of major parameters for conveying black plastic pellets in 96 m long pipeline.

No.	m_f kg s ⁻¹	m_s kg s ⁻¹	Δp_t kPa	Δp_{th} kPa	U_a ms ⁻¹	U_s ms ⁻¹	σ_{wm} kPa	λ	α
1	0.0495	0.568	43.1	25.5	4.022	2.873	0.492	0.834	0.156
2	0.0635	0.555	37.7	23.9	5.577	4.238	0.796	0.841	0.115
3	0.0741	0.560	33.5	22.3	6.407	4.912	0.886	0.808	0.099
4	0.0828	0.550	30.0	21.3	7.411	6.225	1.137	0.781	0.082
5	0.0883	0.564	24.9	17.1	8.210	7.014	1.205	0.753	0.071
6	0.0488	0.828	54.7	36.9	4.074	2.660	0.451	0.814	0.171
7	0.0669	0.829	50.7	33.0	5.801	4.382	0.785	0.812	0.110
8	0.0742	0.825	47.4	32.2	5.935	4.812	0.889	0.830	0.101
9	0.0770	0.841	43.8	31.3	6.672	5.573	1.003	0.801	0.088
10	0.0871	0.830	42.6	31.6	8.001	6.900	1.236	0.787	0.072
11	0.0495	1.012	64.2	45.6	4.344	2.997	0.521	0.792	0.160
12	0.0675	1.030	58.7	43.4	6.386	4.433	0.815	0.838	0.108
13	0.0745	1.024	59.6	41.5	6.320	4.920	0.916	0.834	0.099
14	0.0842	1.023	57.3	39.2	7.497	6.418	1.126	0.765	0.078
15	0.0888	1.024	53.6	39.4	7.913	6.816	1.222	0.798	0.072
16	0.0449	1.208	80.3	56.9	3.903	2.512	0.380	0.774	0.170
17	0.0674	1.241	71.8	49.6	6.226	4.400	0.775	0.795	0.110
18	0.0744	1.198	66.4	46.6	6.271	4.900	0.884	0.812	0.099
19	0.0837	1.203	60.1	43.4	6.983	6.012	1.139	0.829	0.083
20	0.0880	1.205	65.6	44.8	7.638	6.523	1.241	0.837	0.076

Table A.4: Experimental values of major parameters for conveying black plastic pellets in 52 m long pipeline.

No.	m_f kg s^{-1}	m_s kg s^{-1}	Δp_t kPa	Δp_{th} kPa	U_a ms^{-1}	U_s ms^{-1}	σ_{wm} kPa	λ	α
1	0.0384	0.567	29.3	12.0	3.413	2.123	0.290	0.751	0.189
2	0.0498	0.560	25.3	10.2	4.369	2.997	0.458	0.779	0.143
3	0.0656	0.568	21.5	9.6	5.678	4.238	0.759	0.809	0.114
4	0.0727	0.564	19.8	10.0	6.329	4.882	-	-	0.100
5	0.0822	0.565	18.5	10.1	6.865	5.929	1.034	0.803	0.080
6	0.0498	0.840	32.2	16.6	4.325	3.007	0.462	0.780	0.143
7	0.0643	0.849	26.9	14.3	5.499	4.032	0.594	0.797	0.100
8	0.0713	0.848	25.0	15.3	6.036	4.921	0.820	0.795	0.093
9	0.0833	0.850	23.2	13.0	7.160	5.957	0.965	0.848	0.070
10	0.0882	0.846	22.0	14.5	7.560	6.418	1.008	0.763	0.070
11	0.0494	1.074	41.8	20.3	4.300	2.936	0.468	0.828	0.143
12	0.0651	1.057	36.2	19.4	5.535	4.062	0.726	0.794	0.121
13	0.0718	1.058	33.8	19.4	6.246	4.835	0.802	0.805	0.093
14	0.0820	1.067	31.6	19.4	7.039	5.724	1.026	0.786	0.087
15	0.0850	1.067	30.6	18.3	7.174	6.029	1.045	0.785	0.080
16	0.0446	1.214	50.2	24.5	3.831	2.441	0.394	0.798	0.181
17	0.0498	1.219	46.9	24.4	4.185	2.663	0.489	0.907	0.166
18	0.0665	1.244	40.7	23.1	5.560	4.082	0.697	0.801	0.114
19	0.0729	1.248	39.3	20.0	6.134	4.812	0.841	0.853	0.093
20	0.0826	1.220	36.2	21.0	7.116	5.859	1.066	0.847	0.080

Table A.5: Experimental values of major parameters for conveying wheat in 52 m long pipeline.

No.	m_f kg s ⁻¹	m_s kg s ⁻¹	Δp_t kPa	Δp_{th} kPa	U_a m s ⁻¹	U_s m s ⁻¹	σ_{wm} kPa	λ	α
1	0.0495	0.967	55.5	22.0	3.966	1.747	0.334	0.527	0.256
2	0.0663	0.959	45.7	18.0	5.271	3.160	0.671	0.579	0.143
3	0.0733	0.957	40.2	17.1	5.658	3.532	0.726	0.539	0.133
4	0.0828	0.961	38.7	16.9	6.559	4.368	0.896	0.541	0.107
5	0.0882	0.962	36.7	16.0	6.919	4.788	0.978	0.566	0.093
6	0.0495	1.450	80.0	35.4	3.969	1.792	0.341	0.548	0.239
7	0.0665	1.439	57.1	29.0	5.038	3.009	0.639	0.580	0.150
8	0.0742	1.439	55.7	26.9	5.789	3.583	0.785	0.589	0.128
9	0.0836	1.439	54.0	25.5	6.394	4.299	0.892	0.556	0.107
10	0.0885	1.461	47.9	25.2	6.869	4.834	0.997	0.566	0.093
11	0.0545	1.945	100.4	44.3	4.197	2.088	0.442	0.582	0.215
12	0.0676	1.986	82.8	40.6	5.245	3.185	0.711	0.576	0.150
13	0.0747	1.977	72.5	36.6	5.750	3.446	0.746	0.573	0.135
14	0.0796	1.997	69.9	36.8	5.957	3.703	0.814	0.572	0.128
15	0.0868	1.996	63.9	33.2	6.577	4.290	0.909	0.569	0.114
16	0.0543	2.300	125.5	53.9	4.388	2.092	0.403	0.521	-
17	0.0657	2.383	109.7	47.5	5.112	3.027	0.663	0.587	-
18	0.0747	2.403	91.3	45.3	5.583	3.583	0.780	0.572	-
19	0.0838	2.388	83.3	43.8	6.358	4.330	0.952	0.564	-
20	0.0885	2.415	79.1	42.9	6.581	4.466	1.028	0.588	-

Table A.6: Experimental values of major parameters for conveying wheat in 96 m long pipeline.

No.	m_f kg s ⁻¹	m_s kg s ⁻¹	Δp_t kPa	Δp_{th} kPa	U_a m s ⁻¹	U_s m s ⁻¹	σ_{wm} kPa	λ	α
1	0.0557	1.159	92.9	58.3	4.318	2.187	0.420	0.547	0.198
2	0.0676	1.157	81.1	50.1	5.303	3.185	0.702	0.588	0.145
3	0.0749	1.161	74.2	47.5	5.543	3.446	0.706	0.539	0.136
4	0.0838	1.168	70.7	46.1	6.509	4.330	0.926	0.601	0.111
5	0.0870	1.162	69.0	44.7	6.882	4.666	0.969	0.587	0.097
6	0.0559	1.494	111.4	82.6	4.237	2.189	0.423	0.555	0.196
7	0.0678	1.494	95.0	66.2	5.214	3.214	0.737	0.603	0.146
8	0.0745	1.496	93.9	63.4	5.805	3.583	0.796	0.584	0.131
9	0.0833	1.497	82.3	57.7	6.218	4.299	0.882	0.577	0.102
10	0.0869	1.493	81.0	58.3	6.583	4.566	1.009	0.622	0.096
11	0.0560	1.960	105.1	107.3	4.321	2.098	0.423	0.515	0.204
12	0.0678	1.957	112.5	95.9	5.313	3.182	0.707	0.594	0.145
13	0.0739	1.968	105.5	85.8	5.806	3.583	0.788	0.585	0.131
14	0.0838	1.969	99.4	80.4	6.472	4.292	0.948	0.622	0.102
15	0.0878	1.964	95.6	76.4	6.745	4.727	1.008	0.592	0.094
16	0.0556	2.387	101.1	93.6	4.556	2.283	0.423	0.511	0.196
17	0.0677	2.402	135.3	106.0	5.241	3.180	0.673	0.566	0.145
18	0.0744	2.374	111.9	107.3	5.524	3.520	0.781	0.576	0.135
19	0.0835	2.373	109.4	101.1	6.198	4.150	0.928	0.605	0.110
20	0.0873	2.375	109.4	98.5	6.802	4.710	0.996	0.583	0.095

Table A.7: Experimental values of major parameters for conveying barley in 96 m long pipeline.

No.	m_f kg s ⁻¹	m_s kg s ⁻¹	Δp_t kPa	Δp_{th} kPa	U_a m s ⁻¹	U_s m s ⁻¹	σ_{wm} kPa	λ	α
1	0.0490	1.006	95.5	49.1	3.896	1.588	0.282	0.610	0.254
2	0.0665	1.001	72.9	43.3	5.116	3.260	0.731	0.635	0.150
3	0.0739	1.032	63.7	39.2	5.821	3.960	0.964	0.681	0.125
4	0.0798	1.021	60.3	37.5	6.484	5.045	1.120	0.635	0.096
5	0.0888	1.027	57.5	36.3	6.796	5.523	1.343	0.656	0.093
6	0.0562	1.296	106.5	66.7	4.607	2.320	0.548	0.688	0.205
7	0.0671	1.293	91.3	54.8	5.318	3.250	0.749	0.634	0.155
8	0.0766	1.306	79.9	49.9	5.698	4.081	0.946	0.656	0.120
9	0.0837	1.306	73.8	47.8	6.703	5.115	1.235	0.635	0.103
10	0.0885	1.307	72.0	47.7	7.017	5.523	1.397	0.654	0.097
11	0.0560	1.738	137.5	79.0	4.224	2.123	0.431	0.649	0.204
12	0.0675	1.732	114.3	77.1	5.189	3.300	0.741	0.628	0.150
13	0.0745	1.748	103.4	68.8	5.672	3.890	0.958	0.649	0.135
14	0.0857	1.717	95.3	66.0	6.441	5.151	1.159	0.637	0.095
15	0.0885	1.739	90.6	62.2	6.686	5.391	1.276	0.668	0.091
16	0.0560	1.279	105.8	68.3	4.278	2.130	0.471	0.653	0.220
17	0.0678	2.106	121.1	95.6	4.964	3.220	0.742	0.631	0.157
18	0.0749	2.107	123.2	85.9	5.812	3.999	0.933	0.679	0.119
19	0.0846	2.101	120.8	82.5	6.435	5.000	1.145	0.647	0.098
20	0.0876	2.093	114.0	79.0	6.761	5.605	1.376	0.689	0.088

Table A.8: Experimental values of major parameters for conveying barley in 52 m long pipeline.

No.	m_f kg s^{-1}	m_s kg s^{-1}	Δp_t kPa	Δp_{th} kPa	U_a m s^{-1}	U_s m s^{-1}	σ_{wm} kPa	λ	α
1	0.0490	1.017	56.1	23.6	3.948	1.588	0.304	0.655	0.255
2	0.0651	1.045	44.8	18.5	5.293	3.180	0.725	0.662	0.150
3	0.0714	1.048	40.9	17.9	5.713	3.860	0.876	0.679	0.120
4	0.0807	1.046	37.9	17.3	6.570	5.082	1.158	0.627	0.099
5	0.0862	1.036	35.5	17.4	6.842	5.533	1.295	0.658	0.089
6	0.0554	1.311	61.9	25.2	4.415	2.123	0.395	0.601	0.202
7	0.0656	1.312	55.7	23.4	5.209	3.172	0.740	0.657	0.155
8	0.0729	1.311	51.0	23.0	5.590	3.860	0.922	0.675	0.127
9	0.0819	1.313	45.5	21.9	6.326	4.788	1.123	0.685	0.099
10	0.0882	1.321	44.9	22.0	6.934	5.503	1.297	0.666	0.089
11	0.0555	1.729	72.3	35.7	4.284	2.128	0.458	0.667	0.210
12	0.0662	1.745	65.0	32.0	5.035	3.152	0.689	0.654	0.147
13	0.0729	1.741	59.7	30.6	5.634	3.860	0.886	0.649	0.127
14	0.0832	1.731	56.1	29.3	6.351	5.051	1.161	0.637	0.099
15	0.0882	1.740	53.3	28.3	6.693	5.298	1.211	0.671	0.085
16	0.0557	1.881	88.4	41.0	4.273	2.150	0.462	0.675	0.205
17	0.0667	2.096	80.8	41.9	4.992	3.201	0.753	0.656	0.155
18	0.0733	2.120	75.5	37.3	5.662	3.891	0.975	0.697	0.128
19	0.0829	2.106	70.9	36.6	6.244	4.882	1.195	0.674	0.103
20	0.0873	2.115	68.6	36.3	6.740	5.595	1.310	0.644	0.090

Table A.9: Experimental values of pressure along 96 m long pipeline for white plastic pellets.

No.	m _f kgs ⁻¹	m _s kgs ⁻¹	P ₁ kPag	P ₂ kPag	P ₃ kPag	P ₄ kPag	P ₅ kPag	P ₆ kPag	P ₇ kPag	P ₈ kPag	P ₉ kPag
1	0.048	0.519	38.8	26.4	22.9	19.1	17.7	13.2	8.8	5.4	3.1
2	0.065	0.519	36.2	22.7	19.5	16.3	14.5	11.3	8.3	5.6	3.0
3	0.072	0.514	34.2	22.4	19.3	15.7	13.9	10.7	7.9	5.1	2.7
4	0.087	0.520	30.0	22.4	18.5	14.2	11.7	9.8	7.4	4.5	2.4
5	0.097	0.520	26.7	20.6	16.6	11.5	9.5	5.4	3.1	1.7	1.1
6	0.048	0.765	58.4	39.5	34.2	28.0	25.4	19.9	14.0	9.6	3.5
7	0.065	0.746	51.7	38.3	33.7	28.5	25.6	20.6	15.6	10.0	6.1
8	0.072	0.751	49.1	38.0	33.1	28.6	26.3	20.9	15.8	10.6	5.7
9	0.086	0.750	44.7	35.8	30.8	26.3	22.5	18.7	14.0	8.6	4.4
10	0.097	0.757	42.4	33.5	28.0	23.7	19.8	15.9	13.4	8.7	4.4
11	0.047	0.960	73.2	52.3	43.6	35.5	33.0	23.4	16.8	10.0	2.8
12	0.065	0.958	64.3	47.2	40.4	33.9	31.1	23.6	17.7	11.4	5.4
13	0.073	0.969	60.6	44.6	37.5	30.9	27.4	20.8	15.8	10.5	5.1
14	0.086	0.969	56.3	42.3	37.1	31.4	27.8	21.4	16.5	10.6	5.2
15	0.097	0.974	54.4	42.5	36.5	30.3	26.2	21.4	16.7	10.1	5.0
16	0.048	1.115	79.1	57.9	50.5	41.2	38.2	28.8	21.4	14.6	6.5
17	0.066	1.117	70.6	51.3	44.3	37.8	35.1	25.8	19.7	12.6	5.8
18	0.073	1.119	67.3	51.1	44.5	37.4	33.8	26.5	20.8	14.2	6.4
19	0.086	1.114	63.4	49.8	44.0	37.1	32.8	26.1	20.6	13.5	6.5
20	0.120	1.116	55.7	43.1	36.0	28.9	23.0	20.2	15.7	9.6	5.4

Table A.10: Experimental values of pressure along 96 m long pipeline for black plastic pellets.

No.	m_f kgs ⁻¹	m_s kgs ⁻¹	P_1 kPag	P_2 kPag	P_3 kPag	P_4 kPag	P_5 kPag	P_6 kPag	P_7 kPag	P_8 kPag	P_9 kPag
1	0.050	0.568	43.1	25.5	7.8	3.6	3.5	1.7	1.3	0.2	0.0
2	0.064	0.555	37.7	23.9	21.0	16.2	16.2	12.0	9.8	5.8	2.7
3	0.074	0.560	33.5	22.3	19.4	13.8	14.5	10.5	9.0	5.2	3.2
4	0.083	0.550	30.0	21.3	18.6	14.4	14.7	10.7	8.8	4.7	3.1
5	0.088	0.564	24.9	17.1	12.8	8.6	7.7	2.3	1.3	0.9	0.6
6	0.049	0.828	54.7	36.9	32.9	26.9	25.7	17.7	13.3	7.4	3.6
7	0.067	0.829	50.7	33.0	29.1	24.3	23.1	17.6	14.6	9.1	4.4
8	0.074	0.825	47.4	32.2	28.4	22.7	22.4	16.7	13.3	7.1	3.3
9	0.077	0.841	43.8	31.3	26.5	20.5	21.1	15.3	12.7	6.4	4.3
10	0.087	0.830	42.6	31.6	26.3	20.8	21.0	15.1	12.7	6.4	3.6
11	0.050	1.012	64.2	45.6	40.4	33.6	32.0	22.6	17.1	9.2	4.1
12	0.068	1.030	58.7	43.4	38.4	32.8	30.6	21.6	17.3	9.7	4.7
13	0.075	1.024	59.6	41.5	36.1	30.4	28.9	21.6	16.5	9.3	3.9
14	0.084	1.023	57.3	39.2	34.1	29.1	27.3	20.1	15.7	8.5	3.3
15	0.089	1.024	53.6	39.4	34.4	29.3	26.7	18.8	15.3	7.6	4.7
16	0.045	1.208	80.3	56.9	49.6	39.6	37.7	27.2	17.1	8.1	10.0
17	0.067	1.241	71.8	49.6	42.3	34.5	31.1	21.7	17.3	9.8	4.9
18	0.074	1.198	66.4	46.6	41.1	34.9	33.2	24.3	19.6	11.1	7.3
19	0.084	1.203	60.1	43.4	38.2	32.3	30.8	22.7	17.9	10.0	6.9
20	0.088	1.205	65.6	44.8	37.3	28.6	27.7	19.6	16.2	8.1	5.9

Table A.11: Experimental values of pressure along 96 m long pipeline for wheat.

No.	m_f kgs ⁻¹	m_s kgs ⁻¹	P ₁ kPag	P ₂ kPag	P ₃ kPag	P ₄ kPag	P ₅ kPag	P ₆ kPag	P ₇ kPag	P ₈ kPag	P ₉ kPag
1	0.056	1.159	92.9	58.3	53.7	47.7	46.1	33.0	25.7	13.4	6.4
2	0.068	1.157	81.1	50.1	43.7	35.8	34.2	23.3	17.7	8.9	5.0
3	0.075	1.161	74.2	47.5	42.1	35.5	33.8	24.1	19.4	10.4	5.2
4	0.084	1.168	70.7	46.1	40.9	33.6	31.4	22.1	18.0	8.9	5.2
5	0.087	1.162	69.0	44.7	39.7	33.6	31.4	22.1	18.0	8.8	5.9
6	0.056	1.494	111.4	82.6	76.4	66.2	63.3	37.5	31.5	17.9	7.2
7	0.068	1.494	95.0	66.2	58.6	47.9	45.5	29.8	23.4	12.0	6.7
8	0.075	1.496	93.9	63.4	55.2	45.5	43.4	30.2	24.2	14.3	7.7
9	0.083	1.497	82.3	57.7	51.2	42.4	40.3	29.2	24.7	13.5	8.0
10	0.087	1.493	81.0	58.3	50.5	42.4	40.4	29.3	25.3	13.0	7.9
11	0.056	1.960	105.1	107.3	69.2	50.1	43.4	16.0	12.6	7.9	10.7
12	0.068	1.957	112.5	95.9	83.0	61.6	58.2	36.9	26.9	9.9	5.7
13	0.074	1.968	105.5	85.8	78.2	66.3	63.3	46.0	34.3	15.2	8.3
14	0.084	1.969	99.4	80.4	73.1	62.7	59.8	40.3	33.4	18.3	9.0
15	0.088	1.964	95.6	76.4	68.5	58.4	55.4	37.4	28.5	15.2	10.1
16	0.056	2.387	101.1	93.6	72.4	42.0	36.7	30.9	28.8	12.9	5.8
17	0.068	2.402	135.3	106.0	78.9	56.4	56.1	43.2	36.2	19.5	9.5
18	0.074	2.374	111.9	107.3	103.	85.3	80.0	50.5	42.0	27.2	11.6
19	0.084	2.373	109.4	101.1	95.2	84.8	81.8	56.9	44.2	20.5	9.8
20	0.087	2.375	109.4	98.5	92.8	76.5	71.3	40.5	29.3	11.2	8.9

Table A.12: Experimental values of pressure along 96 m long pipeline for barley.

No.	m_f kgs ⁻¹	m_s kgs ⁻¹	P ₁ kPag	P ₂ kPag	P ₃ kPag	P ₄ kPag	P ₅ kPag	P ₆ kPag	P ₇ kPag	P ₈ kPag	P ₉ kPag
1	0.049	1.006	95.5	49.1	41.1	30.4	28.0	17.3	12.3	4.5	1.7
2	0.067	1.001	72.9	43.3	37.7	31.7	30.0	21.3	16.4	8.6	4.5
3	0.074	1.032	63.7	39.2	33.7	26.7	24.7	17.0	13.4	7.0	2.0
4	0.080	1.021	60.3	37.5	32.9	26.1	24.8	17.1	14.1	7.2	5.7
5	0.089	1.027	57.5	36.3	30.7	24.4	23.4	16.9	14.2	7.4	5.0
6	0.056	1.296	106.5	66.7	51.7	42.0	41.0	29.8	22.0	9.3	4.4
7	0.067	1.293	91.3	54.8	48.6	39.7	37.6	25.5	19.3	10.1	4.7
8	0.077	1.306	79.9	49.9	43.0	35.1	34.0	23.9	19.4	10.5	5.1
9	0.084	1.306	73.8	47.8	42.0	34.0	32.3	23.2	19.8	11.1	6.3
10	0.089	1.307	72.0	47.7	41.3	33.0	31.3	20.8	17.3	9.5	6.1
11	0.056	1.738	137.5	79.0	60.5	60.0	60.0	29.4	19.7	12.8	0.0
12	0.068	1.732	114.3	77.1	67.6	55.9	52.8	33.4	25.1	14.1	7.8
13	0.075	1.748	103.4	68.8	60.2	49.0	46.3	30.6	24.4	12.9	7.0
14	0.086	1.717	95.3	66.0	56.4	45.0	43.1	30.4	23.7	12.9	7.6
15	0.089	1.739	90.6	62.2	52.8	43.7	41.5	28.6	21.8	10.2	5.6
16	0.056	1.279	105.8	68.3	58.9	48.0	45.2	28.2	20.1	9.8	6.4
17	0.068	2.106	121.1	95.6	79.4	60.7	60.0	28.8	29.7	27.1	16.6
18	0.075	2.107	123.2	85.9	74.7	59.0	55.3	35.8	28.0	14.3	8.9
19	0.085	2.101	120.8	82.5	71.1	56.2	52.8	35.8	29.1	14.6	8.3
20	0.088	2.093	114.0	79.0	69.4	55.3	52.6	34.7	28.1	13.1	7.4

B Locations of Pressure Transducers

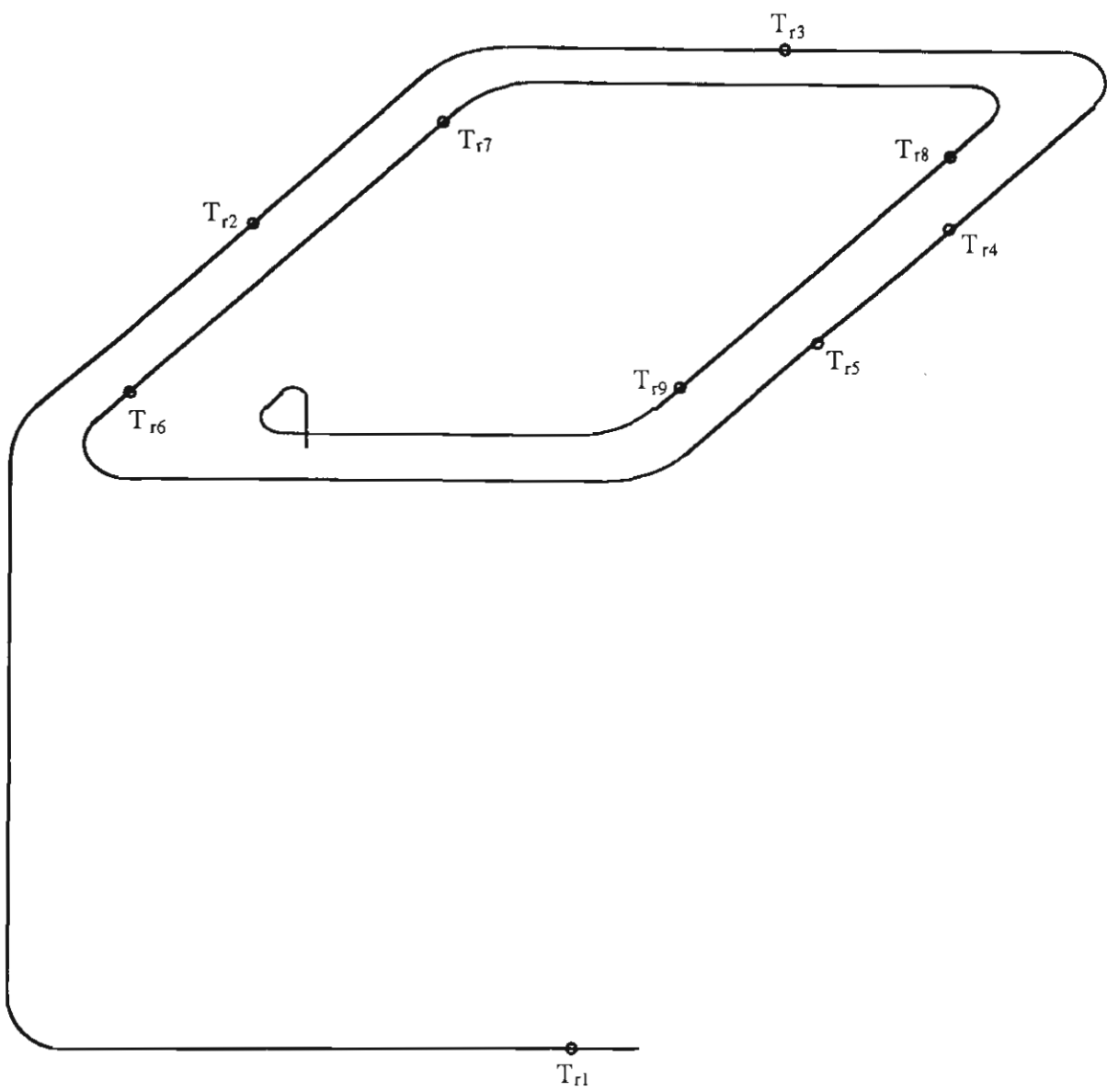


Figure B.1 Schematic layout of 96 m long pipeline and transducer locations.

Table B.1: Pressure transducer location (distance from end of pipeline).

	Pressure Transducer								
	T_{r1}	T_{r2}	T_{r3}	T_{r4}	T_{r5}	T_{r6}	T_{r7}	T_{r8}	T_{r9}
Location (m)	96	78.0	71.2	59.6	57.1	43.9	32.4	22.1	10.9

C Computer Programme for Pressure Drop Prediction

```

DIMENSION MF(100), DPP(100,200), L(100)
REAL MF, MFI, MFE, MFR, MFL, MS, LT, LTT, LS, L
REAL KSI, LMTA, MU, MUW
CHARACTER*10 MFDP, ANS
WRITE(*,5)
5  FORMAT(5X,'PLEASE GIVE INITIAL VALUE OF MF.'/)
   WRITE(*,6)
6  FORMAT(3X,'MFI=')
   READ(*,*) FI
   WRITE(*,7)
7  FORMAT(5X,'PLEASE GIVE END VALUE OF MF.'/)
   WRITE(*,8)
8  FORMAT(3X,'MFE=')
   READ(*,*) MFE
   WRITE(*,9)
9  FORMAT(5X,'PLEASE ENTER THE VALUE OF MS.'/)
   WRITE(*,10)
10 FORMAT(3X,'MS=')
   READ(*,*) MS
   OPEN(1,FILE='PRE.DAT')
   READ(1,*) D, LT, DMF, DLT
   READ(1,*) RB, D1, EPS, FA, FAW
   READ(1,*) TOP, POP
   READ(1,*) EPPS, UMD
   CLOSE(1)
   G=9.8
   A=3.14*D**2/4.
   RS=RB/(1.-EPS)
   GMB=RB/1000.
   FA=FA*3.14159/180.
   FAW=FAW*3.14159/180.
   FAS=4./3.*FAW*GMB**(1./3.)
   OMG=ASIN(SIN(FAW)/SIN(FAS))
   LMTA=(1.-SIN(FAS)*COS(OMG-FAW))/(1.+SIN(FAS)*COS(OMG-FAW))
   MU=TAN(FA)
   MUW=TAN(FAW)
   ATA=1.723*380./(380.+TOP)*((273.+TOP)/273.）**1.5/100000.
   UAMIN=UMD*RS*G*MUW*EPS**3*D1**2/(180.*(1.-EPS)*ATA)
   CK=105.*EPS*(D1/D)*(MUW/MU)**(1./3.)
   WRITE(*,12)
12  FORMAT(5X,'ENTER ASSUMING TOTAL PRESSURE DROP')
   READ(*,*) DPO
   WRITE(*,500)
500  FORMAT(2X,'DO YOU WISH TO OBTAIN THE PRESSURE
      DISTRIBUTION(Y/N)?,')
   READ(*,510) ANS
510  FORMAT(A1)
   NN=INT(LT/DLT+1.)
   IF ((ANS.EQ.'N').OR.(ANS.EQ.'n')) NN=1
   DO 550 J=1,NN
   I=0
   MFI=FI

```

```

      LTT=LT-(J-1)*DLT
30    RA=1.293*(POP+DPO/2.)*273./(101.*(273.+TOP))
35    MFL=0.
      MFR=MFI-MFL
      UA=MFR/(RA*A)
      US=CK*(UA-UAMIN)
c    write(*,*) US
      KSI=1./(1.+US/(0.542*SQRT(G*D)))
      SGMF=KSI*RB*US**2
      SGMW=LMTA*SGMF
      LS=MS*LTT/(A*(1.-KSI)*RB*US)
      DP=(4.*MUW*LMTA*SGMF/D+2.*MUW*RB*G)*LS/1000.
      write(*,*) DP
      IF(ABS(DPO-DP).GT.EPPS)THEN
      DPO=DP
      GOTO 30
      ELSE
      I=I+1
      N=I
      MF(I)=MFR
      DPP(I,J)=DP
      END IF
      IF(MFI.LT.MFE)THEN
      MFI=MFI+DMF
      GOTO 35
      END IF
c    write(*,200) MF(1),MF(N)
c    write(*,300) DPP(1,J),DPP(N,J)
c    write(*,*) PUP
200  FORMAT(2X,'MF=',2X,F10.4,2X,F10.4)
300  FORMAT(2X,'DP=',2X,F10.4,2X,F10.4)
      L(J)=LTT
550  CONTINUE
      WRITE(*,31) CK, UAMIN, US, LS
31   FORMAT(5X, 3HCK=, F8.3, F8.3, 3HUS=, F8.3, 3HLS=,F8.3,/)
      WRITE(*,32)
32   FORMAT(2X,'DO YOU WISH TO SAVE RESULTS TO A DATA
& FILE(Y/N)?',/)
      READ(*,510) ANS
      IF((ANS.EQ.'Y').OR.(ANS.EQ.'y')) THEN
      WRITE(*,40)
40   FORMAT(/,2X,'PLEASE GIVE OUT MF,DP RESULTS NAME')
      READ(*,100) MFDP
      OPEN(16,FILE=MFDP)
      WRITE(16,50) (MF(I),I=1,N)
      WRITE(16,51) (L(J),J=1,NN)
      WRITE(16,52) ((DPP(I,J),I=1,N),J=1,NN)
      CLOSE(16)
100  FORMAT(25A)
50   FORMAT(1X,F8.3)
51   FORMAT(3X,F8.3)
52   FORMAT(5X,F8.3)
      ENDIF
      STOP
      END

```

D Wall Pressure Distribution in Vertical Slug-Flow

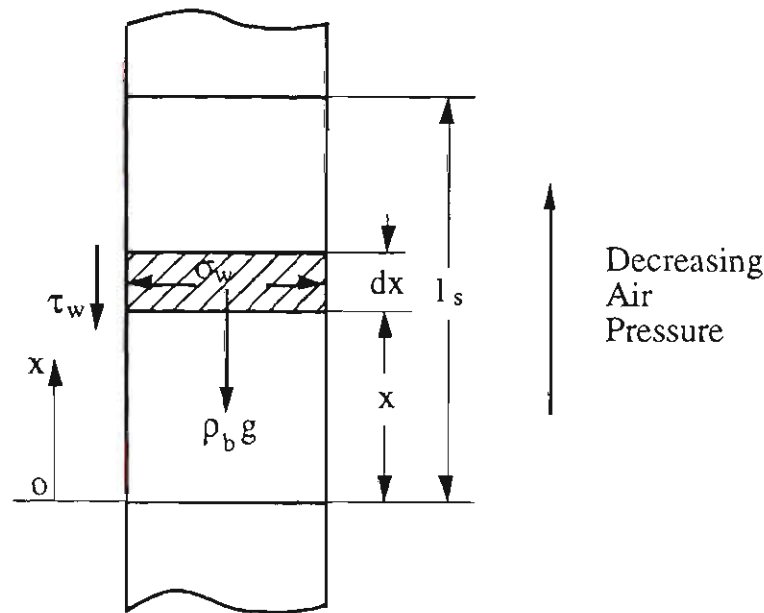


Figure D.1 A particle slug in a vertical pipe

Figure D.1 shows a particle slug flowing in a vertical pipe. Based on an equilibrium of the forces acting on the vertical slug and using Janssen's method, Konrad et al. [69] developed the following equation for predicting the axial stress in the vertical slug.

$$\sigma_x = C e^{-\frac{4\mu_w \lambda}{D}x} + (-\rho_b g + \frac{\Delta p}{l_s}) \frac{D}{4\mu_w \lambda} \quad (D.1)$$

where C is a constant and can be determined by the following boundary condition:

$$\sigma_x = 0, \text{ at } x = 0.$$

Applying the above condition to Equation (D.1) yields

$$\sigma_x = (\frac{\Delta p}{l_s} - \rho_b g) \frac{D}{4\mu_w \lambda} (1 - e^{-\frac{4\mu_w \lambda}{D}x}) \quad (D.2)$$

Konrad et al. [69] also developed the following equation for pressure gradient in vertical slug flow.

$$\frac{\Delta p}{l_s} = \frac{4\mu_w \lambda}{D} \sigma_f + \rho_b g \quad (D.3)$$

where σ_f is the stress on the front surface of the slug.

Substituting Equation (D.3) into Equation (D.2) and replacing σ_x with σ_w/λ :

$$\sigma_w = \lambda \sigma_f (1 - e^{-\frac{4\mu_w \lambda}{D} x}) \quad (\text{D.4})$$

E Publications While PhD Candidate

- 1 Mi, B. and Wypych, P.W., Particle Slug Velocities in Horizontal Slug-Flow Pneumatic Conveying, Powder Handling & Processing, Vol. 5, No. 3, Sep. 1993, pp 227 - 233.
- 2 Mi, B. and Wypych, P.W., Prediction of Pressure Drop and Determination of Optimal Operating Point in Low-Velocity Pneumatic Conveying, to be published in Powder Technology.
- 3 Pan, R., Mi, B. and Wypych, P., Design of Pneumatic Conveying System for Granular Materials, International Conference on Advanced Technology and Equipment of Materials Handling, Shanghai, China, Oct. 25-27, 1994.
- 4 Pan, R., Mi, B. and Wypych, P.W., Pneumatic Conveying Characteristics of Fine and Granular Bulk Solids, to be published in Kona, No. 12, 1994.